The liver microenvironment – a driver of Hepatocellular carcinoma

Marco Youssef William Zaki, MSc, BSc.

PhD thesis

Supervisors:

Prof. Helen Reeves
Prof. Fiona Oakley
Prof. John Lunec
Prof. Dina Tiniakos

Centre for Cancer

Translational and Clinical Research Institute

Newcastle University

December 2019

Abstract

Hepatocellular carcinoma (HCC) is a major health problem and is the third leading cause of cancer-related mortality worldwide. The prevalence of non-alcoholic fatty liver diseases (NAFLD) is on the rise, and the possibility for the development of HCC in NAFLD patients is increasing in the western countries. HCC driver mutations are not druggable and the median improvement of life expectancy in treated HCC patients doesn't exceed, at best, 2 years. Therefore, novel rewarding targets should be identified, from whom the components of the liver microenvironment represent a fertile field of research and drug discovery.

SULFATASE 2 (SULF2), an extracellular sulfatase, was markedly upregulated in the cancer associated fibroblasts (CAFs) in more than half of HCC biopsies, and CAF-SULF2 expression was associated with poor prognosis and sorafenib tolerance in HCC patients. In vitro, stromal SULF2 induced the proliferation, migration, invasion and therapy evasion of HCC cell lines. Stromal SULF2 activated JNK/IL6 pathway in the fibroblast cell lines, while SULF2-rich secretome activated NF-kB/CD44 stemness pathway in the tumour cells justifying the aggressive, SULF2-dependent tumour cell phenotype.

In a mouse model of NAFLD-induced HCC, *Sulf2*, as well as other targets, was upregulated in the non-tumour liver tissue of the dietary-challenged mice compared to matched controls. Pathway analysis and immunohistochemistry (IHC) validation in mouse and human tissue supported the profound role of different immune cells in the process of tumour development. We have identified a novel Cd44-positive macrophage phenotype that worked in concert with certain T cell subsets to develop HCC in mice. The number of CD44 positive macrophages in the non-tumour liver biopsies of NAFLD patients who developed HCC was higher than CD44 positive macrophages in patients who didn't develop malignancy.

In conclusion, non-parenchymal cell compartments play an essential role in HCC development and progression. Therapeutics targeting the activities of these cells represent a novel strategy for disease prevention/management.

Declaration

I hereby declare that the work presented in this thesis is original and has not been previously submitted to any other academic institution.

Acknowledgement

No words can fulfil my gratification to GOD for his hands were always carrying me, making the verse “For in him we live and move and have our being” comes true. I am tremendously grateful to my family; Nardeen, Mariam and my parents for their unconditional support. Your love and encouragement were my fuel for doing this degree.

I would like to acknowledge my supervisors; Professor Helen Reeves, Professor Fiona Oakley, Professor John Lunec and Professor Dina Tiniakos, for their significant role in my scientific progression. Their contribution to the process of improving my intellectual and laboratory skills is always appreciated.

I would also like to thank all members of the Newcastle fibrosis research group and the members of the northern institute for cancer research (NICR) and the institute of cellular medicine (ICM) for the lovely time we had together. Special thanks to Julie Worrell; Hannah Paish; Sari F Alhasan; Ruchi Shukla; Misti McCain; Ben Barksby; Lee A Borthwick; Olivier Govaere; Ahmed K Mahdi; Joao Mauricio; Robyn Watson; Jack Leslie; John Lunec and Sirintra Nakjang.

It is a good chance to thank Professor Fiona Oakley for giving me the chance to work in other projects throughout my PhD. Her support promoted my scientific career and helped me to be a co-author in many manuscripts that are either accepted “in *Hepatology”*, under review or about to be submitted to high impact journals. I would also like to thank Professor Quentin M Anstee for financially supporting my projects through the EpoS grant. Special thanks to Professors Derek Mann and Jelena Mann for including me in their projects that led to me being a co-author in their recent publications in *Gastroenterology*. I am also grateful to our Spanish collaborators; Aitor Esparza-Baquer and Maria J. Perugorria, for including me in their elegant study that is now being reviewed in *Gut*. Also, I am thankful to my Italian friend; Massimo Younis for including me in his nice study that is to be submitted to *Hepatology* very soon.

Table of content

List of figures

List of tables

List of abbreviations

2D	Two-dimension
3D	Three-dimension
4-MUS	4 methylumbelliferyl sulfate
Ab	Antibody
ABC	Avidin-Biotin complex
AFB1	Aflatoxin B1
AFP	Alfa fetoprotein
AIH	Autoimmune hepatitis
ALD	Alcoholic liver diseases
ALIOS	American life style
ALP	Alkaline phosphatase
ALT	Alanine transaminase
ALT	Aspartate transaminase
ApoB	Apo-lipoprotein B
APS	Ammonium persulfate
ARG1	Arginase-1
ATCC	American tissue culture collection
ATM	Ataxia Telangiectasia Mutated
BAD	BCL2 Associated Agonist Of Cell Death
BCA	Bicinchoninic acid
BCL2	B-cell lymphoma 2
BCLC	Barcelona clinic of liver cancer
BCL-XL	B-cell lymphoma-extra large
BMI	Body mass index
BrdU	5-bromo-2'-deoxyuridine
BSA	Bovine serum albumin
CAF	Cancer associated fibroblasts
CCL2	The chemokine (C-C motif) ligand 2
CCL4	The chemokine (C-C motif) ligand 4
CCL5	The chemokine (C-C motif) ligand 5
CCND1	Cyclin D1
CCNE1	Cyclin E1
CD163	Cluster of differentiation 163
CD44	Cluster of differentiation 44
CD68	Cluster of differentiation 68
CDH1	Cadherin 1
cDNA	Complementary DNA
CK1	Casein Kinase 1
CLD	Chronic liver diseases
CM	Conditioned media
COL1a1	Collagen 1A1
COX2	Cyclooxygenase 2
CSC	Cancer stem cells
CSF	Colony stimulating factor
CTNNB1	β-catenin
CXCL10	Chemokine (C-X-C motif) ligand 10

CXCL9	Chemokine (C-X-C motif) ligand 9
CYP1A2	Cytochrome P450 Family 1 Subfamily A Member 2
CYP2E1	Cytochrome P450 Family 2 Subfamily E Member 1
DAA	Direct acting antiviral
DAB	3,3'-diaminobenzidine
DAMP	Danger associated molecular pattern
DAPI	4’,6-diamidino-2-phenylindole
DE	Differentially expressed
DEN	Diethyl nitrosamine
DEPC	Diethyl pyrocarbonate
DEPTOR	DEP Domain Containing MTOR Interacting Protein
DMEM	Dulbecco’s modified Eagle’s medium
DMPA	9,10 dimethyl-1,2-benzanthracene
DMSO	Dimethyl sulfoxide
DNA	Deoxyribonucleic acid
ECL	Enhanced chemiluminescence
ECM	Extracellular matrix
EDTA	Ethylenediaminetetraacetic acid
EGF	Epidermal growth factor
EGFR	Epidermal growth factor receptor
EHD	Extrahepatic diseases
ELISA	Enzyme-linked immunosorbent assay
EpCAM	Epithelial cell adhesion molecule
ER	Endoplasmic reticulum
ERK	Extracellular Signal-Regulated Kinase
FAK	Focal adhesion kinase
FBS	Foetal bovine serum
FDR	False discovery rate
FFPE	Formalin-fixed paraffin embedded
FGF	Fibroblast growth factor
FN1	Fibronectin
Fz	Frizzled
G1	Group1
G2	Group2
GADD45β	Growth Arrest And DNA Damage Inducible Beta
GAGs	Glucose amino glycans
gDNA	Genomic DNA
GEM	Genetically engineered mice
GPC3	Glypican3
GS	Glutamine synthase
GSEA	Gene set enrichment analysis
GSK3β	Glycogen synthase kinase 3 beta
GSTT1	Glutathione S-transferase theta-1
GTSM1	Glutathione S-transferase M1
H&E	Haematoxylin and Eosin
HbSAg	Hepatitis B surface antigen
HBV	Hepatitis B virus
HCA	Hepatocellular adenoma
HCC	Hepatocellular carcinoma

HCV	Hepatitis C virus
HDL	High-density lipoprotein
HFD	High fat diet
HGDN	High grade dysplastic nodules
HGF	Hepatocyte growth factor
HIFα	Hypoxia inducible factor α
HPF	High power field
HR	Hazard ratio
HRP	Horseradish peroxidase
HS	Heparan sulfate
HSBP	Heparan sulfate binding protein
HSC	Hepatic stellate cells
HSPG	Heparan sulfate proteoglycans
IF	Immunofluorescence
IFNɣ	Interferon gamma
IGF	Insulin growth factor
IGT	Impaired glucose tolerance
IHC	Immunohistochemistry
IkBα	nuclear factor of kappa light polypeptide gene enhancer in B-cells inhibitor, alpha
IKKβ	Inhibitor of nuclear factor kappa B kinase subunit β
IL1β	Interleukin 1β
IL6	Interleukin6
IL6ST	Interleukin 6 Signal Transducer
IL8	Interleukin 8
iNOS	Inducible Nitric oxide synthase
INR	International normalised ratio
IP	Intra-peritoneal
IPA	Ingenuity pathway analysis
ITK	IL2 inducible T cell kinase
JAK	Janus Kinase
JNK	c-Jun N-terminal kinases
KD	Kilo Dalton
KD	Knock down
KEAP1	Kelch-like ECH-associated protein 1
KO	Knock out
KRT	Keratin
LDL	Low-density lipoprotein
LECT2	Leukocyte cell-derived chemotaxin 2
LGDN	Low grade dysplastic nodules
Lob.	Lobular
Log2FC	Log2 fold change
LPS	Lipopolysaccharide
LRP5	LDL Receptor Related Protein 5
MAPK	Mitogen activated protein kinase
MCD	Methionine-choline deficient
MCP1	Monocyte Chemoattractant Protein-1
MDM2	Mouse double minute 2 homolog
MDR	Multiple drug resistance

MDSC	Myeloid derived suppressor cells
MICA	MHC class I polypeptide-related sequence A
MIF	Macrophage Migration Inhibitory Factor
mLST8	MTOR Associated Protein, LST8 Homolog
mM	Millimole
MMP	Matrix Metallopeptidase
M-PER	Mammalian protein extraction reagent
MSigDB	Molecular signature data base
mTOR	Mammalian target of rapamycin
mTORC	Mammalian target of rapamycin complex
MTT	3-(4,5-dimethylthiazol-2-yl)-2,5-diphenyltetrazolium bromide
MUP	Major urinary protein
MVA	Multivariate analysis
n	Number
NAFLD	Non-alcoholic fatty liver diseases
NAS	NAFLD activity score
NASH	Non-alcoholic steatohepatitis
NDST	N-deacetylase/N-sulfotransferase
NES	Normalised enrichment score
NF-kB	Nuclear factor kappa-light-chain-enhancer of activated B cells
ng	Nano gram
NK	Natural killer
NRF2	Nuclear factor erythroid 2-related factor 2
NT	Non-targeted
NT	Non-tumour
OLTx	Orthotopic liver transplantation
PBS	Phosphate buffer saline
pCEA	Pan carcino-embryonic antigen
PD1	Programmed death 1
PDGF	Platelet Derived Growth Factor
PDL1	Programmed death ligand 1
PHx	Partial hepatectomy
PI3K	Phosphoinositide 3-kinases
PNPLA3	Patatin-like phospholipase domain-containing protein 3
POSTN	Periostin
PSC	Best supportive care
PST	Performance status
PVT	Portal vein thrombosis
qPCR	Quantitative polymerase chain reaction
REC	Research Ethics Committee
RICTOR	RPTOR Independent Companion Of MTOR Complex 2
RLTD	Relative level of transcriptional difference
RNA	Ribonucleic acid
RNAseq	RNA sequencing
RPTOR	Regulatory Associated Protein Of MTOR Complex 1
RT	Room temperature
RTK	Receptor tyrosine kinase
S.E.M	Standard error mean
SCID	Severe combined immune deficiency

SDC	Syndican
SDF1	Stromal Cell-Derived Factor 1
SDS-PAGE	Sodium dodecyl sulfate- polyacrylamide gel electrophoresis
SF	Serum-free
shRNA	Short hairpin RNA
SI	Staining intensity
SNP	Single nucleotide polymorphism
SOD2	Superoxide dismutase 2
STAT3	Signal transducer and activator of transcription 3
SULF1	Sulfatase1
SULF2	Sulfatase-2
T	Tumour
T2DM	Type-2 diabetes mellitus
TACE	Trans-arterial chemoembolization
TAK1	Transforming growth factor-β activated kinase-1
TAM	Tumour associated macrophages
TBS-T	Tris-buffered saline-tween 20
TCGA	The cancer genome atlas
TEMED	Tetramethylethylenediamine
TERT	Telomerase reverse transcriptase
TFRC	Transferrin receptor
TGFβ	Transforming growth factor beta
TGFβR	Transforming growth factor beta receptor
TIM3	T Cell Immunoglobulin Mucin 3
TIMP1	Tissue inhibitor of metalloproteinases 1
TLS	Tertiary lymphoid structure
TME	Tumour microenvironment
TNFα	Tumour necrosis factor alpha
TNM	Tumour node metastasis
TP53	Tumour p53
T_{reg}	Regulatory T cells
TSC1	Tuberous sclerosis 1
TSC2	Tuberous sclerosis 2
TYK2	Tyrosine Kinase 2
uPA	Urokinase-type plasminogen activator
UVA	Univariate analysis
VEGF	Vasculo-endothelial growth factor
VIM	Vimentin
WB	Western blotting
WT	Wild type
αSMA	Alpha smooth muscle actin

Chapter 1 - Introduction

Hepatocellular carcinoma (HCC)

Primary liver cancer is a major health issue that ranks seventh in world-wide cancer incidence and accounts for around 6% of overall cancer cases[1, 2]. The heterogeneous distribution of liver cancer is due to the regional prevalence of its risk factors; and generally speaking, more than three quarters of liver cancer cases arise in patients from developing countries compared with cases from the developed countries[3]. Indeed, liver cancer is the third most prevalent cancer in developing countries after lung and stomach cancer[4]. While the incidence of liver cancer showed a 30% decline in high risk countries, in other countries Hepatocellular carcinoma (HCC) incidence doubled in the period between 1978 and 1992[4]. HCC; that is liver cancer initiated by malignant changes in hepatocytes, is the most common type of liver cancer and about 800,000 cases were reported in 2012[5]. HCC accounts for 75-80% of total primary liver cancer cases, whilst the remaining cases develop on the background of carcinoma of the bile ducts or cholangiocarcinoma[6].

1.1. Risk factors for the development of HCC

Major risk factors for the development of HCC include the presence of cirrhosis, viral hepatitis B and C, non-alcoholic fatty liver diseases (NAFLD), obesity, presence of type-2 diabetes mellitus (T2DM), ingestion of aflatoxin and alcohol **(Figure 1.1)**.

1.1.1 Cirrhosis

Cirrhosis is the major risk factor for the development of HCC and it typically develops on the background of chronic liver disease. Chronic liver diseases include viral hepatitis, alcohol consumption, NAFLD and hemochromatosis[7]. The incidence of HCC development in cirrhotic patients depends on the background liver disease and the severity of this underlying cause and approximately 2.5 to 4% of cirrhotic patients develop HCC per year, while 80% of HCC cases arise on the background of established cirrhosis[8-10]. It is, hence, better to describe the role of cirrhosis in the development of HCC in the context of other risk factors.

1.1.2 Hepatitis B virus

Hepatitis B virus (HBV) infection accounts for 50% of HCC cases worldwide[11]. HBV infection is acquired vertically in the endemic areas where most of patients became chronic carriers for the disease. On the other hand, blood transfusion and unsafe sexual habits are the major determinants of horizontal HBV infection in the countries with lower viral incidence[12]. HBV-

HCC is linked with other factors including gender, age, concurrent ingestion of Aflatoxins as well as smoking[13]. HBV can be considered as an independent risk factor for the development of HCC; however, more than 70% of HBV-HCC cases are developed on the background of cirrhosis[13]. In a systematic review in Asia, the odds for the development of HBV-HCC were dramatically increased in the presence of cirrhosis[14]. Two important aspects should be highlighted here; the first is that the HBV viral load (estimated by measuring the HBV DNA) was proportional to the increased risk of HCC development in patients from Taiwan independent of other risk factors[15]. Secondly, the genotyping of HBV is associated with the severity of the disease in a regional pattern; that is, genotype D is associated with the development of HCC in western countries and in the USA, whereas, genotype C was associated with cirrhosis and HCC development in the Asian population[13].

1.1.3 Hepatitis C virus

The development of HCC on the background of Hepatitis C virus (HCV) peaked in Mediterranean countries, for example, Egypt and Italy, but also in Japan[16-18]. It is also predicted that the incidence of HCV-induced cirrhosis and subsequently HCC will rise within the next decade in the USA[19]. Other case-control studies showed that HCV-positive individuals were 17 times more susceptible to develop HCC compared to non-HCV patients[20]. Unlike HBV infection, HCV-HCC is developed in the majority of cases after the establishment of cirrhosis; probably because HCV increases the risk of fibrosis and inflammation preceding the cirrhotic changes in the liver tissue[21, 22]. HCV infected patients are more likely to develop HCC in presence of other co-factors like age, male gender, genotype 1b, presence of diabetes, increased alcohol consumption as well as in presence of HIV or HBV co-infection[13]. The high efficacy of the direct acting antiviral (DAA) therapy managed to abolish viral replication and decrease the viral load which should in theory decrease the incidence of cirrhosis and in turn the development of HCC[23, 24]. However, safety studies should be carried on using these drugs due to the reported increase in HCC in DAA-treated patients in certain studies[25]. In addition, once the cirrhosis is established the risk of HCC is still independent on efficient viral eradication with the DAA[23].

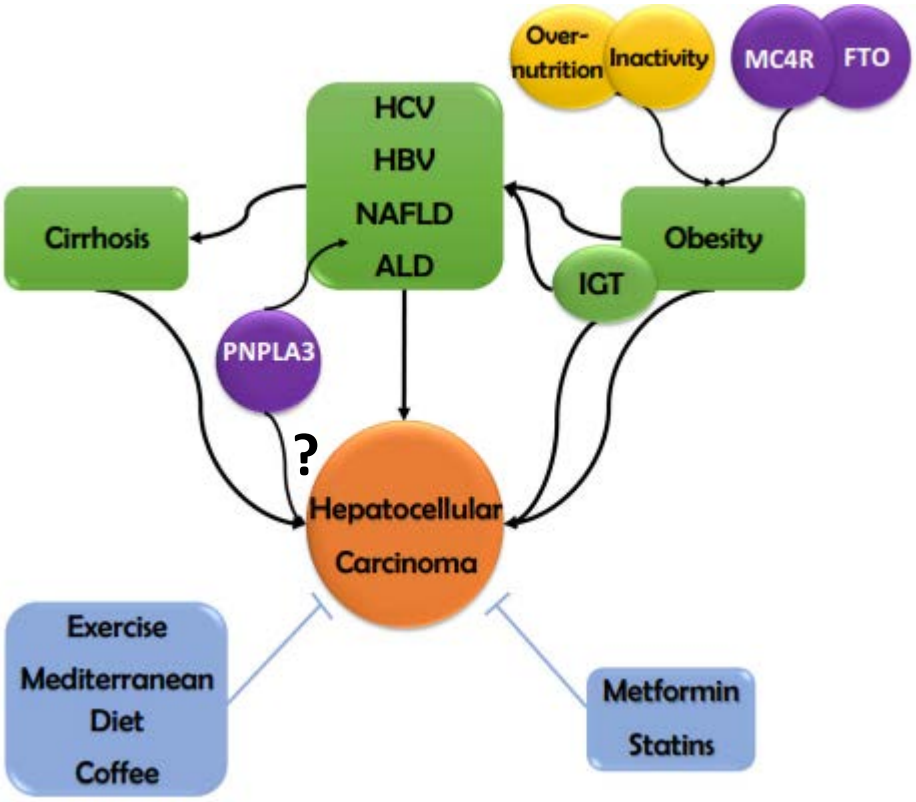

Figure 1.1 The association of HCC with different risk factors; from Reeves et al[26] with permission: The development of HCC is associated with co-infection with clinical factors (cirrhosis), infection with liver viruses (HBV and HCV), or with environmental factors (obesity, excessive alcohol consumption, diet related fatty liver diseases). Preventive strategies for HCC may involve adapting better eating habits and healthier life style. Studies performed on patients having the antidiabetic metformin or the anti-hyperlipidaemic Statins showed delayed or less onset of HCC development[27, 28]. Abbreviations: HCV; Hepatitis C virus, HBV; Hepatitis B virus, NAFLD; non-alcoholic fatty liver disease, ALD; alcoholic liver diseases, IGT; impaired glucose tolerance.

1.1.4 Alcohol

The link between alcohol consumption and HCC development has been extensively studied[29-31]. The correlation between alcohol consumption and HCC revealed a dose-dependent association, with patients drinking more alcohol or over longer period of time being more likely to develop HCC than age matched non-alcoholics[31]. In the US, individuals with a history of alcohol intake were at higher risk to develop HCC relative to those who do not drink. In addition, patients who have more than 80 mL/d alcohol had 4.5 higher risk of developing HCC compared to other individuals[31]. Alcohol intake is associated with the development of cirrhosis and hence favouring HCC development. In addition, increased alcohol intake induces

alcoholic steatohepatitis (ASH) with more fat deposition, more inflammation and accumulated free radicals that all lead to hepatocarcinogenesis[32].

1.1.5 Aflatoxin

Grains, nuts or fermented soybeans stored in humid conditions are susceptible to the development of the liver carcinogen Aflatoxin by the *Aspergillus flavus* and *Aspergillus parasiticus* species[33]. This carcinogen, especially Aflatoxin B1 (AFB1), is prevalent in sub-Saharan Africa and East Asia and resulted in a higher HCC prevalence[32]. Aflatoxin ingestion induces a point mutation in codon 249 of the p53 tumour suppressor gene predisposing to HCC[34]. Studies from Sudan[35], Taiwan[36] and China[37] adopted several ways to detect the exposure to AFB1, for example, AFB1-DNA and AFB1-albumin in tissues and body fluids. Correlation studies revealed an AFB1-synergistic effect on HBV patients developing HCC suggesting that AFB1 might potentiate the carcinogenic effect of HbSAg[38].

1.1.6 Non-alcoholic fatty liver disease (NAFLD)

The Epidemiology of HCC has been significantly altered during the last few years primarily due to major breakthroughs in the treatment of viral hepatitis and the increase in NAFLD prevalence, resulting in a shift towards NAFLD-driven HCC as a key contributor to the burden of HCC. NAFLD prevalence exceeds 25% of the western population given the increase of the onset of other comorbidities including obesity, hyperglycaemia and the metabolic syndrome[39], and this syndrome can progress to the more severe form, non-alcoholic steatohepatitis (NASH), that is strongly associated with the development of HCC[40]. Risk factors for the development of HCC on the background of NASH include male gender, age with criteria of the metabolic syndrome. Although the other factors increase the risk of developing HCC, it is largely after progression to cirrhosis, which is not always the case in patients with NAFLD, where cirrhosis is present in only 70% of those developing HCC. In the other 30% of NAFLD cases, HCC develops in the absence of established cirrhosis. These patients often present at a more advanced stage, as they are not in cirrhosis HCC surveillance programs[41, 42]. The prevalence of NAFLD-HCC in the western countries ranges between 4-22%[43], while one study has shown that 59% of the US HCC patients had NAFLD background[44]. This is not the case in the Eastern countries and the Middle East where other etiologies are more prevalent.

1.1.7 Type-2 Diabetes mellitus (T2DM) and obesity

HCC is closely associated with the prevalence of T2DM, with probably 8-50 % of HCC cases arise in diabetic patients[45, 46]. Different studies from the US[45] and Western Europe[47] showed

that the odds of developing HCC in presence of T2DM are 1.5-4 times higher than the non-diabetic patients. Increased insulin resistance and hyperglycaemia may have also promote DNA and cellular damage consequent to accumulation of hepatic fat and the subsequent escalation to NASH, with associated the oxidative stress and production of free radicals[48]. In addition, T2DM together with obesity can be associated with HCC development independently of the presence of NAFLD[45, 46].

Patients with body mass index (BMI) of more than 30 have a four times higher risk of developing HCC compared to non-obese patients[30]. The development of HCC in obese patients is also associated with environmental factors like alcohol consumption and tobacco[49-51]. The link between obesity and HCC may be through the establishment of NAFLD and T2DM[45, 46].

1.2. Anatomic and histopathological changes in HCC

Benign hepatocellular tumours are hepatocellular adenoma (HCA) and focal nodular hyperplasia, while benign biliary tumours include biliary adeno-fibroma and bile duct adenoma. Liver malignancy, on the other hand, may be of hepatocellular (HCC, hepatoblastoma and HCC fibrolameller variant), cholangiocellular (cholangiocarcinoma) or mixed (hepatocellular cholangiocarcinoma, mixed epithelial mesenchymal hepatoblastoma) cell origin[52]. Macroscopically, HCC may develop as a single lesion or as multiple foci separated by non-tumour liver parenchyma. HCC developed on the background of cirrhosis is often encapsulated with fibrous tissue, but this feature is not as frequent in the non-cirrhotic patients with HCC[52, 53].

Three histological features are assessed in biopsy tissues when considering the diagnosis of HCC, including changes in liver architecture and cytological features, as well as the presence of portal stromal invasion[54]. Loss of the intact portal tract and the presence of unaccompanied arteries, together with an increase in liver cell plates from 1-2 cells thick to 3 cell thick or more are typical features of HCC. Some HCCs have sheet-like growth patterns, while other types form pseudo-like or trabecular structures of the liver cell plates[54]. Changes to cellular morphology are often seen in HCC and can be also be a useful tool for diagnosis. These changes include the presence of clear or giant cells, as well as fatty deposition within tumour associated with some features also seen in their non-tumour counterparts - like Mallory-Denk bodies, intracellular inclusions and hyaline globules. Nuclear polymorphism is also seen in HCC, especially in the presence of abnormal mitotic figures and changes in the nuclear-to-cytoplasmic ratio[54]. These cytological abnormalities together with the changes in the

architecture were the basis for Edmondson and Steiner's classification of HCC tumour grades[55]. This classification includes 4 grades. Grade 1 or well differentiated HCC typically has thin trabecular architecture, with slightly enlarged nuclei and abundant eosinophilic cytoplasm. Grade 2 or moderately differentiated HCC frequently has a pseudo-glandular pattern with a higher nuclear-to-cytoplasmic ratio. Poorly differentiated HCC includes grades 3 and 4, with an exponential increase in nuclear hyperchromatic features[55]. HCC lacks a typical pattern of stromal invasion, although more abundant stroma can be feature in fibrolamellar and scirrhous subtypes of HCC[54].

In addition to histological assessment of diagnostic biopsies, based on the haematoxylin and Eosin stained sections, the presence of other tissue markers can provide a strong additional tool to confirm a diagnosis of HCC and distinguish a primary from a secondary or metastatic tumour. Immunohistochemistry can also distinguish mixed origin tumours and non-cancerous lesions. The presence of canalicular polyclonal carcino-embryonic antigen (pCEA) or CD10, with focal or strong hepatocellular Glypican-3 (GPC3) and Arginase-1 (ARG1) expression are strong indicators of a primary rather than metastatic cancer and are at least moderately sensitive. In parallel, the loss or disorder of reticulin staining with strong sinusoidal expression of CD34, especially if associated with cytoplasmic GPC3 and Glutamine synthase (GS) staining, strongly support a diagnosis of HCC rather than a benign lesion[54].

1.3. Molecular classification of non-tumour/HCC and their link with clinical features

The focus of many liver cancer researchers has been directed towards profiling HCC tumours into different molecular categories, with the aim of developing a more "personalised" approach for the affected patient, with the ability to predict their prognosis, but also their likely outcome to a particular treatment. HCCs typically harbour great inter and intra-tumour heterogeneity and it was hoped that the innovation of microarray and high throughput "omics" techniques would decipher the more meaningful molecular subtypes within a tumour.

One of the first integrated molecular studies was reported in 2007, on tissues from HBV-driven HCC in French patients, and combined gene mutation, DNA methylation and expression microarray data[56]. Mutation in *TP53, AXIN1, TCF1, PIK3CA, and KRAS* genes was evident in this cohort of patients with a unique hyper-methylation in the *CDKN2A* and *CDH1* gene promoters. Unsupervised clustering of the microarray data identified two robust clusters; each of which was divided further into 3 sub-clusters. This 6-G clustering was defined by clinical features as

well as mutational status[56]. A subsequent larger multi-centre study used formalin-fixed, paraffin embedded (FFPE) tumour tissues as well as the adjacent non-tumour tissues from a primary cohort of early HCC in Japanese patients undergoing tumour resection[57]. The derived gene signature was subsequently validated in patients from the US and western countries, with the goals of correlating gene signature from both tumour and non-tumour tissue with patient outcome. Outcomes studied included survival and late recurrence (tumours developed two years or more after resecting the primary tumour). Interestingly, the gene signature of the tumour tissue didn't show any association with the patients' survival or tumour recurrence, while the non-tumour gene signature was significantly associated with patient survival. Particular genes associated with poorer survival were those involved in inflammatory processes, with strong enrichment of genes in both the NF-κB and IL6/STAT3 pathways[57].

One subsequent multi-centre study from *Chiang et al*[58] focused on exploring copy number variation and expression microarray in HCV-driven HCC resection tissues from Spain, US and Italian patients[58]. Most of the characterised tumours harboured 1q gain, 8q gain and 8p loss, with hierarchical clustering of the microarray expression profile identifying 5, rather than 6, patient subgroups. Interestingly, two clusters (*CTNNB1* and the proliferation subclasses) were concordat with the French clustering groups, while concordance between pathway analyses in the *Chiang et al.* clustering and the previous 6G study was also demonstrated[58]. *Hoshida et al*[59] followed this study up with a meta-analysis combining the previous gene expression studies. All the expression data, from the different aetiologies of HCC, was pooled and analysed together, with three suggested human HCC sub-clusters emerging. These were termed S1-S3 and again, associations with clinical and histological data defined[59]. S1 and S2 subgroups shared some common features and together, S1 and S2 were termed the proliferative subtype, as opposed to the non-proliferative subtypes made up of S3 cases **(Figure 1.2)**. Tumours in the proliferative phenotype reportedly had a more aggressive phenotype, with comparatively poorer outcomes for affected patients. This group was characterised by activation of RAS, IGF and mTOR signalling pathways[59]. Two subclasses were defined within this proliferative group, based on activation of either the Wnt/TGFβ pathway or the EpCam progenitor cell pathway[59]. Conversely, the non-proliferative phenotype, in

which patients had a relatively better prognosis compared to the proliferative subtype, included patients with CTNNB1 mutation[60, 61].

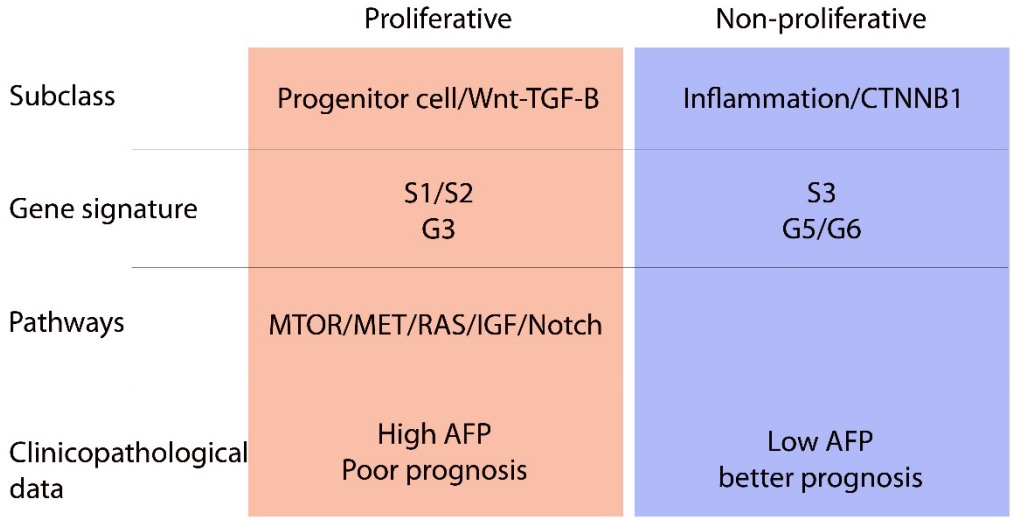

Figure 1.2 Hoshida's classification of HCC patients, from *Hoshida et al*[59] with modification HCC patients were classified according to their gene expression profile and to the deregulated pathways into three classes (S1-S3). Concordance with previous gene signatures revealed an overlap with particular groups (G3, G5/G6) mentioned previously by *Boyault et al*[56]. Overlapped gene signatures represent two groups of patients based on the proliferation index of the tumours; the proliferative phenotype with poor patient outcome and the non-proliferative group with good prognosis.

As a result of these studies, there is the possibility of profiling the gene expression of HCC and classifying affected patients into categories, supported by clinical data, which are associated with outcome. With a view to indentifying signature(s) that predicted disease recurrence, *Villanueva et al*[62] went on to evaluate the gene expression profile of 287 early HCC from patients cared for at four different centres, exploring the overlap with the previously reported gene expression signatures from tumour tissues as well as from the non-tumour regions. The *Chiang et al* proliferation signature[58] was the most prevalent in the *Villanueva et al* cases. Pair-wise comparisons confirmed clustering of the most poor survival gene signatures together. In contrast, analysis centred on V coefficients showed clustering of most signatures into three broad categories. The first category included the proliferation subtype[58], G3[56], cluster A[63], late TGFB[64], Met signature[65] and S1[59] signatures. The second category was defined by the poor survival tumour-adjacent signature[57], while the third category was associated with progenitor cell activation (hepatoblastoma_C2[66], EpCAM[67] and S2[59] signature). Of all the gene signatures within the broader categories, only

the G3[56] signature, poor survival signature and satellites were independently associated with tumour recurrence and overall recurrence.

While these studies have grouped patients based on their gene expression state into certain categories with an ability to predict outcome and tumour recurrence, the role of these groupings in prospective management decisions for patients remains uncertain. A further limitation of these data thus far, is the limitation to HCC predominantly arising in HBV and HCV aetiologies, with little representation of NAFLD-HCC patients. More work is needed to define the gene expression profile of NAFLD-HCC patients and to explore possible overlaps between the transcriptome of these patients and the publically available viral aetiology HCC datasets.

1.4 Pathophysiological changes in HCC

The development of HCC is mostly accompanied by chronic liver diseases, with cirrhosis as the most important known factor predisposing to HCC development. The liver malignant process is believed to start with chronic liver disease that leads to disruption of the normal liver architecture and generating nodules of hepatocytes. These nodules can undergo a number of pre-malignant steps, involving their transformation into low grade dysplastic nodules (LGDN) that progress to high grade dysplastic nodules (HGDN). An accumulation of genetic and epigenetic events with time increase the likelihood of these premalignant structures transforming into malignant early HCC and subsequently more aggressive HCC[68]. This multi-stage process is accompanied by the build-up of different mutational loads, deregulated signalling pathways as well as changes in the premalignant microenvironment.

1.4.1 Genetic Factors predisposing HCC

Several single nucleotide polymorphisms (SNPs) are associated with the development of HCC in combination with one or more from HCC risk factors[69]. SNPs in the cell cycle genes (*TP53* and *MDM2*[70]), inflammatory genes (*TGFβ*[71], *TNFα*[72] or *IL1β*[73]) and oxidative stress genes (*SOD2*[74]) are of special interest. HCV patients with rs4444903 SNP in *EGF*[75] gene and rs2596542 SNP in the *MICA*[76] gene responsible for altering immune response are at higher risk for developing HCC. *PNPLA3*[77] SNP in NAFLD/NASH patients predispose the development of HCC, while SNPs in *GTSM1* and *GSTT1* genes[78] are common in HBV infected patients or AFB1 positive patients who progress to HCC. In isolation these SNPs are not harmful, but they can increase the likelihood of HCC development in the presence of other risk factors.

1.4.2 Pre-carcinogenic gene alteration

As reported below, acquired *TERT* mutations are common in HCC and recently, rare germ line mutations in *TERT* have also recently been reported to increase the risk of HCC[79, 80]. TERT encodes telomerase, an enzyme important for maintaining the integrity of telomeres – the protected DNA repeated sequences at the ends of chromosomes. Changes in the telomere and the tolemerase activities are common in the cirrhotic patients and are associated with high risk of HCC development. *TERT* promoter mutations are present in about 5% of LGDN and in 19% of the HGDN with marked increase in early HCC patients[81]. *TERT* promoter mutation can, thereby, be considered as the "guardian" of the malignant transformation of hepatocytes, while other mutations are acquired afterwards. Hepatocellular adenomas, a rare type of benign hepatic tumours, have β-catenin exon 3 mutations, *HNF1A* or *IL6ST* mutations. The presence of β-catenin mutation in hepatocellular adenoma increases the risk of the development of malignancy. The chromosomal aberrations, hypomethylation and *TERT* promoter mutation are included in the last step of malignant transformation[82].

In human, the insertion of viral DNA particles in the human genes like TERT and CCNE1 can lead to genotoxicity and HCC development[83]. Similarly, infection with adeno-associated virus 2 (AAV2) leads to insertional mutations in the aforementioned genes together with CCNA1 and TNFSF10; being correlated with HCC development[84]. Frequent C>A point mutation and R249S mutation in *TP53* as a result of AFB1-DNA adduct is commonly seen in HCC patients[33]. Aristolochic acid exposure leads to T>A transverion and was associated with HCC development in Chinese population adding another tier of complexity in the process of cancer initiation[85].

In experimental HCC, the mechanism by which carcinogens induced genotoxicity is extensively studied. Discovered in the thirties of the last century, N-nitoso compounds were the most commonly used carcinogen in hundreds of HCC studies [86]. Administration of Diethylnitrosamine (DEN) is responsible for the alkylation of the guanine N^7 atom leading to HCC development in rats. Further investigation identified cytochrome p450 enzyme (CYP2E1)-mediated metabolism of DEN to dimethyl nitrosamine (DMN) to be responsible for the formation of DNA adduct before the development of HCC in mice[86]. The development of DEN-induced HCC was partially mediated through the induction of oxidative stress and consequently the production of reactive oxygen species (ROS) that affect DNA integrity and induce further chromosomal aberrations and genotoxicity[86].

1.4.3 Main DNA driver mutations

Whole genome sequencing studies showed that although the number of somatic mutation in HCC patients can be between 35 and 80 mutation per case, the optimal number of driver mutations required for the initiation of the tumour is between 5 to 8[87]. The rest of these mutations are considered as "passenger" mutations that are not able by themselves to initiate HCC. Key driver mutations usually happen in the key genes regulating the process of the carcinogenesis including genes regulating cell cycle (*TP53, CDKN2A, RB1, CCNE1*), genes preserving telomere function (*TERT*), genes responsible for cell proliferation (*CTNNB1* and *AXIN1*) and oxidative stress (*NRF2* and *KEAP1*) **(Figure 1.3)**.

1.4.3.1 Cell cycle gene mutations

Mutation in the tumour suppressor gene *P53* is common, reported in 12% - 48% of HCC patients[88]. *P53* is crucial for important biological processes like apoptosis, cell cycle arrest and DNA repair, with change in its sequence alters the translation or function of the encoded protein, pushing cells towards malignant transformation[89-94]. HBV, HCV, oxidative stress and ingestion of AFB1 are associated with *TP53* point mutations, leading to G:C to T:A transversion [33, 95-100]. Moreover, the HBV host–integral gene, HBx, reduces the binding of *P53* to important transcription factors responsible for apoptosis, resulting in disruption of this physiological process[101-103]. Other genes involved in cell cycle regulation, like *p21, CCNE1* and *RB1* genes are vulnerable to mutational changes in HCC patients. Approximately 12% of HCC have homozygous deletion in *p21*[104], and a further 8% of patients harbour *RB1* mutations[105]. HBx is found to be integrated in the human genome leading to mutation *CCNE1* gene in about 5% of HCC[83] and amplification of *FGF19/CCND1* locus in 14% of HBV-related HCC[106].

1.4.3.2 Telomerase reactivation mutations

Early changes in the telomere and telomerase activity are seen in liver tissues of cirrhotic patients, and in HCCs - with about 90% of HCC having a higher level of expression of telomerase[107]. This is attributed to amplification in the *TERT* locus in about 6% of patients[108], HBx insertion in the region of *TERT* in 15% of patients and an activating mutation in the *TERT* promoter in more than 50% of patients[83]. *TERT* promoter mutation is associated with *CTNNB1* mutation in a number of HCC patients[108].

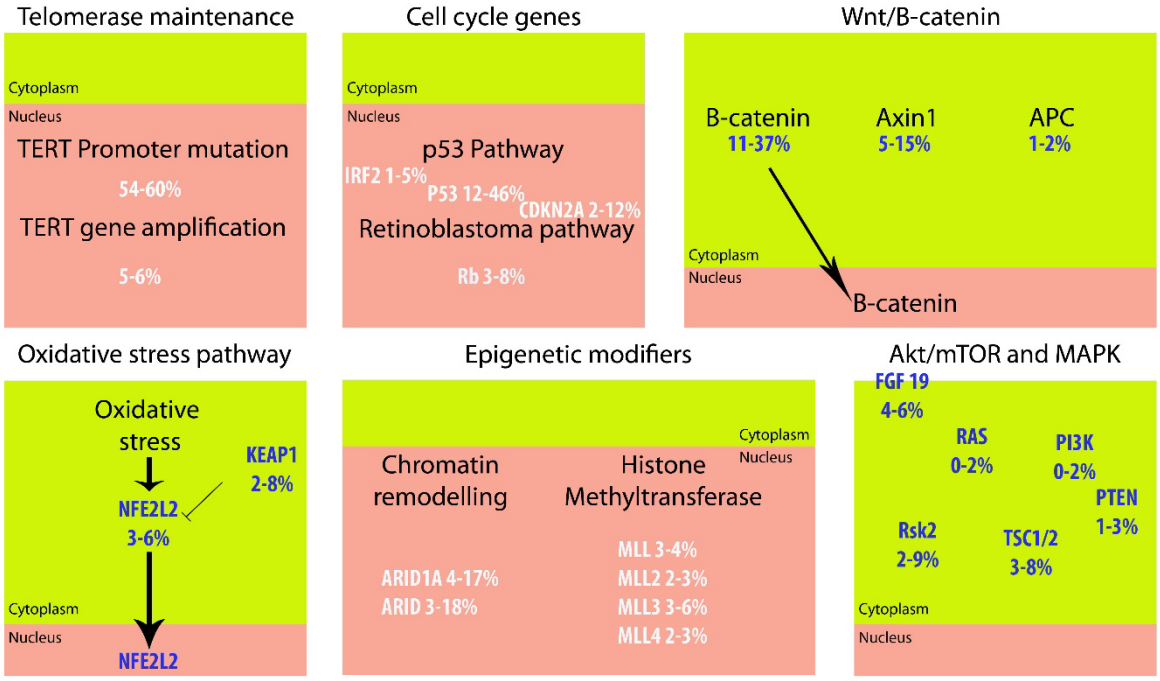

Figure 1.3 Mutational status in HCC patients, *from Zucman-Rossi et al*[109] with modification
Driver mutations in HCC take place in key genes responsible for regulating telomerase function, cell cycle, *Wnt*/β-catenin and oxidative stress. Other less-common mutations include mutations in the genes responsible for epigenetic regulation of gene expression or genes regulating RTK pathways.

1.4.3.3 *CTNNB1* mutation

Wnt/β-catenin pathway is an essential oncogenic pathway in about 40% of HCC and is responsible for cell proliferation and metabolic processes within the tumour. *CTNBB1* encodes β-catenin and in the absence of constitutive activating *CTNNB1* mutations, upstream dysregulation is typically present, promoting *Wnt* ligands binding to the Frizzled receptors leading to the aberrant translocation of wild type (WT) β-catenin from its membranous complex into the nucleus, to activate its specific gene expression. However, *CTNNB1* is mutated in exon 3 in more than 30% of HCCs, leading to constitutive nuclear translocation of β-catenin and persistent activation of the pathway[110]. Other genes involved in the Wnt/β-

catenin pathway, like *APC* and *AXIN1*[111] are also, but less frequently, mutated. Some studies suggested a link between HCV infection and AFB1 exposure to the development of HCC with CTNNB1[110].

1.4.3.4 Receptor tyrosine kinase-related mutations

Receptor tyrosine kinases (RTK) comprise a large group of enzymes that phosphorylate important downstream targets regulating many physiological, but also oncogenic pathways. An activating mutation in any one of these proteins, or deletion mutation in one of their inhibitory regulators, will lead to activation of the whole pathway and increase cellular survival and proliferation. Amplification of *CCND1/FGF19*[106], activation mutation in *PIK3CA* or deletion mutation in the pathway inhibitor *TSC1* or *TSC2* will lead to activation of the PI3K/AKT/mTOR pathway[108]. Although RAS mutation is rare in HCV and HBV-infected HCC patients (2%), inactivating mutations in the RAS inhibitor *RSK2* occurs in about 9% of HCC patients leading to activation of this whole pathway[104]. Mutations in RAS family members also include activation mutation in codon 61 in *NRas*, in codon 12 in both *HRas* and *KRas*[112-118]. Lack of genome wide studies in NAFLD-HCC patients might explain the underestimation and the low number of HCC patients harbouring mutations in the RAS family members.

1.4.4 Oncogenic pathways in HCC development and progression

HCCs are a very heterogeneous group of tumours and many factors can be involved in the process of tumour development and progression. As mentioned before, DNA damage and the resulting pattern of mutation is essential to the development of the disease. Unfortunately many of these changes in the human genome are deemed un-correctable or 'undruggable' and the focus of the current research is to understand the consequences of changes in the gene at the protein level, with the hope of identifying chemopreventive or therapeutic targets for HCC. A number of key pathways promoting tumourigenesis are those maintaining the oncogenic conditions within the premalignant liver or in the tumour microenvironment. Infiltration of different stromal or immune cells to the tumour niche can directly favour oncogenesis or activate key pathways that promote chronic liver disease progression to cirrhosis, paving the route to HCC development. The interplay between different cell types within the liver tissue and the oncogenic pathways potentially activated by cell-cell cross talk are summarised here.

1.4.4.1 NF-κB pathway

Inflammatory cytokines like TNFα, IL6, IL8 and IL1β released from dead or damaged cells or the bacterial cell wall component Lipopolysaccharides (LPS) can activate the classical NF-κB pathway by phosphorylation and degradation of IκBα. Unphosphorylated IκBα sequesters members of the NF-κB family in an inactive form in the cytoplasm. As a result of IκBα degradation, released NF-κB dimers, typically RelA and P50 homodimers, enter the nucleus to activate NF-κB targets. In the alternative pathway, p100 is degraded resulting in a p52 molecule and enabling the free p52/RelB to translocate to the nucleus promoting transcription of a discrete subset of NF-κB dependant genes. Genes regulated by the NF-κB pathway include pro-inflammatory genes (*iNOS, IL6, TNFα* and *IL1β*), fibrogenic genes (*TGFβ*), cell survival and apoptosis genes (*BCL2, BCL-XL, cIAP, GADD45β*) and metabolic genes (*SOD2*)[119].

Activation of NF-κB can be associated with the development and progression of HCC regardless of its cellular source. In *Mdr2* knockout mice that develop spontaneous HCC on a background of cholestasis-induced chronic inflammation, the release of TNFα from the bile ducts and different inflammatory cells activates the NF-κB pathway in the adjacent hepatocytes by recruiting RelA to the nucleus and leading to HCC. Activation of the NF-κB pathway reported in this model was associated with the late phase of tumour initiation[120], mediated by upregulation of the anti-apoptotic and cell survival genes *GADD45β* and *BCL2*[120]. Activation of NF-κB in non-parenchymal cells can also contributes to the initiation of HCC. NF-κB-mediated iNOS production from macrophages and neutrophils can abrogate P53 transcription, via an increase in free radicals and an enhanced production of macrophage Inhibitory Factor, or MIF [121, 122]. This pro-tumorigenic effect of macrophages can also be promoted by dead or apoptotic hepatocytes, which release characteristic molecules known as Danger Associated Molecular Patterns (DAMPs), which activate NF-κB signalling within macrophages. This in turn leads to the production of IL6 and TNFα, which have well established mitogenic effects on adjacent hepatocytes[123-126].

After tumour initiation and development, activation of NF-κB can contribute to progression and a poorer outcome. Tumour cells or tumour associated macrophages secretes CCL22 and CC17 chemokine that attract a specific subset of Tcells ($T_{regulatory}$ or T_{reg} cells) to the site of the tumour. This type of T cell is responsible for induction of an immunosuppressive phenotype that supresses anti-tumour immunity[127]. NF-κB activation induces the expression of different

matrix modifying proteins and enzymes that are essential for tumour progression[128-130]. The Cyclooxygenase-2 (*COX-2*) enzyme, a transcriptional target for NF-κB, is responsible for production of hypoxia inducible factor-α (*HIF-α*) that stimulates production of the angiogenic factor *VEGF* [131].

1.4.4.2 JNK pathway

The cJun NH_2-terminal kinase (JNK) is included in different physiological and pathological pathways in the liver as well as in other organs. The JNK pathway regulates the expression of different downstream genes that are implicated in apoptosis and proliferation, including *cJun*, *JunD* and *JunB*[132]. The role of JNK pathway activation and the development and the progression of HCC has been extensively studied using human and murine models. Early reports showed that livers of *JNK1*-deficient mice[133], or those treated with a specific JNK inhibitor[134], or those of *cJun*-deficient mice[135] , did not regenerate after partial hepatectomy (PHx) and were also protected from the development of carcinogen-induced HCC. Moreover, deficiency of JNK activation in mouse embryonic fibroblasts impaired cellular proliferation[136]. To dissect the role of JNK activation in different cell types in liver microenvironment, Das *et al* tested the potential of *JNK1/JNK2* global or conditional deletion on the ability of the livers to regenerate and to develop HCC[137]. Global deletion of *JNK1/JNK2* did not affect liver regeneration after PHx, and *JNK1/JNK2* hepatocyte conditional-knockout (KO) promoted the initiation of HCC in mice liver implying that activation of JNK1/2 in hepatocytes is one of the pro-apoptotic mechanisms. However, specific deletion of *JNK1/2* from the hepatocytes and the non-parenchymal cells did protect mice from DEN-induced HCC by regulating compensatory proliferation and regulation of production of pro-tumourigenic cytokines like IL6 and TNFα[137]. In conclusion, the role of JNK seems to be cell-specific, with JNK activation in the non-parenchymal cells favouring the development of carcinogenesis by regulating the inflammatory secretome, which in turn, through paracrine signalling mediates hepatocyte trans-differentiation and tumourigenecity.

1.4.4.3 Wnt/β-catenin pathway

The Wnt/β-catenin pathway is implicated in several functions within the liver microenvironment, with roles in liver regeneration, metabolism and cellular proliferation. About 19 Wnt members are involved in the Wnt pathway. Upon synthesis, the Wntless receptors transfer the Wnt members to the plasma membrane[138-142]. In the absence of receptor ligand, the intracellular, wild type β-catenin molecule is bound to a membrane-

anchored complex - a destruction complex that involves Axin, APC, GSK3α/β and CK1α/β proteins. The pathway is switched on when Wnt ligands bind to and facilitate the dimerization of the Frizzled (Fz) and LRP5/6 extracellular receptor complex. Dimerization of Fz-LPR receptors stimulates the binding of Dishevelled (Dsh) protein to the cytoplasmic tail of the Fz receptor that facilitates further interaction and phosphorylation of Axin and its bound kinases GSK3 and CK1 to LPR cytoplasmic tail. This inhibits β-catenin (CTNNB1) proteasome degradation and encourages saturation of the destruction complex [143-145146]. Downstream targets to the β-catenin pathway involve genes responsible for metabolism (*GS*, *CYP2E1* and *CYP1A2*), cell cycle regulation (*CCND1*; Cyclin D1 and *Myc*), cytoskeleton remodelling (*CDH1* and *MMP7*), some fibroblast growth factors (*FGF*s), epidermal growth factor receptor (*EGFR*) and chemokines (leukocyte cell-derived chemotaxin 2 (*LECT2*))[147-165]. Subcellular localisation of β-catenin in the healthy and diseased liver, including its role in liver regeneration and HCC, has been comprehensively reviewed [166].

All the recent molecular characterisations attribute β-catenin mutations or activation in the WT Wnt/β-catenin pathway as major contributors to HCC malignancy. In the *Hoshida et al* classification[59], the TGFβ-Wnt signalling pathway was enriched in the S1 subgroup of HCC patients. This group of patients was characterised by poor outcome and high AFP levels. Conversely, patients in the S3 subgroup, who showed good prognosis compared to other subgroups, were characterised by the activation mutation in exon 3 of the *CTNNB1*. Murine models of β-catenin activation mutations were not able to initiate HCC in isolation. However, in the presence of co-activated pathways like the Ras pathway, β-catenin is potentially involved in the development of HCC[167-171]. Any mutational or transcriptional changes in the other members of the β-catenin pathway are also associated with the incidence of human HCC. Inactivation of the β-catenin negative regulator *GSK3β* or upregulation of the Wnt receptor Frizzled7 (*Fr7*) were frequently seen in HCC [57, 172-174]. Patients with T2DM have SNPs in *WNT5b* and *TCF7L2* genes which might predispose HCC[175]. NF-κB and PI3K/AKT activation was linked to the upregulation of cytoplasmic or membranous β-catenin inducing experimental HCC in mice, highlighting the importance of the upregulation of the β-catenin irrespective to its subcellular localisation[166].

1.4.4.4 TGFβ pathway

The TGFβ pathway comprises three ligands; TGFβ1, TGFβ2 and TGFβ3 and three receptors TGFβR1, TGFβR2 and TGFβR3. Binding of any TGFβ ligand to TGFβR3 induces its binding to the

TGFβR2 which then recruites TGFβR1 and the activation of the downstream pathway. Classical activation of the TGFβ pathway induces the phosphorylation of *SMAD2* and *SMAD3*, facilitating their nuclear translocation and initiation of TGFβ-related gene expression[176-182].

The role of TGFβ in the process of tumourigenesis was highlighted in the high-throughput transcriptomic analysis, in which patients in the S1 group were characterised by activation of the TGFβ pathway in association with a poorer overall survival compared to the other groups[59]. In a clear contrast, TGFβ is typically considered as a tumour suppressor gene, with its dysfunction linked with the development HCC[183]. This discrepancy was highlighted further by a recent study from *Chen et al.* that was published in gastroenterology in 2018[184]. By RNA sequencing, TGFβ-related genes were deregulated in more than 25% of HCC patients versus controls. TGFβ protein expression was absent in normal hepatocytes, although evident in both tumour cells and HCC stroma. Unsupervised clustering of their data showed four distinct clusters, with descending activation of the TGFβ pathway from cluster A (highest) towards cluster D (lowest). Survival analysis revealed that *inactivation* of the TGFβ pathway (cluster D) was linked with shorter survival emphasising the importance of loss of TGFβ tumour suppressor function. The active TGFβ groups were enriched with other oncogenes, like *MDM2*, *KRAS, IGF2* and *KEAP1* in comparison to the other group. In particular, the active group was linked with hepatic fibrotic genes (collagens), cytokines (*IL6* and *IL6ST*) together with growth factors like *PDGF* and *EGF* confirming the active role of TGFβ in the tumour microenvironment and the cross talk between different cell types in the process of carcinogenesis. On the other hand, loss of TGFβ activity was associated with the deficiency of other tumour suppressor genes like *ATM, BRCA1* and *FANCF*[184]. This implies that treatment with TGFβ pathway inhibitors should be targeted for a certain subclass of HCC rather than being a global therapy.

1.4.4.5 JAK/STAT pathway

Activation of the JAK/STAT pathway is cytokine-dependent and is usually, but not always secondary to activation of other oncogenic pathways, including NF-κB and JNK pathways. Both NF-kB and JNK pathways primarily activate gene expression of different cytokines, including those activating the JAK/STAT pathway[120, 137]. Although activation of the JAK/STAT pathway in HCC is evident in the epithelial cells, the role of this pathway is more prominent in the non-parenchymal cell types that foster an aggressive niche and immune suppressive environment. Receptor signalling via the JAK/STAT pathway includes 4 members, namely JAK1, JAK2, JAK3 and TYK2. Activation of these receptors leads to phosphorylation and subsequent

homo/heterodimerisation of different STAT members (STAT1, STAT2, STAT3, STAT4 or STAT5), followed by their translocation to the nucleus. In the nucleus they activate a plethora of downstream target genes[185].

IL6 is a classical activator of the STAT3 pathway and is one of the well-known protumorigenic cytokines in the tumour microenvironment. The major non-parenchymal sources of IL6 are tumour associated macrophages (TAMs) and cancer associated fibroblasts (CAFs). Recently, a study from Michael Karin's group[186] has shown that the release of IL6 from TAMs induced the expression of *CD44* in liver parenchymal cells, via the activation of STAT3. CD44 is a cell surface glycoprotein and its upregulation in the centrilobular areas lead to its dimerization with EGFR and expression of the P53 antagonist *MDM2*. The consequent loss of *P53* function lead to the development of tumours in mice challenged with DEN[186]. In addition, IL6 is known to promote inflammation-induced HCC, as well as neo-angiogenesis in established tumours[187]. Activation of STAT3 by IL6 modulates the tumour microenvironment by increasing the infiltration of inflammatory cells to the tumour area, while reducing the maturation of dendritic cells and inducing the proliferation of the immune suppressive TH17 T-cell subtype[188-191]. Activation of this pathway also increases the expression of cell survival and cell cycle progression genes favouring more proliferative niche within the tumour area[192-196].

Other interleukins activating the JAK/STAT pathway can play a role in inflammation-associated cancers. The NF-κB related upregulation and secretion of IL23 from myeloid derived suppressor cells activates the JAK/STAT pathway together with Wnt pathway, which in turn promote an increase in the proliferation index of colorectal cancer cells[197]. IL10 supresses the anti-tumour T-cell activity in premalignant and malignant conditions, via activation of the IL10/IL22 receptor family[198-203].

1.4.4.6 mTOR pathway

The mTOR pathway is activated in a sub-group of HCCs and is usually linked with metabolic processes[204, 205]. This pathway includes two distinct effector complexes, namely mTOR complex1 (mTORC1) and mTOR complex2 (mTORC2). mTORC1 includes *mTOR, mLST8, DEPTOR, RAPTOR* and *PRAS40*, while mTORC2 is composed of *mTOR, mLST8, DEPTOR, PROTOR* and *RICTOR*. Activation of mTORC1 is mediated via different growth factors, amino acids, nutrients and cytokines, which induce activation of the MAPK pathway, leading to phosphorylation and inactivation of the mTOR inhibitors TSC1 and TSC2. Although mTORC2 is not sensitive to nutrients, it is very sensitive to growth factors that control actin cytoskeleton

and cell metabolism[206]. Activation of mTOR pathway regulates different physiological and pathological pathways including ageing, autophagy, metabolism and cell growth[207, 208]. The main determinant of activation of mTORC1 is the over-nutrition that induce metabolism, *DE NOVO* lipogenesis and protein synthesis, while at the same time inhibit autophagy. Activation of the mTORC2 pathways is independent on nutrient status but dependent on other growth factors like IGF[207, 208].

The mTOR pathway is activated in response to the increased lipogenesis in steatotic liver compared to healthy controls, and the pathway is further activated in association with liver malignancy. This mechanism is particularily essential for "feeding" the tumour cells as a nutrients' supplier[209]. It also regulates another process which is key for cancer progression; autophagy. In the process of cancer initiation, autophagy plays a protective role by eliminating cell debris and damaged cells; however, after the development of tumour, autophagy increase tumour cell survival and increase tumour resistance to many anticancer therapies[210, 211]. In human HCC, more than 50% of patients show upregulation of one or more from the mTOR family, and the prognosis of this group of patients is unfavourable and characterised by poor survival[212, 213]. In contrast, the inhibition of the mTOR pathway may be protective. Metformin treatment in diabetic patients reportedly halves the incidence of HCC development compared to the diabetic patients receiving non-metformin treatments. The protective effects of Metformin therapy is proposed to be via activation of the AMPK pathway, a known inhibitor of the mTOR pathway[214, 215].

1.4.5 The role of the liver premalignant/microenvironment in the development of HCC

The development of HCC is usually preceded by chronic liver diseases which alter the cellular landscape in the liver microenvironment and favour certain conditions that permit the malignant transformation of hepatocytes or cancer stem cells[216]. Livers of patients with HCV infection are characterised by more hepatocyte damage and infiltration of inflammatory cells that contribute to viral clearance, but also to the development of pro-inflammatory, pro-malignant environment. On the other hand, the double stranded HBV can integrate into the human genome and if this occurs in certain areas, the integration can activate oncogenes or supress important genes responsible for cellular homeostasis, leading to malignant transformation. This is predisposed by infiltration of other stromal cells and cycles of liver regeneration that help tumour development. The role of the microenvironment in NASH-driven HCC is still poorly investigated, but reports link the high oxidative stress status and

accumulation of lipids within the hepatocytes as a trigger for their transformation into malignant cells[26].

Regardless of the cause of the chronic liver disease, the liver has its own defence mechanism against any invading/foreign bodies. In response to chronic liver disease, certain type of cells like hepatic stellate cells or fibroblasts, together with inflammatory cells such as macrophages and leukocytes, produce or alter the composition of the component proteins in the liver microenvironment. The component proteins in the liver microenvironment are termed the extracellular matrix (ECM) proteins. This remodelling process of the ECM is associated with the development of new blood vessels (neo-angiogenesis) and fibrosis. Although being a physiological process for normal wound healing, persistent injury that occurs during chronic disease can lead to the establishment of unresolved fibrosis that progresses to cirrhosis. Cirrhosis is characterised not just by permanent fibrosis, but also distortion of the architecture of the liver by nodules of regenerating hepatocytes, within which malignant transformation can occur. Hence, it is important to understand the role of the tumour premalignant niche, including the contribution of factors that elicit the growth of a particular clone of cells to form the malignant tumour[216].

The tumour premalignant microenvironment is composed of ECM, within which there are different types of non-parenchymal cells, each with their own profile of secreted cytokines or other factors. This environment can promote the growth of transdifferentiated hepatocytes, as well as their invasion and migration through the disrupted basement membrane[217, 218].

1.4.5.1 Cellular components of tumour microenvironment

The role of the immune cells in the development and progression of HCC is a hot topic, in part owing to the breakthrough of immune check-point inhibitors as therapies for other malignancies[219]. It is now widely accepted that one of the key the cells responsible for anti-tumour immunity is the CD8 T-cell, which plays a critical role in immune surveillance. Active CD8 T-cells recognise damaged or transformed hepatocytes and help eliminate them. Notably, exhausted non-proliferating CD8 T-cells are not able to perform this function properly. T-cell exhaustion is initiated via binding of inhibitory receptors on the T-cells, such as PD1 and TIM3, to ligands on immune suppressor cells – a so called 'check-point' to prevent the immune system causing tissue damage as a result of continuing T cell activity. In persistent liver injury, the 'check' which switches off the T cells in the microenvironment can help transformed

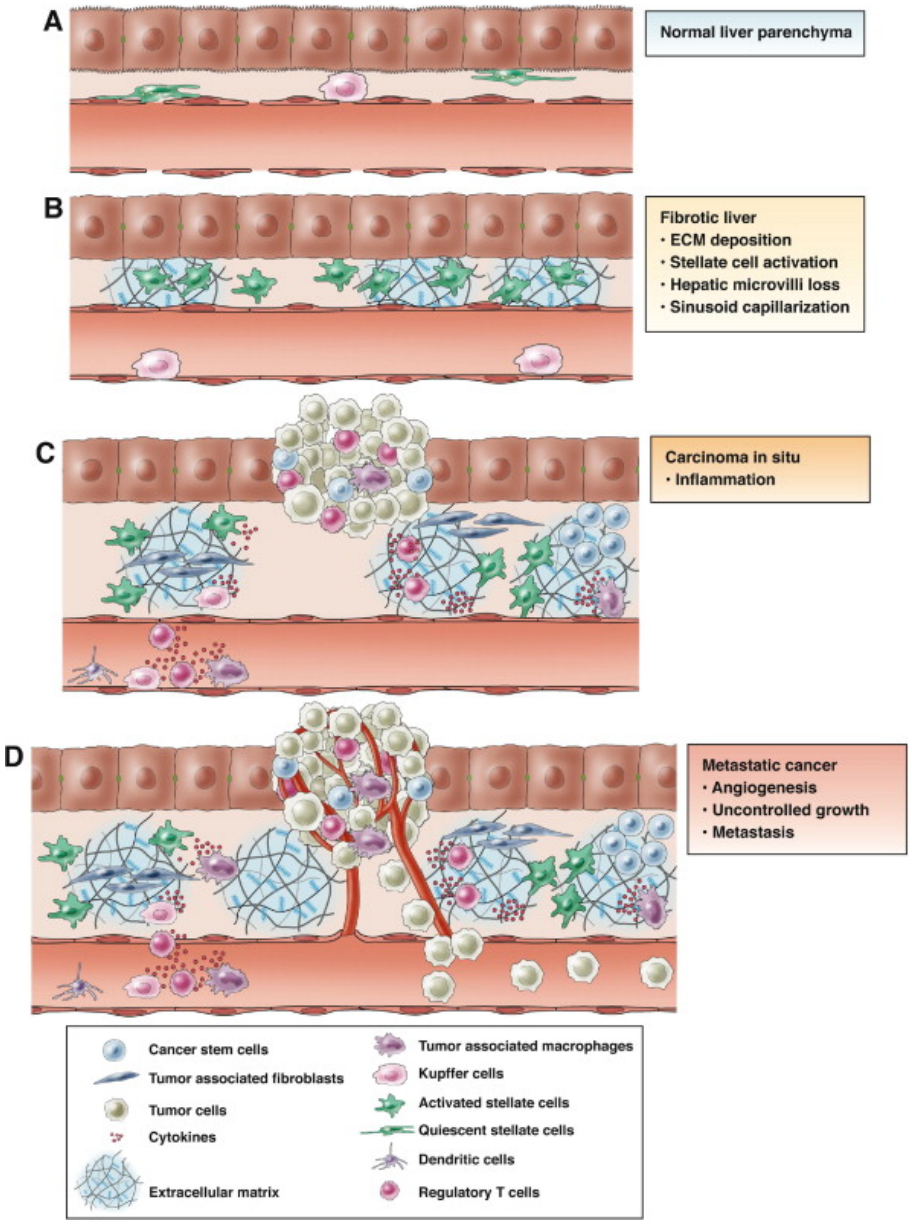

Figure 1.4: The role of the the premalignant/tumour microenvironment in the development and progression of HCC; from Hernandez-Gea et al[216] with permission: The cascade of the development of abnormal microenvironment in the liver starts from the activation of Quiescent stellate cells to hepatic active stellate cells which secrete ECM proteins. This provides a mechanical stiffness which is linked to the development of HCC. After the primary tumour is formed, infiltration of different immune components and proliferation of endothelial cells help the process of tumour progression and metastasis.

hepatocytes or tumour cells evade host immunity. Tumour cells can also express the ligands which bind the inhibitory receptors on T cells, such as PD-L1 , similarly altering the tumour microenvironment in a way which leads to tumour progression[219]. The class of anti-cancer drugs called 'Check-point inhibitors' disrupt this 'switch off' mechanism, potentially unleashing an anti-tumour immune response.

Other types of T-cells which are frequently found within the tumour microenvironment are the CD4 T-cells and Treg cells. While CD8 T cells promote an active immune response, Treg cells are immunosuppressive and dampen an immune response. The presence of Treg cells in particular is linked with poorer patient prognosis, attributed to roles in immune-evasion of the tumour cells[220]. The number of Treg cells is associated with HCC stage and a ratio of higher Treg to CD8 T-cell number can predict a worse patient outcome [221]. Treg cells secrete cytokines that dampen the host immunity, encouraging an immune-null environment that facilitates tumour growth. Activation and infiltration of Treg cells in tumour areas is partly mediated by myeloid-derived suppressor cells (MDSC) and macrophages, that secrete chemotactic cytokines that specifically attract Treg cells[220].

Macrophages, or 'big eaters' in the Greek language from which the term comes, are large cells recruited to sites of injury. They detect and phagocytose pathogens or debris, for purposes of elimination, but also presentation of antigens from the source of potential harm to T cells. They can also release cytokines that activate other immune cells. Macrophages can be phenotypically diverse, with different lineage or polarisation – most commonly termed macrophage 1 (M1) or macrophage 2 (M2) - according to the disease state. M1 macrophages are an inflammatory subset of macrophages that secrete a wide spectrum of cytokines and growth factors with pro-inflammatory functions within the diseased liver. M2 macrophages, on the other hand, adopt a restorative phenotype, with anti-inflammatory and tissue regenerative functions[222]. In malignant conditions, the interaction between the tumour cells and the macrophages favours the development of M2-polarised macrophage subset that is known as tumour activated macrophage (TAM)[223]. TAMs have immune supressing roles in the tumour microenvironment by cross-talking with other immune cells and increasing the infiltration of immune suppressive cells[224]. TAMs also release other angiogenic and tumour cell proliferating factors increasing the proliferation but also the migration and invasion of the tumour cells. In human HCC, the number of TAM has been reported an unfavourable prognostic marker associated with disease progression[225].

Although the role of immune system is pivotal in the development and the progression of HCC, other non-parenchymal cells are still fundamentally important for supporting the tumour microenvironment. As mentioned the TGFβ pathway plays a role in tumour development. The cellular sources of TGFβ in the tumour niche are the tumour cells, but also activated stromal cells known as cancer associated fibroblasts (CAF) and macrophages which have tumour

promoting functions within the tumour microenvironment [226]. CAFs are the major source of collagen that is responsible for increasing tissue stiffness, which is also associated with a more aggressive tumour microenvironment. Compared to normal fibroblasts, CAFs secrete a different repertoire of chemokines, like CXCL12 and SDF-1 that promote tumour metastasis and chemoresistance[227]. CAFs can also secrete VEGF and HGF, respectively inducing neo-angiogenesis within the tumour microenvironment and supporting growth and proliferation of the tumour cells[228].

By interrogating changes in the immune profile in HCC patients at the transcriptomics level, the Llovet group has identified a group of HCC patients characterised by the enrichment of immune genes, immune signatures for T-cells, macrophages, tertiary lymphoid structure (TLS), PD-1 and immune metagene-related pathways[229]. This "immune subclass" was defined by the upregulation of 108 immune-related genes, with strong enrichment of the TGFβ, JAK/STAT signalling pathways. Integration of this subclass with the previously published HCC transcriptomic data showed a strong enrichment with the previously described S1 subclass (Wnt/TGFβ activation pathway), while immunohistochemistry (IHC) staining confirmed significant associations with PD-1 and PD-L1 protein expression. Notably, within the immune subclass two distinct groups were further defined. The first group, comprising 33% of cases and termed the "exhausted immune group", was characterised by active stroma, T-cell exhaustion, TGFβ expression and an M2 macrophage signature. The other group was termed the 'active immune group' as it was associated with an "active immune response" characterised by T-cell activation and IFN expression. These latter features have previously been reported in other cancer types as predictive of a response to treatment with a checkpoint inhibitor called pembrolizumab. Patients in the HCC 'active immune response group' had a lower tumour recurrence after resection and a trend towards better survival. This subclass was an independently associated with better overall survival (OR=0.58, p=0.04), reflecting the importance of the activation of T-cells in anti-tumour control[229].

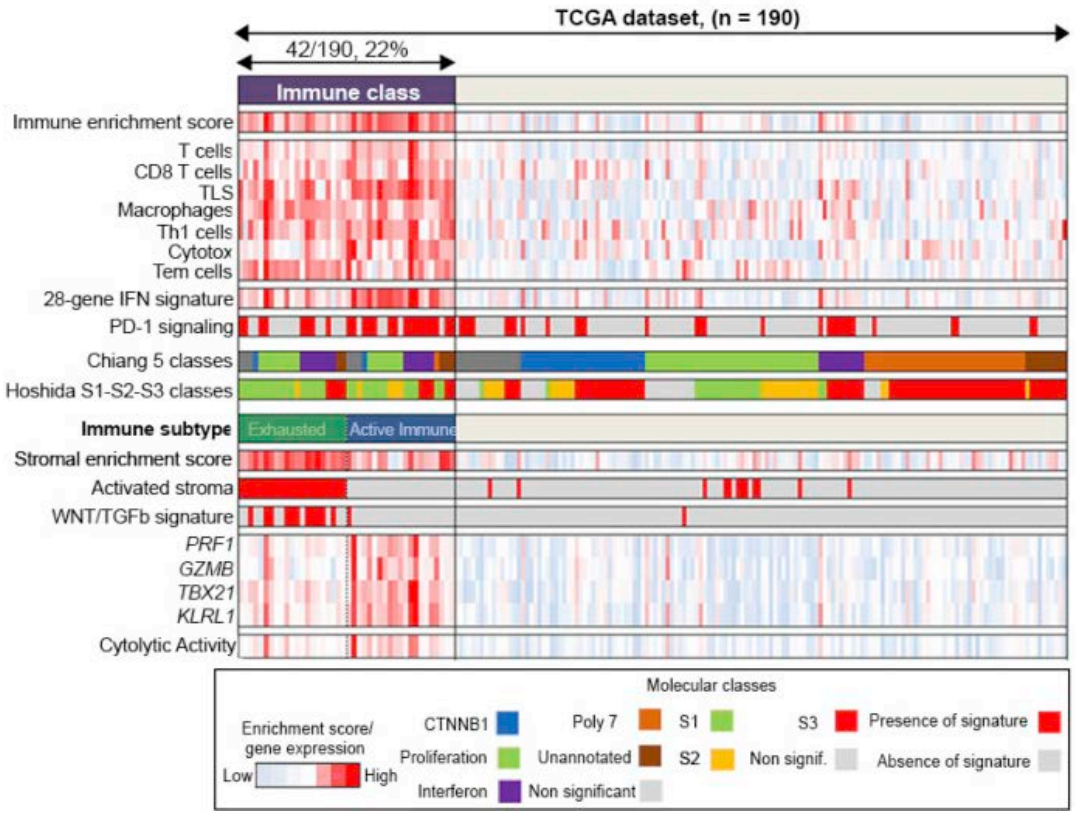

Figure 1.5: The integration of different component/pathways of the microenvironment to construct immune response in HCC patients; from *Sia et al*[229] with permission: less than quarter of HCCs were characterised by activation of certain immune-related genes. This Immune class was characterised by activation of the stroma as well as activation of TGFβ pathway. Within this immune class, one third of HCCs had exhausted T cell gene signature in association with poor patient prognosis. The rest of tumours showed active CD8 cytotoxic T cell and favourable outcome after resection confirming the active anti-tumour immunity.

1.4.5.2 Extracellular matrix proteins and their regulators

1.4.5.2.1 Heparan sulfate proteoglycans (HSPGs)

The ECM is a complex network of secreted and post-transcriptionally modified proteins that act as a storage platform for growth factors and cytokines. ECM proteins also act as co-receptors facilitating the ligation of bound growth factors to their receptors on the cell surface. Modifiers to the structure and/or function of ECM proteins play an important role in changing the structure of these proteins, but also in the liberation and availability of growth factors to their binding sites. One important category of the ECM proteins are the heparan sulfate proteoglycans (HSPGs), which are composed of heparan sulfate (HS) chains covalently bound to a core protein[230]. The importance of HSPGs derives from their versatile functions within the tissue microenvironment. With more than a million HSPG available binding sites, groups of proteins can bind, forming the so called 'Heparan sulfate interactome'[231, 232].

Heparan sulfate binding proteins (HSBP) include enothelial growth factors (VEGFs), Wnt ligands, sonic hedgehog signalling and ligands activating the TGFβ pathway[233-236]. FGF, HGF, RAGE and APP family of protein undergo HS-induced oligomerisation facilitating binding to their ligands/receptors[237-245]. HSPGs may also act as scaffold proteins that block or favour – dependent on their post translational modifications - the most suitable configuration for associated HSBPs to bind their receptors[246].

Members of the HSPGs family include Syndicans (SDC1-SDC4), Glypicans (GPC1-GPC6), perlecan, agrin and collagen XVIII, ECM proteins [247-252]. The HS component is a hetero-polysaccharide chain comprised of heparin, hyaluronic acid, chondroitin sulfate, keratan sulfate and dermatan sulfate[253-255]. Generally, HS chains include repeated di-saccharide units of glucuronic acid or its epimer L-iduronic acid, linked in the 1-4 position with unsubstituted, N-sulfated or N-acetylated glucosamine. Synthesis of the HS chain is a multi-step process and starts with chain initiation where a linker arm is introduced between the core protein and the glucose amino glycans (GAGs). Subsequently, glucosamine-transfer and exostosin glycosyltransferases enzymes start the second step; chain elongation or polymerisation. Further enzyme-directed post transcriptional modifications on the HS chains include 2O-sulfation on uronic acid moieties or 3O and 6O-sulfation on the glucosamine[255]. This process is not random, but rather specific to the type of cell, the physiological function of the parent HSPG and can be influenced by pathological processes within the host organ[256-259]. Three groups of post translational modifying enzymes are involved in the post-polymerisation step in the HS synthesis, including (1) N-deacetylase/N-sulfotransferases (NDST1-4) which replace the acetyl groups with sulfate groups; (2) epimerases which convert D-glucuronic acid into its epimer L-iduronic acid, which has a more flexible ring confirmation; and (3) sulfotransferases, which direct O-sulfation of the substituted sulfate groups at the 2,3 and 6-O positions[260-266].

The functional importance of the HSPGs extends beyond the physiological status to exert a pivotal role in liver pathology. At first glance, the pattern of HSPGs within the liver microenvironment is significantly different between the physiological and pathological state. This difference implicates a role of HSPGs in many liver diseases. In viral hepatitis, the viral particles invade the host hepatocytes for replication, with entry of both HBV and HCV mediated by different kinds of HSPG. In human fibrotic and cirrhotic conditions, the quantity and distribution of different HSPGs change in association with the severity and the stage of the disease, particularly on the liver non-parenchymal cells. In the physiological state, SDC2,

SDC3 and perlican are expressed in the resting myofibroblasts, smooth muscle cells, endothelial cells in the portal blood vessels, with SCD1 and perlican expressed in the endothelial cells of the sinusoidal wall. In chronic liver diseases, the expression of these HSPGs is upregulated and their level of sulfation is altered. In viral hepatitis, SDC1 is unusually expressed in the non-sinusoidal hepatocyte interface[267], in line with its mechanistic role promoting viral invasion of hepatocytes[268, 269]. As such, SDC-1 has been proposed as a candidate therapeutic target for viral hepatitis.

The role of HSPGs in the tumour microenvironment has also been described in relation to disease staging and prognosis[267]. GPC3 , for example, is absent or scanty in normal or diseased liver, but markedly upregulation in a subset of HCCs and has been adopted as a tissue diagnostic marker in HCC[270]. *GPC3* level is upregulated in HCC diagnostic biopsies and resections, but not in control nor in chronically diseased livers. GPC3 protein is only detected in HCC, while it was absent in the adjacent non-tumour counterparts. GPC3 is usually present in the tumour cell membrane, and it can be occasionally detected in the tumour cell cytoplasm[271] Due to tumour heterogeneity, GPC3 is included in an HCC diagnostic panel including GS, Heat shock protein 70 and CD34[272]. *In vitro* studies have shown that upregulation of GPC3 in HCC cell lines enables Wnt ligands such as Wnt3a to bind to the frizzled receptor, activating the Wnt3a/β-catenin pathway. This oncogenic GPC3-mediated activation of the β-catenin pathway was notably regulated by an important post translational modifier of HSPG structure, namely Sulfatase-2 (SULF2)[273].

1.4.5.2.2 Sulfatase 2(SULF2) physiological and pathological roles

SULF2 belongs to a larger group of 17 sulfatase enzymes[274, 275]. SULF2, rather than the other sulfatases, is an extracellular post-translational modifiers of HSPGs. *SULF2* transcript was identified as sonic hedgehog response genes involved in the activation of Wnt signalling[276], [277]. Subsequent functional analyses at the protein level revealed a role in the selective modification (desulfation) at the 6O position of HSPGs – a position known to be associated with regulation of ECM binding of multiple cytokines and growth factors, including FGFs [278-281], HGF [282], fibronectin [283], PDGF [284] and VEGF [285]. Subsequent to SULF2-mediated removal of the 6O sulfate, bound factors can be liberated from their storage sites to bind and activate their target pathways, regulating cell survival, differentiation, ECM remodelling and angiogenesis. Hence any upregulation or change in SULF2 function or expression level can, in

theory, significantly alter the function and composition of the tissue microenvironment - making it an interesting protein to study.

1.4.5.2.2.1. Structure of SULF2

The structure and maturation of SULF2 is illustrated in **(Figure 1.6)**. Immature SULF2 is composed of 870 amino acids comprising 4 unique domains, namely the signal peptide, enzymatic, hydrophilic and sulfatase domains[286]. The similarity of amino acid sequences between mouse and human SULF2 exceeds 90%, highlighting a high conservation amongst different species[286]. Much of the protein structure is also common to both SULF1 and SULF2 proteins, with the most notable differences being in the heparin binding motifs in the hydrophilic domain[287, 288], perhaps suggesting different target specificity.

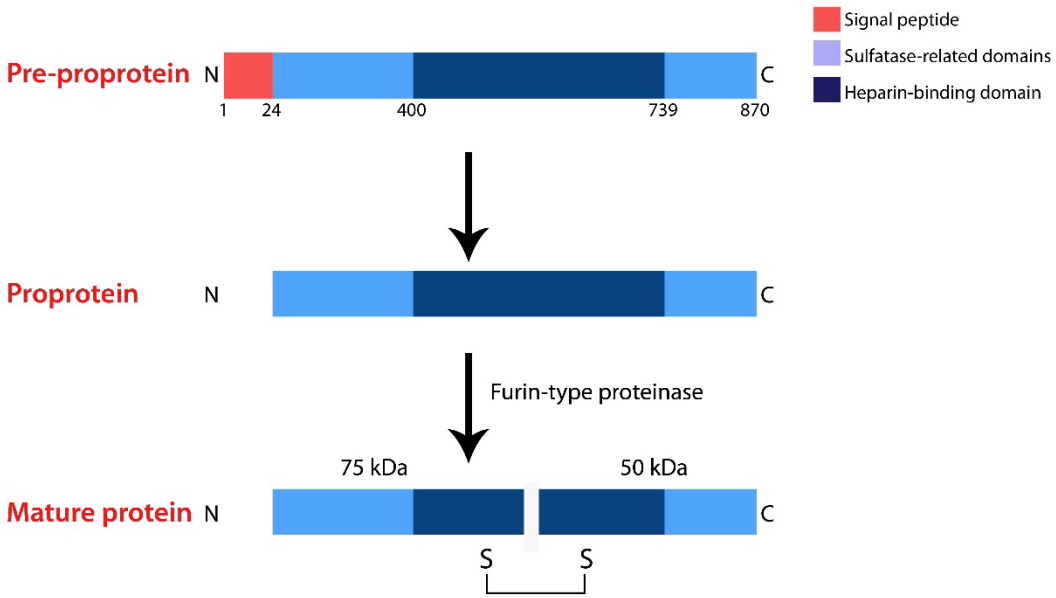

Figure 1.6 SULF2 structure and activation, from Rosen and Lemjabbar [289] with modification
Immature SULF2 undergoes a two-step activation; loss of signal peptide and cleavage of the SULF2 pro-protein into two peptides linked via a di-sulphide bond. Abbreviations: C; C-terminal, N; N-terminal, S-S; disulphide bond, kDa; Kilo Dalton

The hydrophilic domain is responsible for the membrane anchorage process as well as the interaction of the enzyme with its substrate HSPGs[288, 290, 291]. The sulfatase cleavage in the target HSPG is mediated by the oxidation of a cysteine residue into a Cα-formylglycine[276, 286].

The SULF2 pre-proprotein has its signal peptide removed within the endoplasmic reticulum (ER) **(Figure 1.6).** A Furin-type proteinase then acts on the hypdrophilic domain of the proprotein, cleaving it into two 75 KD and 50 KD[288, 292] isoforms. The mature SULF2 is created by the binding of these two fragments with a disulphide bond. The resulting active protein has membrane-anchored and secreted forms[286, 288, 291]. Although SULF2 is responsible for the post transcriptional modification of the HSPGs, this enzyme is also vulnerable to post-translational

modification. The N-terminal region of SULF2 contains more than 10 glycosylation sites, although the exact role of glycosylation and whether this affects the enzyme activity or membrane binding is unclear. Glycosylation of SULF1 is known to affects its biological functions in terms of secretion, activity and membrane binding[286, 293].

1.4.5.2.2.2. The function of SULF2

Early evidence of the role of SULFs in normal physiological processes came from knock-out (KO) mice. SULF2$^{-/-}$ mice had poorer survival, decreased weight gain and developed lung abnormailites compared to their wild type littermates[294]. The mortality of SULF1$^{-/-}$ SULF2$^{-/-}$ double mutant mice was nearly 50%, although the mice were able to give birth to normal embryos with smaller adult organs[295]. The double mutant mice had swallowing difficulties attributed to weak oesophageal muscles, implicating the importance of both the enzymes in muscle cell homeostasis[296]. The phenotype was similar to that seen in Hs2st, EphrinB1 and BMP deficient mice [295].

The process of desulfation, in which SULF2 eliminates the sulfate group specifically from the 6O position of the wide range of HSPGs[291], is summarised in **(Figure 1.7).** Briefly, the hydrophilic domain of SULF2 binds to its target HS chain, while the sulfatase catalytic domain binds to the last 6O-sulfate group in the chain. The process desulfates the entire chain at the 6O position, before the enzyme dissociates from the desulfated chain, in order to target other HSPG members [297].

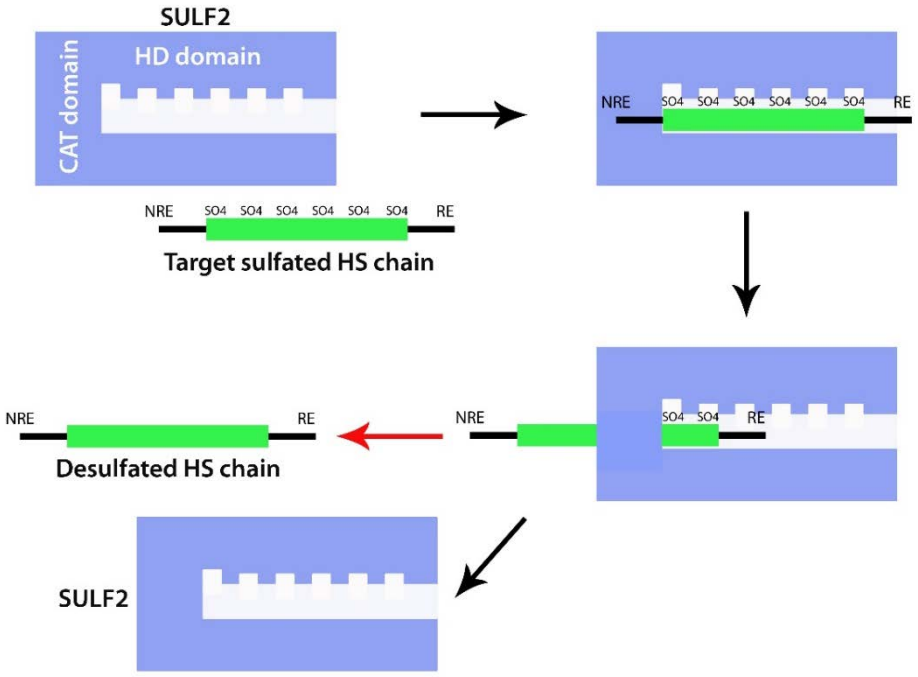

Figure 1.7 SULFs-mediated desulfation of different members of HSPGs; *from* [297] with modification Abbreviations: CAT; catalytic domain, HD; hydrophilic domain, NRE; Non-reducing end, RE; reducing end.

A tool to assess the sulfatase activity of the SULFs was developed by Morimoto-Tomita et al[286]. In brief, 4-methylumbelliferyl sulfate (*4-MUS*) is used as a sulfatase substrate, with quantification of intensity of a released fluorescent moiety being proportional to sulfatase activity[286]. The SULF2-mediated desulfation of HSPGs chains in the liver reportedly increases the release of endotheial (VEGF, EGF, PDGF), fibrotic (FGF1, FGF2, CXCL12, FN1, SOD), hepatocellular (HGF) and inflammatory (IL8, CCL21, TNFα, CSF1, IL7, IFNγ) factors from their binding sites within the microenvironment to activate their downstream targets[296, 298-300].

1.4.5.2.2.3. The tumour promoting role of SULF2

Alongside the important physiological role of SULF2, it is also implicated in pathological processes, including malignancy. A malignant proangiogenic role for SULF2 was reported in $SULF2^{-/-}$ mice that developed less HCC than their wild type littermates after exposure to the carcinogen DEN. Further investigation revealed that SULF2 induced neo-angiogenesis via a TGFβ/Periostin (POSTN) dependant mechanism, increasing liver tumour size, number and distant metastasis into the lungs[301]. SULF2 – active at physiologically neutral pH only - initiated angiogenesis, with heparinise taking over cleavage of HS chains in more hypoxic and acidic conditions in the tumour microenvironment [302, 303].

Microarray data exploring gene expression in HCC resections previously reported that *SULF2* was upregulated in about 57% of HCC patients[304]. An elevated level of *SULF2* was associated with early disease recurrence in these patients. The researchers also reported that SULF2 stimulated FGF2/GPC3 upregulation and activation in HCC cell lines, as well as in a mouse xenograft model. Additionally, SULF2 induced Akt/ERK oncogenic pathways that promoted cell growth and migration via phosphorylation of the Akt substrate GSK3β, an established anti-apoptotic factor [273, 304]. Further support for a role regulating apoptosis comes from knockdown of SULF2 in HCC cells showing upregulated *BAD*, a pro-apoptotic molecule that forms heterodimer with BCL-2 and BCL-xL survival factors, and hence induces apoptosis [305]. Finally, *SULF2* has also been found to be a transcriptional target of P53 in different types of cancer, as well as in HCC cell lines [306, 307].

1.5 Experimental mouse models for HCC- a focus on diet-induced HCC

The use of an experimental mouse model provides a powerful tool for the study of tumour biology and for testing new therapeutic targets in preclinical studies in an *in vivo* context. The use of mouse models in cancer research, and particularly in HCC, is context dependent and needs careful study design before running any model. HCC usually arises in the background of

chronic liver disease, and consequently, inducing these tumour-inducing conditions in mice will better reflect the human disease. However, testing new therapeutic treatments doesn't require these conditions especially if the duration of the study is relatively short. Mouse models used in HCC can be categorised in four different categories; genetically engineered mice (GEM), mice with HCC induced with genotoxic drugs, mice with HCC induced by implementation methods and Diet induced HCC.

1.5.1. Genetically engineered mice (GEM)

As mutations in certain oncogenes and tumour suppressor genes are actively responsible for the development of human HCC, mice with CRISPR/CAS9-induced mutations are commonly used in cancer research. This approach is applied if the research group is interested in the effect of a certain mutation(s) rather than looking at other aspects like tumour stroma interaction or the role of the tumour microenvironment. Mice with activation mutations in the oncogene *cmyc* alone are commonly used in HCC studies[308], as are mice with *cmyc* mutations in combination with *β-catenin*[309] or *E2F1* overexpression mutations[310]. Combination of more than one mutation decreases the latency period for tumour development[311]. Specific deletion of *p53* was sufficient to induce experimental HCC after 56 weeks[312], while deletion of both *p53* and *pten* from mice hepatocytes successfully developed visible HCC after 4 month from this manipulation[313]. Other techniques to induce targeted mutations in hepatocytes include the hydrodynamic injection of plasmids in mouse tail vein, which induces the permeability of the hepatocytes to the plasmids with high transgene expression[311]. One emerging technique used to produce GEM is the Cre-Lox recombination system. Originally developed to manipulate mammalian cell lines genes[314], the Cre-Lox system is now widely used to target certain genes in cell-specific manner[315]. This is of particular importance if targeting a specific gene globally is lethal. The Cre-recombinase enzyme targets LoxP flanked specific chromosomal DNA sequences to control gene expression[316]. Cre recombinase binds 13bp from the beginning and the end of the LoxP site forming a dimer that binds to another LoxP site forming a tetramer. The Cre-recombinase enzyme cuts at the LoxP sites, which are then joined together with a DNA ligase, leading to either gene inversion (in case of two LoxP-flanked sequences in the same chromosomal arm) or gene deletion (in case of repeat LoxP-flanked sequences). Gene knock-in (KI) can be achieved by adding floxed cassette sequences that compete with the LoxP floxed-cut sequences[316].

1.5.2 HCC-inducing genotoxic chemicals

This is probably the most common way of inducing HCC in genetically wild-type mice, thus avoiding the use of GEM that have higher costs. The idea behind using the genotoxic chemicals is to induce changes in the DNA that eventually lead to more damage, chromosomal aberrations and HCC[317]. Factors affecting the development of HCC using this approach are the age and sex of the animal as well as the type of carcinogen used. Diethyl nitrosamine (DEN) is a DNA alkylating agent that increases the level of free radicals and oxidative stress in the liver microenvironment leading to HCC[318]. In younger mice (less than 2 weeks old), DEN IP injection can alone induce liver carcinogenesis, while in older mice, a second hit of either liver enzyme accelerators like phenobarbital or a HCC-inducing diet for tumours to form[319]. Other less commonly used liver carcinogens include the RAS mutation inducer 9,10-dimethyl-1,2-benzanthracene (DMBA)[320].

1.5.3 HCC-inducing implanted pro-malignant or malignant hepatocytes or progenitor cells

The idea behind this technique is to implant tumour cell lines from human or mouse origin into immunocompromised mice to study the impact of new therapeutic targets on the growth or the metastasis of the implanted tumour[321]. In orthotopic models, tumour cells are implanted directly into the liver of the mice to see the interaction of liver stroma to the newly existing tumour, while heterotopic models inject tumour cells subcutaneously in mice and monitor the development of the tumour[216]. The mice used have a compromised innate immune system to eliminate the possibility of tumour rejection by the immune system, and NOD-SCID mice[322] and CD1 deficient nude mice are more likely to be used due to lack of T and B cells. To knock out the effect of natural killer cells (NK) cells together with other immune cell subsets, the NOD/SCID-*IL2g*$^{-/-}$ is now frequently used in cancer research[323].

1.5.4 Diet-induced NAFLD/NASH and NASH/HCC

Many attempts have been made to develop a murine model that recapitulates the human NAFLD and NASH-driven HCC. As the human disease includes symptoms of the metabolic syndrome - including hyperglycaemia, hyperlipidaemia, obesity, insulin resistance - together with liver inflammation, a physiologically relevant model should also ideally have these deregulated features. Models of liver inflammation includes the major urinary protein (MUP)-urokinase-type plasminogen activator (*uPA*) transgenic mice, that develop severe inflammation, ballooned hepatocytes and HCC with age[324]. Upregulation of uPA induces the production of ROS as a result of the elevation of oxidative stress; a mechanism driven mainly by the activation of the NF-κB pathway. The *mdr*$^{-/-}$ model is also a classical model of

inflammation-induced HCC where phospholipids are trapped in the hepatocytes leading to cholastatic inflammation, portal hypertension and bile duct dysplasia with subsequent malignancy[325]. Upregulation of *tnfα* in the ductular epithelia and in some inflammatory cells associate with translocation of the RelA (p65) subunit of the NF-κB from the hepatocytes cytoplasm into the nucleus, leading to activation of the whole survival and oncogenic pathway[120].

Diet-induced NAFLD and NASH models typically use diets with high levels of fats and trans-fats with/without sugar intake in drinking water, or diets deficient in one or more important amino acids. Animal model studies generally use the C57BL6 wild type mouse strain. In the methionine-deficient and choline-deficient (MCD) diet, mice liver develops severe hepatic inflammation with infiltration of different subset of immune cells into the liver leading to severe fibrosis and steatohepatitis at 8 weeks from diet intake[326]. The MCD diet-challenged mice, however, don't develop any signs of insulin resistance or obesity within the time course of the study. In fact they have signficant weight loss (>40%)[326]. The other frequently used dietary model is the high fat diet (HFD) that succeeds in producing features of metabolic syndrome - like obesity, severe steatosis, impaired glucose tolerance and insulin resistance[327]. Of note, the degree of liver injury is less than observed in the MCD diet model and the development of HCC using the high fat diet alone or with sugar water in C57BL/6 mice is questioned[328]. On the other hand, in the HFD-fed B6/129 isogenic mouse model (by crossing the C57BL/6 with the 129S1/SvImJ mice), mice do develop insulin resistance with some histological features of steatohepatitis, including hepatocellular ballooning and Mallory-Denk bodies. These features can be accompanied by the development of predysplastic regenerative nodules which progress to HCC after a year from the diet-intake[329].

In 2008, *Tetri et al.*[330] fed C57BL/6 mice with a diet that resembles the fat composition in the fast food market. They called this diet the American life style (ALIOS) diet and it included partially saturated vegetable oil (this fat is composed of a mixture of saturated, mono and polyunsaturated fats) with corn syrup in the drinking water. In their experimental settings, the mice developed weight gain, higher plasma triglycerides, higher serum liver enzymes, and steatosis. On the other hand, mice failed to show any fibrotic changes, portal inflammation or any hepatocyte ballooning in the course of the study (16 weeks)[330]. In order to see whether or not the ALIOS diet can induce liver tumourigenesis with time, *Dowman et al*[331] fed C57BL6 x 129 mice with the ALIOS diet and monitored the development of tumours with other

histopatholigical features of NASH at two time points; 6 month and 12 month. ALIOS-fed mice became obese and developed glucose intolerance at 6 month but not at 12 month compared to age-matched controls. ALIOS fed mice had higher triglycerides levels and higher liver enzyme levels at 12 months compared to their controls. Histologically, ALIOS fed mice had more steatosis, fibrosis and higher NAS score compared to the mice on normal chow. These mice did not develop hepatocellular ballooning at any time point. They did, however, develop small tumours (9 lesions in 6 mice out of 10), while in the control mice, no detectable malignant nodules were captured[331].

In summary, the use of a particular type of murine models is subjected to the purpose of the study, with no model being able to reflect all the features of the human disease. Manipulating the existing diets/mice strains to reach a more universal mouse model that recapitulate all the human disease histological, biochemical and transcriptomic spectra may help to understand the biology of this disease and evaluate new therapies.

1.6 Project objectives

1.6.1 Hypothesis:

The overarching *hypotheses* being explored: Host and local factors influence the liver microenvironment, promoting the development and progression of NAFLD-HCC. Non-parenchymal cells in the liver premalignant conditions are “gatekeepers” for expansion of abnormal parenchymal clones preceding the development of HCC. Capture of novel therapeutic targets for HCC management is achieved using unsupervised clustering of murine and human RNA-sequencing transcriptome data. After the establishment of the HCC, the tumour cells establish bidirectional relation with tumour infiltrating stromal cells to maintain their proliferation and therapy resistance.

SULF2 is a key modifier of the tumour microenvironment and candidate therapeutic target. Initial immunohistochemistry studies exploring SULF2 at the protein rather than mRNA level in HCC in the *Reeves* lab suggested expression in tumour cells, but also non-parenchymal cells. Focused on this critical modifier of hepatic HSPGs, the primary goal of this project was to further characterise SULF2, including its cellular origin in non-tumour and tumour liver tissues and its functional impact on the tumour microenvironment.

NAFLD-HCC is an emerging global threat and has been the primary HCC aetiology studied in this thesis. In addition to studies in formalin fixed human tissues, high through-put RNA

sequencing data from tissues generated from an *in vivo* mouse model of a well characterised dietary induced chronic liver disease of NAFLD progressing to HCC (*Reeves, Oakley*) was analysed with bioinformatics tools, alongside publically available HCC transcriptomic data. *In-vitro* work included models to explore cross-talk between hepatic cells. In combination, these studies facilitated the characterisation of the contributions of SULF2 in HCC, but also provided the resource to explore other key elements of the tumour microenvironment in NAFLD-HCC.

1.6.2 Specific Aims

1.6.2.1. To characterise SULF2 within the *in vivo* tumour microenvironment and explore associations with disease stage and patient outcome.

1.6.2.2 To define the functional impact of SULF2 *in vitro*, by developing models to assess the contribution of different cell types expression or secreted isoforms on the phenotypic behavior of HCC cells.

1.6.2.3 To explore the impact of SULF different oncogenic, cell survival and chemoresistance signaling pathways in HCC.

1.6.2.4 To explore the role of SULF2 in the progression of non-alcoholic fatty liver disease (NAFLD) and NAFLD-HCC in a relevant animal model.

1.6.2.5 To explore additional features promoting the development and progression of diet-induced HCC in a biologically relevant model recapitulating human disease.

1.6.2.6 Combine histological data with transcriptomic data to identify SULF2 or novel mechanistic pathways relevant to the development and the progression of NAFLD-HCC.

Chapter 2: Materials and methods

2.1 General Laboratory Practice

Established experiments in the Institute of Cellular Medicine (ICM) and in the Northern Institute for Cancer Research (NICR) followed Newcastle Universities set standards which act in accordance with the Control of Substances hazardous to Health Regulations 2002 (COSHH) and Biological COSHH (BioCOSHH).

2.2 Patients

Human HCC biopsies: This study was classified as retrospective case series involving those with sufficient residual tissue for research purposes. The initial pilot study and subsequent larger series of cases were approved by and the Newcastle upon Tyne NHS Foundation Trust Research and Development department and the Newcastle and North Tyneside Local Research Ethics Committee (REC)(Reference 2004/012) and (Reference 04/Q0905/168 and 10/H0906/41) respectively. Anonymised code-linked datasets were adopted to maintain patients' confidentiality and proper data protection. Preliminary investigation of SULF2 tissue protein expression was performed in formalin fixed paraffin embedded tissues (FFPE) from HCC diagnostic biopsies collected in the period between 2000 and 2002 of 6 patients. The study was then expanded to include 54 more biopsies in the period between 2003 and 2010 from patients who consented to the availability of their tissues for research use. Exclusion criteria included patients with histologically-proven benign tissue or patients with other types of liver cancer i.e. cholangiocarcinoma. Patient information was collected from the histopathology reports together with patient's records and radiology data. This data included etiology of the underlying liver disease, age, gender, BMI, presence of T2DM, presence of cirrhosis, tumour size (in cm), tumour number, tumour grade, presence of portal vein thrombosis (PVT), Edmondson-Steiner tumour grade[55], tumour node metastasis (TNM) stage, Albumin level (g/l), Bilirubin level (µmol/l), AFP, presence of Ascites, Child-pugh score, combined Barcelona Clinic for Liver Cancer (BCLC) stages[332], patients survival from the time of biopsy and the administered treatments (orthotopic liver transplantation (OLTx), resection, ablation, trans-arterial chemoembolization (TACE), medication and best supportive care (PSC))

Human HCC biopsies from sorafenib treated patients: Biopsies from small cohort of HCC patients who received sorafenib treatment were also stained for SULF2. Biopsies were collected from patients at the time of diagnosis before the start of the treatment. In this cohort, patients

were classified as sorafenib responders, who had a stable disease on imaging for at least 6 months, or sorafenib non-responders where treatment was discontinued due to poor tolerance or if the disease progressed within three months.

2.3 Immunohistochemistry

2.3.1 For the SULF2 study:

In order to investigate the SULF2 and SULF2-regulated proteins in FFPE diagnostic biopsy tissue sections containing both HCC and non-neoplastic liver parenchyma, IHC was performed for SULF2, α-smooth muscle actin (αSMA), GPC3, β-Catenin, RelA-P-ser536 and CD44. Slides were scanned and assessed digitally with Aperio Imagescope Software. All cases were stained for SULF2 and GPC3, while representative cases were stained for αSMA and β-Catenin. 21 cases previously stained and scored for SULF2 were then stained for RelA-P-ser536 and CD44. Details of the antibodies are listed in **Table 2.1**

Staining	Catalogue number	Producer	Clonality/ host species	Antigen retrieval (IHC)	Experiment
SULF2	MCA5692GA	AbD Serotec	Mouse mAb	Triology system Cell Marque,UK	1:200
αSMA	ab7817	Abcam	Mouse mAb	The pressure cooker 'decloaking'	1:200
GPC3	sc-65443	Santa Cruz	Mouse mAb	The pressure cooker 'decloaking'	1:200
β-catenin	610514	BD Transduction Labs	Mouse mAb	The pressure cooker 'decloaking'	1:400
RelA-P-Ser536	ab86299	Abcam	Rabbit pAb	Tris buffer (pH 9)	1:200
Pan CD44	ab157107	Abcam	Rabbit pAb	Citrate buffer (pH6)	1:1000
CD68	OABB00472	Aviva systems biology	Rabbit pAb	Citrate buffer (pH6)	1:200
F4/80	Ab6640	Abcam	Rat mAb	20ug/ml Proteinase-K	1:100

Table 2.1 list of antibodies used in IHC

2.3.1.1 Human SULF2 staining

SULF2 IHC staining was performed using an automated Ventana processor (Roche). Slides were deparaffinised using series of Xylene (Fisher Chemicals Code: X/0200/17 Lot: 1556167) and then rehydrated through descending concentrations of alcohol (Alcohol (C_2H_6O): Ethanol Absolute from Fisher Chemicals Code: E/0650DF/17). Slides were exposed to cell conditioning and antigen retrieval (programme 245) followed by 1:50 SULF2 1^{ry} antibody treatment. Tissues

were then incubated with Multimer (AKA Secondary) 2nd antibody (discovery OmniMap anti-Ms HRP cat 4310) for 16 minutes and SULF2 positive brown colour was developed by treating slides with DAB (cat 4304). Slides were counterstained with standard Heamatoxylin II (cat 790-2208) for 8 minutes followed by Blueing reagent (cat 760-2037) for 4 minutes. Slides were then removed, washed with Tris-buffered saline- tween 20 (TBS-T) for 5 minutes and then dehydrated in ascending concentrations of alcohol for 30 seconds each and 2X 4 minutes in Xylene. Finally, slides were mounted using DPX mounting media (Sigma-Aldrich Code: 06522-500mL Lot: BCBH4393V).

2.3.1.2 Human RelA-P-ser536 staining

RelA-p-Ser536 staining was manually performed using an overnight protocol. On the first day, slides were deparaffinised and rehydrated by passing them through Xylene and descending serial concentrations of ethanol (100, 70 and 50 %) for 5 minutes each. Tissue endogenous peroxidase was blocked by incubating slides with 3% H_2O_2 in methanol for 15 minutes. Slides were then rinsed in phosphate-buffered saline (PBS) before proceeding into the antigen retrieval protocol.

High pH antigen retrieval protocol (Tris-EDTA antigen unmasking solution, pH9, vectors lab, catalogue H-3301) was applied in the RelA-P-Ser536 IHC. Slides were microwaved in the retrieval buffer at power 80 for 20 minutes. After cooling down with water, slides were permealised with 0.25% triton-x100/PBS for 10 minutes and then mounted into a sequenza for further processing. Slides were then blocked with an avidin/biotin blocking kit (catalogue SP-2001, Vector laboratories) for 15 minutes each separated by three washes with PBS for 5 minutes. Slides were blocked with 20% goat serum (45 minutes) prior to incubation with the primary antibody diluted in 5% of goat serum at 4°C. On the next day, slides were warmed up and then incubated with 2 drops of anti-rabbit Envasion+ system HRP labelled polymer (DAKO, catalogue K4003) for 30 minutes. Slides were washed 3 times with PBS before incubating with 100 µl DAB mix (reference number SK 4100, Vector labs) for a maximum of 12 minutes. Slides were counterstained with Haematoxylin for 2.5 minutes followed by Scotts water for 1 minute before dehydrating, clearing and mounting with DPX mounting media.

2.3.1.3 Human CD44 staining

CD44 staining was manually performed in a one-day protocol. Slides were deparaffinised and rehydrated by passing them through Xylene and descending serial concentrations of ethanol (100, 70 and 50 %) for 5 minutes each. Tissue endogenous peroxidase was blocked by

incubating slides with 3% H_2O_2 in methanol for 15 minutes. Slides were then rinsed in phosphate-buffered saline (PBS) before proceeding into the antigen retrieval protocol; low pH antigen retrieval protocol (Citrate antigen unmasking solution, pH6, vectors lab, catalogue H-3300). Slides were microwaved in the retrieval buffer at power 80 for 20 minutes. After cooling down with water, slides were mounted in sequenza vertical slides racks for further processing. Tissues were then blocked with avidin/biotin blocking kit (catalogue SP-2001, Vector laboratories) for 15 minutes each separated by three washes with PBS for 5 minutes. Slides were blocked with 20% goat serum prior to incubation with the primary antibody diluted in 10% goat serum for 2 hours. Slides were washed with 5X PBS and then incubated with 2 drops of anti-rabbit Envasion+ system HRP labelled polymer (DAKO, catalogue K4003) for 30 minutes. Slides were then washed 3 times with PBS before incubating with 100 µl DAB mix (reference number SK 4100, Vector labs) for a maximum of 12 minutes. Slides were counterstained with Haematoxylin for 2.30 minutes followed by Scotts water for 1 minute before dehydrating, clearing and mounting with DPX mounting media.

2.3.1.4 Scoring system for the applied stains

For SULF2: Two pathologists blinded to patient outcome assessed SULF2 and GPC3 immunostained slides. SULF2 in tumour cells was graded as absent or present, where present included 5% or more of tumour cells with positive cytoplasmic immunostaining. SULF2 in CAFs was graded as absent or present, where 'absent' included cases with either no or scant SULF2 and 'present' included cases with intense focally positive or diffusely positive SULF2.

For GPC3: GPC3 expression in tumour cells was scored from (0-3), corresponding to negative, focal or dot like cytoplasmic positivity, more diffuse cytoplasmic positivity, and intense cytoplasmic or membranous positivity.

For RelA-P-ser536: RelA-P-ser536 expression in the tumour cell nuclei was scored as 0 (negative), 1 (scattered positive nuclei), 2 (more than 50% positive nuclei) or 3 (more than 90% positive nuclei).

For CD44: CD44 expression in the tumour cells was scored from (0-3), corresponding to negative, scant cytoplasmic or membranous tumour cell positivity, moderate cytoplasmic or membranous positivity and strong membranous positivity.

2.3.2 For the C3H/He mouse model study:

As a validation to the RNA-sequencing data, a group of markers was chosen for IHC, which included CD44, CD68 and F4/80. The details of the antibodies are listed in **Table 2.1**

2.3.2.1 Mouse CD44 staining

The same human staining protocol was applied to the mouse CD44 staining.

2.3.2.2 Mouse CD68 staining

The one-day CD68 staining was manually performed as previously described for CD44 until the blocking step. Slides were blocked with 20% pig serum for 45 minutes prior to incubation with the primary antibody diluted in the blocking solution for 1.5 hours. Slides were washed with 5X PBS and then incubated for 60 minutes with 1:200 of biotinylated swine anti-rabbit antibody (Dako, catalogue E0353) diluted in PBS. After washing with PBS, the vector avidin biotin complex (ABC) was added to each slide (Vector labs, catalogue PK 7100), and incubated for 30 minutes. DAB and further processing was performed as previously described in the human and mouse CD44 staining.

2.3.2.3 Mouse F4/80 staining

F4/80 staining was performed using a one-day protocol, and after deparaffinisation and blocking of endogenous peroxidases, slides were then rinsed in phosphate-buffered saline (PBS). Antigen retrieval was performed using 20 µg/ml proteinase K in pre-warmed PBS for 20 minutes at 37°C. Slides were mounted into sequenza vertical slides racks for further processing. Tissues were then blocked with avidin/biotin blocking kit (catalogue SP-2001, Vector laboratories) for 15 minutes each separated by three washes with PBS for 5 minutes. Slides were blocked with 20% goat serum for 45 minutes prior to incubation with the primary antibody diluted in the blocking solution for 1.5 hours. Slides were washed with 5X PBS and then incubated for 60 minutes with 1:200 of biotinylated goat anti-rat antibody (star 131B, Biorad) diluted in PBS. After washing with PBS, the vector avidin biotin complex (ABC) was added to each slide (Vector labs, catalogue PK 7100), and incubated for 30 minutes. DAB and further processing was like what was described in the human and mouse CD68 staining.

2.3.2.4 Scoring procedure for the applied stains

As the three stains applied to the mouse tissue exclusively stained macrophages, the scoring system for these markers depended on counting the number of positive macrophages in matched 10 high-power fields (HPF) and the mean number of positive macrophages/10 HPFs was representative to number of positive macrophages in each case.

2.4 Cell culture

A combination of different cell lines was used to assess SULF2 function *in vitro*. Two HCC cell lines with different SULF2 expression levels were used including SULF2-null HCC cell line; Hep3B cells and the SULF2-expressing Huh7 cells. Both cell lines were from the NICR cell line bank and were exported originally from the American Tissue Culture Collection (ATCC).Huh7 is an adherent, malignant epithelial cell line previously isolated from 57-year old Japanese patient in the eighties of the last century, while Hep3B is another malignant hepatocyte cell line that was isolated from HCC male patient. Both cell lines are widely used to study different HCC oncogenic pathways alongside with testing the effect of new therapeutic targets against liver malignancy. LX-2 myofibroblast cell line[333] was a kind gift from Professor Scott Friedman, Mount Sinai University. LX2 cells represent a model of hepatic activated myofibroblasts and are accepted as a tool in preclinical studies for new therapeutic targets. LX2 cells provide a valuable source of information in cell-cell cross talk with other cell types in the diseased liver environment.

2.4.1 Culture conditions

Cells were incubated in Panasonic incubator in 5% CO_2 at 37°C degrees in 95% humidified conditions. All cell-based experiments were performed under sterile conditions in a class II laminar flow BioMAT2 hood (Medair Technologies, USA). Cell lines were cultured in Dulbecco's modified Eagle's medium (DMEM) media with high glucose concentration (Biosera, UK). Other supplements to the media included 10% heat deactivated foetal bovine serum (FBS) (Sigma), 1% penicillin/streptomycin (100 unit/ml penicillin and 100 µg/ml streptomycin; sigma) and 2 mM L-glutamine (Sigma).

2.4.2 Cell line sub-culturing

When cells reached 60-70% confluency, the media was aspirated and cells were washed with 5 ml of sterile PBS. 2 ml of ready-to-use trypsin (sigma) was then incubated with cells at 37°C for 5 minutes for the purpose of cell detachment. 4 ml of complete media was added to deactivate trypsin and cell pellet was collected by centrifugation at 1000 r.p.m for 4 minutes at room temperature (RT). Cells were cultured in T75 flasks in fresh media for future use, or they were counted for further experiments.

2.4.3. Mouse hepatocyte isolation

Hepatocytes were isolated from C57BL/6 mice livers using a two-step perfusion method. Mice were culled by an overdose of Ketamine and Xylazine anaesthesia. After opening the abdomen, the inferior vena cava was cannulated and the superior vena cava was clamped.

Liver retro-perfusion was performed using 50ml of Krebs-ringer bicarbonate buffer (Sigma) with EDTA followed by 50ml of Krebs-ringer bicarbonate buffer with calcium chloride and 1mg/ml Collagenase, and the portal vein was the outlet for the perfusing solutions. Hepatocytes from the perfused liver were isolated in Krebs-Ringer buffer and were filtered through 70µm cell strainers. Hepatocytes were then centrifuged (50xg for 3minutes) and washed with Krebs-Ringer buffer. At the end of the procedure, the pellet was resuspended in 10% Williams medium E (Gibco) containing 10%FBS, 2mM L-glutamine, 100 u/ml penicillin and 100 µg/ml streptomycin and plated in rat tail collagen-coated plates. 4 hours later, dead floating cells with the old media were replaced by fresh complete Williams E medium.

2.4.4 Isolation of mouse bone marrow-derived macrophages

After sacrificing the mice, the femur and tibia are excised and kept in HBSS-. Bone marrow was then flushed out using 5ml HBSS- and a 23 gauge needle under laminar flow hood. Cell suspension was then disaggregated using 18 gauge needle, and cells were transferred into 50 ml falcon tube where they were centrifuged at 400xg for 5 minutes. Pellet was resuspended in Ammonium Chloride-Potassium (ACK) lysis buffer for 1 minute, and then 1x PBS was added to restore osmolarity. Cell suspension was layered onto a 62.5% percoll density gradient, and the mixture was centrifuged at 1000 xg for 30 minutes. Cells in the gradient interface; the immature mono-nuclear cells, were collected and washed twice with 1X PBS before resuspension in RPMI media containing 10% FCS, 1 mM pyruvate-glutamine, penicillin-steptomycin and 10ng/ml M-CSF. Immature monocytes were kept for 7 days at 37°C with 5%CO_2 to mature into macrophages.

2.4.5 Macrophage polarisation

Polarisation of BMDM into M1 and M2 macrophage phenotypes was achieved by treating seeded macrophages with either 100ng/ml LPS and 50ng/ml Ifnɣ (for M1 macrophages) or 10 ng/ml of Il4 and Il13 in the media for 24 hours.

To collect M0, M1 and M2 CM, media was aspirated after polarisation and cells were washed with PBS before adding fresh media for 24 hours. The collected media was 10 x concentrated and stored for the desired experiments.

2.4.6 Cell counting

Cell counting was performed automatically by using EVE™ Automatic Cell Counter (Germany). 10 µl of homogenous cell suspension was mixed with 10 µl of trypan blue dye. 10 µl from this mix was pipetted into the Eve counting slide to be inserted in the automatic cell counter.

2.4.7 Freezing cells

Cells to be frozen were cultured in T75 flask to reach 60-70% confluency. After trypsinisation and cell centrifugation, the resulting pellet was re-suspended in 1 ml of cell freezing media (0.8 ml of culture media+0.1 ml FBS+0.1 ml DMSO (Sigma)). Cells were then transferred to cryo-vials and loaded into cryo-chamber filled with isopropyl alcohol (Nalgene) to achieve -1°C/min rate of cooling for overnight. Cryo-vials were then transferred into liquid nitrogen for long-term storage.

2.4.8 Collection and concentration of cell conditioned media

1 x 10^6 of LX-2 cells were cultured in 10 mls of media in a 10 cm dishes for 48 hours. Cell-conditioned media (CM) were then collected and centrifuge at 1600 r.p.m for 5 minutes to pellet any cell debris. CM was enriched by 10-fold by using the Amicon Ultra 15 (3000 NMWL) centrifugal filters (Merk Millipore, UK, catalogue UFC900324). Media was centrifuged in these concentration tubes at 2600 g for 45 minutes at 4°C, and the concentrated CM was sterile filtered before storage at -80°C for further experiments.

2.4.9 Sorafenib, inhibitors and other reagents

Sorafenib was purchased from Cell signalling technologies (catalogue number 8705). SP600125 (JUN N-Terminal Kinase (JNK) inhibitor, catalogue number 1496), (5Z)-7-Oxozeaenol (transforming growth factor-β-activated kinase 1 (TAK1) inhibitor, catalogue number 3604) and FR 180204 (Selective Extracellular Signal-Regulated Kinase1/2 (ERK1/2) inhibitor, catalogue number 3706) pathway inhibitors were purchased from Tocris. IKK-2 Inhibitor IV (Inhibitor Of Nuclear Factor Kappa B Kinase Subunit Beta, catalogue number 401483) was purchased from Calbiochem. Wnt-3a was purchased from R&D systems.

2.4.10 Stable SULF2 Knockdown

LX-2 cells were transduced with mission TRC2 shRNA lentiviral particles targeting SULF2 (TRCN0000364518, Sigma-Aldrich, USA) or TRC2-pLKO-puro non-targeting (NT) with hexadimethrine bromide (shRNA sequences in **Table 2.2**). Cells were selected using puromycin. Successful SULF2 knockdown was confirmed by both real-time PCR and western blotting.

Target	Sequence
SULF2 shRNA	CCGGGGGCGAAAGTCATTGGAATTTCTCGAGAAATTCCAATGACTTTCGCCCTTTTTG
NT shRNA	CCGGCAACAAGATGAAGAGCACCAACTCGAGTTGGTGCTCTTCATCTTGTTGTTTTT

Table 2.2 shRNA sequences of mission TRC2 SULF2 and non-targeting shRNA lentiviral particles.

2.4.11 2D Trans-well assay

Cancer cells were co-cultured with stromal cells with different SULF2 expression levels in order to see the impact of stromal SULF2 on the behaviour of the tumour cells as previously described in similar conditions[334-336]. Huh7 and Hep3B cells were incubated in 12- and 24-well plates in different cell densities i.e. 10000, 20000 and 50000 cells/well, while control or SULF2 KD LX-2 cells were cultured in ThinCerts™-TC inserts, pore size 3.0 µm (Greiner bio-one, Switzerland, catalogue 662631) in 1:1 ratio on top of the tumour cells. 24, 48 and 72 hours later, the impact of the stromal SULF2 on the growth and viability of the tumour cells –after removal of the trans-wells with the cultured stromal cells- was assessed with MTT viability assay and BrdU cell proliferation ELISA assay as mentioned below.

2.4.11.1 MTT viability/metabolic activity assay

The principle of the MTT colorimetric assay is the mitochondrial reduction of the 3-(4,5-dimethythiazol2-yl)-2,5-diphenyl tetrazolium bromide (MTT) by the mitochondrial enzyme succinate dehydrogenase. Such reaction only takes place in viable and metabolically active cells where the MTT dye penetrates the cell membrane until reaching the mitochondria where it is reduced by succinate dehydrogenase to give a purple insoluble formazan product. The resulting product is solubilised with 1-propanol and the intensity of the purple colour (which reflects the metabolic activity of the parent cells) is measured using a spectrophotometer.

At the desired time point, trans-wells including the incubated stromal cells were discarded, and the media was replaced by 500µl of 5mg thiazoyl blue tetrazolium bromide (Sigma-Aldrich, USA, catalogue M2128) /ml complete media. The dye was then incubated with cells for 3 hours at 37°C, and then media was aspirated and the plate was allowed to dry at RT for 5 minutes. The insoluble formazan crystals were dissolved using 1-propanol with shaking for 5 minutes on an orbital shaker. The resulting solution was then transferred into 96-well plate and colour intensity was analysed using plate reader at 570 and 620 nm.

2.4.11.2 Cell proliferation ELISA, BrdU assay

The assay principle for this assay relies on the use of 5-bromo-2'-deoxyuridine or Bromodeoxyuridine, a synthetic thymidine analogue which replaces thymidine during the DNA synthesis of the replicating cells and hence can be used as a marker for cell

proliferation[337]. The ELISA kit (Roche, Germany, catalouge 11647229001) involves BrdU labelling agent together with anti-BrdU antibody that recognises the BrdU-labelled DNA.

Tumour cells were treated with 10µM BrdU labelling agent 20 hours before the desired end point to allow the incorporation of BrdU into the newly synthesised DNA of dividing cells. Labelling media was removed and cells were fixed for 30 minutes at RT. Anti-BrdU antibodies were then incubated with the cells for 90 minutes with subsequent washing with PBS for 5 minutes at the end of the incubation period. The intensity of the green colour developed after adding the substrate solution to the plate was stopped by using H_2SO_4 stop solution and was measured at 450 nm.

2.4.12 Tumour cell migration assay

The ability of the stromal SULF2 to regulate the migration of the tumour cells was tested using the cell migration inserts (Ibidi, Germany, catalogue 80209). 30000 tumour cells/70 µl media were cultured overnight on both sides of the migration inserts to allow for cell attachment. The migration insert was removed and media was replaced with CM from control LX-2 or SULF2 KD LX-2 cells in 1:1 ratio with complete media. Pictures of the migration front were taken 24 hours after incubation with the stromal CM using a Zeiss inverted microscope. Pictures were captured at 50x magnification and gap closure was assessed by measuring the gap distance at each time point using ImageJ software.

2.4.13 Tumour cell invasion assay

Tumour cell invasion assay depends on the ability of the tumour cells to invade through the ECM proteins from the Engelbreth Holm-Swarm (EHS) mouse tumour[338] forming an artificial basement membrane that is dried over the wall of 8 µM pore size polycarbonate inserts.

After rehydrating the interior of the Boyden chambers with serum-free (SF) media at RT for 2 hours, tumour cells (300,000 cells per chamber) were suspended in 300µl SF media and were pipetted inside the invasion chamber. The chamber was then inserted in 24-well plate including different densities from overnight-attached control or SULF2-KD LX-2 cells as a living source of SULF2. 72 hours later, inserts were carefully removed using sterilised forceps and the un-invading cells together with the ECM matrix gel were carefully, but thoroughly, removed from the interior of the chamber inserts using a cotton swab to reduce the background. Inserts were then transferred to new 24-well plate containing 500 µl of the staining solution to stain for the invading cells on the outer surface of the polycarbonate

membrane for 20 minutes. Chambers were then washed with water and the dye was dissolved using 10% aceitic acid and the developed colour was measured at 560 nm on a plate reader.

2.4.14 3D spheroid hanging droplets

3D spheroid models provide more *in vivo*-like conditions, which reflect the complexity of the tumour microenvironment in terms of drug penetration and absorption as well as the growth of cells in a multi-layer, rather than a monolayer[339, 340]. The rationale of doing this experiment in the SULF2 context was to investigate the effect of stromal SULF2 on tumour cell proliferation shown by the degree of spheroids growth, and for this reason two procedures were adopted; mixed fibroblast-tumour cell spheroids and single tumour spheroids.

The optimum number of cells forming a single, rounded sphere was investigated by culturing different cell densities (12000, 6000, 3000, 1500, 1000, 750, 500, 250, 125 and 62 cells) in 20µl of media on the interior surface of a 10 cm^3 lid that was then inverted to allow the media including the cell suspension to hang over humid environment by adding 10 ml of sterile PBS to the bottom of the dish. Droplets were left for 3 or 4 days to reach the best time upon which spheroids were formed.

Mixed cell-type spheroids; Huh7 or Hep3B cells combined in a 1:1 ratio with control or SULF2 KD LX-2 cells in 20µl media per sphere on a 10cm^3 dish lid (n=10 per group). The total number of cells mixed to form a single sphere was 3000 cells. Pictures were taken at 50X magnification using a Zeiss inverted microscope from day 3 after mixing single cells until day 8 of culture.

Tumour cells' spheroids; Huh7 or Hep3B cells were suspended in hanging droplets to form spheres. The total number of cells mixed to form a single sphere was 3000 cells. Spheroids were transferred into the stromal CM at either 3 days (Hep3B spheroids) or 4 days (Huh7 spheroids) after the date of hanging the droplets. Pictures were taken at 50X magnification using Zeiss fluorescent microscope from day 3 or 4 after mixing single cells until the seventh day.

Calculation of the spheroids volume: the spheroids' growth was calculated as follows:

- Spheroids were numbered from 1-10 so that images from matched spheroids could be captured daily.
- Pictures of the growing spheroids were analysed using the imageJ image analysis software.

- Software sittings were changed to allow using the freehand selection to the analysed object; spheroid.
- The analysis option in the software toolbar was chosen to set the analysis measurement for the “area” option. This gave the area of the selected object on pixel count.
- The volume of each sphere was calculated using the invented formula:

$$V_{mm3} = 0.09403 \times ((A_{pixel} \times 0.28)/1000)^{1.5}$$

- The output from this experiment was the change of the matched-spheroid volume from the first day of image capture. This was to allow for exclusion of any variability due to the difference of the initial volume of the spheroids.

2.5 RNA Extraction, Reverse Transcription and Polymerase Chain Reaction

2.5.1 RNA extraction

Total Ribonucleic acids (RNA) was extracted from cell lines seeded in 300,000 cell/well in 6-well plate at the desired time point and after specific treatment. Media was aspirated, and cells were washed with ice –cooled PBS. Isolation of RNA was performed using the Qiagen RNeasy Mini kit according to the manufacturer’s protocol. The concentration of the isolated RNA was detected using Nanodrop 2000 machine and software (thermos-scientific) and the samples were kept undiluted at -80°C for further experiments.

2.5.2 Reverse transcription

1µg RNA was used to make complementary DNA (cDNA) using the Promega reverse transcription (RT) protocol. The required RNA concentration was added to a total volume of 8µl using RNase-free water (Qiagen) and the mixture was treated with 1µl RNase-free DNase enzyme with 1µl of 10x RQ1 DNase reaction buffer to eliminate any contamination from genomic DNA (gDNA). The reaction was kept at 37°C for 30 minutes in GeneAmp PCR system 2700 thermal cycler (Applied Biosystems). 1 µl of RQ1 DNase stop solution was then added for 5 minutes to stop the action of the DNase enzyme. Next, 0.5µl random hexamers were annealed to the RNA at 70°C for 5 minutes before proceeding into the RT step. To reach a RT reaction volume of 20µl, 8.5 µl of RT working solution was added to every sample. The RT working solution contained (per sample): 1µl M-MLV RT enzyme, 4µl of 5x M-MLV RT buffer, 1 µl 10 mM dNTP, 0.5µl of RNasin ribonuclease inhibitor and 2µl of RNase free water. Mixture was pipetted and incubated on the thermocycler for 1 hour at 42°C to allow the RT reaction to take place. Samples were kept at -80°C for future experiment.

2.5.3 Quantitative polymerase chain reaction (qPCR)

The resulting cDNA (50ng/µl) was diluted 1:5 to 10ng/µl with Nuclease-free water and then 2µl of the diluted cDNA (20ng/µl) was used for the gene expression protocols. 6.5µl of 2x SYBR® Green JumpStart™ Taq ReadyMix (Sigma, catalogue S4438) was mixed with 3.5µl of nuclease-free water and with 1µl of both forward and reverse primers (at 10 µM concentration) designed for genes of interest. A total reaction volume of 13µl was loaded onto 96-well plate (MicroAmp optical plate, Applied Biosystems) and the qPCR reaction was performed using the 7900HT Fast Real-Time PCR System (Applied Biosystems) equipped with the SDS 2.3 software. The standard program was used (50°C for 2 min, 95°C for 10 min followed by 40 cycles of 95°C for 15 sec and 60°C for 1 min).

2.5.4 Primer design

List of all the designed primers is in **Table 2.3** All primers used for this study were self-designed using three online bioinformatics software: primer 3 version 1.4 software, PubMed nucleotide blast tool software and Primer bank website. Nucleotide sequence of the target genes was obtained from PubMed website using Nucleotide search engine. The sequence of the designed primers was checked against whole genome using the BLAST option on the PubMed website to ensure good alignment and high specificity towards the target gene. Primers were ordered from sigma website in dry format, reconstituted in DEPC water to 10µM. Both the

Gene	Forward primer 5'-3'	Reverse primer 5'-3'
SULF2	ATGAGTTTGACATCAGGGTCCCGT	ATGGATTTCCCGTCCATATCCGCA
PDGFRβ	AGACACGGGAGAATACTTTTGC	AGTTCCTCGGCATCATTAGGG
αSMA	GAAGATCAAGATCATCGCCC	CTCGTCGTACTCCTGCT
Col1a1	GTGCGATGACGTGATCTGTGA	CGGTGGTTTCTTGGTCGGT
VIM	TGCAGGAGGCAGAAGAATGG	AAGGGCATCCACTTCACAGG
TIMP1	CCTTCTGCAATTCCGACCTC	GTATCCGCAGACACTCTCCA
TNFα	GAGGGCTGATTAGAGAGGTC	ATGAGCACTGAAAGCATGATCC
IL6	CCTGAACCTTCCAAAGATGGC	TTCACCAGGCAAGTCTCCTCA
CD44	TCCAACACCTCCCAGTATGACA	GGCAGGTCTGTGACTGATGTACA
CDH1	AAAGGCCCATTTCCTAAAAACCT	TGCGTTCTCTATCCAGAGGCT
EpCAM	GAACACTGCTGGGGTCAGAA	CTGAAGTGCAGTCCGCAAAC
KRT7	CAGGATGTGGTGGAGGACTT	AGCTCTGTCAACTCCGTCTC
KRT19	TGAGTGACATGCGAAGCCAAT	CTCCCGGTTCAATTCTTCAGTC
AXIN2	TACACTCCTTATTGGGCGATCA	TTGGCTACTCGTAAAGTTTTGGT
LGR5	AGCAAACCTACGTCTGGACA	ACAGAGGAAAGATGGCAGCT
CDH2	AGCAGTGAGCCTGCAGATTT	CTGCCACTTGCCACTTTTCC
PDGFRα	TTTTTGTGACGGTCTTGGAAGT	TGTCTGAGTGTGGTTGTAATAGC
TCF4	ACTGTAGCCTGCATCCACAT	TTTCCCCAGAGCATCTCCAG
CXCR4	CTGGCCTTCATCAGTCTGGA	TCATCTGCCTCACTGACGTT
FZD7	GTGCCAACGGCCTGATGTA	AGGTGAGAACGGTAAAGAGCG
FGFR1	CGCCCCTGTACCTGGAGATCATCA	TTGGTACCACTCTTCATCTT
GADD45β	TACGAGTCGGCCAAGTTGATG	GGATGAGCGTGAAGTGGATTT
MDR1	CACGTGGTTGGAAGCTAACC	GAAGGCCAGAGCATAAGATGC
HPRT	TTGCTTTCCTTGGTCAGGCA	ATCCAACACTTCGTGGGGTC

Table 2.3: list of primers used in the current study

forward and reverse primers were diluted 1:10 in DEPC water for semi-quantitative PCR and qPCR. 1:10 serial dilution from control cDNA (20ng/µl) was prepared to test the efficiency of the designed primers using the standard curve drawn by 7900HT Fast Real-Time PCR System (Applied Biosystems) equipped with the SDS 2.3 software. The slope of the standard curve was used to calculate primer efficiency using the qPCR Efficiency Calculator online software (Thermo-scientific). Primers with a % of efficiency ranging from 90-110% were considered for gene expression analysis. Data analysis of the gene expression experiments adopted the Comparative quantification algorithms-ΔΔCt methods in which the expression of the target gene in an experimental context is compared to the expression results of both a calibrator

(control or untreated sample) and a normaliser (house-keeping gene, HPRT in our case). The resulting ΔΔCt value was used to calculate the fold difference in gene expression.

2.6 Western blotting

2.6.1 Total protein extraction

Protein was extracted from cell lines seeded in 300,000 cell/well in 6-well plate at the desired time point and after specific treatment. Media was aspirated, and cells were washed with ice –cooled PBS prior to adding the Mammalian Protein Extraction Reagent (M-PER) (thermo-scientific, catalogue 78503). 10µl of protease inhibitor cocktail (Roche) and 20µl of Phosphatase Inhibitor Cocktail 2 (sigma, catalogue p5726) were added per 1ml of the protein extraction buffer, and around 70-90µl from this mixture was incubated with cells in 6-well plate for 2 minutes on ice to allow detergents and buffer component to lyse the cells. Cells were then scrapped from the surface of the plate and the whole lysate was transferred into 1.5 ml Eppendorf tubes to be centrifuged at 13,000 r.p.m for 20 minutes at 4°C. the supernatant including all the soluble proteins was collected in new Eppendorf tube for protein quantification.

2.6.2 Protein quantification and preparation

The bicinchoninic acid (BCA) assay procedure was performed to measure the total protein concentration (Pierce BCA Protein Assay Kit, Thermo Scientific). The intensity of the purple colour produced by the reduction of CU^{+2} into CU^{+1}, by the amino acids present in the total proteins, and subsequent detection of the CU^{+1} ion by the BCA, was proportional to the quantity of the total protein present in every tested sample. A serial dilution from the standard bovine serum albumin (BSA) was used to create a standard curve from which the concentration of the sample protein was interpolated. 10µl of sample was mixed with 80µl of the working reagent (50:1 ratio of reagent A and reagent B) and the reaction mix was left for 30 minutes at 37°C. The absorbance was read by the spectrophotometer at 562 nm. The desired concentration of protein (10-20µg) was mixed in a 1:4 ratio with 4x protein loading dye and the mixture was heated up at 95°C in the heat-block for 5 minutes for protein denaturing purposes.

2.6.3 SDS-PAGE electrophoresis

According to the size of the tested protein, the resolving gel was made in 7.5, 10 or 12%, while the stacking gel was always made in 4% using the formula listed in **Table 2.4**

	Resolving gel (ml)			Stacking gel (ml)
	7.5%	**10%**	**12%**	**4%**
MilliQ water	5.5	4.85	4.35	6.4
1.5 M Tris pH 8.8	2.5	2.5	2.5	
0.5 M Tris Ph 6.8				2.5
40%Acrylamide/bis (Biorad, 1610148)	1.9	2.5	3	1
10% SDS	0.1	0.1	0.1	0.1
10% APS	0.05	0.05	0.05	0.05
TEMED (Sigma, T9281)	0.01	0.01	0.01	0.01

Table 2.4 composition of the SDS-PAGE gels

Samples were loaded on the custom made SDS-PAGE gel and the PageRuler Prestained Protein Ladder (thermos-scientific, catalogue 26616) was used as a protein size marker. Samples were run at 90 volts for 2 hours and at the end of the electrophoresis, the gel was prepared for blotting.

2.6.4 Protein transfer

Proteins separated on the SDS-PAGE gel were transferred to Nitrocellulose membrane (HyBond-C Extra, Amersham Biosciences, UK) using the wet-transfer method in tris-glycine buffer (pH 8.3). The gel, the nitrocellulose membrane, two filter pads and two blotting pads were pre-immersed in the transfer gel and the transfer sandwich was set that the negatively charged proteins were transferred from the gel (nearest to the cathode probe) to the membrane (nearest to the anode probe). Protein transfer was run on 100 volts for 1.30 hours. Ponceau s solution (Sigma, catalogue 7170) was used to confirm the correct transfer of the proteins to the blotting membrane.

2.6.5 Membrane blocking and immunoblotting

Membrane was blocked with either 5% skimmed milk or 5% BSA in 1x TBS-T solution (60 g of Tris, 90 g of NaCl and 5 ml of Tween 20 in 1 L of H_2O; pH 7.5) to eliminate any unspecific binding. All the primary antibodies were incubated with the membrane overnight with gentle shaking over orbital centrifuge at 4°C. The following day, the primary antibodies were aspirated and the membrane was washed thoroughly with TBS-T 3x 5 minutes while shacked

to ensure precise removal of the unbound antibody remnants. 1:2000 of the HRP conjugated secondary antibodies were then incubated with the membrane for 1 hours RT on the orbital shaker. List of the antibodies used in WB is in **Table 2.5**

Staining	Catalogue number	Producer	Clonality/ host species	Dilution
SULF2	MCA5692GA	AbD Serotec	Mouse mAb	1:1000
Phosphor-SAPK/JNK (Thr183/Tyr185)	9251	Cell signalling	Rabbit pAb	1:1000
SAPK/JNK (Thr183/Tyr185)	9252	Cell signalling	Rabbit pAb	1:1000
Phospho- NF-Kb p65 (Ser536)(93H1)	3033	Cell signalling	Rabbit mAb	1:1000
NF-Kb p65 (C-20)	sc-372	Santa cruz biotechnology	Rabbit pAb	1:1000
Phospho-stat3 (Tyr705)(D3A7)	9145	Cell signalling	Rabbit pAb	1:1000
Stat3	9132	Cell signalling	Rabbit pAb	1:1000
Phospho-p44/42 MAPK (ERK1/2)(Thr202/Tyr204)	9101	Cell signalling	Rabbit pAb	1:1000
p44/42 MAPK (ERK1/2)	0102	Cell signalling	Rabbit pAb	1:1000
phospho-ERK	4370	Cell signalling	Rabbit mAb	1:2000
ERK1/2	9107	Cell signalling	Mouse mAb	1:2000
phospho-AKT	4060	Cell signalling	Rabbit mAb	1:2000
AKT	4691	Cell signalling	Rabbit mAb	1:2000
GAPDH	ab37168	Abcam	Rabbit pAb	1:2000
β-actin	A-5441	Sigma-Aldrich	Mouse mAb	1:2000
Anti-rabbit IgG, HRP-linked	7074	Cell signalling	Goat	1:2000
Anti-Mouse IgG, HRP-linked	A4416	Sigma-Aldrich	Goat	1:2000

Table 2.5 List of antibodies used in Western blotting

2.6.6 Immunodetection

The membrane was washed 3x 5 minutes after the removal of the 2nd antibodies, and was then incubated with the chemiluminescence substrate Pierce ECL Western Blotting Substrate (Thermo Scientific, catalogue 23106) for 1 minute before developing the bands using x-ray films in the dark room. The film was developed using developing solution (RG X-ray developer, Champion) and fixative (RG X-ray fixer, Champion) in the Mediphot 937 developing system.

2.6.7 Membrane stripping

For the detection of the phosphorylated and total proteins, the phospho-antibodies were applied first to the membrane and after developing the protein bands, the membrane was

stripped for the purpose of re-blotting with the total protein primary antibody. The membrane was washed with TBS-T for 15 minutes at RT and was then incubated with Restore™ Western Blot Stripping Buffer (Thermo-scientific, catalogue 21059) for 20 minutes at RT on orbital shaker. The membrane was then re-washed with TBS-T buffer for another 10 minutes before blocking with the specific blocking agent prior to retreating with total protein primary antibody.

2.7 Immunofluorescence (IF)

Cells stained for GP3 and β-Catenin were seeded in 8-chamber slides at 40,000 – 80,000 cells/ chamber. At the end of the treatment, the media was aspirated and the cells were washed with PBS before fixing them with 6% formalin for 30 minutes at RT. Formalin was removed and cells were further fixed and permablised with acetone for 10 minutes prior to wash with 0.25% PBS-Triton for another 10 minutes. 20% goat serum was used for blocking purposes at RT for 45 minutes and the primary antibody was diluted in PBS (1:75 for GPC3 and 1:100 for β-Catenin) and incubated with cells in the chambers for 45-60 minutes at RT. The primary antibody was then aspirated and cells were washed before incubating them with the fluorescent-labelled secondary antibody for 45-60 minutes in the dark. The secondary antibody was removed and cells were treated after washing with DAPI (4',6-Diamidino-2-Phenylindole, Dihydrochloride)(Thermo scientific, catalogue d1306) in 1:5000 dilution. Cells were finally washed with distilled water and mounted with the glycerol mounting media.

2.8 Animal procedures

6-8 week old male C3H/he mice (Harlan Laboratories, UK) were used in this study and were housed 4 per cage to reduce fighting injuries. A simple procedure to remove preputial glands was routinely performed at 28 weeks, without complications. Mice were fed an American lifestyle diet (ALIOS: 45 % calories from fat, high trans-fat with high sucrose/fructose drinking water, TD.110201, Harlan Laboratories, Wisconsin, USA) or a control diet (15% calories from fat, low trans-fat without sugar, TD.110196, Harlan Laboratories, Wisconsin, USA) *ad libitum*. Culling was at 4 time-points, namely 12 weeks (1 month on diet; n=8 per group), 24 weeks (4 months on diet; n=8 per group); 36 weeks (7 month on diet; n=8 per group) and 48 weeks (10 month on diet; n=24 per group). Additional groups of 12 mice on control diet and 12 on the ALIOS diet received a single intraperitoneal injection of DEN (Sigma, N0258-1G) at 16 weeks.

Upon humane killing, body/liver weight and the macroscopic number and size (using callipers) of tumours were recorded. Liver tissues were dissected to fit in to three groups depending on

further tissue processing: the first set of liver tissues was treated with RNA later solution for RNA long preservation and RNA-sequencing process. Samples were kept in the 4°C overnight to ensure adequate tissue penetration, and for long-term storage samples were stored at -80°C. The second set of tissues was immersed in 10% formalin for fixation and tissue staining purposes. Samples were kept in 10% formaldehyde solution overnight and tissues were exposed to further procedures to keep them in paraffin-embedded blocks. The last part of samples was fresh-frozen in OCT media using liquid nitrogen and was then kept in -80°C for further applications. The *in vivo* experiments were performed according to ethical guidelines under a UK home office licence.

2.9 Tissue studies

Formalin fixed paraffin embedded (FFPE) tissue from tumour and non-tumour liver was sectioned 5 microns thick for histological assessments. An expert liver pathologist, who was blinded to the experimental dietary group assessed the histological features of non-tumour and tumour liver using Haematoxylin and eosin (H&E) and Sirius Red stained slides. The degree of steatosis (0-3) according to the percentage of fat deposition in the liver tissue with zero is <5%, 1= 5-33%, 2= 33-66% and 3 >66%, hepatocellular ballooning (0-2) with zero means no ballooning, 1 is few ballooned hepatocytes and 2 is moderate or marked ballooning, and lobular inflammation (0-2) counting the inflammatory foci/HPF with 0=no foci, 1=1-2 foci, 2=2-4 foci and 3= >4 foci was quantified and the NAFLD activity score calculated[341]. Other features of liver injury and inflammation, including, Mallory-Denk bodies, lipogranulomas, microvesicular steatosis was also documented and the degree of fibrosis (pericellular, portal/periportal, bridging) was assessed using a four-grade scoring system[341]. Histological assessment of the tumours was performed using H&E and reticulin staining[342] and defined as adenomas or HCC grade 1 or 2. Parameters considered included the presence and degree of nuclear atypia, the presence of cytoplasmic hyaline globules and mitotic figures, and the thickness of liver cell plates. Additionally, the presence and extent (percentage of the tumour area) of steatosis, features of degeneration (Mallory-like bodies, ballooning) and inflammation inside the tumours were also assessed.

2.10 RNA sequencing, statistics and data analysis

10-20 mg of non-tumour and tumour tissues were shipped in RNAlater on dry ice to AROS Applied Technology (Denmark), where RNA was extracted and the quality of each sample checked using a Bioanalyser (Agilent). Only samples with at least 400ng of total RNA and a

RNA Integrity Number (RIN) greater than 8.0 were included. RNA sequencing was performed using Illumina's Stranded mRNA kit for library preparation, with 100 bp Paired End Reads, five samples to be sequenced across one lane. RNA expression and sequence analyses were performed with the Newcastle Bioinformatics Support Unit. The mouse genome sequence was obtained from "Ensemble" to construct a reference genome index and reads were mapped to this using Bowtie tool within the R package. Differentially expressed genes were calculated using "DESeq2" tool and data were filtered by adjusted p-value of 0.05 and |Log2FC|in different tissues groups. Data visualisation was performed using Heatmapper software[343].

2.10.1 Unsupervised Hierarchical clustering of the mouse model data

Hierarchical clustering of the mouse non-tumour and tumour RNAseq data was performed to visualise the grouping of individual mice and to see whether this grouping reflects the actual histopathological criteria and the dietary/carcinogen intervention. Because this grouping was not pre-defined with a response variable, this method is considered as un-supervised clustering way of gathering the data. The output of this hierarchical cluster is a tree-like graph showing the observations; called dendrogram. Unsupervised clustering was performed on the R package using the "hclust" function.

In this function, the hierarchical clustering was performed on the transcriptome of 49 mice with every mouse assigned to individual cluster with the algorithm gathering every two most similar mice into an individual cluster until there is only one cluster exists. The distance "dissimilarity" between the individual mice is every time recalculated by the Lance-Williams dissimilarity update formula according to the wards minimum variance method using the "Ward.D2" option[344]. The Euclidean distance is the method that R script uses by default to calculate the distance between the two objectives (mice) based on the formula:

$$d_{euc}(x,y) = \sqrt{\sum_{i=1}^{n}(x_i - y_i)^2}$$

In the non-tumour tissue, a DE gene list was created from the two non-tumour clusters identified by the cluster dendrogram.

2.10.2 Unsupervised k-means clustering of the human TCGA data

In order to correlate the human data with the mouse transcriptomics data, clustering of the human TCGA publically available transcriptomics data without guide from a response variable "unsupervised". Human data was partitioned using K-means clustering that classifies the data into group of k clusters with k representing the number of pre-selected groups. Group of observations "patients" with the lowest dissimilarity (high intra-class similarity) were classified within the same group, and patients with different transcription profiles were separated in different subclasses. This is to determine the major determinants responsible for this grouping.

Unsupervised class discovery by NMF-metagene and K-means clustering was performed on the TCGA LIHC project (374 liver cancer samples + 50 normal tissue samples) testing all combination of 3-12 metagenes and clusters with a bootstrapped resampling method to test for reproducibility. A metagene is a single score that reflects the expression level of several genes. This was followed by projecting the mouse transcriptomics onto the identified clusters to see the overlapping signatures. This was performed by Sirintra Nakjang from Newcastle bioinformatics support unit.

2.10.3 cBioPortal software analysis

cBioPortal is an online available software which includes wide amount of information about genomic data of different types of cancer based on the TCGA database. This can be a useful *in silico* tool to study the prevalence of a certain gene mutation and copy number variant within the TCGA dataset. It also provides a wide group of data concerning the association between genes concerning co-expression versus mutual exclusivity, correlation of genes with survival, networks in which a particular gene is involved and the clinical data of the group of patients expressing this particular gene. The cBioPortal website uses the Spearman and Pearson correlation methods to predict the association between the enquired genes.

In order to confirm the association between SULF2 and other downstream gene, the cBioPortal tool was used by searching for SULF2 with correlated genes using the mRNA expression z-score in the TCGA dataset. The correlation between SULF2 and other candidate genes with spearman's and Pearson's correlation coefficients and p-value were retrieved with the correlation plot from the website.

2.10.4 Ingenuity Pathway Analysis (IPA) software

The IPA (QIAGEN Inc., https://www.qiagenbioinformatics.com/products/ingenuitypathway-analysis) is a powerful tool for mapping and networking of the DE gene list calculated elsewhere to explain the effect of gene expression on different pathways and downstream diseases and functions. The IPA database is constructed from findings manually or automatically curated from top journals forming the ingenuity findings, while the ingenuity-modelled knowledge is an aggregation of the ingenuity expert knowledge and ingenuity supported third party information.

Data uploaded to the IPA software should include gene ID (Observation) with the Log2FC and the adjusted p-value for every gene. Data were uploaded on the IPA on an Excel file format and data was analysed based on pre-selected cut off values. The ideal number of analysed gene in every data set ranges between 200 and 3000. The IPA output shows the pathways involved in this particular analysis, the downstream functions of the changed DE genes, the upstream genes that regulate the change in the gene list and networks enriched from the current analysis.

IPA uses two statistical tools to explain the analysis; the p-value of overlap between the IPA curated list and the current analysis dataset and the activation z-score. P-value is calculated using Right-Tailed Fisher's Exact Test with Benjamin correction for multiple testing in predicting the p-value of the canonical pathways and diseases and biofunction. Activation z-score is used to give a prediction for the direction of change in the particular pathway(s) influenced by the analysed gene set.

Canonical pathways: the first provided piece of information provided by the software gives an idea about the IPA pathways directed by the analysed gene list. The bar chart provides the significance of the gene enrichment in pathways deregulated from this gene list. The colour of the bar chart detects the direction of change in these pathways predicted from the change in individual genes' direction. An absolute z-score of 2 is considered significant in the IPA context.

Upstream regulators: this tool is helpful to identify the transcription factors "or any molecule that affects the expression of another molecule" that regulate the changed gene in the analysed dataset. The upstream analysis is calculated by defining the direction of change in DE genes and mapping them to the already present transcription factors on the IPA dataset.

Generally, if the direction of change of certain gene is consistent with a certain activation state of the transcription factor either activated or inhibited, a prediction of activation is made by the software. Activation z-score in the IPA is calculated from the formula:

$$z = \frac{x}{\sigma_x} = \frac{\sum_i w_i x_i}{\sqrt{\sum_i {w_i}^2}}$$

Where

$$x_i \in (-1,1)$$

When +1 is activation sate and -1 is deactivation state of the gene in response to the transcription factor

$$w_i = \frac{|M_{activating} - M_{inhibiting}|}{M_{activating} + M_{inhibiting} + 1}$$

With w_i is the weight of an edge "relationship between the gene and the relevant transcription factor" and $M_{activating}$ is the number of activation finding between the gene and the transcription factor and $M_{inhibiting}$ is the number of inhibiting finding (this data is from what was published before concerning these two genes).

Diseases and functions: the output from this analysis specifies the cellular processes that are changed due to the change in the examined gene list. This analysis also predicts the activation or inhibition of the top diseases and functions enriched from the previous analysis. All the genes related to every changed function can be retrieved and visually presented for subsequent validation. The colours of the heat map produced from this analysis detects the direction of change in the function as detected by the activation z-score, and the size of each square in the heat map represents the p-value of overlap between the mapping genes and the IPA enriched diseases and function.

Networks: this option in the IPA software allows for concentrating on more "focused molecules" or molecules that have high connectivity with other molecules in the dataset. These important molecules are the seed to which other important genes are connected and the gaps are then filled from the IPA dataset and networks are finally annotated with high-level functional categories. The networks are ranked according to the number of focused molecules in every network.

2.10.5 Gene Set Enrichment Analysis (GSEA)

Gene set enrichment analysis (GSEA) software includes around 18,000 gene lists uploaded in the Molecular Signatures Database (MSigDB)[345, 346]. This large number of gene lists is arranged in 8 main categories with smaller sub-categories. Main categories of the GSEA software include:

- Hallmark gene sets (H): the most popular well-defined biological processes and functions.
- Positional gene sets (C1): include gene lists for every human chromosome.
- Curated gene sets (C2): include gene from publically available databases.
- Motif gene sets (C3): include lists of genes regulated by the most common transcription factors and miRNAs.
- Computational gene sets (C4): gene listed by reconstructing the large cancer microarray data.
- Gene Ontology (GO) gene sets (C5): include three categories; genes annotated with the GO biological processes, CO cellular processes and CO molecular functions.
- Oncogenic signatures (C6)
- Immunologic signature (C7)

The output of the GSEA analysis is the GSEA enrichment score that includes the enrichment score (the degree of which DE genes are overrepresented by the GSEA gene list), normalised enrichment score (NES) that corrects for the number of gene sets and false discovery rate (FDR) that estimate the probability of false positivity of the enrichment score. The larger the NES, the smallest the FDR value for a given analysis.

2.11 Statistical analysis

Statistical analyses were performed using SPSS version 23 or GraphPad Prism version 7.00. The principal documented endpoint in the clinical cases studied was overall survival, recorded as months from diagnosis until 01/01/2019. Differences in cumulative survival were determined using the Kaplan-Meier method and a Log-Rank test. The Cox proportional hazards-regression model was used to identify parameters associated with survival. Data are show as a mean ± the standard error of the mean (SEM). Associations were explored by linear regression, with differences between groups of continuous variables assessed by t-test (parametric data) or Kruskal Wallis (non-parametric data) tests. Differences between

categorical variables were assessed by Pearson Chi Square. A p-value of <0.05 was considered significant.

Chapter 3: Characterisation of SULF2 protein expression and Function in human HCC

3.1 Background

HCC represents the majority of Liver cancer cases and is ranked the third cause of cancer related mortality worldwide[6]. Hepatocarcinogenesis is a multi-step process that arises on the background of chronic liver diseases, most commonly liver cirrhosis[26]. Despite the advances in diagnostic and predictive tools including high through-put sequencing and novel immune-therapies that limit the development and the progression of other types of cancers, HCC remains a global problem that affects about 850,000 people all over the world[6]. Molecular profiling studies of tumours resected from HCC patients revealed distinct molecular subgroups, generating hopes for personalised therapy approaches[57, 59], as yet with limited success[87, 347]. DNA changes in HCC patients have also been thoroughly investigated hoping to find targetable candidates[109], but the trunk "driver" mutations identified have proven to be difficult therapeutic targets[88]. Recent studies have also focused on the role of the tumour microenvironment as a potential driver for the development and the progression of HCC[57, 229]. Anti-PD-1 antibodies (eg. Nivolumab) appear to improve the outcome of patients[348] beyond sorafenib, the standard of care 1st line therapy for HCC[349], and have gained approval from the FDA for use as 2nd line therapies.

SULF2 is an endosulfatase enzyme that selectively removes sulfate group from the 6-O position in the HSPGs[286]. In a previous study, elevated *SULF2* mRNA levels in resection samples from HCC patients was associated with worse outcome and a link with the HCC tissue marker GPC3 was suggested[304]. *In vitro* studies showed that SULF2 upregulated GPC3 expression and facilitated the binding of Wnt-3a ligand to its receptor, leading to activation of the non-mutated β-catenin pathway[273]. A further link between SULF2 and HCC was reported in a study where SULF2 knock-out mice were shown to develop fewer tumours compared to their matched WT controls. In this study, SULF2 reportedly induced neo-angiogenesis via activation of the POSTN/TGF-β pathway[301]. However, the protein expression and cellular distribution of SULF2 in HCC tissues, together with the impact this may have on its clinical significance or mechanistic roles in HCC have been poorly investigated so far.

3.2 Chapter 3 aims

3.2.1 To characterise SULF2 within the *in vivo* tumour microenvironment and explore associations with disease stage and patient outcome.

3.2.1 To define the functional impact of SULF2 in vitro, by developing models to assess the contribution of different cell types expression or secreted isoforms on the phenotypic behaviour of HCC cells.

3.3 SULF2 expression in liver tissues from patients with HCC

SULF2 protein level was determined by IHC in diagnostic biopsies from 60 HCC patients. The IHC was performed by technical staff in the *Reeves* lab, with details of patients' selection and IHC protocols described in the materials and methods. The demographic and clinico-pathological features are presented in **Table 3.1.** and summarised here. The median age of the studied cohort was 69 years. Although at least 80% of HCC arise in cirrhotic livers, liver cirrhosis was absent in 29/60 (49%) of the cases studied. This reflects the majority of HCC being diagnosed radiologically in patients with cirrhosis, with biopsy – which carries the risks of haemorrhage and tumour seeding - advocated either when there is doubt radiologically, or in patients without established cirrhosis[332]. Patients were those with BCLC A-C stage disease, rather than those with end stage BCLC-D, as biopsy diagnosis is generally reserved for those patients fit enough for therapy. The overall median survival was 20.3 months in this selected group. While many did not have cirrhosis or established chronic liver disease (CLD), etiological associations included T2DM in 29 patients out of 60 (49%), with NAFLD or ALD being common in those that did have CLD.

3.3.1 SULF2 expression was scant in the non-tumour tissue

Generally, SULF2 expression in non-tumour liver was low, with scant SULF2 expression occasionally detected on the canalicular surface of hepatocytes (**Figure 3.1**). Notably, SULF2 expression was detected in smooth muscle cells of the portal tract arteries as well as in the non-parenchymal sinusoidal cells and in the endothelial cells. Low background, with expression of SULF2 in either smooth muscle or the endothelial cells, were used as an internal controls in all cases, to ensure reproducible quality of the IHC.

Figure 3.1: Expression of SULF2 in HCC tissue compared to the adjacent non-tumour tissue.

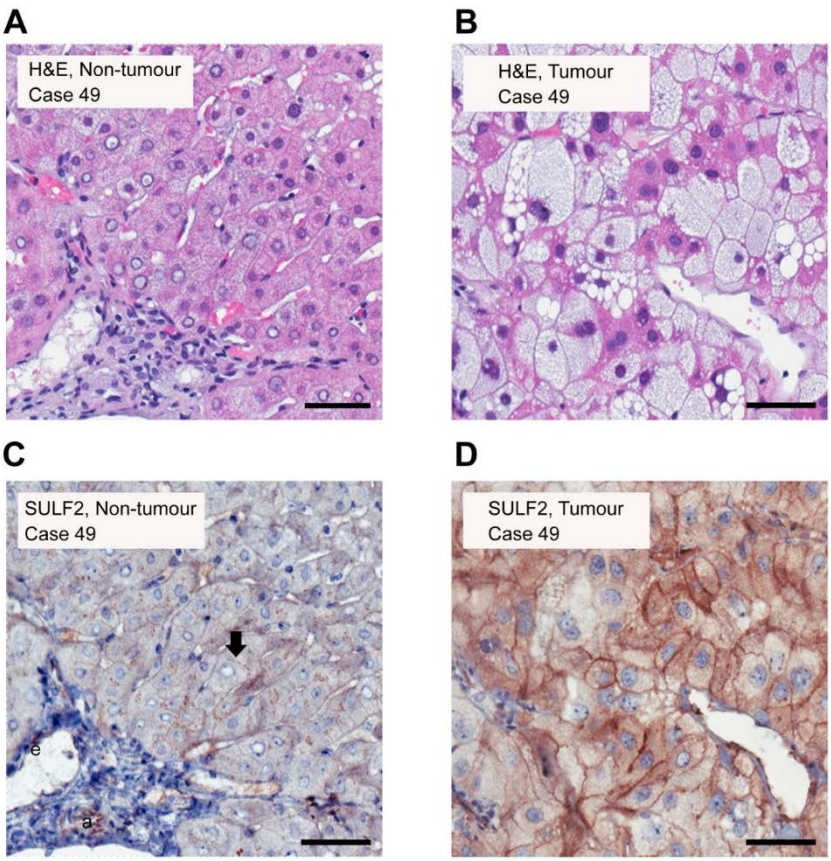

Representative images from patient 49 showed H&E staining of the non-tumour **(A)** and the tumour **(B)** tissues. In the non-tumour tissue, normal hepatocytes were arranged in chords with an intact portal tract and inflammatory cells starting to infiltrate into the tissue, while cytological atypia, dense chromatin together with loss of liver architecture were the criteria of the tumour tissue. Representative images showed SULF2 immuno-positivity in the non-tumour **(C)** versus the tumour tissue **(D)**. SULF2 was scantly expressed in the membrane of normal hepatocytes (black arrow) as well as different non-parenchymal cells including smooth muscle cells of the arteries (a), the endothelial cells (e) and the sinusoidal cells (white arrow). Images were captured at x20 magnification and scale bars represent 50 microns, n=60 patients.

3.3.2 SULF2 was upregulated in the tumour cells in biopsies from a subset of patients with HCC

In contrast to the SULF2 levels in the non-tumour cases, SULF2 was upregulated in 35/60 (58%) of HCC biopsies. This finding supports the previous study that reported upregulation of the *SULF2* mRNA level in about 57% of HCC resection specimens[304]. Of the cases characterised here, SULF2 upregulation relative to non-tumour tissues was common, but more commonly in tumour associated stromal cells rather than tumour cells themselves. SULF2 positivity in the membrane/cytoplasm of the tumour cells was present in only 9/60 (15%) of cases **(Figure 3.1)**. Tumour cell SULF2 positivity was significantly associated with larger tumours (9.6±1.6 versus 6.2±0.8 cm, p=0.026) and higher median AFP serum level (1400 ng/ml versus 5ng/ml, p=0.03), when compared to the negative cases. Notably, most of the tumour-cell positive SULF2 patients (7/9) had T2DM compared to 41% (21/51) where SULF2 was absent (p=0.042). SULF2 tumour-cell positivity was also associated with extrahepatic diseases (p=0.003) as well as advanced TNM stage (p=0.034). Patients were more likely to receive supportive care only.

Median survival was reduced compared to the whole cohort, although not significantly so in the small numbers considered **(Table 3.1)**.

	All patients	**SULF2 in HCC cells**		
	60	Absent 51	Present 9	p value
Age (median)	69	69	65	ns
Gender (male/female)	49/11	42/9	7/2	ns
BMI (median)	27	27	27	ns
T2DM no/yes	32/28	30/21	2/7	0.042*
Cirrhosis no/yes	31/29	25/26	6/3	ns
CLD none/ALD/NAFLD/other	19/10/15/16	16/9/13/13	3/1/2/3	ns
Grade 1/2/3	18/27/15	17/23/11	1/4/4	ns
Size (cm)	6.7±0.7	6.2±0.8	9.6±1.6	0.026*
Tumour number	2.2±0.4	2.0±0.4	3.3±1.1	0.11
PVT no/yes	52/8	46/6	6/3	0.056
EHD no/yes	52/8	47/4	5/4	0.003**
TNM stage 1/2/3/4	29/12/11/8	26/11/10/4	3/1/1/4	0.034*
INR	1.0±0.02	1.0±0.02	1.0±0.03	ns
Albumin (g/l)	38.8 ± 0.67	39.2±0.7	36.8±1.9	ns
Bilirubin (µmol/l)	21.4±7.9	14.1±1.1	63.1±52	ns
AFP (median)	6	5	1400	0.03*
Ascites no/yes	55/5	47/4	8/1	ns
Childs-Pugh A/B/C	53/6/1	46/5/0	7/1/1	ns
BCLC stage A/B/C/D	17/13/28/2	15/12/22/2	2/1/6/0	ns
ECOG PST 0/1/2	32/22/6	28/19/4	4/3/2	ns
Therapy OLTx/Res/Ablation	3/7/12	3/5/12	0/2/0	0.037*
TACE/Med/ BSC	28/1/9	25/0/6	3/1/3	
Median survival (months)	20.3	28.7	11.6	ns
No Surgical treatment	n=50	n=43	n=7	
Median survival (months)	16.2	19.7	9.9	0.054

Table 3.1: Demographic and clinico-pathological features of patients Continuous data are presented as mean ± standard error unless otherwise stated, with statistical comparisons using a Mann Whitney test. Categorical data were compared using a Chi Square test. Survival was assessed by the Kaplan Meier method. 'Other' included small numbers with Hepatitis C (n=4); haemochromatosis (n=4), cryptogenic cirrhosis (n=4); Hepatitis B (n=1); autoimmune hepatitis (n=2); and α-1-antitrypsin deficiency (n=1). Abbreviations: T2DM, Type 2 diabetes mellitus; AFP, alphafetoprotein; BMI, body mass index; ALD, alcoholic liver disease; NAFLD, non-alcoholic fatty liver disease; HCV, Hepatitis C; HBV, Hepatitis B;AIH, autoimmune hepatitis; A1AT, α-1-antitrypsin deficiency; PVT, portal vein thrombosis; EHD, extra-hepatic disease; INR, international normalised ratio; BCLC, Barcelona Clinic for Liver Cancer.

3.3.3 SULF2 upregulation in the Cancer-Associated Fibroblasts (CAFs) identified HCC patients with poorest outcomes

Further characterisation of the HCC biopsies revealed intense positive SULF2 expression in the non-parenchymal cancer associated fibroblasts (CAFs) invading the tumour area in 52% of tumour cases (31/60) **(Figure 3.2)**. To confirm SULF2 positivity in this particular cell type

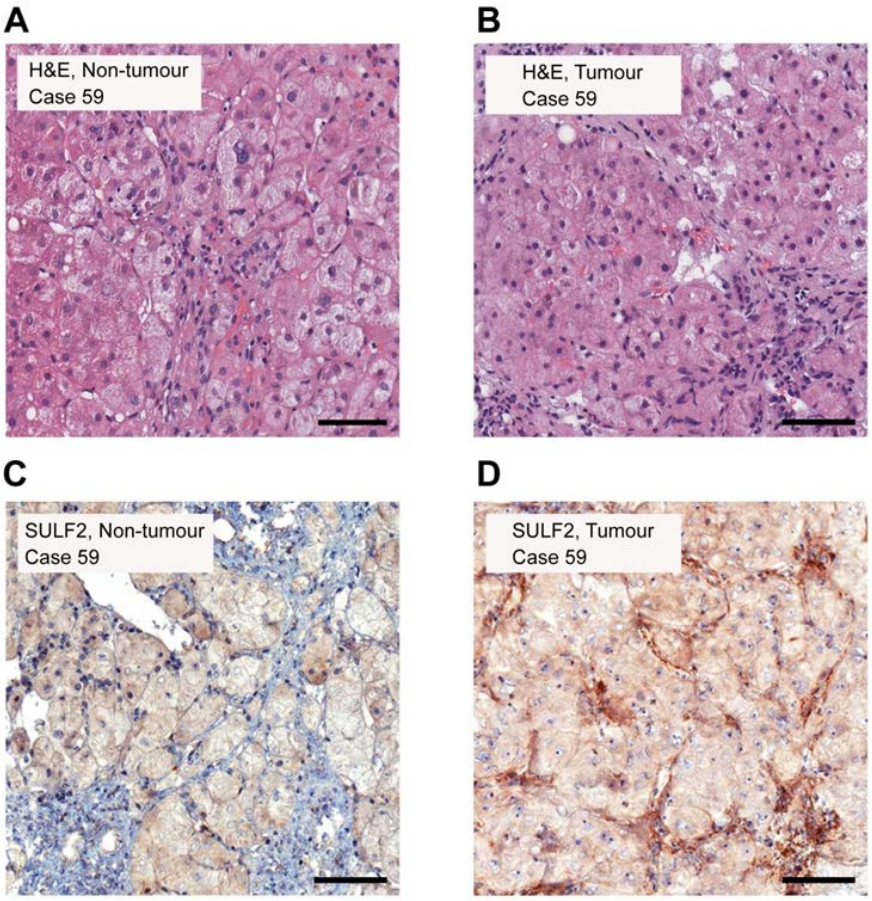

Figure 3.2: Expression of SULF2 in HCC-CAFs compared to the adjacent non-tumour tissue. Representative images from patient 59 show H&E staining of the cirrhotic non-tumour **(A)** and the tumour **(B)** tissues. Cirrhotic changes in the non-tumour area were evident with micro-nodules and inflammatory infiltrate. The tumour tissue was characterised with stromal invasion and a solid pattern. Representative images showed SULF2 immuno-positivity in the non-tumour **(C)** versus the tumour tissue **(D)**. SULF2 positivity was stronger and more evident in the CAFs in the tumour tissue compared to the non-tumour. Images were captured at x20 magnification and scale bars represent 50 microns.

rather than other infiltrating cells such as elongated TAMs, serial section for selected cases were stained with αSMA; the classical marker for activated CAFs. Indeed, SULF2 positive cells were also positive for αSMA **(Figure 3.3)**. SULF2 expression was not as positive in the αSMA positive activated hepatic stellate cells in the portal tract or bridging fibrous septa of the non-tumour liver **(Figure3.3)**.

Compared to SULF2 expression in the tumour cells, CAF-SULF2 positivity was more frequent. CAF-SULF2 expression was not associated with specific tumour criteria, however, overall survival was reduced in CAF-positive SULF2 HCC cases (12.2 months versus 35 months) **(Table 3.2)**. In subsequent survival analyses, the small numbers of patients undergoing potentially curative treatments (7 that underwent resection and 3 that had a liver transplantation), were excluded. CAF-SULF2 positivity in the remaining 50 patients was significantly associated with poorer survival (7.2 months versus 29.2, p=0.005 Kaplan Meier) **(Figure 3.4)**. Moreover, SULF2

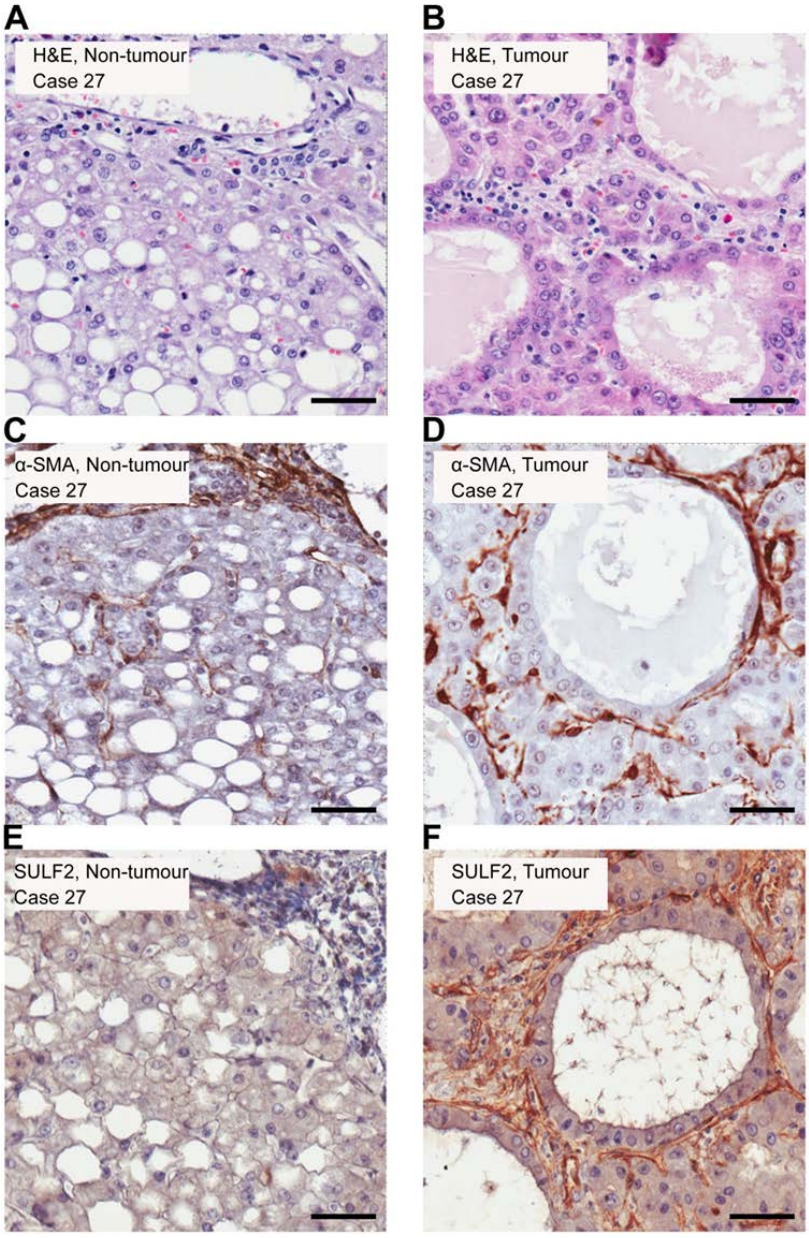

Figure 3.3: Expression of SULF2 in αSMA positive CAFs but not αSMA positive fibroblasts. Representative images from patient 27 show H&E staining of the non-tumour **(A)** and the tumour **(B)** tissues. This case was characterised by fatty deposition and immune filtration of the non-tumour tissue. The tumour tissue resembled the pseudo-glandular pattern. Representative images showed αSMA and SULF2 IHC in the non-tumour **(C,E)** versus the tumour tissue **(D,F)**. αSMA stained activated fibroblasts in the portal tract in the non-tumour tissue and the CAFs in the tumour tissue. SULF2 positivity was restricted to the CAFs but not fibroblasts of the normal non-tumour liver. Images were captured at x20 magnification and scale bars represent 50 microns.

upregulation in either HCC cells or HCC and CAFs was also strongly associated with poorer survival (9.9 versus 29.2 months, p=0.005, Kaplan Meier).

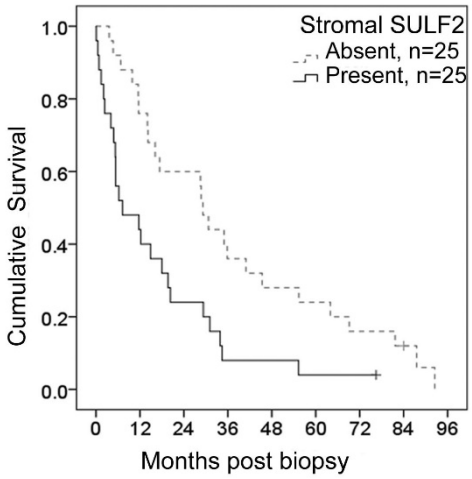

Figure 3.4 Stromal SULF2 was associated with poorer survival. Kaplan Meier survival curve for patients scored as having absent or scanty SULF2 in tumour stromal cells, versus those with either widespread or focally intense expression is shown. The median survival was 7.2 months versus 29.2 months, p=0.005, n= 50 patients

Univariate analyses to identify factors associated with survival are shown in **Table 3.3**. Those with a p value <0.01 were entered into a multivariate cox regression analysis and included

	All patients	**SULF2 in cancer associated fibroblasts (CAFs)**		
	60	Absent 29	Present 31	p value
Age (median)	69	69	69	ns
Gender (male/female)	49/11	23/6	26/5	ns
BMI (median)	27	25	28	ns
T2DM no/yes	32/28	14/15	18/13	ns
Cirrhosis no/yes	31/29	14/15	17/14	ns
CLD none/ALD/NAFLD/other	19/10/15/16	9/4/7/9	10/6/8/7	ns
Grade 1/2/3	18/27/15	12/10/7	6/17/8	ns
Size (cm)	6.7±0.7	6.2±1.1	7.2±1.0	ns
Tumour number	2.2±0.4	1.6±0.2	2.7±0.7	ns
PVT no/yes	52/8	27/2	25/6	ns
EHD no/yes	52/8	27/2	25/6	ns
TNM stage 1/2/3/4	29/12/11/8	12/7/3/2	15/2/8/6	ns
INR	1.0±0.02	1.0±0.02	1.03±0.04	ns
Albumin (g/l)	38.8 ± 0.67	39.4±0.9	38.3±1.0	ns
Bilirubin (µmol/l)	21.4±7.9	12±.9	30.3±15.2	ns
AFP (median)	6	6	6	ns
Ascites no/yes	55/5	28/1	27/4	ns
Childs-Pugh A/B/C	53/6/1	28/1/0	25/5/1	ns
BCLC stage A/B/C/D	17/13/28/2	10/7/12/0	7/6/16/2	ns
ECOG PST 0/1/2	32/22/6	17/10/2	15/12/4	ns
Therapy OLTx/Res/Ablation	3/7/12	2/2/8/	1/5/4	ns
TACE/Med/ BSC	28/1/9	14/1/2	14/1/7	
Median survival (months)	20.3	35.0	12.2	ns
No Surgical treatment	n=50	n=25	n=25	
Median survival (months)	16.2	29.2	7.2	0.005**

Table 3.2: Demographic and clinico-pathological features of patients

Continuous data are presented as mean ± standard error unless otherwise stated, with statistical comparisons using a Mann Whitney test. Categorical data were compared using a Chi Square test. Survival was assessed by the Kaplan Meier method. 'Other' included small numbers with Hepatitis C (n=4); haemochromatosis (n=4), cryptogenic cirrhosis (n=4); Hepatitis B (n=1); autoimmune hepatitis (n=2); and α-1-antitrypsin deficiency (n=1). Abbreviations: T2DM, Type 2 diabetes mellitus; AFP, alpha fetoprotein; BMI, body mass index; ALD, alcoholic liver disease; NAFLD, non-alcoholic fatty liver disease; HCV, Hepatitis C; HBV, Hepatitis B;AIH, autoimmune hepatitis; A1AT, α-1-antitrypsin deficiency; PVT, portal vein thrombosis; EHD, extra-hepatic disease; INR, international normalised ratio; BCLC, Barcelona Clinic for Liver Cancer.

tumour grade, presence of extrahepatic disease, portal vein thrombosis, or ascites, serum albumin, performance status (PST), treatment received and SULF2 status. Tumour grade, serum albumin and PST were strongly and highly significantly associated with survival.

However, SULF2 presence contributed independently of these factors, whether considered only in CAFs, or combined in either tumour cells or CAFs **(Table 3.3)**.

Variable	UVA	MVA entering elevated stromal SULF2		MVA entering elevated tumour or stromal SULF2	
	p value	p value	HR (CI)	p value	HR (CI)
Age	0.195				
Gender	0.197				
AFP	0.014				
Tumour Number	0.046				
Tumour size	0.015				
EHD	0.006	0.057		0.048	0.31 (0.10-0.99)
PVT	<0.001	0.116		0.130	
Edmondson-Steiner Grade **Grade 1 (n=17)** **Grade 2 (n=22)** **Grade 3 (n=11)**	0.006 0.001 0.014	0.003 0.001 0.283	 0.18 (0.06-0.51) 0.56 (0.19-1.62)	0.002 0.001 0.196	 0.16 (0.06-0.47) 0.49 (0.17-1.44)
Cirrhosis	0.795				
Ascites	<0.001	0.714		0.668	
Albumin	<0.001	0.002	0.88 (0.81-0.96)	0.002	0.88 (0.81-0.95)
Bilirubin	0.036				
INR	0.433				
ECOG PST **PST 0 (n=23)** **PST 1 (n=21)** **PST 2 (n=6)**	<0.001 <0.001 0.01	0.001 0.021 0.592	 0.11 (0.02-0.72) 0.62 (0.10-3.64)	0.001 0.002 0.630	 0.10 (0.02-0.73) 0.64 (0.10-3.94)
Treatment **Ablation (n=12)** **TACE (n=28)** **Medical (n=1)** **Supportive (n=9)**	<0.001 <0.001 <0.001 0.595	0.066		0.013 0.304 0.221 0.001	 0.50 (.13-1.87) 0.48 (0.15-1.55) 0.01 (0.00-0.15)
Tumour SULF2 **Absent (n=43)** **Present (n=7)**	0.061				
Stromal SULF2 **Absent (n=25)** **Present (n-25)**	0.006	0.045	0.46 (0.22-0.98)		
Tumour or Stromal (CAFs) SULF2 **Absent (n=22)** **Present (n=28)**	0.005			0.016	0.38 (0.18-0.73)

Table 3.3: Multivariate analysis of factors associated with survival in non-surgically treated patients Factors associated with survival in 50 patients for whom surgical treatment was not an option were assessed by univariate analysis (UVA). Factors with a p-value less than 0.01 were entered into a multivariate Cox Regression analysis. Two distinct multivariate analyses (MVA) are shown, the first considering stromal SULF2 and the second (shaded in grey) showing a similar analysis, but in which SULF2 overexpression in either HCC cells or stromal cells was classed as 'present'. Significance and Hazards Ratio (HR) with upper and lower 95% confidence intervals are shown.

3.4 Investigation of the impact of CAF-SULF2 on the behaviour of the tumour cells

As SULF2 was predominantly expressed in the αSMA positive CAFs in half of the patients, rather than the tumour cells, subsequent studies were directed towards understanding the role of stromal SULF2 and/or SULF2 regulated factors. The accumulation of activated hepatic stellate cells in patients with chronic liver disease contributes to the tissue mechanical stiffness and reportedly enhances tumorigenicity[350]. Studies by other groups have also previously shown the presence of CAFs to be linked with poorer response to treatment in patients with HCC patients[334, 351]. CAFs reportedly also promote cancer stem cell (CSC) properties in the neighbouring tumour cells, as well as regulate the secretion of a wide range of inflammatory and pro-oncogenic cytokines that regulate intercellular crosstalk within the tumour microenvironment (TME)[352, 353]. The contribution of CAF-derived SULF2 had not been previously explored.

3.4.1 The expression level of SULF2 varied between different HCC and myofibroblast cell lines.

The protein and mRNA level of SULF2 was investigated in three different HCC cell lines, including Huh7, Hep3B and HepG2 cells, in addition to the αSMA positive myofibroblast LX-2 cell line. SULF2 was expressed in both Huh7 and HepG2 cell lines, while it is expression in Hep3B cell line was minimal, as confirmed by WB and q-PCR **(Figure 3.5).**

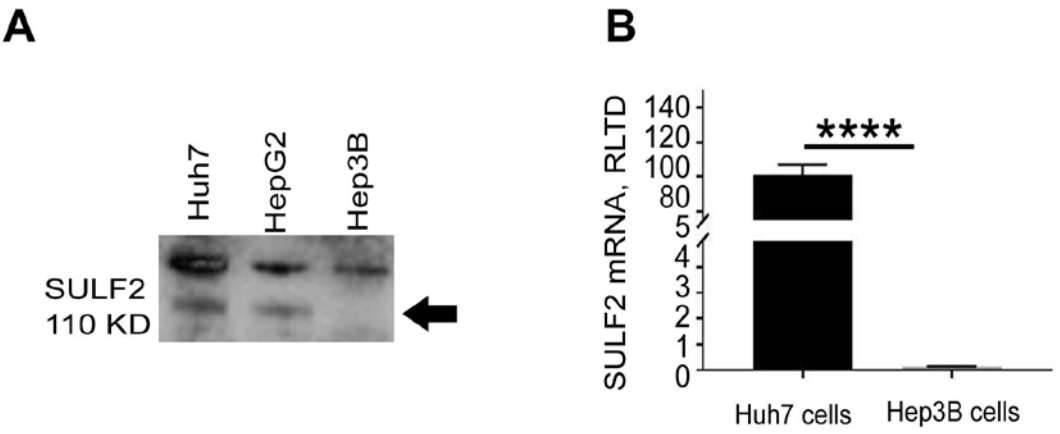

Figure 3.5: Characterisation of SULF2 expression in different HCC cell lines Western blot shows the protein expression of SULF2 in Huh7, HepG2 and Hep3B **(A)**. Huh7 and HepG2 showed a SULF2 band at 110 kiloDalton (kDa) with a non-specific band at 150 kDa, while Hep3B protein extract showed no SULF2 expression. Graph shows mRNA expression of SULF2 in Huh7 and Hep3B cell lines **(B)**. The level of SULF2 in both cell lines was calculated using the relative level of transcriptional difference (RLTD) using HPRT as a control. List of antibodies and primers is provided in the materials and methods. Experiments were repeated three times (n=3) and data are expressed as mean ± s.e.m; ****p<0.0001

SULF2 was expressed by the LX-2 myofibroblasts, which we planned to use to model the interactions between HCC cells and stromal cells. To create a further *in vitro* modelling tool, SULF2 was knocked-down by shRNA, as described in the materials and methods section. LX2 SULF2 expression and SULF2 KD were confirmed by WB **(Figure 3.6)**. Conditioned media (CM) was collected from LX-2 cells and SULF2 KD LX-2 cells and the level of SULF2 in the CM from both cell lines was measured by ELISA **(Figure 3.6),** as described in the materials and methods section.

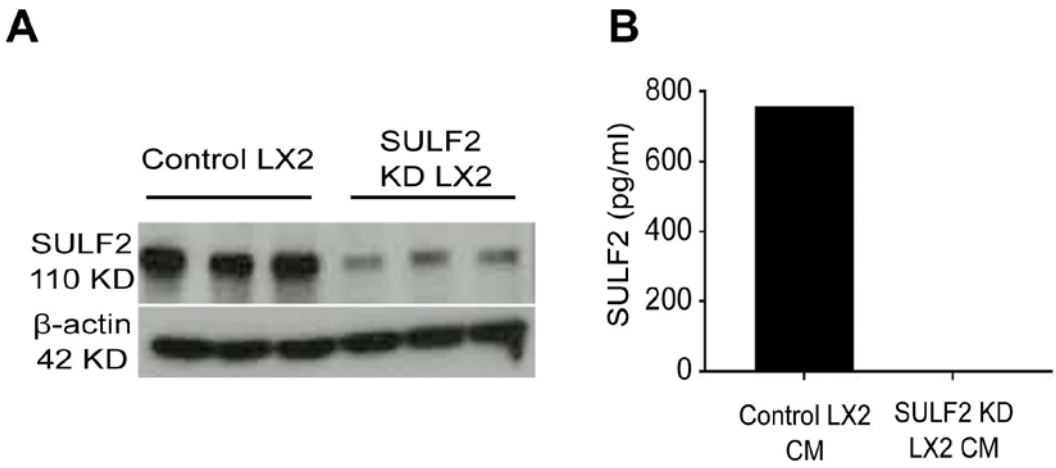

Figure 3.6: Confirmation of SULF2 KD from the LX-2 myofibroblast cell line Western blot shows SULF2 levels in control and SULF2 KD LX-2 protein extracts **(A)**. SULF2 (110 kDa) was successfully knocked down (KD) from the LX-2 cell line. β-actin (42 kDa) was used as a loading control. The experiment was repeated three times (n=3). Graph shows the level of secreted SULF2 in CM from control and SULF2 KD LX-2 cells **(B)**. SULF2 level in the SULF2 KD LX-2 CM was below the SULF2 ELISA kit's detection limit (313 pg/ml). Details of ELISA are in the materials and methods.

3.4.2 Optimisation of conditions for the 2D co-culture between myofibroblasts and HCC cell lines

Based on the aforementioned characterisation, Hep3B cells (with no endogenous SULF2 expression) and Huh7 cells that expressed SULF2 were chosen for further experiments. Previous studies showed induction of tumour cell proliferation stimulated by co-culture with CAFs and LX-2 fibroblasts cells or cell CM[350, 352]. In order to optimise the conditions for co-culturing HCC cell lines with SULF2 manipulated LX-2 cells in the 2D trans-well system, the parent LX-2 cell line was cultured in the trans-well in a 1:1 ratio with 10000, 20000 and 50000 Hep3B and Huh7 cells for different time points.

Co-culture with LX-2 induced the viability of Hep3B cells after 24 hours at 10000 cell densities (p=0.002), after 48 hours at 10000 (p=0.027) and 20000 (p=0.005) cell densities and after 72

hours at 50000 cell density (p=0.001), as compared to matched Hep3B controls, measured by an MTT viability/metabolic activity test **(Figure 3.7)**.

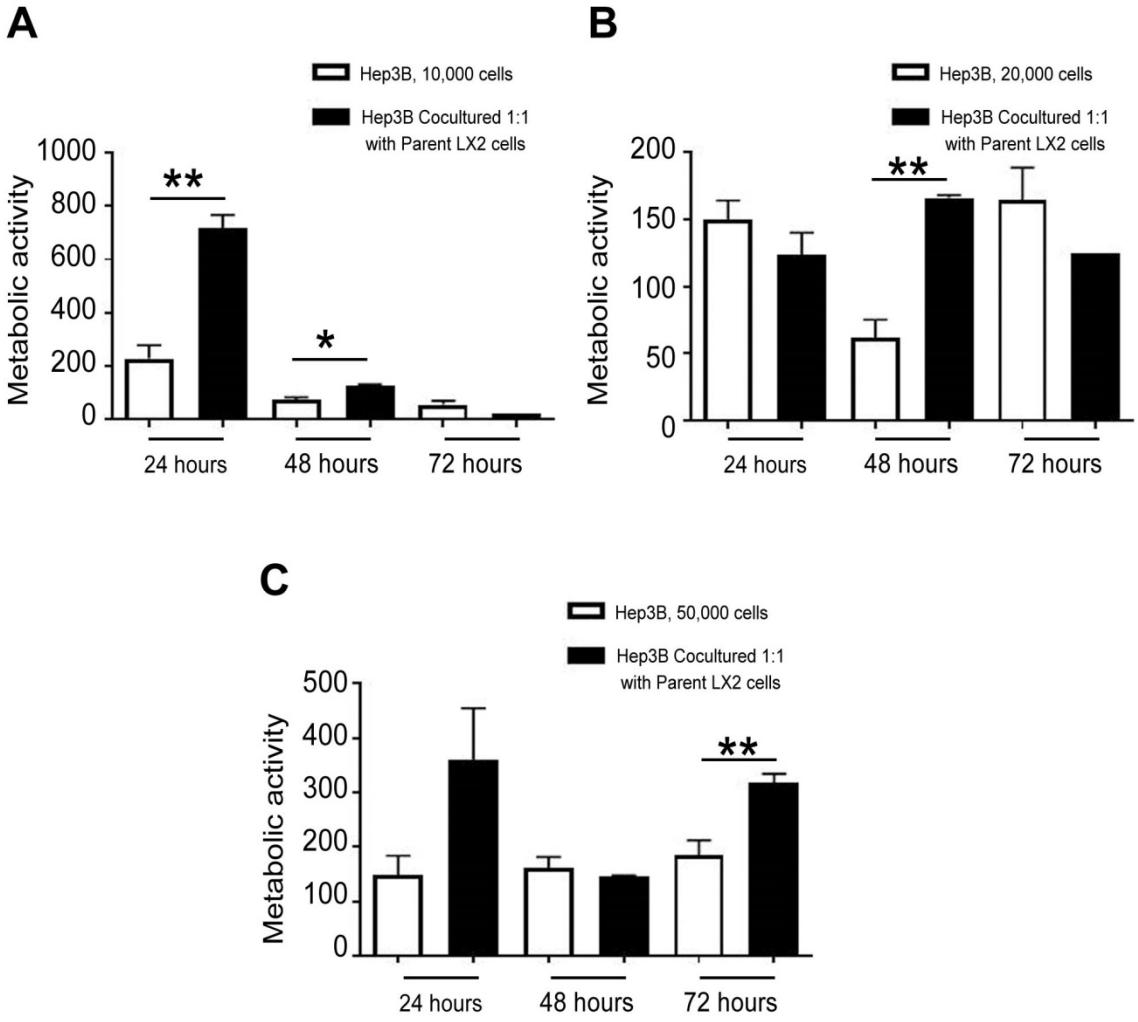

Figure 3.7: Effect of LX-2/Hep3B co-culture on the viability of the tumour cells Graphs show viability of Hep3B cells cultured alone or in co-culture with parent LX-2 cells at 1:1 ratio of 10000 **(A)**, 20000 **(B)** and 50000 **(C)** cells at three different time points (24, 48 and 72 hours). The experiment was repeated 3 times and data are presented as mean ± s.e.m, * p<0.05; ** p<0.01; *** p<0.001; ****p<0.0001, n=3 replicates.

MTT viability of Huh7 co-cultured with LX-2 showed trend towards increase at the 10000 cell density at 72 hours (p=0.078) and the 20000 cell density after 24 hours (p= 0.077). This increase was significant after 24 (p= 0.04) and 72 hours at the 50000 cell density co-culture (p=0.011) **(Figure 3.8)**. Other changes towards increase or decrease in viability upon fibroblast-tumour cells co-culture failed to reach significance.

To avoid cells becoming over-confluent and to standardise the protocol for the two different HCC cell lines, 1:1 co-culture at the 20000 cells per well density for 48 hours was adopted for further co-culture protocols.

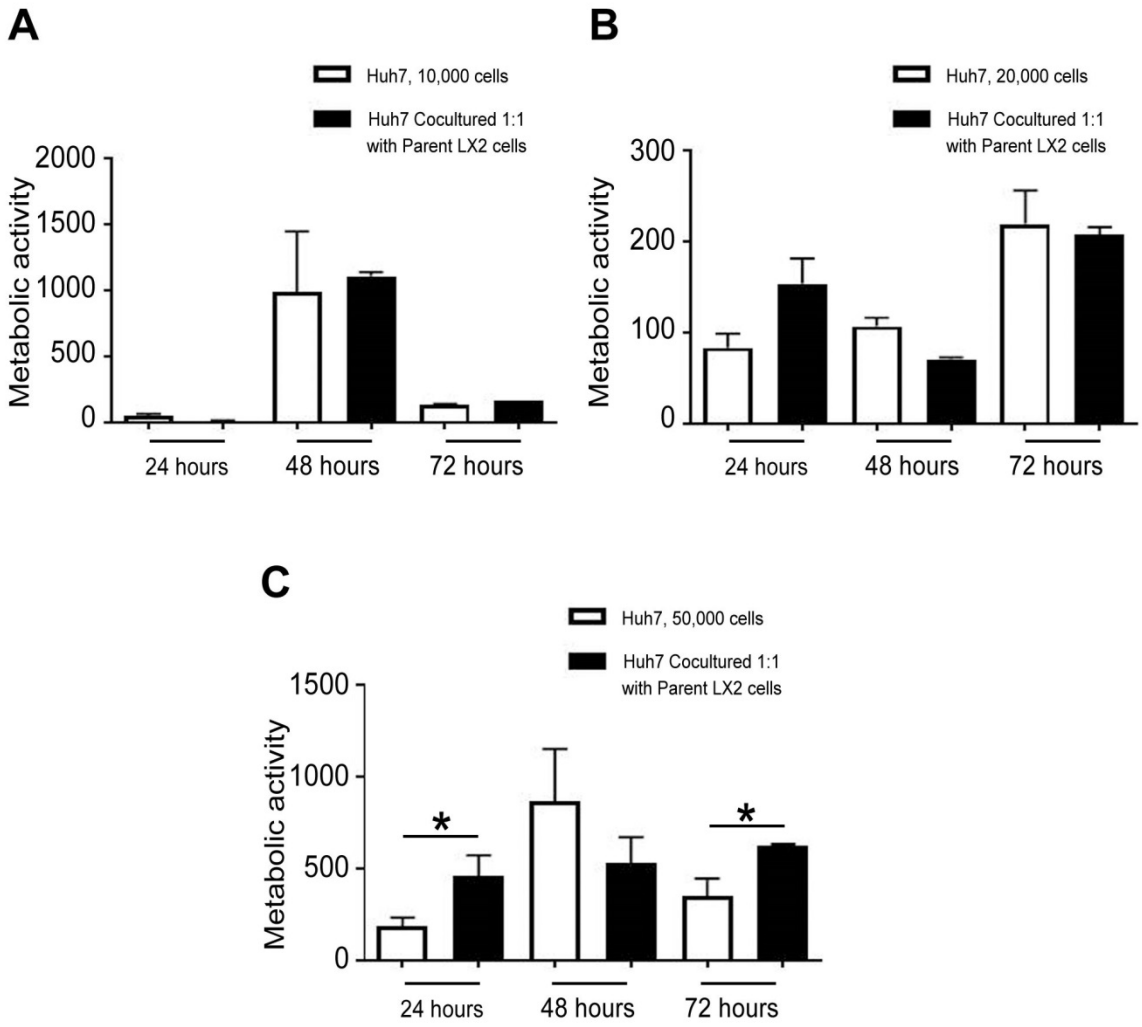

Figure 3.8: Effect of LX-2/Huh7 co-culture on the viability of the tumour cells Graphs show viability of Huh7 cells cultured alone or in co-culture with parent LX-2 cells at 1:1 ratio of 10000 **(A)**, 20000 **(B)** and 50000 **(C)** cells at three different time points (24, 48 and 72 hours). The experiment was repeated 3 times (n=3) and data are presented as mean ± s.e.m, * $p<0.05$.

3.4.3 Stromal SULF2 induced the viability/metabolic activity of the HCC tumour cell lines

Hep3B and Huh7 HCC cell lines were co-cultured with media, control LX-2 cells or with SULF2 KD LX-2 cells **(Figure 3.9)** to assess the impact of stromal SULF2 on the viability of the tumour cells as measured by MTT assay. Secreted SULF2 from control LX-2 cells induced the viability/metabolic activity of Hep3B and Huh7 cells compared to cells co-cultured with SULF2 KD LX-2 ($p=0.0067$ and 0.0013 respectively). Co-culture with control LX-2 cells also significantly

increased the MTT activity of the Hep3B and Huh7 cells compared to HCC cells grown in media only (p=0.002 and <0.0001 respectively)**(Figure 3.10)**.

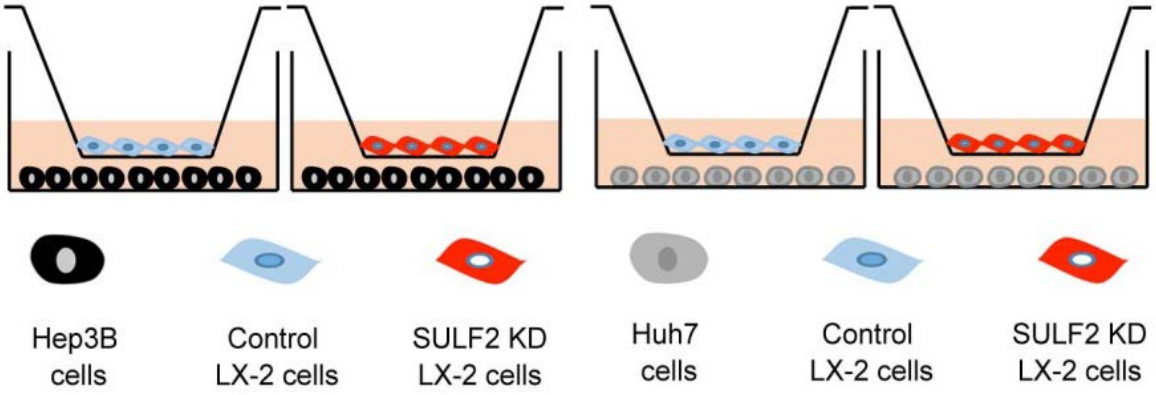

Figure 3.9 Schematic diagram for the fibroblast-tumour cells co-culture experiment. Hep3B cells (black cells) or Huh7 cells (grey cells) were co-cultured with Control LX-2 cells (blue) or with SULF2 KD LX-2 cells (red) on the 2D trans-well inserts. At the due time point, inserts were removed and an MTT assay was performed on the tumour cells.

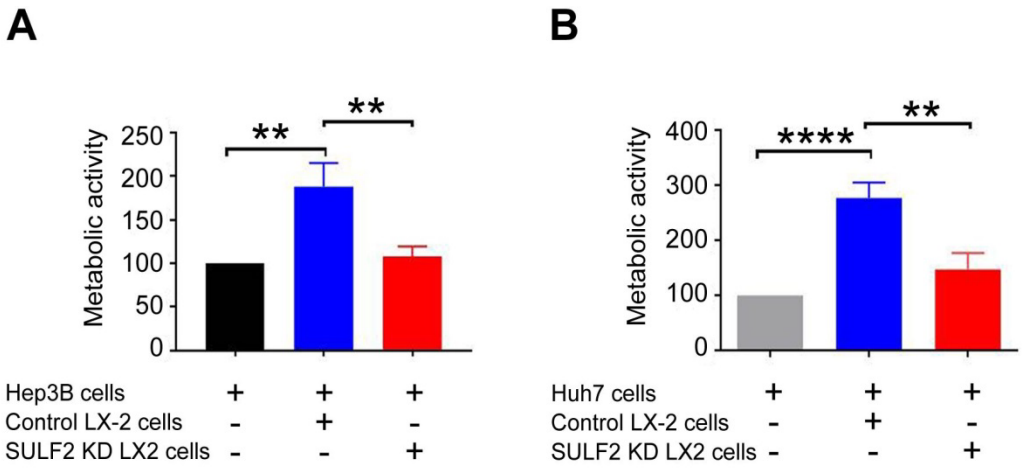

Figure 3.10 Stromal SULF2 induced the viability of the tumour cells Graphs show the impact of stromal SULF2 on the viability of HCC Hep3B **(A)** and Huh7 **(B)** cell lines. The experiment was repeated 3 times (n=3) and data are presented as mean ± s.e.m, ** p<0.01; ****p<0.0001.

3.4.4 Stromal SULF2 promoted the proliferation of the HCC tumour cell lines

A BrdU proliferation assay was performed to confirm the stromal SULF2-induced proliferation of tumour cells within the TME niche. Consistent with the MTT results, stromal SULF2 induced the proliferation of both Hep3B and Huh7 cells compared to co-culture with SULF2 KD LX-2

cells (p=0.0008 and 0.0094 respectively), an effect that was also significantly higher than cells without co-culture (p=0.0033 for both cell lines) **(Figure 3.11)**.

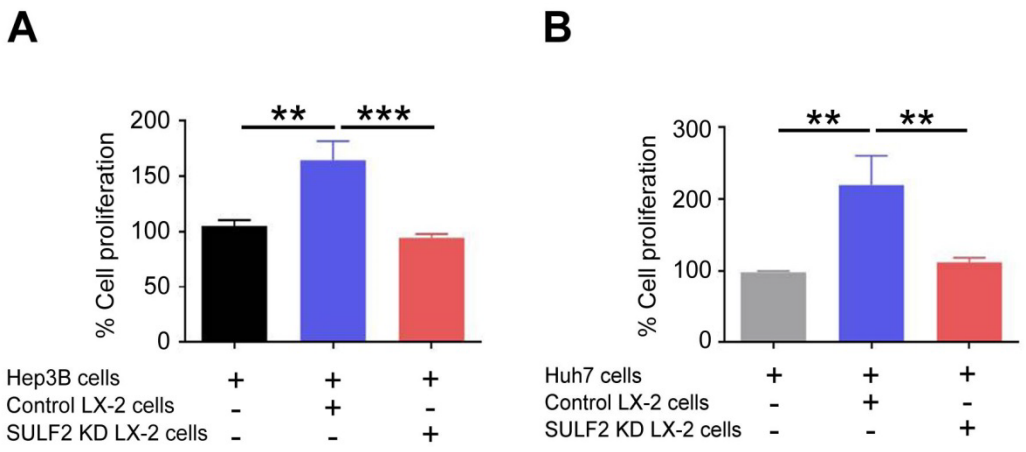

Figure 3.11. The proliferation of the tumour cells was accelerated in the presence of stromal SULF2. Graphs show the impact of stromal SULF2 on the proliferation of the HCC Hep3B **(A)** and Huh7 **(B)** cell lines. The experiment was repeated 3 times (n=3) and data are presented in mean ± s.e.m, * p<0.05; ** p<0.01; *** p<0.001; ****p<0.0001.

3.4.5 Stromal SULF2 potentiated the migration of SULF2-null Hep3B cells, but not the Huh7 cells

In addition to the *in vitro* impact of stromal SULF2 on the proliferation of the tumour cells, we explored the possible impact of stromal SULF2 on the migration of the tumour cells. Hep3B cells (with no SULF2 expression) were able to migrate faster into the 'scratch assay gap' when co-cultured with control LX-2 cell CM compared to CM concentrated from the SULF2 KD LX-2 cell, or Hep3B cells grown without fibroblast CM (p<0.0001 for both conditions) **(Figure 3.12).**

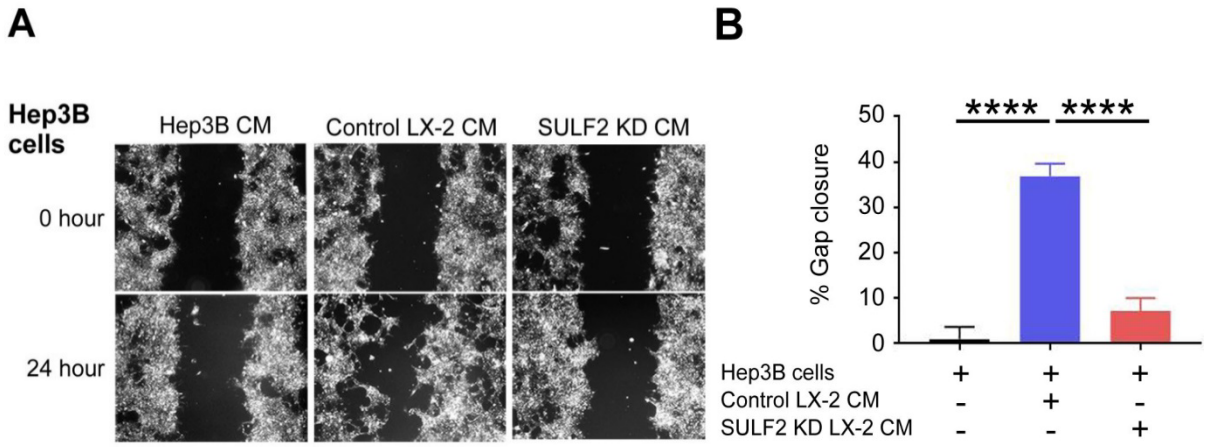

Figure 3.12 Migration of Hep3B cells under the influence of stromal SULF2 Representative images show migration of Hep3B cells at 0 hours (upper row) versus a 24 hour time point **(A).** Stromal SULF2 in CM potentiated the migration of Hep3B cells (middle column) compared to Hep3B cell migration without co-culture with CM (left column) or Hep3B cells grown in CM from SULF2 LX-2 CM (right column). Graph shows the migration of Hep3B as a percentage of Gap closure and the effect of SULF2 on tumour cell migration **(B)**. The experiment was repeated 3 times (n=3) and data are presented in mean ± s.e.m, ****p<0.0001.

Notably, stromal SULF2 did not significantly impact the migration of the Huh7 cells grown without CM (p=0.714), possibly because Huh7 cells express their own SULF2. Migration of Huh7 cells in the presence of stromal SULF2 in the CM, however, was higher than Huh7 cells co-cultured with SULF2 KD LX-2 CM, although not statistically significantly so (p=0.0614) **(Figure 3.13).**

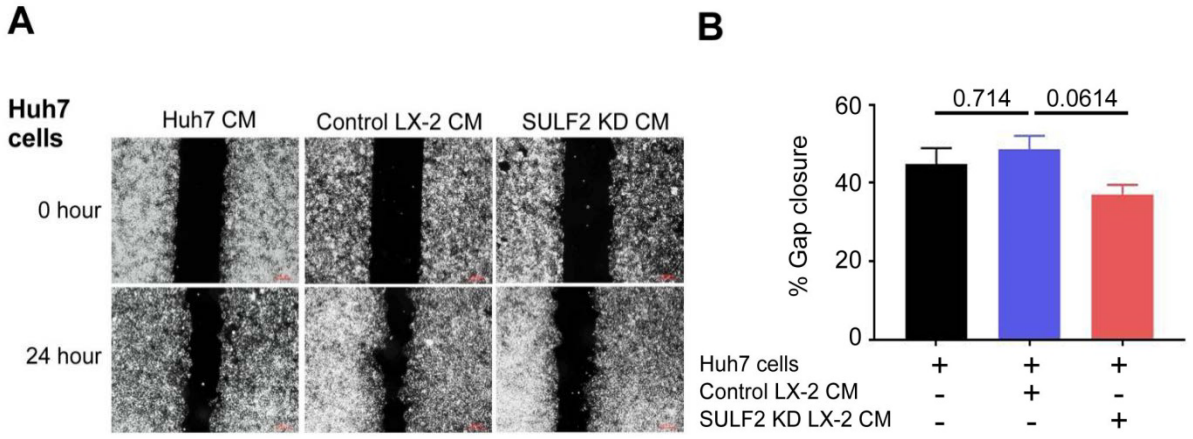

Figure 3.13 Migration of Huh7 cell line under the influence of stromal SULF2 Representative images show migration of Huh7 cells at 0 hours (upper row) versus a 24 hour time point **(A)**. Stromal SULF2 in CM slightly increased the migration of Huh7 cells (middle column) compared to Huh7 cell migrated without co-culture with CM (left column) or Huh7 grown In CM from SULF2 LX-2 CM (right column). Graph shows the migration of Huh7 as a percentage of Gap closure and the effect of SULF2 on tumour cell migration **(B)**. The experiment was repeated 3 times (n=3) and data are presented as mean ± s.e.m, *p<0.05.

3.4.6 Fibroblast-derived SULF2 increased the invasion of the tumour cells.

Characterising the ability of the stromal cells to promote tumour cells invasion of the basement membrane using a Boyden-invasion chamber was the next goal. As a pilot study, SULF2-manipulated LX-2 cells were seeded at the bottom of the 24-well plate to act as a source of SULF2 that might induce the invasion of Hep3B cell from inner surface of the Boyden chamber out to the outer surface **(Figure 3.14)**.

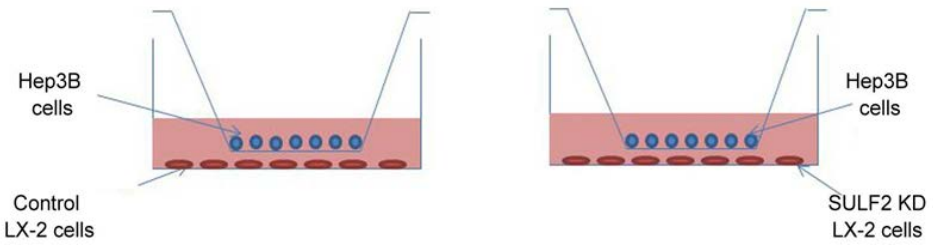

Figure 3.14 Schematic diagram for the chemotaxis of the tumour cells influenced by stromal SULF2. Control and SULF2 KD LX-2 cells (red) were cultured in the bottom of 24-well plate at different concentration overnight. 300000 Hep3B cells (blue cells) were then incubated in the Boyden-invasion chambers and co-cultured with the fibroblasts for 72 hours. The invasion of the tumour cells to the outer surface of the chamber was investigated.

Stromal SULF2 from 5000 cell/well control LX-2 cells significantly increased Hep3B cell invasion compared to Hep3B cultured without fibroblast cell lines at 5000 cell/well (p=0.0013) **(Figure 3.15)**. However, this effect was not significant when compared to Hep3B/SULF2 KD

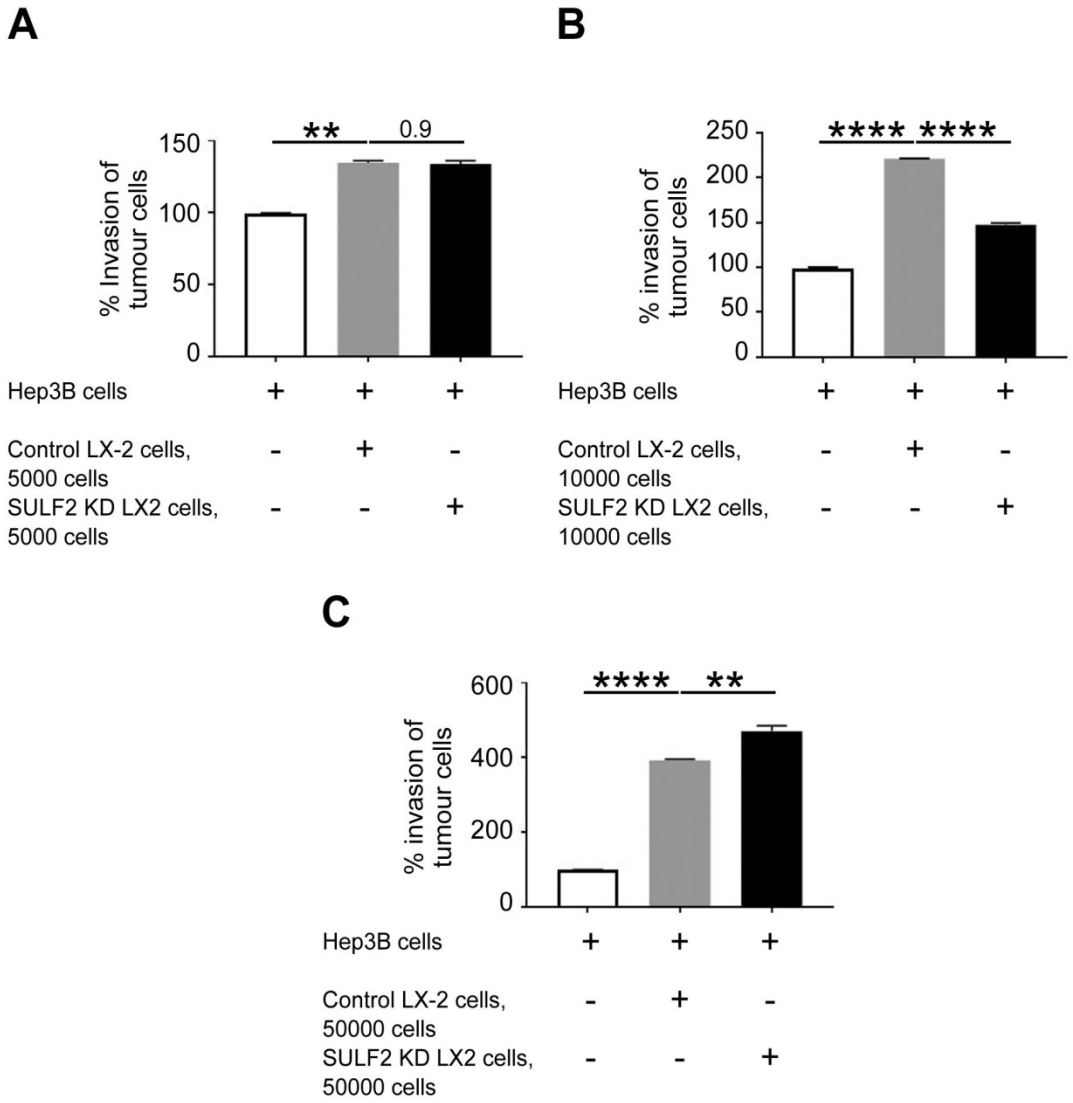

Figure 3.15 Optimisation for the tumour invasion assay Graphs show the invasion of the Hep3B cells (300000 cells/chamber) influenced by media only, SULF2-producing control LX-2 and SULF2 KD LX-2 cells at 5000 fibroblast cell/well **(A)**, 10000 fibroblast cell/well **(B)** and 50000 fibroblast cell/well **(C)**. Experiments were repeated twice (n=2) and data are presented as mean ± s.e.m, * p<0.05; ** p<0.01; *** p<0.001; ****p<0.0001**.**

LX-2 co-culture at this cell number. At 10000 fibroblast cell/well, secreted SULF2 significantly induced tumour cell invasion compared to tumour cells alone or tumour cells co-cultured with SULF2 KD LX-2 cells (p<0.0001) **(Figure 3.15)**. This effect was reversed when 50000 fibroblast cell/well were co-cultured with the tumour cells (p<0.0001 and 0.005 respectively) **(Figure 3.15)**. Taken together, co-culture of tumour cells with SULF2 +/- fibroblasts at 10000 fibroblast cell/well revealed the impact of SULF2 on Hep3B cell invasion.

The experiment was then repeated at 10000 fibroblasts cells/ well to confirm our finding and again control LX-2 induced the invasion of Hep3B cells compared either to tumour cells growing alone ($p<0.0001$) or compared to tumour cells co-cultured with SULF2 KD LX-2 ($P=0.0011$) **(Figure 3.16)**.

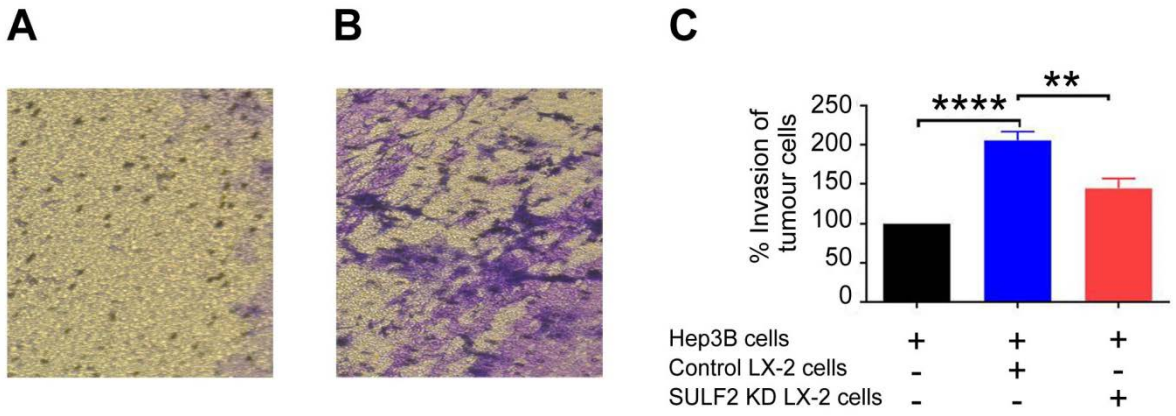

Figure 3.16 Impact of Stromal SULF2 on the invasion of the tumour cells Representative images show invasion of Hep3B cells (stained purple with crystal violet) into the outer surface of the Boyden chambers co-cultured with SULF2 KD LX-2 cells **(A)** and control LX-2 cells **(B)** at 10000 cells/well. Graph shows the impact of stromal SULF2 on the invasion of Hep3B tumour cells **(C)**. The experiment was repeated three times (n=3) and the data are presented as mean ± s.e.m, **p<0.01; ****p<0.0001.

3.4.7 The impact of stromal SULF2 on the proliferation of 3D tumour spheroids

3D tumour spheroids (organoids) are emerging models for improved assessment of drug effectiveness for number of reasons, as recently reviewed by Drost J and Clevers H[354]. Essentially, 3D models are considered more physiological models of human cancer, representing an advance in the preclinical models necessary for more effective translation of basic research into clinical practice. As stromal SULF2 modulated the viability/metabolic activity, proliferation, migration and invasion of the tumour cells on various 2D systems, we went on to investigate the interaction between SULF2 and tumour 3D spheroids in the TME niche *in vitro*.

Huh7 cells in hanging droplets failed to form spheres at 62, 125 and 250 cells/droplet after 4 days **(Figure 3.17)**. At 500, 750 and 1500 cells/droplet, cells started to form a partial sphere like structure that improved at 3000 cells/droplet. Conversely, increasing the number of cells to 6000 and 12000 generated irregular cell aggregates rather than rounded spheres **(Figure3.17)**.

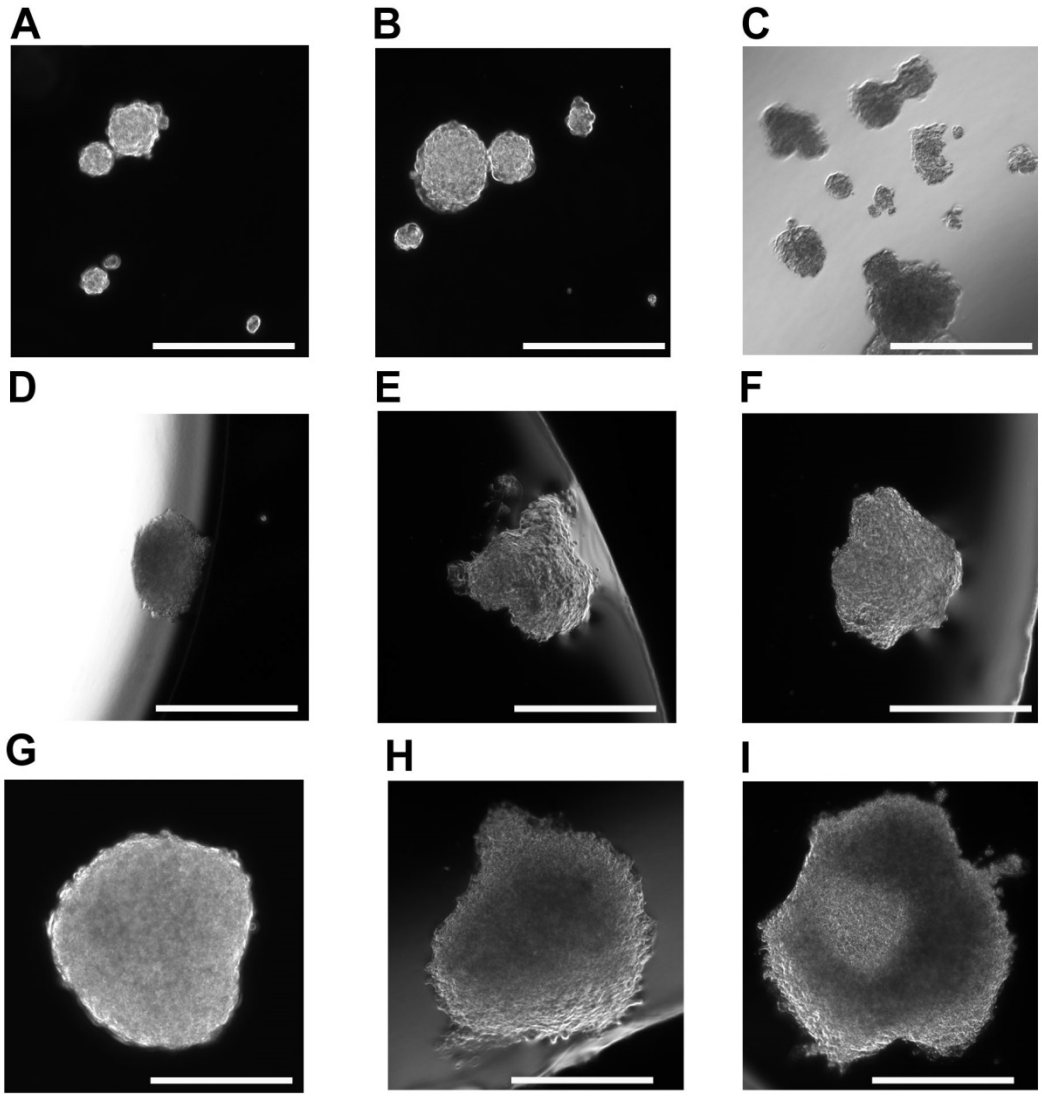

Figure 3.17 Characterisation of Huh7 3D spheroids Representative images show the formation of Huh7 spheroids in hanging droplets after 4 days at 62 **(A)**, 125 **(B)**, 250 **(C)**, 500 **(D)**, 750 **(E)**, 1500 **(F)**, 3000 **(G)**, 6000 **(H)** and 12000 **(I)** cells/droplet. Separate multi-spheres were formed at lower cell concentrations (**A, B, C** and **D**), while at slightly higher cell numbers, single spheres began to exist, yet with a less spherical configuration (**E and F**). Perfect rounded spheroids were formed at 3000 cells/droplets **(G)** and, hence, adapted for further Huh7 spheroids experiments. Less ideal cell aggregates were formed at higher cell concentrations (**H** and **I**). Experiment was repeated 10 times/condition (n=10).

Consistent with Huh7 cells, Hep3B cells also formed single nicely spherical spheroids with all cells attached to the main spheroid at 3000 cells/droplet after 3 days **(Figure 3.18)**. Hence, 3000 cells/hanging droplet was our standard number of cells for the 3D spheroid experiments.

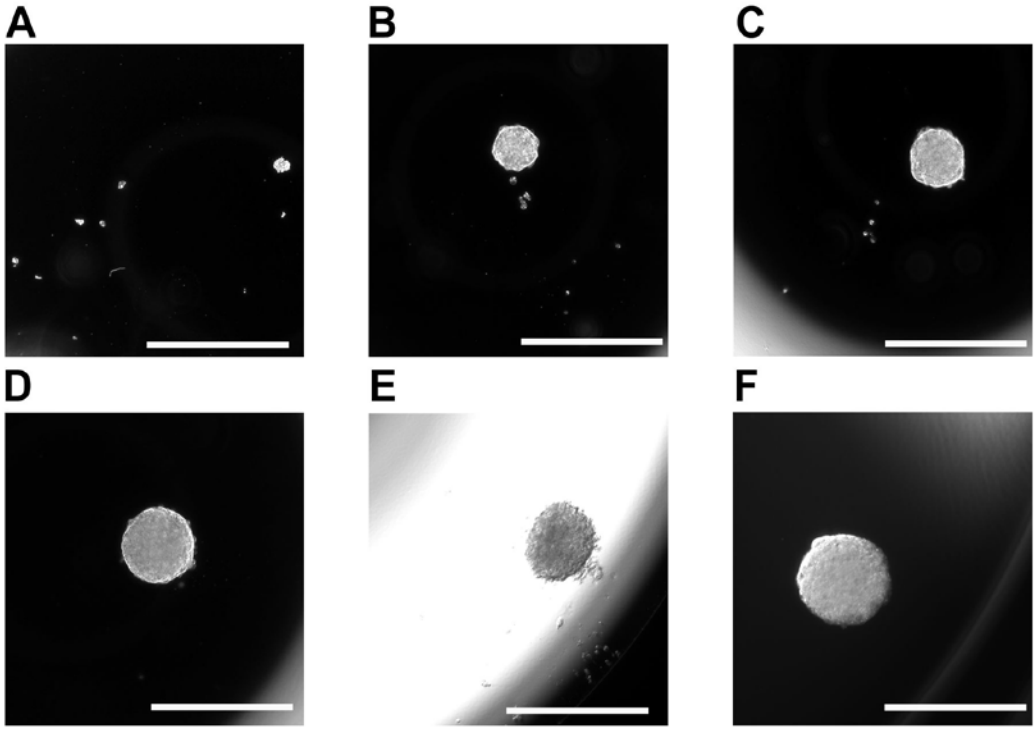

Figure 3.18 Characterisation of Hep3B 3D spheroids Representative images show the formation of Hep3B spheroids in hanging droplets after 3 days at 62 **(A)**, 125 **(B)**, 250 **(C)**, 500 **(D)**, 1500 **(E)** and 3000 **(F)** cells/droplet. Separate multi-spheres were formed at lower cell concentrations (**A-B** and **C**). Nicely rounded spheroids were formed at 500 and 3000 cells/droplets **(D** and **F).** Spheroids formed from 1500 cells/droplet were quite fragile **(E)**. 3000 cell/droplet was the cell concentration that was taken further. The experiment was repeated 10 times/condition (n=10).

3.4.7.1 The impact of stromal SULF2 on the proliferation of the 3D mixed spheroids

Huh7 and Hep3B HCC cells were mixed in 1:1 ratio with either control or SULF2 KD LX2, and cell suspension was left 3 days in hanging droplets to form spheres **(Figure 3.19)**.

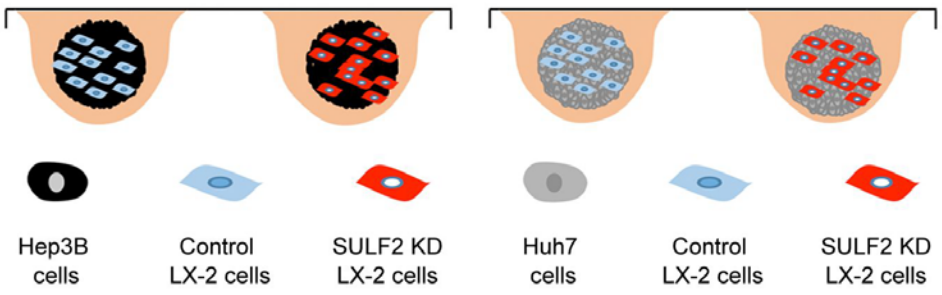

Figure 3.19 Schematic diagram for the mixed spheroid experiment 1500 cells from Hep3B (black cells) or Huh7 (grey cells) were mixed in 1:1 with either control LX-2 cells (blue) or SULF2 KD LX-2 cells (red). Cell slurry was suspended in hanging droplets with complete media for 3 days to form spheres. The impact of stromal SULF2 on mixed spheroids growth was measured via assessing the change of spheroids volume at days 4, 5, 7 and 8 compared to the initial volume at day3.

Huh7 cells directly mixed with control LX-2 cells in 1:1 ratio showed significant increase in the spheroid volume compared to Huh7 cell mixed with SULF2 KD LX-2 cells. This SULF2-derived proliferative effect was significant starting from 5 days after mixing both cell types together for the duration of the experiment (p=0.0089 at 5 days, p<0.0001 at 6 and 8 days) **(Figures 20,21)**. Notably, the change in the volume of the Huh7/control LX-2 mixed spheroids was

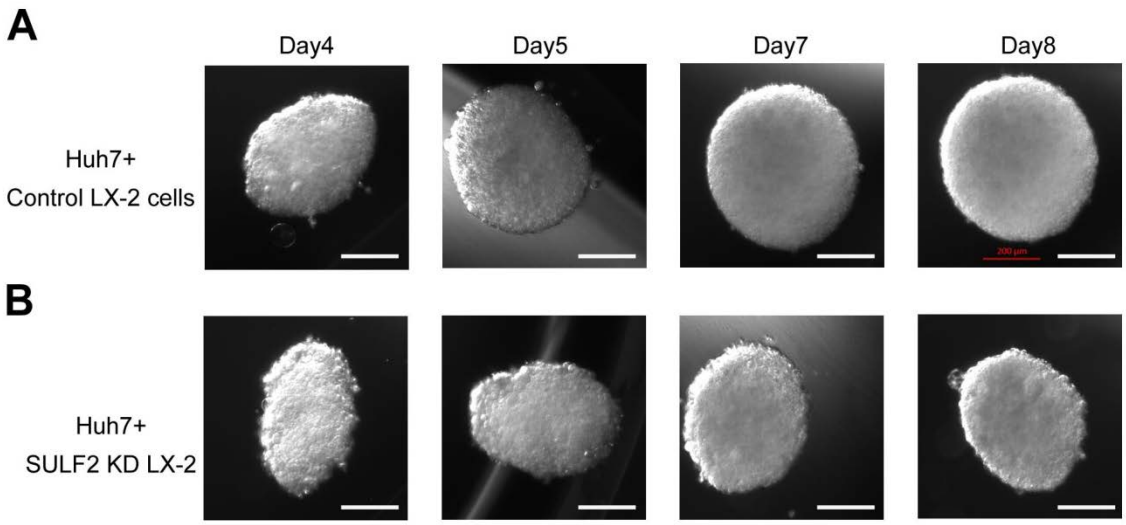

Figure 3.20 Growth rate of Huh7/LX-2 3D mixed spheroids was affected by stromal SULF2 Representative images show the growth of an Huh7/control LX-2 mixed spheroid **(A)** versus the growth of an Huh7/SULF2 KD LX-2 spheroid **(B)** starting from day 4 through to day 8. The experiment was repeated 10 times (n=10). Scale bars represent 200 microns.

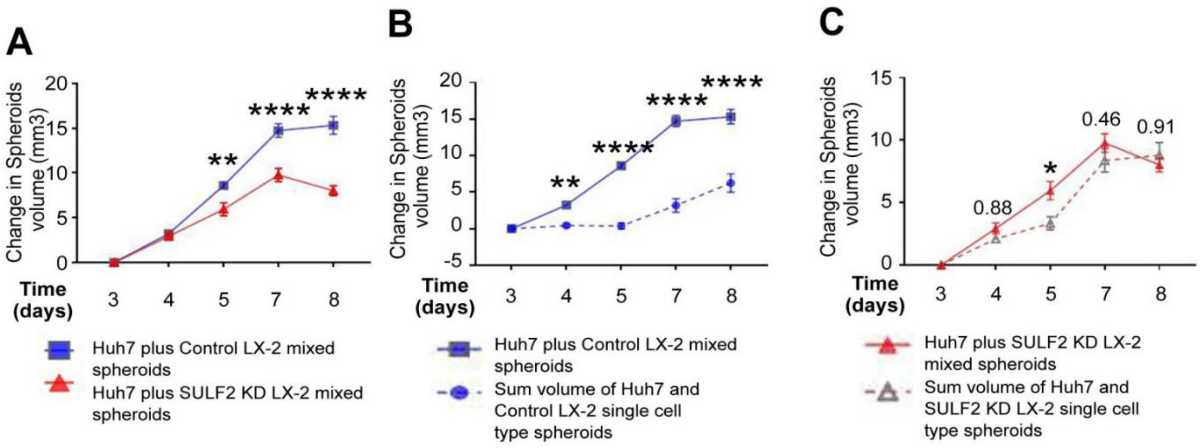

Figure 3.21 stromal SULF2 induced the proliferation of Huh7/LX-2 mixed 3D spheroids Graph shows the change of the volume of Huh7/control LX-2 3D spheroids (blue line) compared to Huh7/SULF2 KD LX-2 spheres (red line) from day 3 to day 8. Graph shows the change in the volume of Huh7/control LX-2 mixed spheroids (solid blue line) versus the sum change in the volume of Huh7 and control LX-2 single cell type spheroids (dashed blue line) **(B)**. Graph shows the change in the volume of Huh7/SULF2 KD LX-2 mixed spheroids (solid red line) versus the sum change in the volume of Huh7 and SULF2 KD LX-2 single cell type spheroids (dashed red line)**(C)**. The experiment was repeated 10 times/condition (n=10). Data are presented as mean ± s.e.m, **p<0.01; ****p<0.0001.

significantly higher than the volume of both Huh7 and control LX-2 matched single cell type spheroids (p=0.0059 at 4 days and p<0.0001 at 5, 7 and 8 days), while the growth rate of Huh7/SULF2 KD LX-2 was more or less the same (except at day 5) to the growth rate of the volume of both Huh7 and SULF2 KD LX-2 matched single cell types **(Figure 21)**.

Co-culturing Hep3B cells with either control LX-2 or SULF2 KD LX-2 in tumour/fibroblast mixed spheroids also showed the same SULF2-dependent growth (p=0.0052 at 5 days, p<0.0001 at 7 and 8 days) **(Figures 22-23)**. Again, this increase of spheroid volume was SULF2 dependent rather than being a result of the difference in the volume of spheroids formed from each individual cell type **(Figure 23)**.

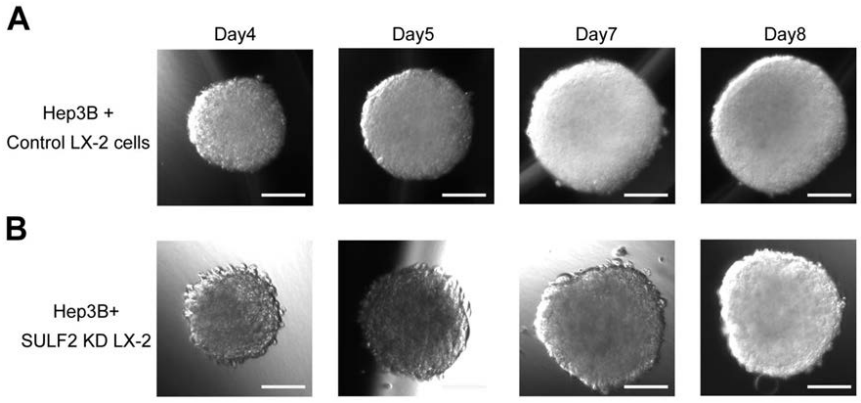

Figure 3.22 Growth rate of Hep3B/LX-2 3D mixed spheroids was affected by stromal SULF2

Representative images show the growth of a Hep3B/control LX-2 mixed spheroid **(A)** versus the growth of a Hep3B/SULF2 KD LX-2 spheroid **(B)** starting from day 4 to day 8. The experiment was repeated 10 times (n=10). Scale bars represent 200 microns.

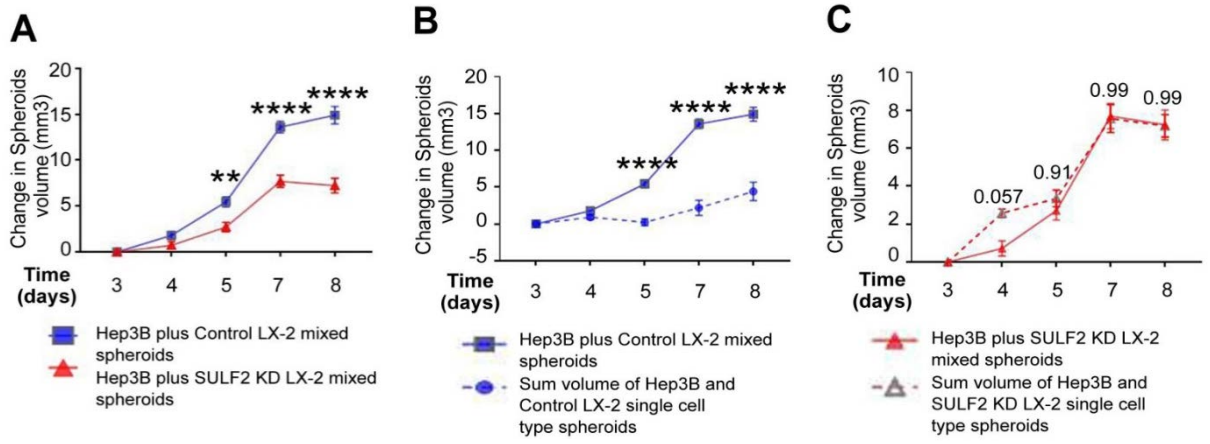

Figure 3.23 stromal SULF2 induced the proliferation of Hep3B/LX-2 mixed 3D spheroids

Graph shows the change of the volume of Hep3B/control LX-2 3D spheroids (blue line) compared to Hep3B/SULF2 KD LX-2 spheres (red line) from day 3 to day 8 **(A)**. Graph shows the change in the volume of Hep3B/control LX-2 mixed spheroids (solid blue line) versus the sum change in the volume of Hep3B and control LX-2 single cell type spheroids (dashed blue line) **(B)**. Graph shows the change in the volume of Hep3B/SULF2 KD LX-2 mixed spheroids (solid red line) versus the sum change in the volume of Hep3B and SULF2 KD LX-2 single cell type spheroids (dashed red line)**(C)**. The experiment was repeated 10 times/condition (n=10). Data are presented as mean ± s.e.m, **p<0.01; ****p<0.0001.

3.4.7.2 The impact of stromal SULF2 in CM on the proliferation of the 3D tumour spheroids

Hep3B single type 3D spheroids were bigger when grown in CM from control LX-2 cells or SULF2 KD LX-2 CM compared to Hep3B cells in non-fibroblast CM at day 5 ($p<0.0001$ and $p=0.0009$ respectively) **(Figure 3.24)**. Although Hep3B spheroids grew larger in control LX-2 CM than in SULF2 KD LX-2 CM, from day 4 until the end of the experiment, it was significant only at day 6 ($p<0.0001$). At this time point, the difference in spheroids grown in SULF2 KD LX-2 was not statistically significant compared to Hep3B in non-fibroblast CM ($P=0.078$). On the other hand, the difference between tumour spheroids in SULF2-containing CM was significantly different from tumour spheroids in non-fibroblasts CM ($P<0.0001$) **(Figure 3.25)**.

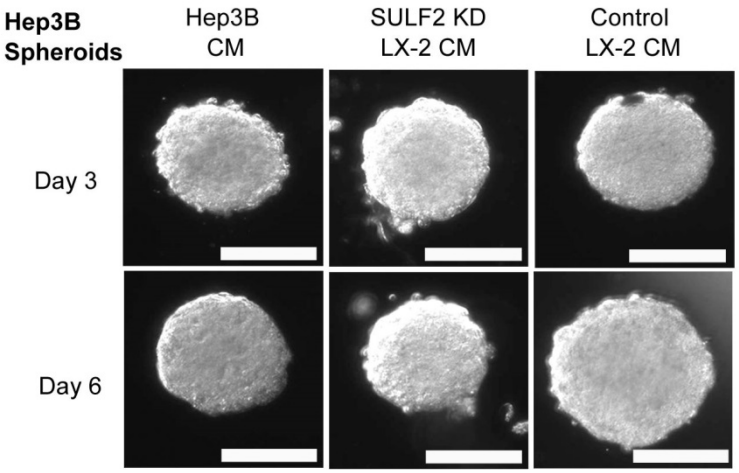

Figure 3.24 Growth rate of Hep3B 3D spheroids was affected by stromal SULF2. Representative images show the growth of matched Hep3B 3D spheroids in complete, non-fibroblast (left column), SULF2 KD LX-2 (middle column) and control LX-2 (right column) CM at 3 days (upper row) and 6 days (lower row) from pipetting individual cells in hanging droplets to form the 3D spheroids. Scale bars represent 200 microns. The experiment was repeated 10 times/time point/condition (n=10).

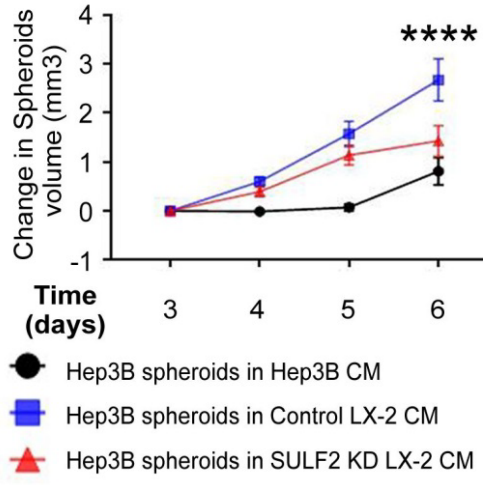

Figure 3.25 stromal SULF2 induced the proliferation of Hep3B 3D spheroids Graph shows the change in volume of Hep3B tumour spheroids when grown in non-fibroblast media (black line), CM from control LX-2 cells (blue line) or in CM from SULF2 KD LX-2 cells (red line). The experiment was repeated 10 times, per time point, per condition (n=10). Data are presented as mean ± s.e.m, ****$p<0.0001$ using two way anova.

3.4.8 The effect of SULF2 blockade on the behaviour of the tumour cells

A SULF2 monoclonal antibody (Ab) was used to test whether targeting SULF2 *in vitro* in the 3D spheroid system would limit their SULF2-dependent proliferation. The SULF2-dependent proliferation of Hep3B spheroids in control LX-2 CM was significantly diminished at 10, 20 and

50 ng/ml of SULF2 Ab at days 4 (p=0.0034, p=0.0054 and p<0.0001), 5 (p<0.0001 for all) and 6 (p<0.0001 for all) **(Figure 3.26)**. The isotype control IgG Ab did not affect the growth of Hep3B spheroids at 10 ng/ml (p=0.9967 at day 4, p=0.91 at day 5 and p=0.08 at day 6), but at higher concentrations (20 and 50 ng/ml) there was a significant, dose dependent, non-SULF2 related growth inhibitory effect on the Hep3B spheroids, attributed to toxicity **(Figure 3.26)**. As a result, 10ng/ml for both antibodies was chosen as the optimal concentration in further experiments on Hep3B spheroids.

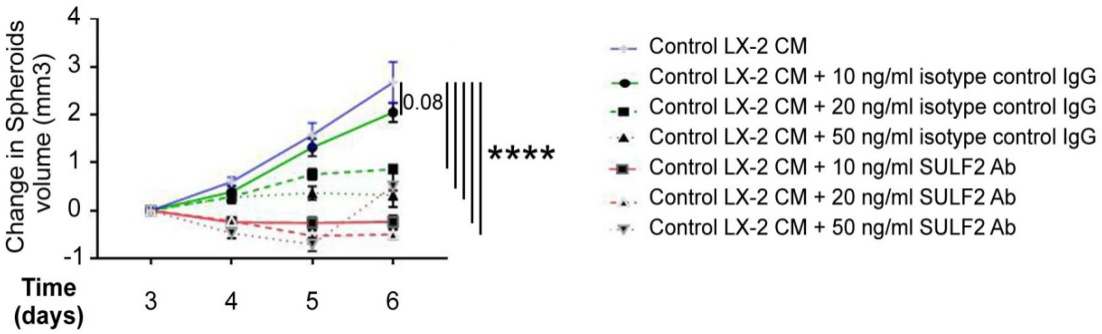

Figure 3.26 Optimisation of SULF2 Ab concentration Graph shows the growth of Hep3B spheroids in control LX-2 CM (blue line), in control LX-2 plus SULF2 Ab at 10 ng/ml (solid red line), 20 ng/ml (dashed red line) or 50 ng/ml (dotted red line) concentration, or in control LX-2 cells plus isotype control IgG at 10 ng/ml (solid green line), 20 ng/ml (dashed green colour) or 50 ng/ml (dotted green line). The experiment was repeated 10 times/condition (n=10). Data are presented as mean ± s.e.m, ****p<0.0001.

Hep3B spheroids grown in CM from either control or SULF2 KD LX-2 cells were subsequently treated with either the SULF2 or IgG control antibody at 10ng/ml. Confirming the previous result, the SULF2 Ab significantly diminished the SULF2-dependent growth of Hep3B spheroids (p<0.0001), with no effect on the growth of spheroids in SULF2 KD CM (P<0.99) **(Figure 3.27)**. The growth of the tumour spheroids in both CMs was not affected by adding the IgG control Ab (p<0.99) **(Figure 3.27).**

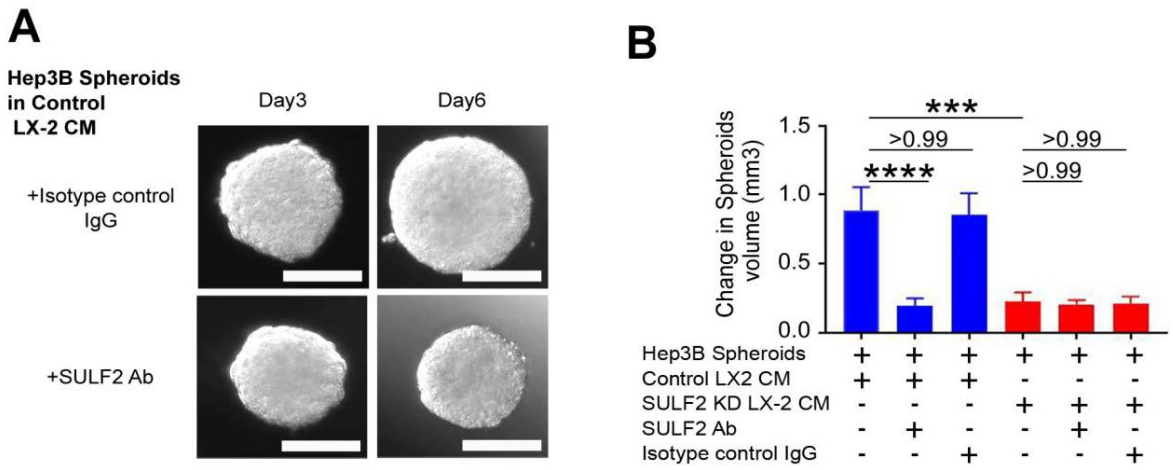

Figure 3.27 Blockade of stromal SULF2 diminished the growth of Hep3B tumour spheroids Representative images show the growth of matched Hep3B spheroids in the SULF2 containing stromal CM in presence of either control isotype IgG (upper row) or SULF2 Ab (lower row) at day 3 (left column) and day 6 (right column) after hanging individual Hep3B cells to form 3D spheroids **(A)**. Graph shows the effect of treating Hep3B spheroids grown CM from control or SULF2 KD with either SULF2 or isotype control IgGs at day 6 **(B)**. The experiment was repeated 10 times/condition (n=10). Data are presented as mean ± s.e.m, ***p<0.001;****p<0.0001.

The growth of the Huh7 spheroids (with a continuous production and secretion of tumour SULF2 in their media) was blocked by adding the SULF2 Ab (p=0.0074 at day 6 and p<0.0001 at day7), but not by adding the isotype control IgG Ab (p=0.37 at day6 and p=0.08 at day7) **(Figure 3.28)**.

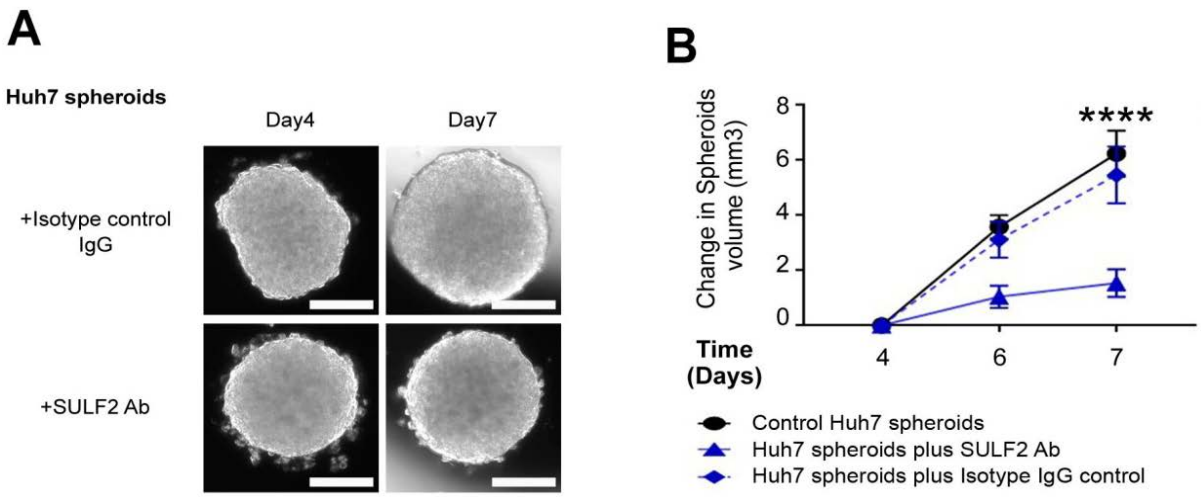

Figure 3.28 Blockade of tumour SULF2 diminished the growth of Huh7 spheroids Representative images show the growth of matched Huh7 spheroids in the presence of either control isotype IgG (upper row) or SULF2 Ab (lower row) at day 4 (left column) and day 7 (right column) after hanging individual Huh7 cells to form 3D spheroids **(A)**. Graph shows the effect of treating Huh7 spheroids with either the SULF2 or isotype control IgG at days 6 and 7 **(B)**. The experiment was repeated 10 times/condition (n=10). Data are presented as mean ± s.e.m, ****p<0.0001.

Moreover, the growth promoting effect of Huh7 CM (SULF2 positive) on the Hep3B spheroids ($p<0.0001$) was significantly diminished by addition of the SULF2 Ab ($p<0.0001$) **(Figure 3.29)**.

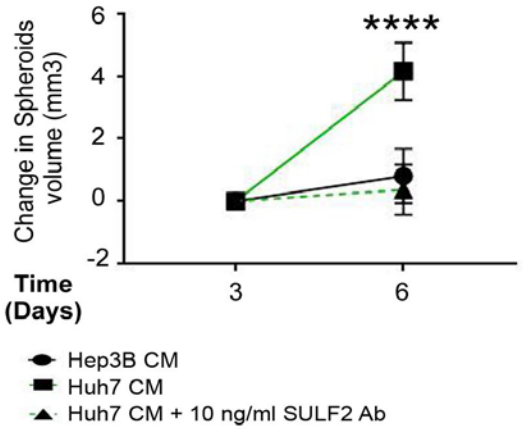

Figure 3.29 Blockade of tumour SULF2 diminished the growth of Hep3B spheroids Graph shows the effect of treating Hep3B spheroids in Huh7 CM with either SULF2 or isotype control IgG at day 6. Experiment was repeated 10 times/condition (n=10). Data are presented as mean ± s.e.m, ****$p<0.0001$.

3.4.9 Stromal SULF2 reduced the sensitivity of tumour cells to sorafenib therapy

Sorafenib is the standard of care, 1st line therapy for patients with advanced HCC, although the benefit afford to most patients is modest[349]. There are no clinically useful biomarkers to predict response and novel approaches to select monotherapies or combination therapies are needed for this group of patients. Elevated SULF2 expression in tumour cells was associated with advanced stage disease, while elevated in either tumour cells or CAFs it was associated with poorer patient outcome. Hence we investigated whether SULF2 had a modulatory effect on the response of tumour cells to sorafenib therapy.

To test the cytostatic/cytotoxic effect of sorafenib on both Hep3B and Huh7, the cells were treated with different concentrations of sorafenib and a viability assay was performed **(Figure 3.30).** Viability of both cell lines was reduced by sorafenib in a dose dependent manner as measured by an MTT viability assay. Huh7 cells were less sensitive to sorafenib treatment than the Hep3B cells, demonstrated by more viable residual Huh7 cells than Hep3B cells at 5 µM sorafenib at both 48 (55.2% versus 42.2%) and 72 hours (46.2% versus 20.9%). Huh7 have more endogenous expression of SULF2 than Hep3B cells, potentially rendering them more resistant to sorafenib, was one potential explanation **(Figure 3.30)**.

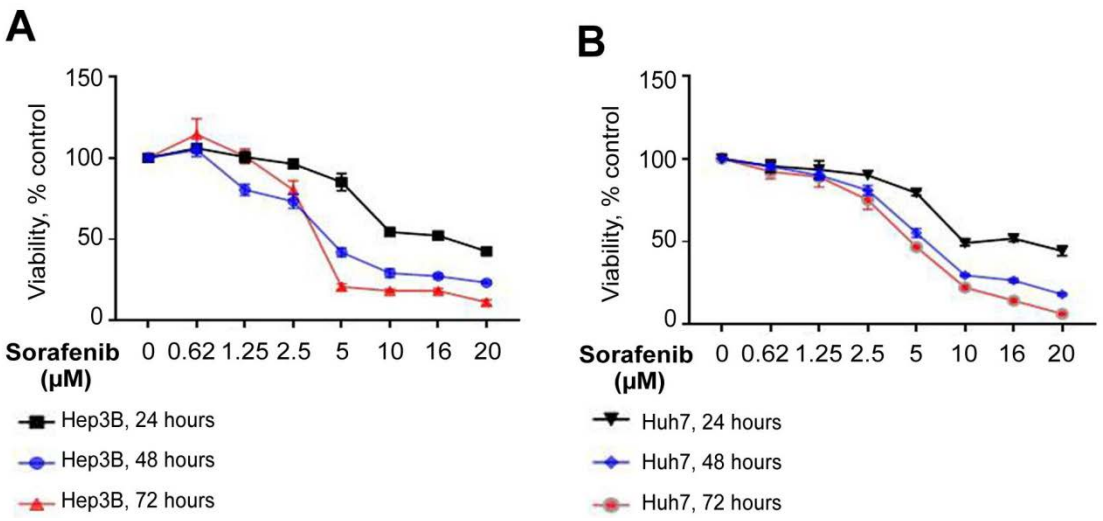

Figure 3.30 viability of Hep3B and Huh7 in response to sorafenib treatment Graphs show viability of Hep3B **(A)** and Huh7 **(B)** treated with 0.62, 1.25, 2.5, 5, 10, 16 and 20 μM sorafenib for 24 hours (black line), 48 hours (blue line) and 72 hours (red line) calculated as percentage viability compared to control cells treated with DMSO. Read-out was MTT cell viability assay. The experiment was repeated 3 times (n=3). Data are presented as mean ± s.e.m.

In BrdU proliferation assay of the tumour cells co-cultured with fibroblast in the 2D co-culture system, sorafenib failed to significantly reduce the proliferation of Hep3B cells co-cultured with control LX-2 cells compared to the co-cultured cells treated with DMSO only (p=0.23). However, Hep3B cells co-cultured with SULF2 KD LX-2 cells were sensitive to sorafenib treatment compared to cells in DMSO (P=0.0085). In addition, the proliferation of the sorafenib-treated control non-co-cultured Hep3B cells was also significantly reduced compared to DMSO-treated cells (p=0.02) **(Figure 3.31)**.

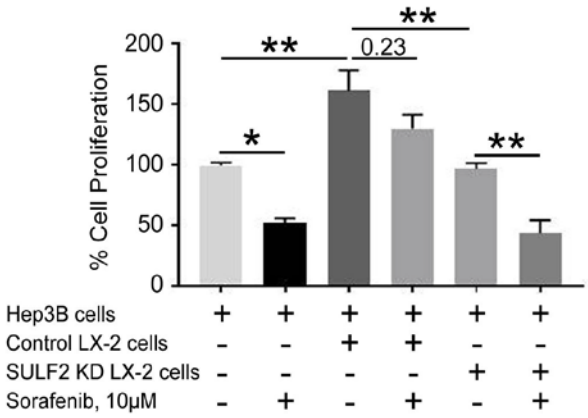

Figure 3.31. The impact of stromal SULF2 on Hep3B cells response to sorafenib Graph shows the proliferation of Hep3B cells co-cultured with either control LX-2 or SULF2 KD LX-2 cells in the presence of sorafenib treatment, expressed as % BrdU proliferation compared to Hep3B treated with DMSO only. The experiment was repeated 3 times (n=3). Data are presented as mean ± s.e.m, *p<0.05;**p<0.01.

Interestingly, Huh7 cells co-cultured with control LX-2 cells with or without sorafenib proliferated at the same rate (p<0.99). Tumour cells responded to sorafenib treatment when

co-cultured with SULF2 KD LX-2 compared to cells treated with the vehicle, yet this did not reach statistical significance (p=0.6). Sorafenib had the same trend with no statistical significance in the non-co-cultured Huh7 cells (p=0.6), supporting a role for SULF2, either from tumour cells or LX-2 cells, in sorafenib resistance *in vitro* **(Figure 3.32)**.

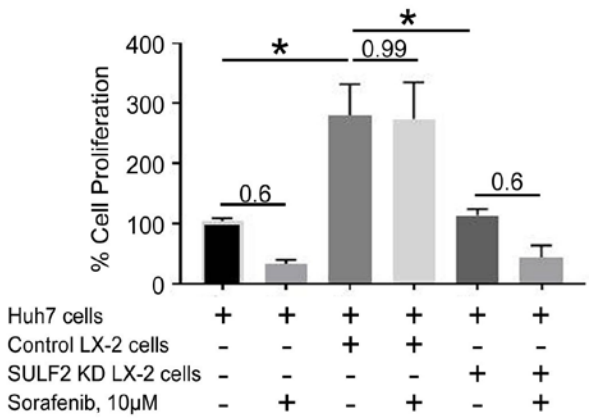

Figure 3.32. The impact of stromal SULF2 on Huh7 cells response to sorafenib Graph shows the proliferation of Huh7 cells co-cultured with either control LX-2 or SULF2 KD LX-2 cells in the presence of sorafenib treatment, expressed as % BrdU proliferation compared to Huh7 treated with DMSO only. The experiment was repeated 3 times (n=3). Data are presented as mean ± s.e.m, *p<0.05.

Sorafenib exerted its cytostatic/cytotoxic effect on the 3D Hep3B spheroids at 4 different concentrations ranging from 1.25 to 10 μM **(Figure 3.33)**. However, Hep3B spheroids in CM

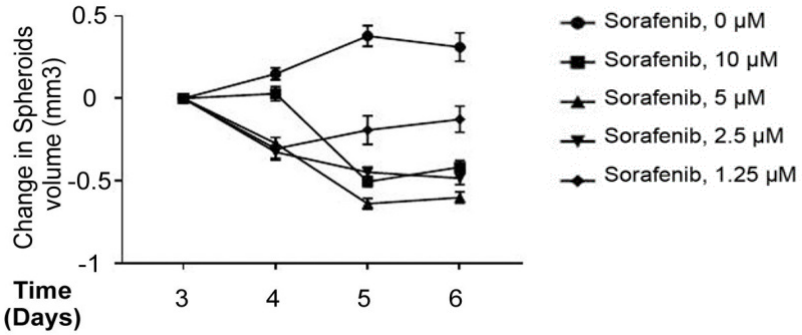

Figure 3.33. Sorafenib diminished the proliferation of Hep3B tumour spheroids Graph shows the proliferation of Hep3B spheroids, as a change in spheroid volume, treated with DMSO, 1.25, 2.5, 5 and 10 μM sorafenib from day 3 to day 6 after hanging individual cells to form spheres. Experiment was repeated 10 times/condition (n=10).

from control LX-2 cells proliferated in the same rate with/without adding sorafenib to the CM at 1.25, 2.5 and 5 μM. In the absence of SULF2 from the stromal CM, the anti-tumour effect of sorafenib on the spheroids was restored, compared to spheroids grown in SULF2 KD CM with DMSO (p=0.0029)**(Figures 3.34 and 3.35).**

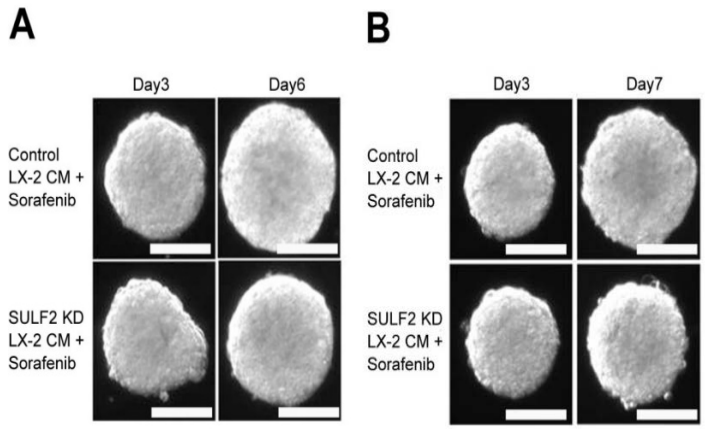

Figure 3.34 Stromal SULF2 decreased the sensitivity of Hep3B tumour spheroids to sorafenib treatment at 5 and 2.5 µM concentrations. Representative images show the growth of matched Hep3B spheroids in CM from control LX-2 (upper rows) or SULF2 KD LX-2 cells (lower rows) at day 3 (left rows) and 6 days (right rows) after adding 5 µM **(A)** or 2.5 µM sorafenib **(B)**. Experiment was repeated 10 times/condition (n=10).

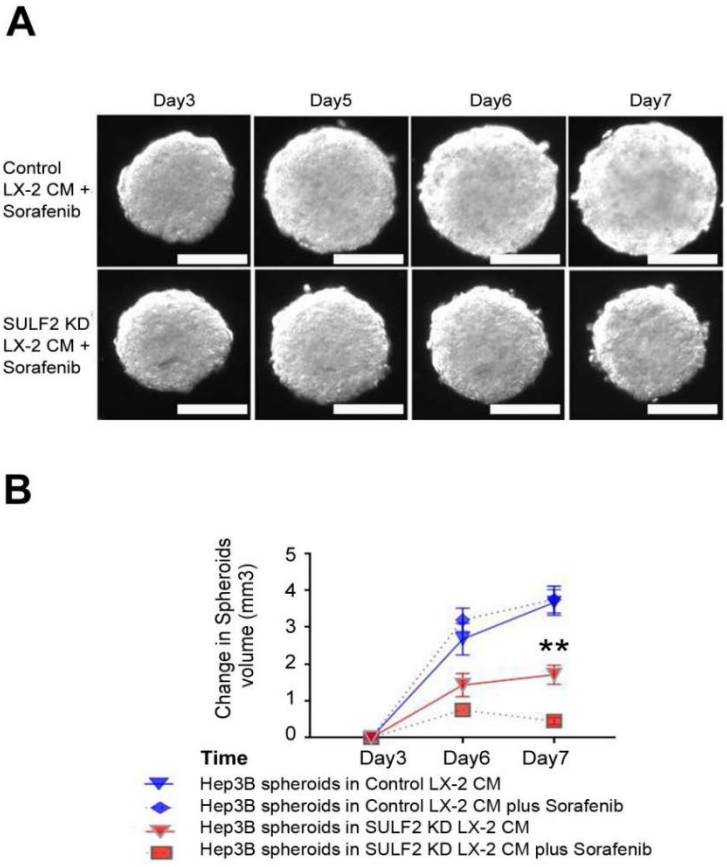

Figure 3.35 Stromal SULF2 decreased the sensitivity of Hep3B tumour spheroids to sorafenib treatment at 1.25 µM concentration Representative images show the growth of matched Hep3B spheroids in CM from control or SULF2 KD LX-2 cells in the presence of 1.25 µM sorafenib **(A)**. Spheroid proliferation was comparable in presence or absence of sorafenib in control LX-2 CM. The cytostatic effect of sorafenib was restored when spheroids were cultured in SULF2 KD LX-2 CM. Graph shows the proliferative rate of Hep3B spheroids, as a change in spheroid volume, treated with 1.25 µM sorafenib from day 3 to day 7 after hanging individual cells to form spheres **(B)**. The experiment was repeated 10 times/condition (n=10). Data are presented as mean ± s.e.m, **p<0.01.

Blockade of stromal SULF2 in the control LX-2 CM using SULF2 Ab retrieved the sorafenib impact on the growth of the Hep3B spheroids (p<0.001) **(Figure 3.36)**.

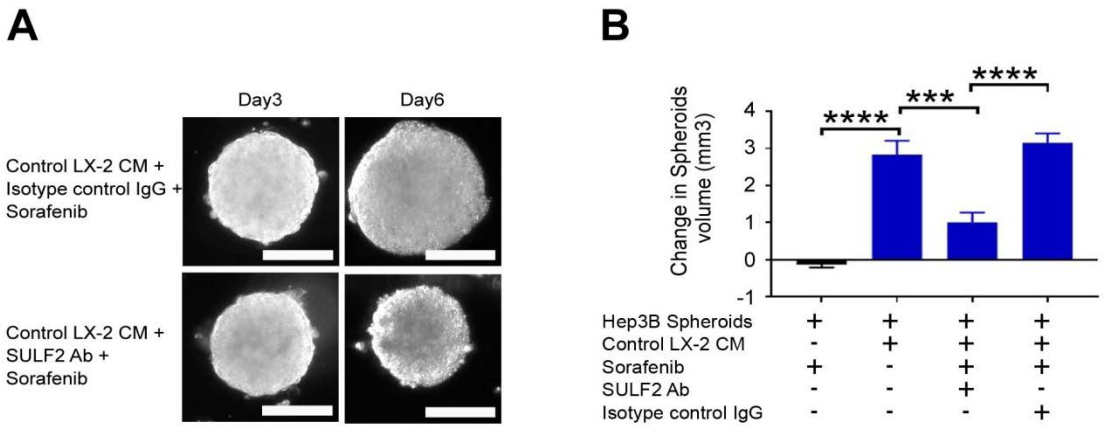

Figure 3.36 stromal SULF2 induced resistance to sorafenib was inversed by blocking SULF2
Representative images show the growth of matched Hep3B spheroids in CM from control LX-2 cells in the presence of 1.25 µM sorafenib and SULF2/isotype control IgG **(A)**. Spheroids proliferated with the same rate in presence or absence of sorafenib in control LX-2 CM with the Isotype control IgG. The cytostatic effect of sorafenib was restored when spheroids were cultured in control LX-2 CM plus SULF2 Ab. Graph shows the proliferation of Hep3B spheroids, as a change in spheroid volume, treated with 1.25 µM sorafenib ± SULF2/isotype control IgG at day 6 after hanging individual cells to form spheres **(B)**. The experiment was repeated 10 times/ condition (n=10). Data are presented as mean ± s.e.m, ***p<0.001; ****p<0.0001.

The potential translational impact of these findings was investigated *in vivo* by performing SULF2 IHC staining in biopsies from nine patients with HCC who received sorafenib treatment. Biopsies were at the time of diagnosis and the patients were classified as responders if they had a partial response or stable disease for at least 3 months. Those patients who showed progression of their disease on imaging at 3 month or who did not tolerate the treatment, were classified as non-responders. In one patient sorafenib was stopped because of toxicity. In six patients there was evidence of progression on their scan at 3 months. These patients were classed as non-responders and all of them had SULF2 positive CAFs present on their tumour biopsy **(Figure 3.37)**. In one of these patients, CAF SULF2 positivity was scant, but the HCC cells were SULF2 positive. By contrast, two patients who maintained stable disease on imaging at 6 months, classed as responders, had no evidence of SULF2 positive CAFs **(Figure 3.37)**. The observed difference in SULF2 expression in non-responders versus responders in this pilot study (non-responders 7/7; responders 0/2; p=0.028, Pearson Chi-Square), in combination with the *in vitro* experiments, these data, support a role for presence of stromal SULF2 in the mediation of sorafenib resistance.

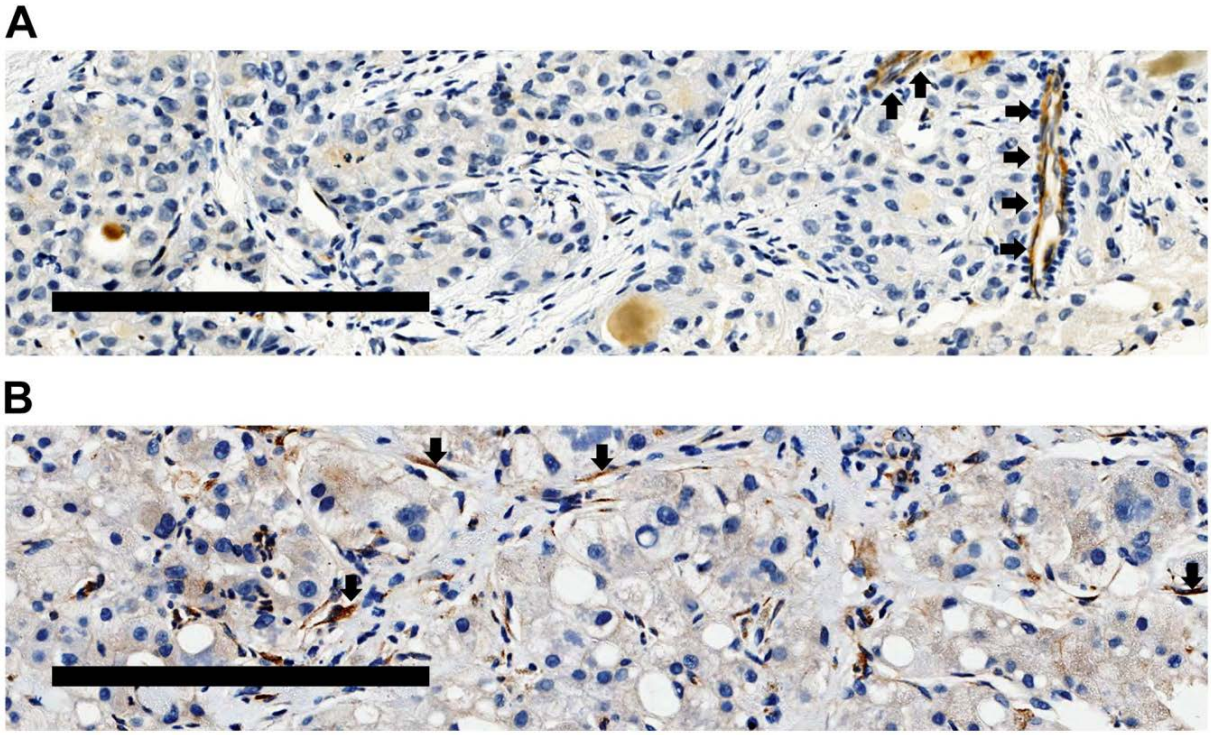

Figure 3.37 Expression of SULF2 in biopsies from sorafenib treated HCC patients Representative images show SULF2 IHC staining in biopsies from a sorafenib-responder **(A)** versus a sorafenib non-responder **(B)**. The presence of endothelial cell SULF2 is marked with black arrows and served as an internal positive IHC control. Scale bars are equivalent to 200 microns (n=9).

3.5 Discussion

The realisation and understanding of the importance of the tumour microenvironment in the development, behaviour and progression of HCC has steadily increased in the last decade. This has followed the application of sophisticated and high-throughput multi-Omics technologies – focused initially on characterising the molecular aberrations in the tumours - opening the door to a new era of research, but largely failing to deliver significant improvements in prognosis for patients with liver cancer. It is recognised that the treatment paradigm of targeting the highly proliferative tumour cells may be insufficient and that strategies aimed at targeting components of the TME, either alone or in combination, may be more beneficial. While the immune TME has received a lot of attention, CAFs are at the heart of the TME and help to nourish the tumour cells and stimulate their growth. CAFs are the predominant non-parenchymal cells in the TME and can modulate the behaviour of the neighbouring tumour cells[355]. They are believed to be derived from the hepatic stellate cells (HSC)[356]. The overall predictive value of both HSC and CAFs in patients with HCC was described previously in an elegant study that identified an activated hepatic stellate cell (A-HSC) gene signature in the

non-tumour tissues, but not the matched tumour pairs, that could predict the prognosis of well-defined HCC patients with metastasis promoting microenvironment. The gene signature was associated with the presence of cirrhosis, the size of the tumour and with vascular invasion in a univariate analysis and was independently associated with poorer survival in a multivariate analysis[357]. Similarly, another research group defined a 122-HSC gene signature that included many ECM proteins related to fibrosis[358]. Combining the 122-HSC gene signature with bilirubin and platelet count created a prognostic index that was associated with HCC, Child-Pugh class and overall survival[358]. Notably, presence of αSMA in the peritumoural area as a predictor of poorer prognosis in HCC patients after curative resection has been recognised for over a decade[351].

Here, we have introduced SULF2 as a key regulator of TME associated HCC progression. SULF2 was upregulated in 58% of diagnostic biopsies from HCC patients. Of these cases, SULF2 expression was elevated in the tumour cells in 15% of patients. Albeit small numbers, tumour SULF2 was associated with T2DM, tumour size, AFP level and TNM stage. Notably, SULF2 was upregulated in 52% of cases in the αSMA positive CAFs and this unique pattern was independently associated with poorer patient survival as shown by multivariate analysis. The pattern of SULF2 expression in the adjacent non-tumour tissues was different from the tumour tissue. In the non-tumour tissue, SULF2 was expressed in the smooth muscle cells lining the portal tract arteries, in the endothelial cells, in the sinusoidal cells and in the immature bile ductules, raising a potential role of SULF2 in both the premalignant as well as in the tumour microenvironments. The expression of SULF2 in more than half of the biopsies together with its predictive significance in the CAFs was the justification for the subsequent thorough investigation of the role of CAF-derived SULF2 and its impact on the behaviour of the tumour cells.

To discern the role of SULF2 from stromal cells on the behaviour of the tumour cells, two different HCC cell lines with different levels of SULF2 were co-cultured with SULF2 producing/SULF2 deficient LX-2 cells or CM. In our 2D trans-well co-culture system, secreted stromal SULF2 induced the viability and the proliferation of the HCC cells regardless of their SULF2 status. An advantage of using the 2D trans-well system was that the two different cell types were kept physically separate, although cultured as a monolayer, enabling us to ascertain that the changes observed in cell phenotype were mediated by soluble

communication, rather than direct cell-cell contacts. Stromal SULF2 also increased the migration of the SULF2 null Hep3B cell line, supporting a role promoting invasive capacity.

Advantages of the 2D systems used include them being less expensive and convenient, as they are relatively easily handled. On the other hand, 2D systems have significant limitations, the major one being that cells grown in 2D systems, as monolayers on polystyrene surfaces, do not recapitulate the *in vivo* conditions[359]. Monolayer cultures cannot mimic the actual 3D cell aggregates that impact penetration and response of solid tumours to anti-cancer therapies. The rounded 3D structured spheroids are an excellent alternative to the conventional 2D cultures, especially in the field of cancer research, due to their ability to recreate the structural features of human tumour *in vitro*. 3D spheroids reportedly recapitulate essential features of human malignancies, including tumour 3D multi-layered composition, physical cell-cell interaction in the tumour context, deposition of ECM protein as well as response to anti-cancer drugs[340, 359, 360].

Stromal SULF2 induced the growth of the tumour 3D spheroids, either when directly mixing tumour/fibroblasts cells together, or by growing tumour 3D spheroids in stromal CM with different levels of SULF2. These 3D data complimented our 2D results. Moreover, blockade of SULF2 from the SULF2-rich stromal or tumour CM successfully limited SULF2-dependent growth on the tumour 3D spheroids. Tumour 3D spheroids responded to sorafenib treatment in a dose dependent fashion, but interestingly, the presence of stromal SULF2 in the CM converted this drug-responsive phenotype into a drug-resistant one. Finally, in a small cohort of patients, we could identified fewer SULF2 positive CAFS in sorafenib responders.

In conclusion, SULF2 mainly upregulated in the CAFs in HCC, was associated with poor outcome in HCC patients. *In vitro* studies showed that stromal SULF2 could induce a more aggressive tumour cell phenotype by increasing tumour cell viability, proliferation, migration, invasion and resistance to therapy.

Chapter 4: The mechanistic role of SULF2 in HCC progression and therapy resistance

4.1 Background

The potential importance of SULF2 in HCC had been previously reported by the Roberts's group, in two successive publications in 2008 and 2010, implicating it in the regulation of FGF/AKT and β-catenin signalling pathways[273, 304]. They showed that overexpression of SULF2 in cell lines facilitated the binding of FGF2 to its receptor on the tumour cells. This binding then induced the phosphorylation and activation of the AKT oncogenic pathway. In the same context, they demonstrated the SULF2-dependent upregulation of GPC3 using knock-down and overexpression experiments in cell lines with different levels of SULF2. They linked the two arms of their study by showing that upregulation of GPC3 mediated by tumour SULF2 increased the autocrine binding of FGF2 to FGF receptors on the tumour cell surface[304]. In the follow up paper in 2010, they focused on the role of SULF2 in activating the β-catenin pathway, known to be deregulated in more than 30% of HCC[273]. Activation mutation in β-catenin, restricting it to the nucleus of the tumour cells, can be detected in about 25% of HCC and promotes cell survival and proliferation[361]. Alternatively, binding of different Wnt ligands to the Frizzled receptor on the tumour cell surface can liberate wild-type β-catenin from the receptor complex enabling translocation to the nucleus and activation of the Wnt/β-catenin pathway[362]. Using a cell line system together with *in vivo* studies in nude mice, Roberts *et al* showed that SULF2 induced endogenous levels of Wnt3a, one of the Wnt ligands that activates Wnt/β-catenin signalling, and that this effect was boosted by adding exogenous Wnt3a recombinant protein. SULF2-induced upregulation of GPC3 further facilitated the binding of Wnt3a to the Frizzled receptor, activating the downstream pathway[273]. The group went on to report that overexpression of SULF2 protected tumour cell lines from cell death and apoptosis induced by inhibitors to PI3K, JNK and ERK pathways. SULF2 knock-down abolished the expression of cyclin-D1 and BCL-2 and induced the expression of the pro-apoptotic protein BAD. This was driven via P13K/AKT pathway activation *in vitro*[305].

Earlier studies predating any focus on HCC had revealed a role for SULF2 in the liberation of important angiogenic and chemotactic factors from cell surfaces[298]. SULF2 removal of sulfate groups from the 6-O-positions of HSPGs immobilized heparin, releasing VEGF, CXCL12 and FGF1 from their heparin binding site to activate their downstream targets[298]. Studies reporting

factors released or secreted into the microenvironment, such as SULF2, which itself promotes the release of other factors from the ECM, are of particular relevance to the search for serum level biomarkers[363]. Serum levels of these factors offer less invasive tools, potentially for predicting patient prognosis, but also for enrichment, by predicting patients that may respond to a therapeutic strategy targeting SULF2.

Another SULF2 regulated signalling pathway to highlight is that of TGF-β. As previously described in chapter 3, SULF2 KO mice were protected from DEN-induced liver tumorigenesis compared to their WT control mice. *In vitro* and *in vivo* studies showed that SULF2 regulates the expression and secretion of certain angiogenic factors involving POSTN[301]. This effect was initiated via SULF2-dependent desulfation of TGFBR3 receptor releasing the bound TGFB1 that, in turn, induced the expression of *POSTN* activating ERK and Focal adhesion kinase (FAK) pathways in the endothelial cells[301].

All the cited studies relied on transcriptomic data to quantify SULF2, with limited focus on its cellular origin. Therefore the role of CAF-derived SULF2, CAFs being the predominant source of SULF2 in the HCC TME, as described in Chapter 3, has not been previously studied. Characterising the cellular source may inform best way of targeting the protein in the clinical context. Importantly, mechanistic pathways often have cell-type specific, even contradictory, roles[137]. In Chapter 3 we showed that stromal SULF2 induced tumour cell proliferation, migration, invasion and resistance to sorafenib treatment. The focus here was to explore the mechanisms involved – using *in vitro* models, but also publically available transcriptome data.

4.2 Chapter 4 aim

4.2.1 To explore the impact of SULF2 on different oncogenic, cell survival and chemoresistance signalling pathways in HCC.

4.3 Investigation of the impact of SULF2 KD from LX-2 fibroblasts

4.3.1 The effect of SULF2 levels on the expression of different mesenchymal markers and inflammatory cytokines

In human HCC, the CAFs were the predominant cellular source of SULF2 within the TME. We initially set out to understand the role of autocrine stromal SULF2 signalling on CAFs. Successful KD of SULF2 was confirmed by q-PCR **(Figure 4.1A)** as well as by WB and ELISA as shown in Chapter3 in **Figure3.6**. SULF2 KD from LX-2 fibroblasts led to the down-regulation of *PDGFRβ* **(Figure 4.1B)** and *COL1α1* **(Figure 4.1C)** expression, with no impact on the expression of the mesenchymal markers *αSMA* **(Figure 4.1D)**, *VIM* **(Figure 4.1E)** and *TIMP1* **(Figure 4.1F)**. This implied that SULF2 regulated a specific phenotype within the stromal cells, potentially mediated by PDGFRβ signalling. An increase in collagen deposition and tissue stiffness has been previously reported to be strongly associated with poor disease outcome[226]. Notably, *αSMA, TIMP1* and *VIM* levels in LX-2 cells were not SULF2 dependent, indicating that SULF2 KD did not affect the activation status of the fibroblasts.

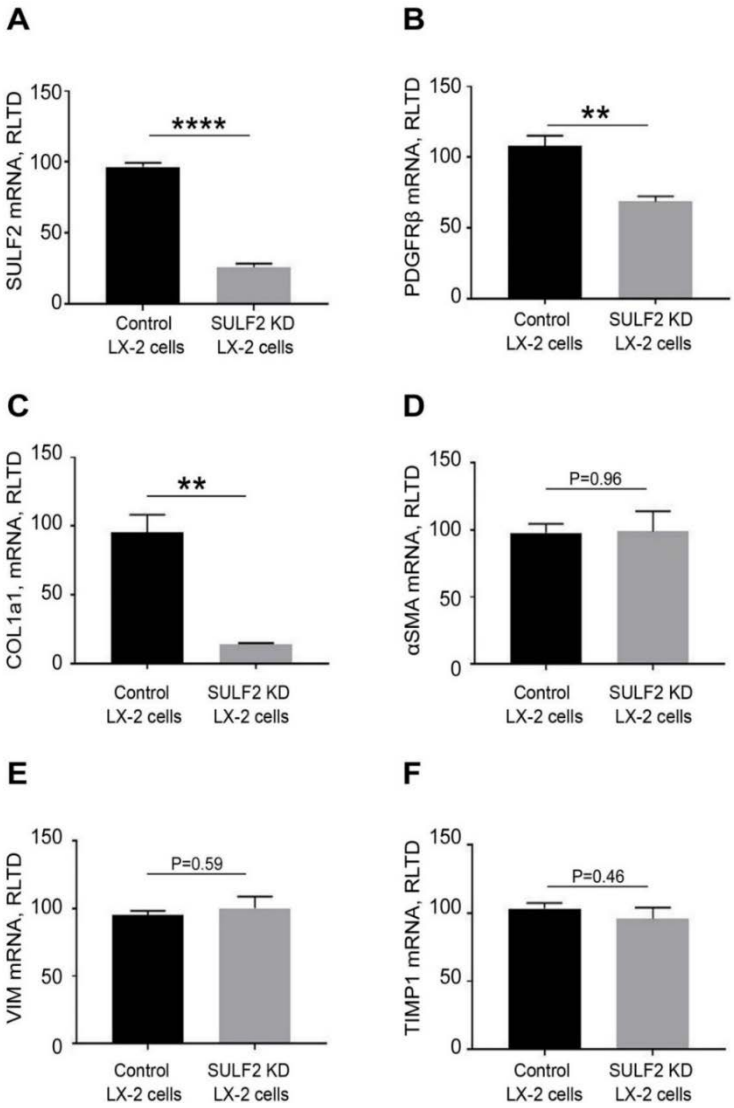

Figure 4.1 SULF2 KD suppressed the expression of certain markers in LX-2 myo-fibroblasts. Graphs show suppression of *SULF2* **(A)**, *PDGFRβ* **(B),** and *COL1α1* **(C)** in association with SULF2 KD in LX-2 cells, while *αSMA* **(D)**, *VIM* **(E)** and *TIMP1* **(F)** were unaffected. Expression is shown as the relative level of transcriptional difference (RLTD) using HPRT as a control. Experiments were repeated three times (n=3) and data are expressed as mean ± s.e.m; ** p<0.01; ****p<0.0001.

Given that CAFs are an abundant source of pro-inflammatory cytokines and growth factors in the malignant niche[226], gene expression of key inflammatory cytokines *IL-1β, TNF-α, IL-6* and *IL-8* was compared between control and SULF2 KD LX-2 fibroblasts. SULF2 KD from LX-2 cells significantly decreased the expression of *IL-6* **(Figure 4.2A)**, *IL-8* **(Figure 4.2B)** and *TNF-α* **(Figure 4.2C)** compared to the control fibroblasts, while *IL-1β* levels were expressed at comparable levels regardless of SULF2 status **(Figure 4.2D).**

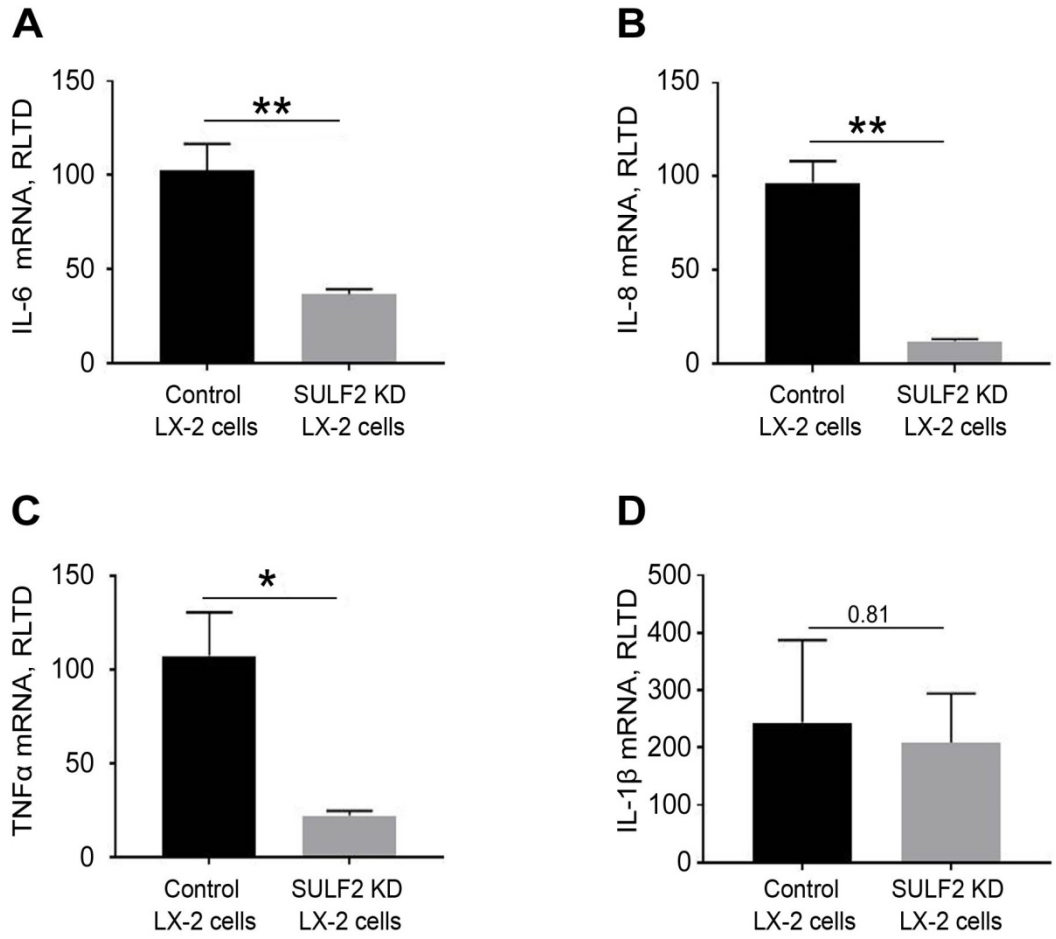

Figure 4.2 SULF2 KD decreased the expression of protumourigenic cytokines in LX-2 myofibroblasts. Graphs show decreased of *IL-6* **(A)**, *IL-8* **(B),** *TNFα* **(C)** and *IL-1β* **(D)** expression in association with SULF2 KD in LX-2 cells. The expression level is shown as relative level of transcriptional difference (RLTD) using HPRT as a control. Experiments were repeated three times (n=3) and data are expressed as mean ± s.e.m; * P<0.05; ** p<0.01.

As a confirmation to the mRNA expression data, ELISA was performed to measure the protein level of COL1a1, IL-6, IL-8, TNFα and MCP1 in concentrated CM from control and SULF2 KD LX-2 cells. IL-6 **(Figure 4.3A)**, IL-8 **(Figure 4.3B)** and COL1a1 **(Figure 4.3C)** protein levels were significantly higher in CM from control LX-2 cells than in SULF2 KD LX-2 CM. On the other hand,

there was no change in TNF-α **(Figure 4.3D)** and MCP1 **(Figure 4.3E)** protein levels in CM from both cell lines.

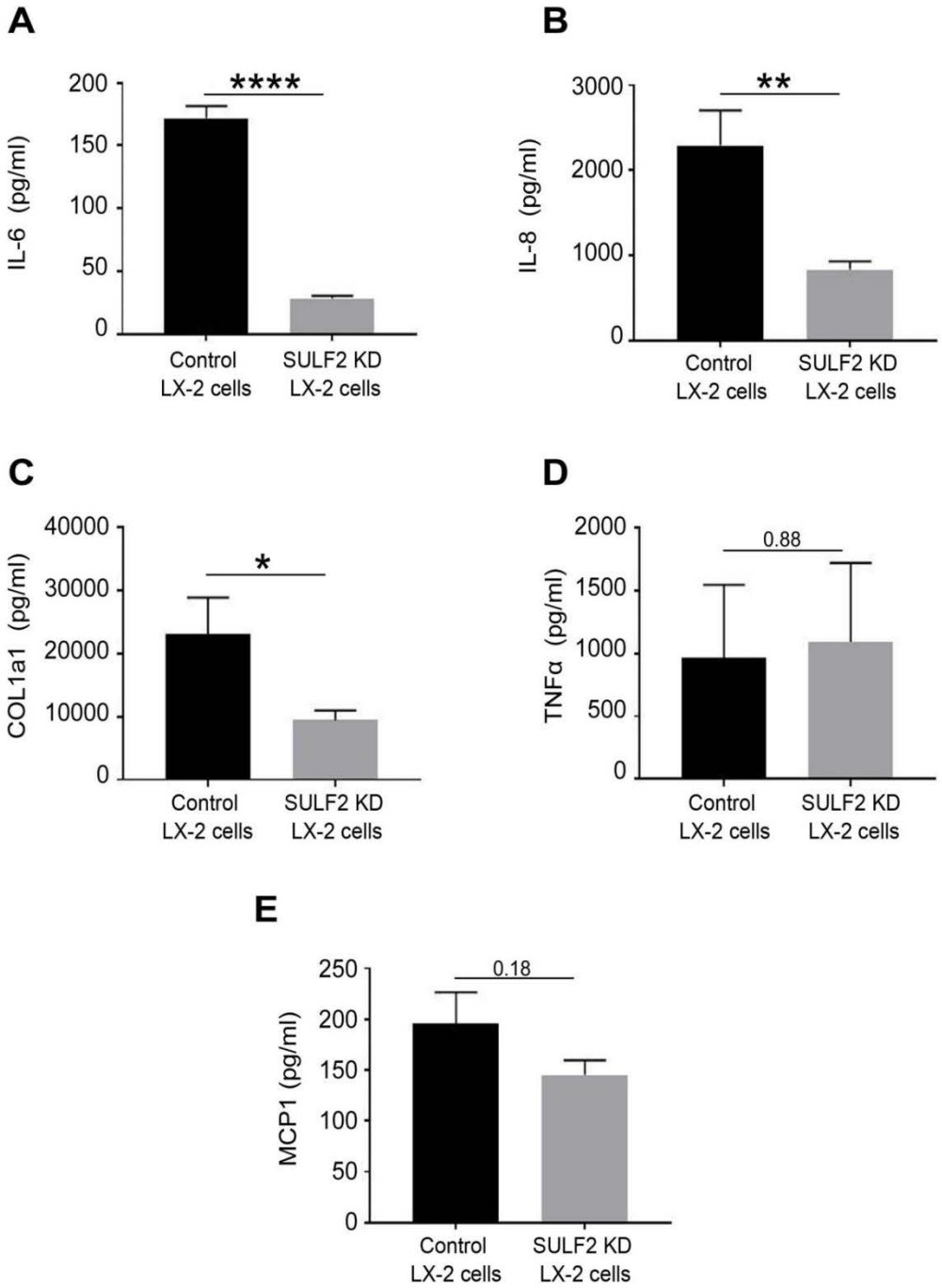

Figure 4.3 SULF2 KD supressed the secretion of key cytokines in LX-2 myo-fibroblasts. Graphs show decreased protein levels of IL-6 **(A)**, IL-8 **(B)**, COL1a1 **(C)** in association with SULF2 KD from LX-2 cells, while the protein levels of TNFα **(D)** and MCP1 **(E)** remained unchanged. Data are presented in mean ± s.e.m; * p<0.05; ** p<0.01; ****p<0.0001, n=3 repeats

4.3.2 The impact of SULF2 on the activation of different pathways in LX-2 fibroblasts

Expression data of control and SULF2 KD LX-2 cells confirmed the deregulation of *PDGFRβ*, together with key inflammatory markers. To understand the underlying mechanism

responsible for this change in the fibroblast secretome, WB of protein lysate from control and SULF2 KD LX-2 cells grown in SF conditions first confirmed the stable KD of SULF2 at 24 and 48 hours from cell seeding **(Figure 3.6).** Control LX-2 cells showed higher levels of p-PDGFRβ compared to SULF2 KD LX-2 cell at 24 hours with modest levels between cell lines at 48 hours. The upregulation of total PDGFRβ in the control LX-2 cells compared to SULF2 KD LX-2 fibroblasts was evident at 24 hours but similar at 48 hours **(Figure 4.4)**. In summary, mRNA and WB confirmed the SULF2-dependent activation and upregulation of PDGFRβ in the LX-2 fibroblasts.

Looking downstream of PDGFRβ signalling, p-JNK1/2 and p-STAT3 levels were strongly downregulated upon SULF2 KD from LX-2 fibroblasts compared to control cells, with no change in the total JNK1/2 and STAT3 levels between the two cell lines **(Figure 4.4)**. While the increase in phosphorylation of the RelA subunit of NF-κB at serine 536 (pP65) was more obvious in control LX-2 compared to SULF2 KD LX-2 cells at 48 hours, there was no change in p-AKT and p-ERK1/2 levels between both fibroblasts cell lines at either time point. In conclusion, stromal SULF2 might activate PDGFRβ/JNK/STAT3, but not ERK and AKT pathways in the LX-2 fibroblasts **(Figure 4.4)**.

Previous reports confirmed the link between JNK and STAT3 pathways with the production of different inflammatory cytokines[137]. The development of HCC depended on the activation of JNK pathway in liver fibroblasts via an increase in cytokines levels and especially IL-6[137]. This was consistent with our hypothesis that SULF2-mediated activation of the PDGFRβ/JNK pathway contributed to the production of IL-6 and IL-8 pro-inflammatory and tumour promoting cytokines. Indeed, addition of recombinant IL-6 protein to the CM from SULF2 KD LX-2 cells partially rescued the proliferative phenotype of Hep3B spheroids compared to SULF2 KD LX-2 CM **(Figure 4.5).** Thus, in addition to the direct mitogenic effect of stromal SULF2 on tumour cells (demonstrated previously by adding SULF2 antibody to tumour cells – Chapter 3), SULF2 may indirectly increase tumour cell proliferation via activation of the PDGFRβ/JNK/IL-6 pathway in the activated stromal cells within the tumour niche.

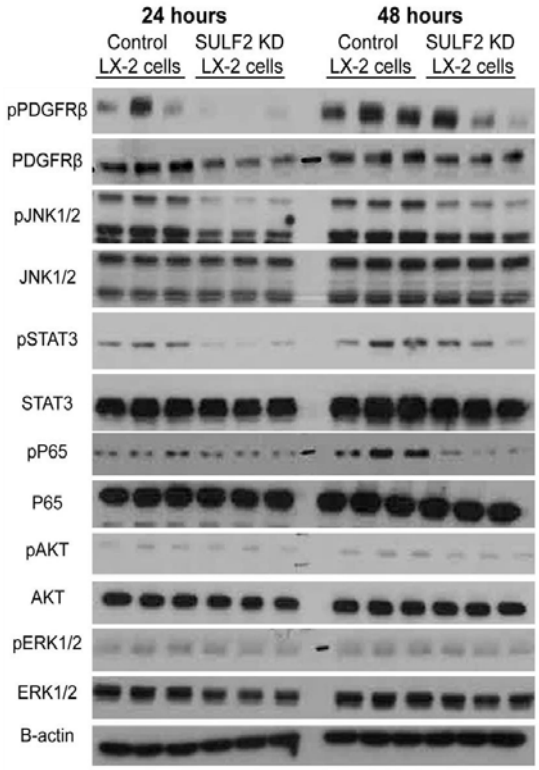

Figure 4.4 SULF2 KD deactivated PDGFRβ, JNK and STAT3 pathways in LX-2 myo-fibroblasts. Western blots show reduced phosphorylation of pPDGFRβ, pJNK1/2 and pSTAT3 in response to SULF2 KD from LX-2 cells. Phosphorylation levels of AKT and ERK1/2 were unaffected with SULF2 KD. The experiment was repeated three times (n=3).

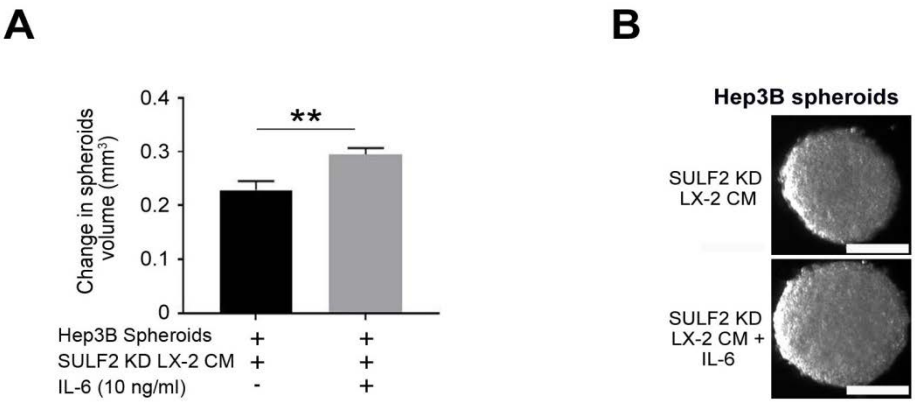

Figure 4.5 Addition of recombinant IL-6 to SULF2 KD CM rescued the proliferative phenotype on Hep3B spheroids. Graph Shows increase in the growth of Hep3B spheroids when IL-6 was added to SULF2-deficient LX-2 CM **(A).** Representative images show the partial rescue of Hep3B spheroids growth phenotype after adding IL-6 recombinant protein to the SULF2 KD LX-2 CM. Data are presented as mean ± s.e.m of 10 spheroids per condition (n=10); ** p<0.01.

4.4 Validation of the association between SULF2, PDGFRβ and IL-6

Interrogation of the publically available (TCGA) human liver cancer dataset on the cBioPortal website (http://www.cbioportal.org/) revealed that SULF2 expression positively associated with the expression of both PDGFRβ (Spearman's Rho 0.58, q-value=2.53e-32) and IL-6 (Spearman's Rho 0.38, q-value=2.42e-13) **(Figure 4.6)**. In combination, these data support a key role for SULF2 in modulating autocrine secretion of pro-tumourigenic IL-6 from fibroblasts, via activation of the PDGFRβ/JNK pathway.

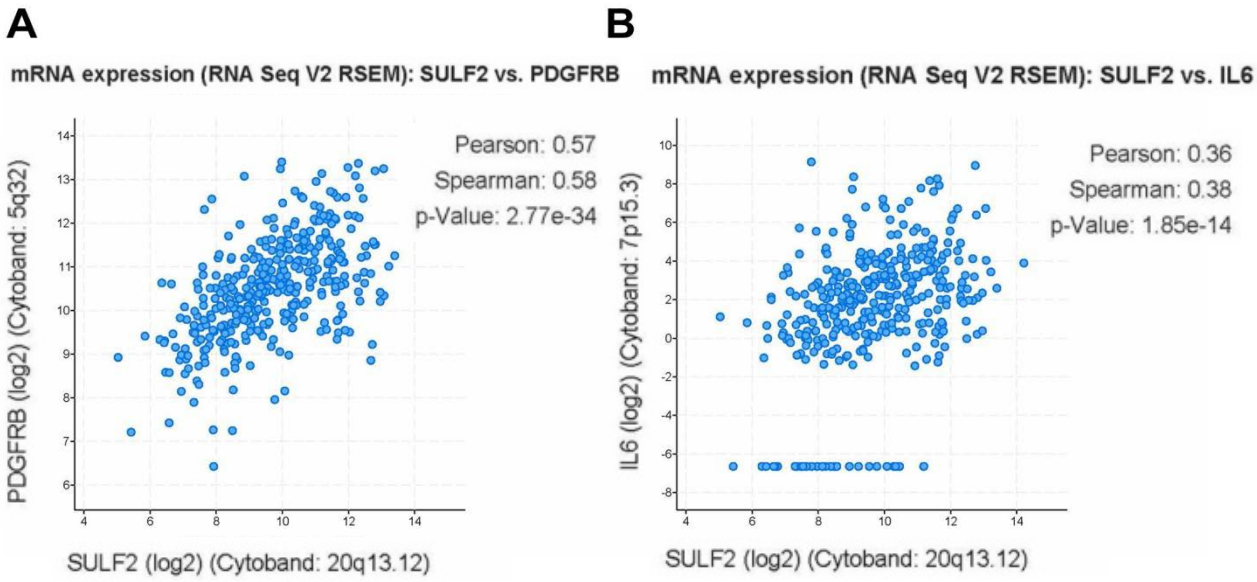

Figure 4.6 Significant associations between SULF2 and PDGFRβ and IL-6 expression in human TCGA gene expression data. Graphs show the correlation between log2 SULF2 expression and log2 PDGFRβ **(A)** or log2 IL-6 expression **(B)** expression. Data are presented as mRNA expression (RNA seq V2 RSEM) for 373 samples.

4.5 Investigation of the paracrine role of stromal SULF2 on the tumour cells

The paracrine role of stromal SULF2 on activation of different oncogenic pathways within the tumour cells was then investigated by culturing Hep3B spheroids in CM from control or SULF2 KD LX-2 cells in the presence of inhibitors to various oncogenic pathways. Inhibitors to JNK pathway (SP600125), TAK-MAPK pathway ((5Z)-7-Oxozeaenol), IKKβ-NF-κB pathway (CAS 507475-17-4), ERK1/2 pathway (FR 180204) and TGFβ pathway (SB525334) were applied to the tumour spheroids to test whether or not they would limit stromal-SULF2 mediated HCC proliferation. Before treating tumour spheroids with inhibitors, the optimal, non-toxic dose from each inhibitor was assessed first in 2D HCC cultures. Hep3B cells seeded in 96-well plate were treated with different concentrations from each inhibitor and the dose that inhibited the growth of cells (measured by MTT viability assay) without being toxic over 24, 48 and 72 hour time points was considered for the 3D spheroids experiment.

As Hep3B spheroids grown in SULF2-rich CM were protected from the sorafenib-induced cytostatic/cytotoxic effect compared to spheroids in SULF2-deficient CM, we wanted to know whether or not the pathways activated by stromal SULF2 would also be responsible for the SULF2-induced sorafenib resistance. So in parallel to the spheroid experiment, Hep3B cells in 6-well plate were treated with SF media, SF-CM from control or SULF2 KD LX-2 cells in absence and presence of sorafenib. Protein lysates of the treated cells were then immuno-blotted for possible SULF2-dependant phosphorylated and total forms of downstream targets of the deregulated pathways.

The JNK inhibitor SP600125 was able to limit both SULF2-dependent and independent growth of Hep3B spheroids **(Figure 4.7)**.

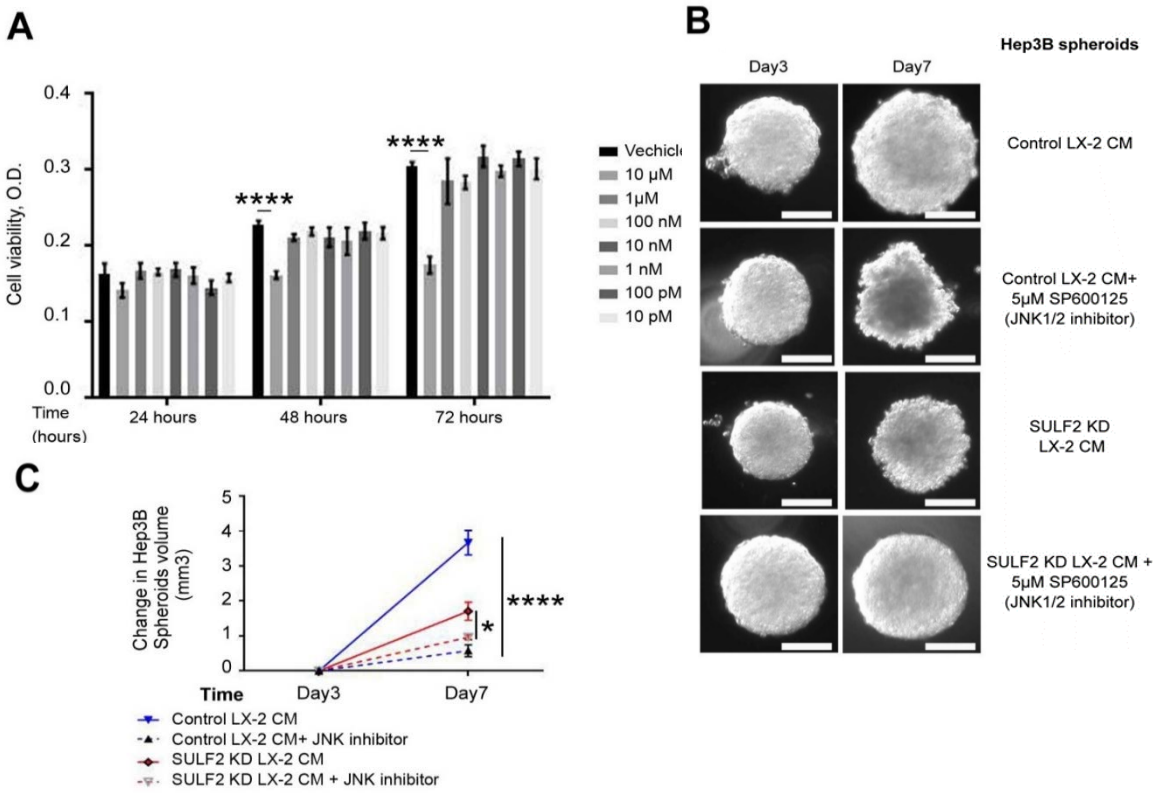

Figure 4.7 The JNK1/2 inhibitor had no stromal SULF2-dependent impact on tumour growth. Graph shows MTT viability data for Hep3B cells treated with different concentrations of a JNK inhibitor for a number of time points **(A),** presented as mean ± s.e.m of three experiments. Representative images **(B)** and graph **(C)** show changes in the growth of Hep3B tumour spheroid treated with CM from both control and SULF2 KD LX-2 cells in presence or absence of 5µM of JNK1/2 inhibitor. Data are presented are expressed as mean ± s.e.m of 10 spheroids/condition (n=10); * $p<0.05$; ****$p<0.0001$.

WB for phospho- and total JNK1/2 showed that addition of CM promoted an increase in p-JNK1/2 phosphorylation and activation of the pathway in the tumour cells independent of

SULF2 **(Figure 4.8)**. Moreover, sorafenib inhibited p-JNK1/2 activation in a SULF2-independent manner **(Figure 4.8)**. The same pattern was shown in p-STAT3 and STAT3 proteins **(Figure 4.8)** implying that stromal SULF2-induced oncogenic and sorafenib-evading mechanisms were driven via activation of neither JNK nor STAT3 pathways.

Figure 4.8 Stromal SULF2 had no independent impact on JNK or STAT3 signalling in tumour cells. Western blots show that stromal CM induced the phosphorylation of pJNK1/2 and pSTAT3 in Hep3B cells in a SULF2-independent fashion. Sorafenib blocked the phosphorylation of pJNK1/2 and pSTAT3 in the Hep3B cells regardless to the SULF2 level in the stromal CM. The experiment was repeated two times (n=2).

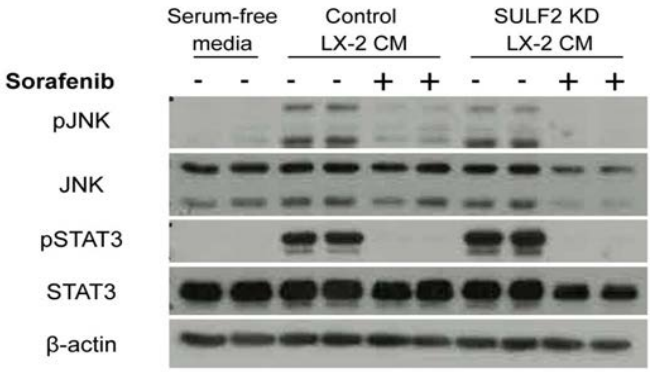

Consistent with this, inhibitors to ERK1/2 and TGFβ-1 pathways blocked the growth of Hep3B spheroids grown in SULF2 positive and negative CM **(Figure 4. 9)**.

Figure 4.9 The ERK1/2 and TGFβ inhibitors had no stromal SULF2-dependent impact on tumour growth. Graphs show MTT viability data for Hep3B cells treated with different concentrations of either ERK1/2 **(A)** or TGFβ **(C)** inhibitors for a number of time points is shown, and data are presented as mean ± s.e.m of three experiments. Graphs show changes in the growth of Hep3B tumour spheroid treated with CM from both control and SULF2 KD LX-2 cells in presence or absence of ERK1/2 **(B)** or TGFβ **(D)** inhibitors. Data are presented are expressed as mean ± s.e.m of 10 spheroids/condition (n=10); * p<0.05; ****p<0.0001.

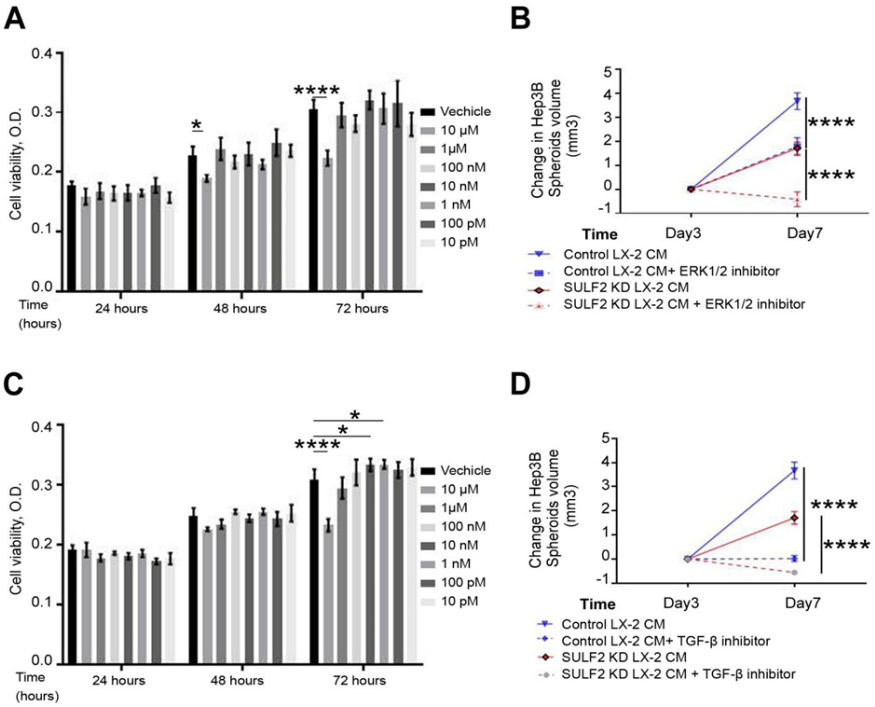

On the other hand, inhibitors to the MAPKKK (TAK1) **(Figure 4.10)** and its downstream target IKK-β **(Figure 4.11)** blocked only the SULF2-dependent spheroids growth.

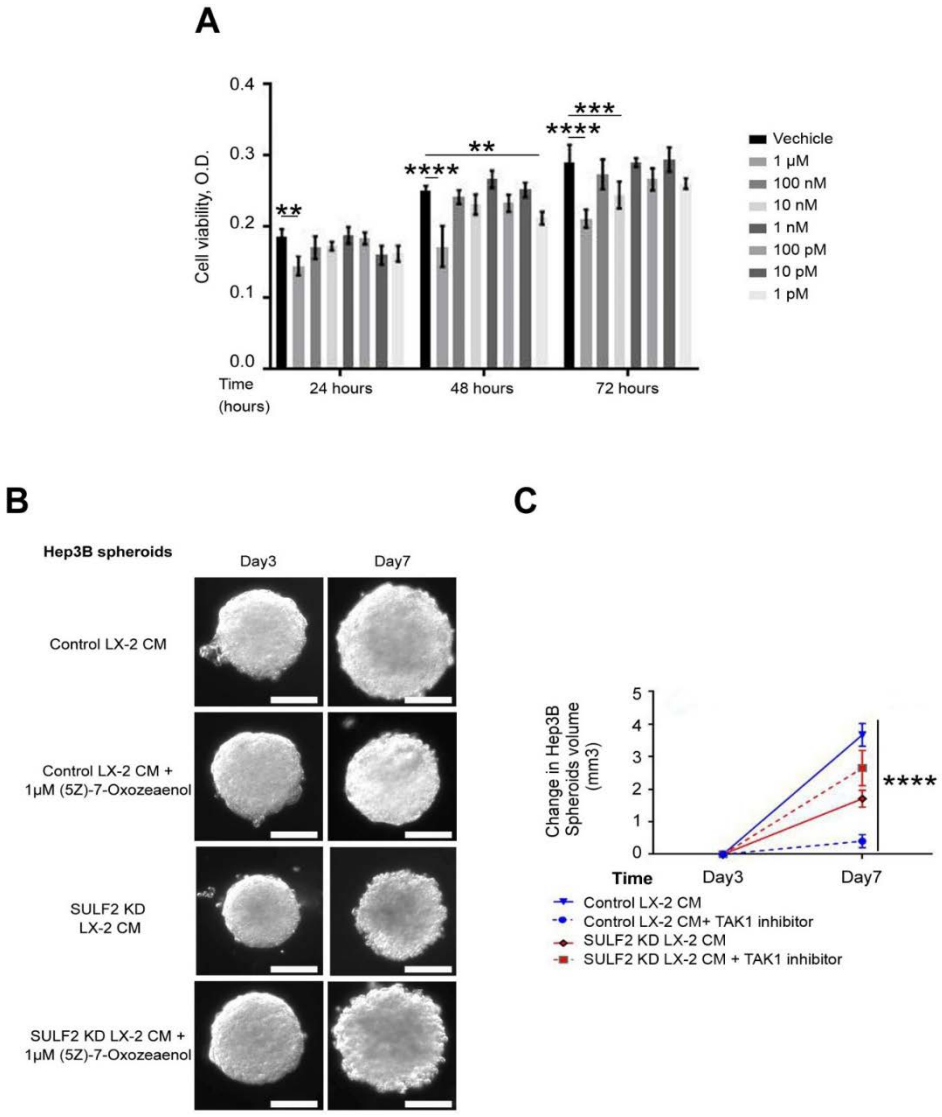

Figure 4.10. TAK1 inhibitor blocked SULF2-dependent growth of Hep3B spheroids. Graph shows MTT viability of Hep3B cells treated with different concentrations of TAK1 inhibitor **(A).** Data are presented as mean ± s.e.m of three experimental repeats. Representative images **(B)** and graph **(C)** show changes in the growth of Hep3B tumour spheroid treated with CM from both control and SULF2 KD LX-2 cells in presence or absence of TAK1 inhibitor. Data are presented as mean ± s.e.m of 10 spheroids/condition (n=10); * p<0.05; ** P<0.01; *** P<0.001; ****p<0.0001.

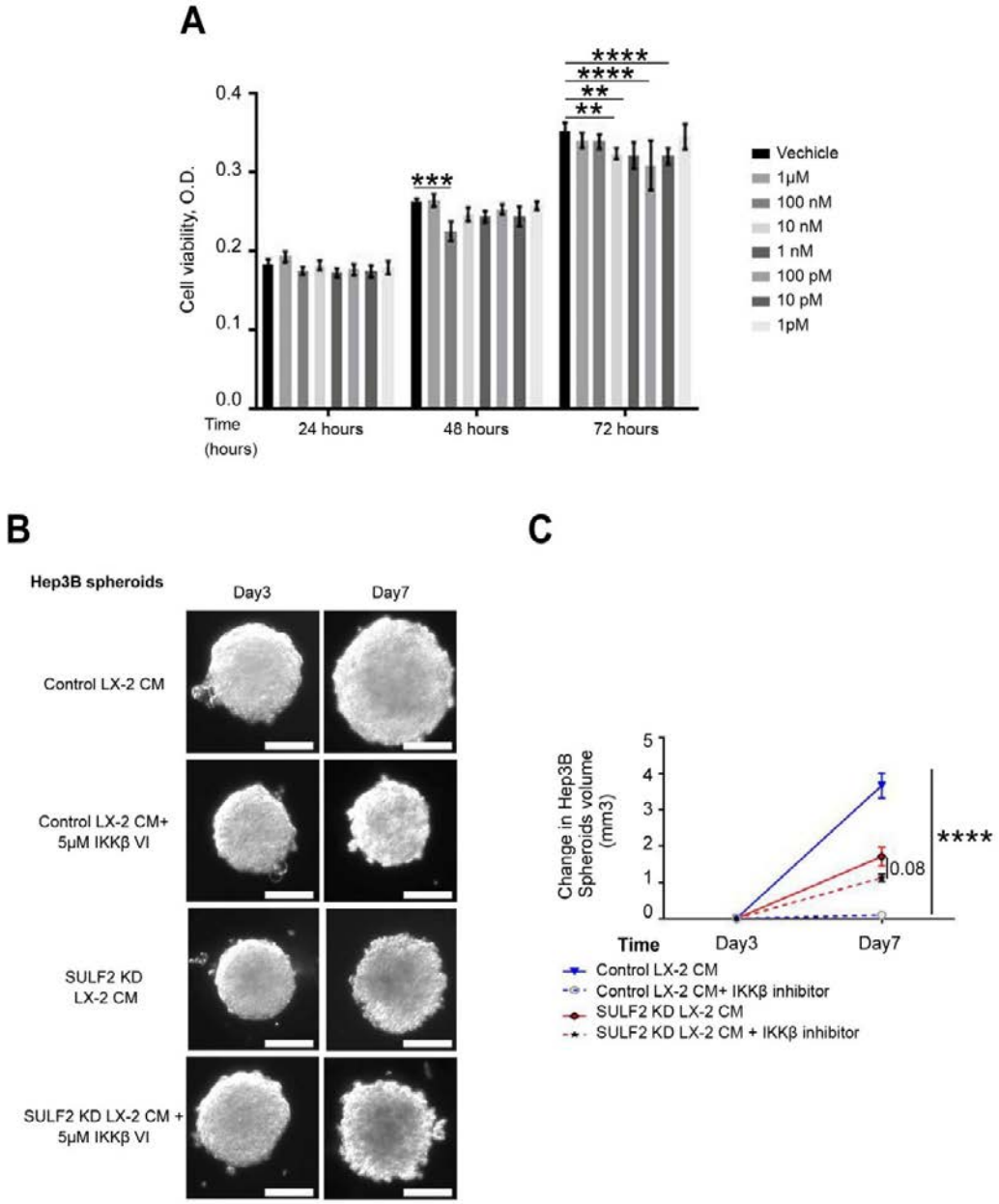

Figure 4.11 IKKβ inhibitor blocked SULF2-dependent growth of Hep3B spheroids. Graph shows MTT viability of Hep3B cells treated with different concentrations of IKKβ inhibitor **(A).** Data are presented as mean ± s.e.m of three experimental repeats. Representative images **(B)** and graph **(C)** show changes in the growth of Hep3B tumour spheroid treated with CM from both control and SULF2 KD LX-2 cells in presence or absence of IKKβ inhibitor. Data are presented as mean ± s.e.m of 10 spheroids/condition (n=10); P<0.01; *** P<0.001; ****p<0.0001.

WB for the phospho- and total RelA ser(536) subunit of NF-κB pathway, a classical target of TAK1/IKKβ pathway, showed upregulation of p-RelA ser(536) in Hep3B cells treated with SULF2-containing CM compared to both SF CM or SF CM from SULF2 KD LX-2 **(Figure 4.12).** Total RelA ser(536) remained unchanged, confirming the SULF2-dependent activation of this particular pathway. Furthermore, this SULF2-induced RelA ser(536) phosphorylation persisted

even in presence of sorafenib, suggesting a link between NF-κB activation and sorafenib resistance in a SULF2-dependent manner. Consistent with the inhibitor data, neither the activation of AKT nor ERK1/2 pathways were SULF2 dependent **(Figure 4.12)**.

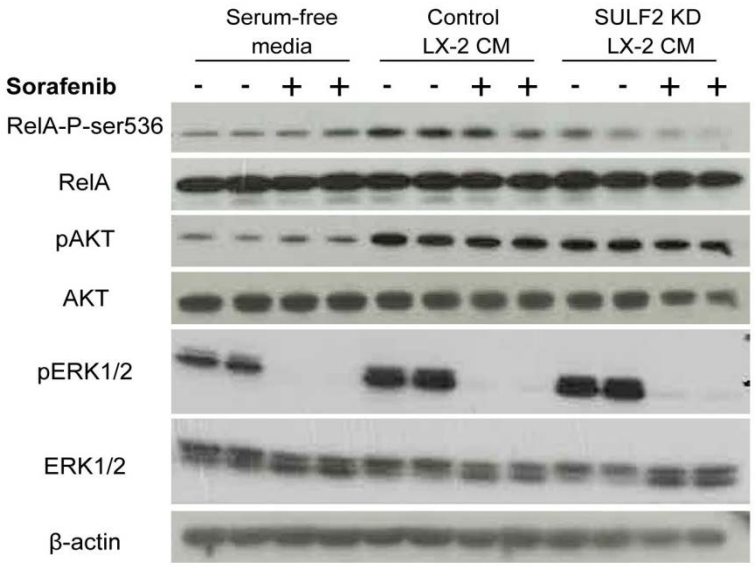

Figure 4.12 Stromal SULF2 activation of NF-κB, not AKT and ERK, persisted in the presence of sorafenib in tumour cells. Western blots show that stromal SULF2 induced the phosphorylation of RelA-P-ser356 (pP65), but not pAKT or pERK1/2 in Hep3B cells. This SULF2-dependent phosphorylation of P65 remained even in the presence of sorafenib, n=4 repeats.

These data confirm that stromal-SULF2 and its related secretome induced the activation of the TAK1/IKKβ/NF-κB pathway in the tumour cells in a paracrine manner. The impact was associated with an increase in the tumour cell proliferative capacity, but also an increase in their ability to resist chemotherapy.

4.6 The role of SULF2 in promoting a cancer stem cell (CSC) phenotype in tumour cells

The stromal SULF2-driven aggressive tumour behaviour was in keeping with a CSC phenotype[364, 365], known to be regulated by NF-κB pathways in different human cancers including HCC[366]. Sorafenib resistance was also reminiscent of this phenotype[367]. The mRNA expression level of different CSC markers was investigated in Hep3B cells challenged with DMSO, control LX-2 CM and SULF2 KD LX-2 CM, with or without sorafenib **(Figures 4.13 - 4.19)**. The presence of SULF2 in the fibroblast CM dramatically induced *CD44* compared to either untreated cells or cells treated with SULF2 KD CM at 12 and 24 hours. This SULF2-dependent upregulation of *CD44* persisted with concurrent sorafenib treatment. Thus, stromal SULF2 induced CSC features and sorafenib resistance in association with the upregulation of *CD44* in

the tumour cells **(Figure 4.13 A,B)**. Sorafenib-only treatment also upregulated *VIM* and *CDH1*, but in a SULF2-independent manner **(Figure 4.13 C-F).** Neither sorafenib nor SULF2 significantly changed the expression profile of *EpCAM, KRT7, KRT19, AXIN2, LGR5, CDH2, PDGFRα, PDGFRβ, TCF4, COL1α1* and *FZD7* **(Figures 4.14 – 4.17)**.

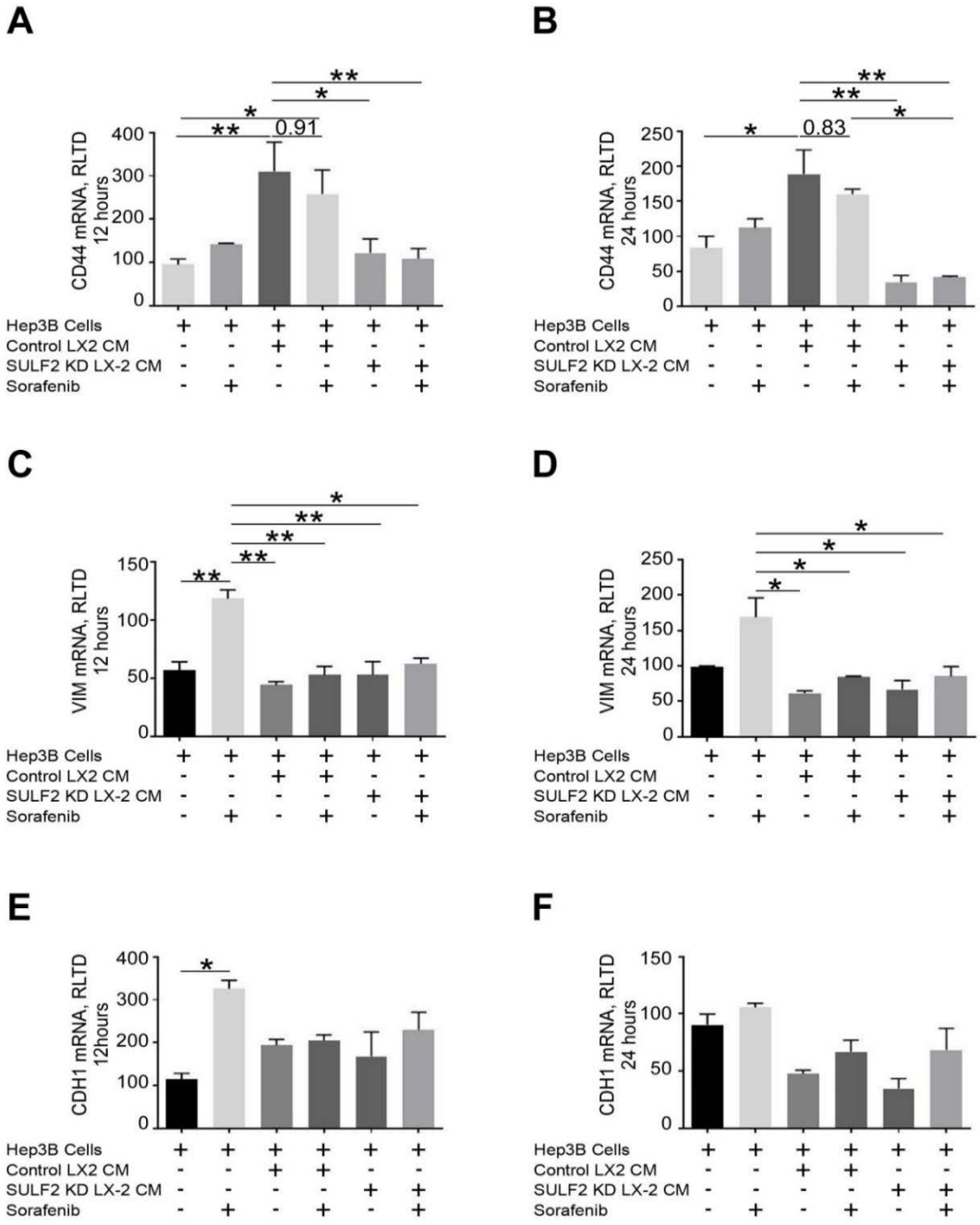

Figure 4.13 Stromal SULF2 induced the expression of CD44, but not VIM or CDH1 in Hep3B cells. Graphs show elevated *CD44* **(A,B)**, but not *VIM* **(C,D)** and *CDH1* **(E,F)** in Hep3B cells treated with control or SULF2 KD LX-2 CM, which persists in the presence of sorafenib at 12 and 24 hours. The expression level is presented as relative level of transcriptional difference (RLTD) using HPRT as a control. Experiments were repeated three times (n=3) and data are expressed as mean ± s.e.m; * $p<0.05$; ** $p<0.01$.

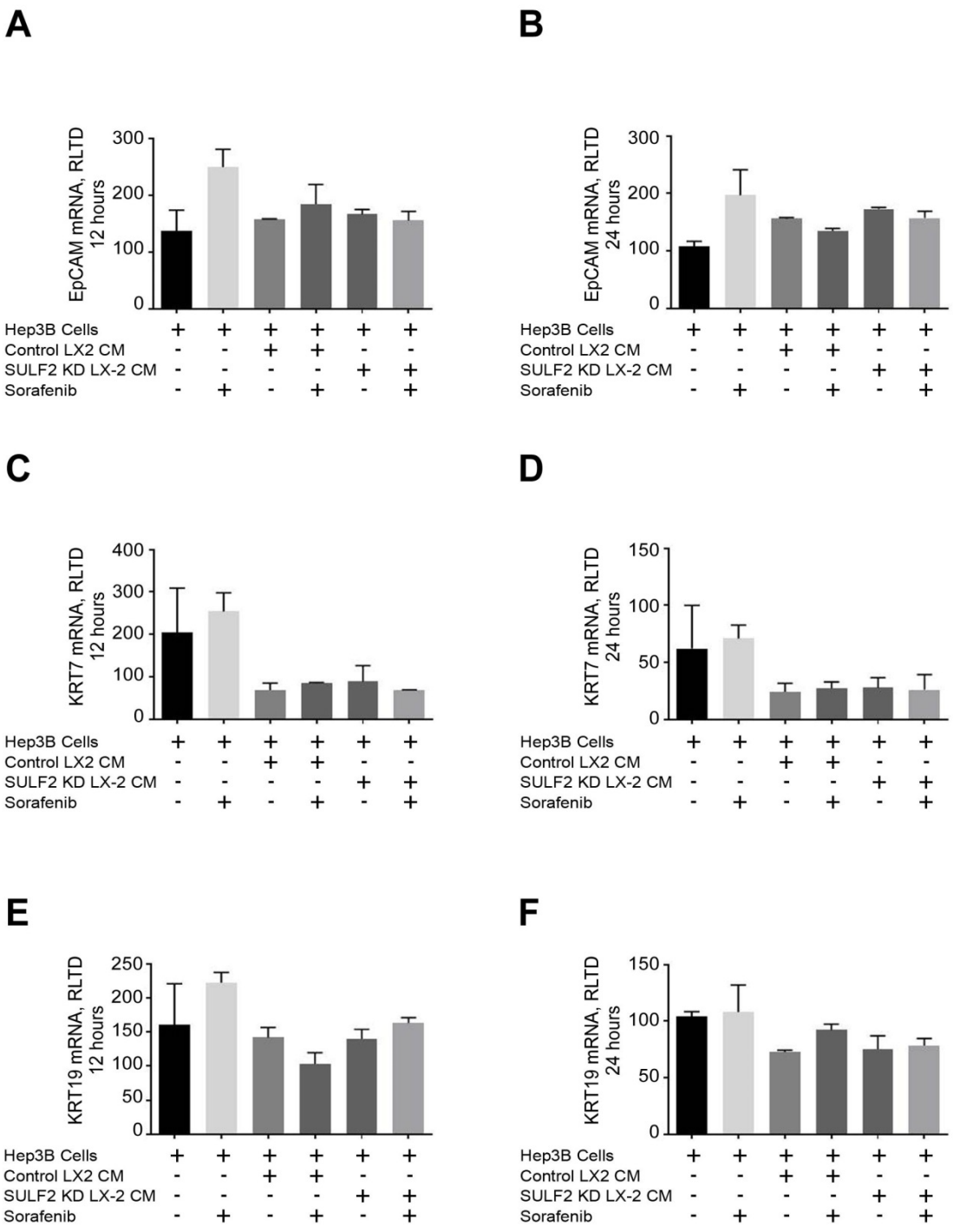

Figure 4.14 Stromal SULF2 didn't affect the expression of EpCAM, KRT7 or KRT19 in Hep3B cells. Graphs show comparable levels of *EpCAM* **(A,B)**, *KRT7* **(C,D)** and *KRT19* **(E,F)** in Hep3B cells treated with control or SULF2 KD LX-2 CM in presence or absence of sorafenib. The expression level is presented as relative level of transcriptional difference (RLTD) using HPRT as a control. Experiments were repeated three times (n=3) and data are expressed as mean ± s.e.m.

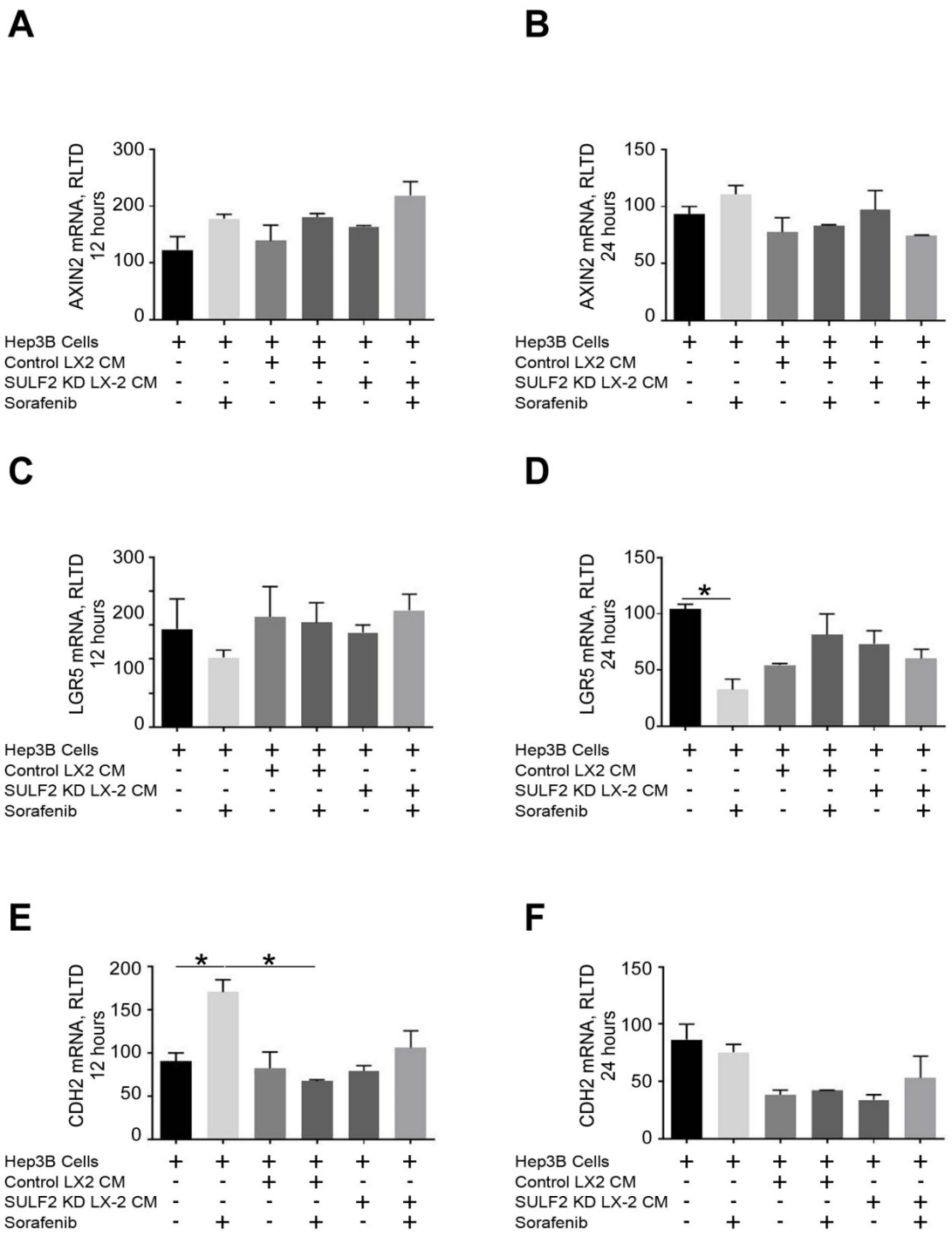

Figure 4.15 Stromal SULF2 didn't affect the expression of AXIN2, LGR5 or CDH2 in Hep3B cells. Graphs show comparable levels of *AXIN2* **(A,B)**, *LGR5* **(C,D)** and *CDH2* **(E,F)** in Hep3B cells treated with control or SULF2 KD LX-2 CM in presence or absence of sorafenib. The expression level is presented as relative level of transcriptional difference (RLTD) using HPRT as a control. Experiments were repeated three times (n=3) and data are expressed as mean ± s.e.m.; * $p<0.05$.

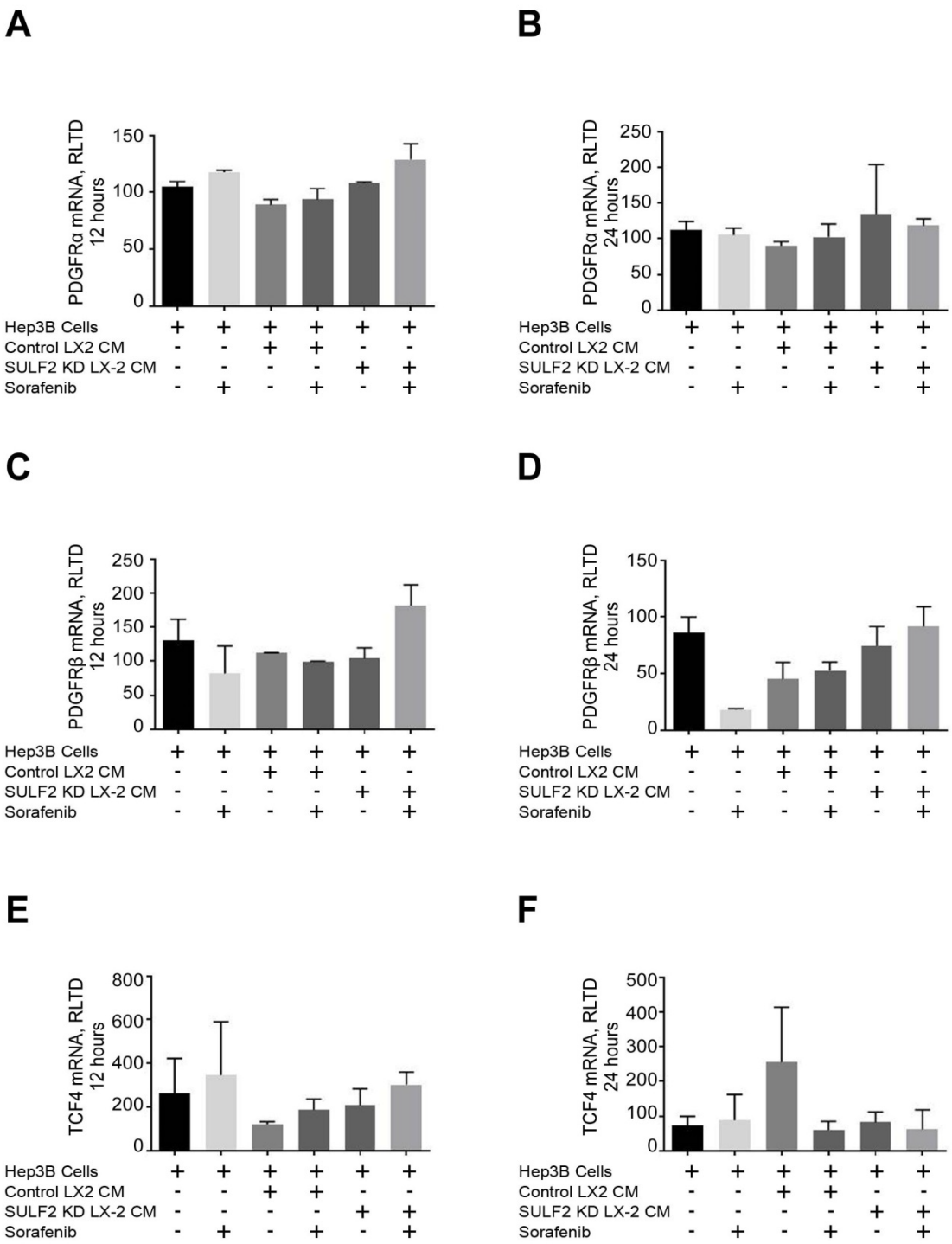

Figure 4.16 Stromal SULF2 didn't affect the expression of PDGFRα, PDGFRβ or TCF4 in Hep3B cells. Graphs show comparable levels of *PDGFRα* **(A,B)**, *PDGFRβ* **(C,D)** and *TCF4* **(E,F)** in Hep3B cells treated with control or SULF2 KD LX-2 CM in presence or absence of sorafenib. The expression level is presented as relative level of transcriptional difference (RLTD) using HPRT as a control. Experiments were repeated three times (n=3) and data are expressed as mean ± s.e.m.

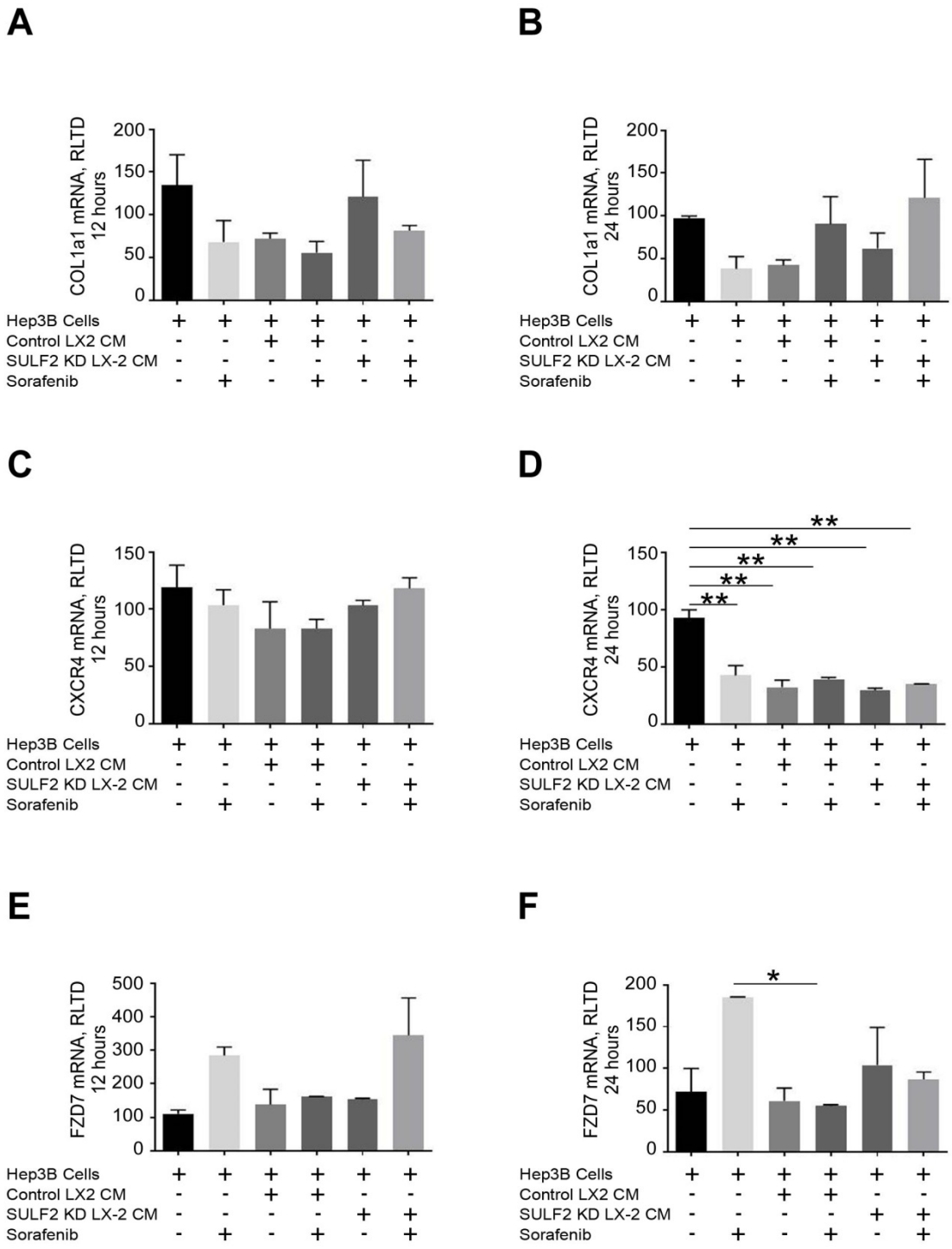

Figure 4.17 Stromal SULF2 didn't affect the expression of COL1A1, CXCR4 or FZD7 in Hep3B cells. Graphs show comparable levels of *COL1A1* **(A,B)**, *CXCR4* **(C,D)** and *FZD7* **(E,F)** in Hep3B cells treated with control or SULF2 KD LX-2 CM in presence or absence of sorafenib. The expression level is presented as relative level of transcriptional difference (RLTD) using HPRT as a control. Experiments were repeated three times (n=3) and data are expressed as mean ± s.e.m; * $p<0.05$; ** $p<0.01$.

Of note, *IL-6* expression in the tumour cells was induced by stromal SULF2 and also persisted in SULF2/sorafenib treated tumour cells at 12 hours, but this failed to reach statistical significance **(Figure 4.18 A)**. The expression levels of *FGFR1, GADD45β, MDR1* and TNF-α was not altered by stromal SULF2.

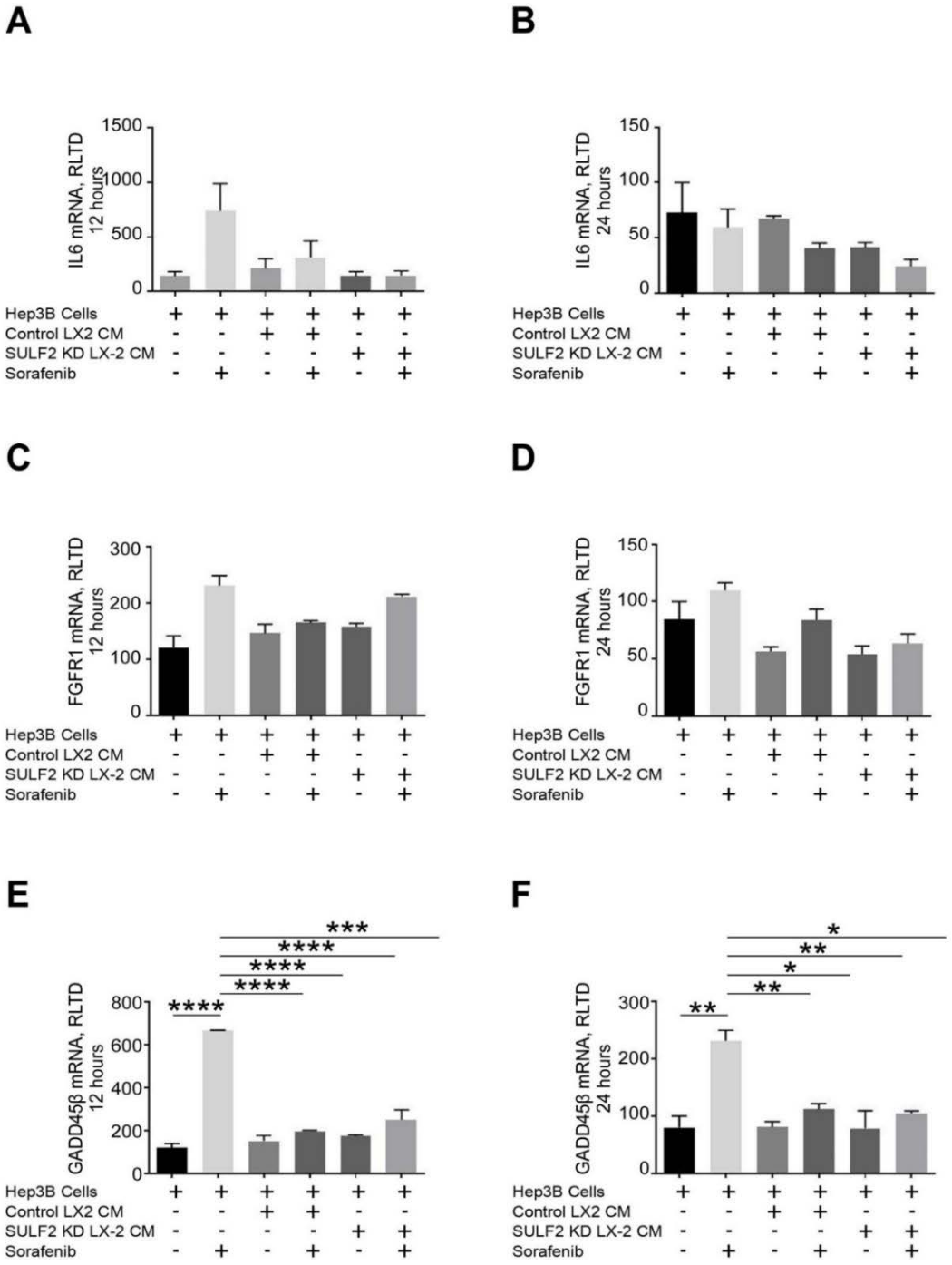

Figure 4.18 Stromal SULF2 didn't affect the expression profile of the inflammatory cytokines IL6, FGFR1 or GADD45β in Hep3B cells. Graphs show comparable levels of *IL6* **(A,B)**, *FGFR1* **(C,D)** and *GADD45β* **(E,F)** in Hep3B cells treated with control or SULF2 KD LX-2 CM in presence or absence of sorafenib. The expression level is presented as relative level of transcriptional difference (RLTD) using HPRT as a control. Experiments were repeated three times (n=3) and data are expressed as mean ± s.e.m; * p<0.05; ** p<0.01.; * P<0.05; ** p<0.01; ***p<0.001; ****p<0.0001.

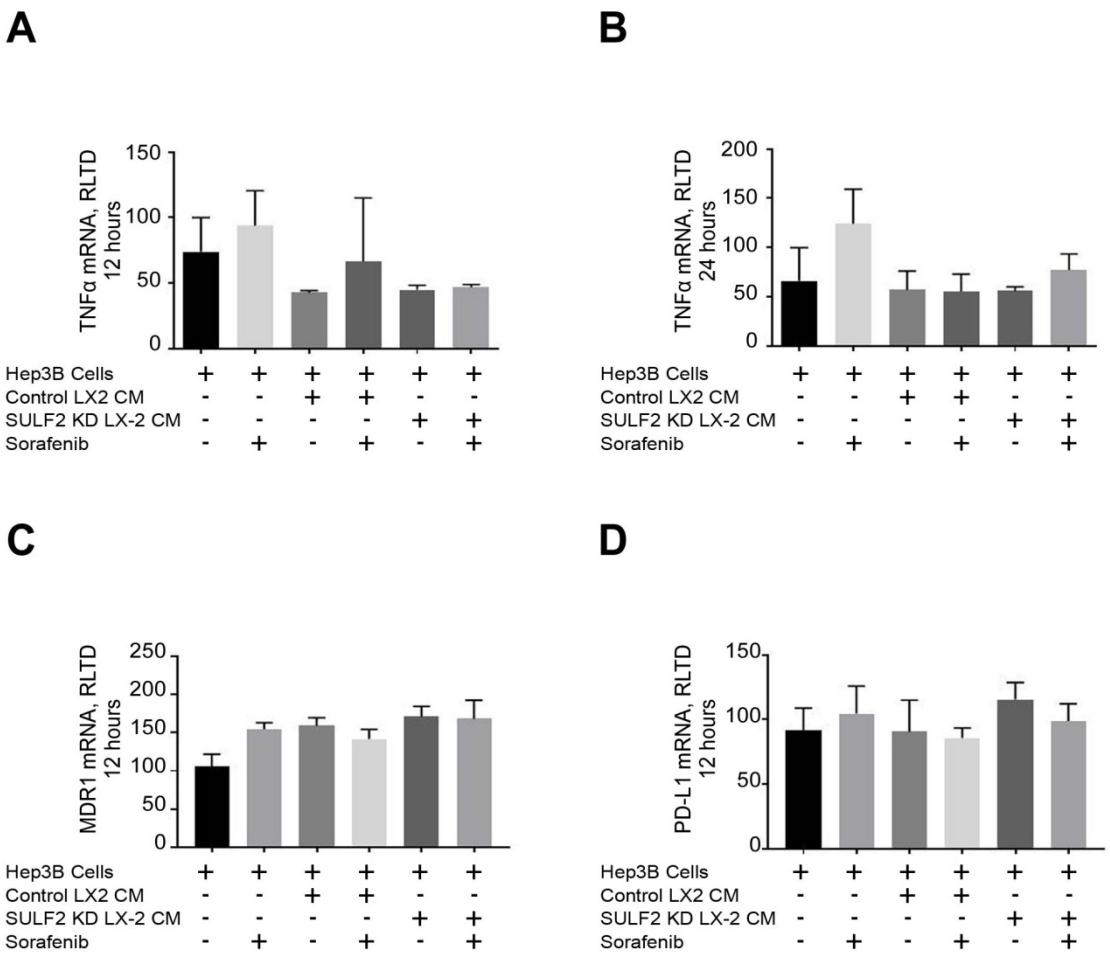

Figure 4.19 Stromal SULF2 didn't affect the expression of TNFα and MDR1 in Hep3B cells. Graphs show comparable levels of *TNFα* **(A,B)** and *MDR1* **(C,D)** in Hep3B cells treated with control or SULF2 KD LX-2 CM in presence or absence of sorafenib. The expression level is presented as relative level of transcriptional difference (RLTD) using HPRT as a control. Experiments were repeated three times (n=3) and data are expressed as mean ± s.e.m.

In summary, in association with enhanced prolferation, invasivion and therapy resistance, stromal SULF2 activated NF- κB and preferentially induced the expression of *CD44* in HCC cells. *CD44* is an established direct target of the NF-κB pathway[366, 368]. In Hep3B cells treated with SULF2-rich stromal CM in presence of an IKKβ inhibitor, the inhibitor abrogated SULF2-induced upregulation of *CD44,* confirming stromal SULF2 as a regular of the tumour IKKβ/NF-κB/CD44 axis **(Figure 4.20)**.

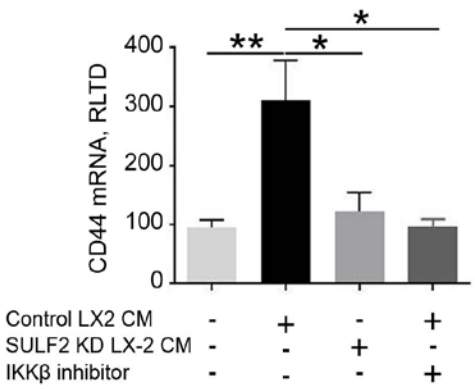

Figure 4.20 IKKβ inhibitors abrogated the stromal SULF2-dependent upregulation of CD44 in Hep3B cells. Graph shows comparable levels of *CD44* in Hep3B cells treated with SULF2 KD LX-2 CM or with IKKβ inhibitor added to the SULF2-rich CM, while *CD44* level was significantly higher in tumour cells treated with control LX-2 CM. The expression level is presented as relative level of transcriptional difference (RLTD) using HPRT as a control. Experiments were repeated three times (n=3) and data are expressed as mean ± s.e.m.; *p<0.05, ** p<0.01.

4.7 Validation of the CAF-SULF2 driven activation of tumour NF-κB/CD44 axis *in vivo*

IHC staining in human biopsies further supported the CAF-tumour cross-talk driven by SULF2. In 20 of the HCC cases previously assessed for SULF2, the presence of CAF-SULF2 **(Figure 4.21 A,D)** was strongly associated with nuclear localisation of p-RelA ser(536) in the adjacent tumour cells (Spearman's Rho 0.776 p<0.001, Pearson Chi-squared test p=0.005) **(Figure 4.21 B,E)**. Membranous CD44 expression in the tumour cells correlated with SULF2 positivity in the contacting CAF (Spearman's Rho correlation 0.744 p<0.001, Pearson Chi-squared test p=0.001) **(Figure 4.21 C,F)**. In addition, CD44 protein expression was associated with the p-RelA ser(536) nuclear positivity (Spearman's rho 0.741 p<0.001, Pearson Chi-squared test 0.047). In CAF-SULF2 null tumours, nuclear p-RelA ser(536) and membranous CD44 protein expression was not evident in the tumour cells **(Figure 4.21 G-I)**.

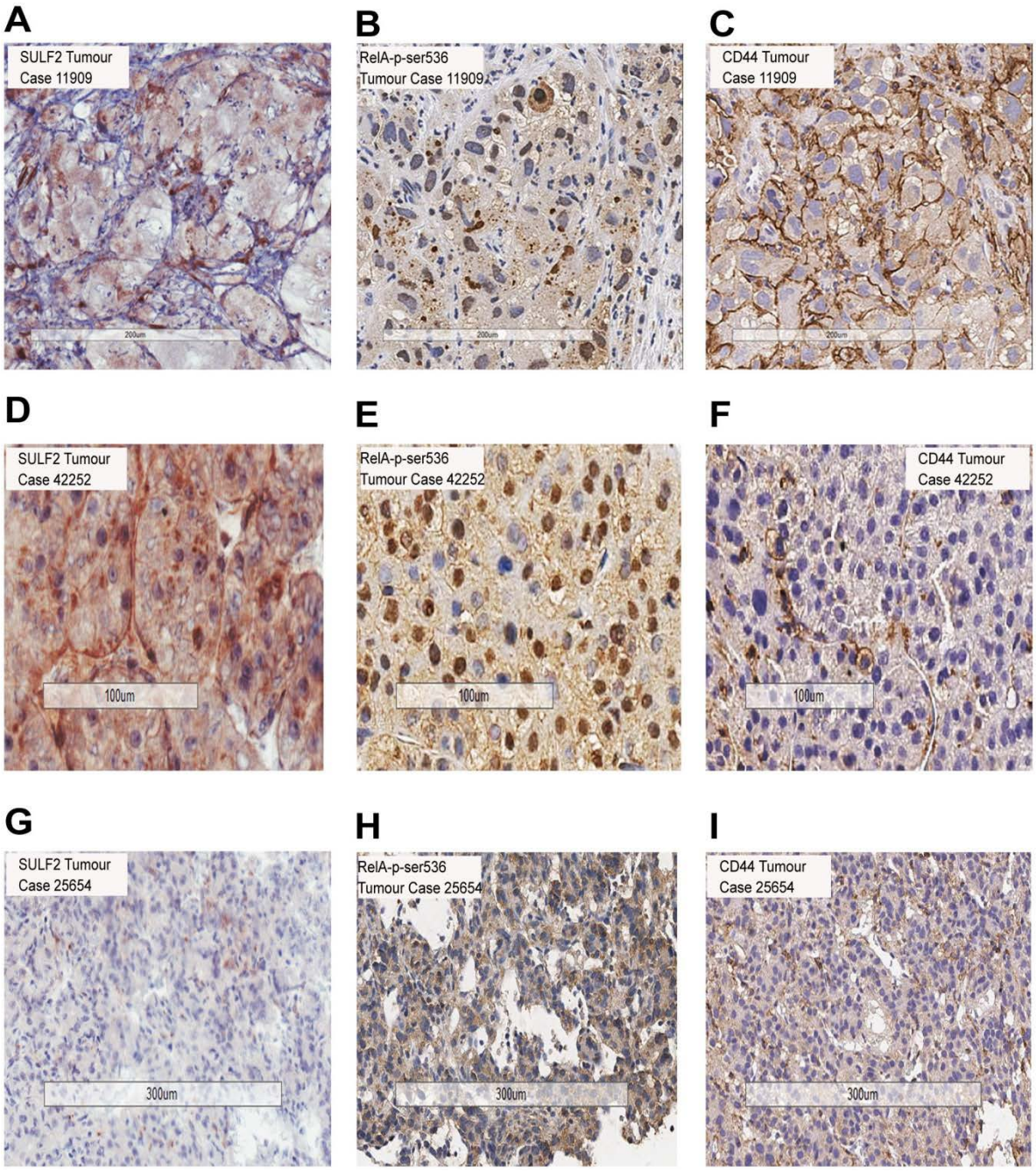

Figure 4.21 Co-expression of SULF2, CD44 and pRelA ser536 in human HCC biopsies Representative images show IHC staining SULF2 **(A,D)**, pRelA ser536 **(B,E)** and CD44 **(C,F)** in two different HCC patients. CAF-SULF2 positivity was evident with nuclear positivity of pRelA ser536 and membranous CD44 positivity in the adjacent tumour cells. Representative images show IHC staining SULF2 **(G)**, pRelA ser536 **(H)** and CD44 **(I)** in HCC patient biopsy. The three markers were negative in this particular case. Images were captured using Aperio Imagescope software at x20, x10 and x5 magnifications, n=20 biopsies.

4.8 SULF2 co-expression with Glypican-3 promotes Wnt signalling and a poor prognosis

GPC3 is a HSPG morphogen often upregulated in HCC tissues and its immunohistochemical detection has been proposed as an HCC histopathology diagnostic biomarker[369]. GPC3 overexpression stabilises cytoplasmic β-catenin in HCC cells and stimulates canonical Wnt

signalling *in vitro*[370], while SULF2 reportedly regulates both expression and 6-O sulfation of GPC3[304]. Our own studies in patient tissues and cell lines indicate that SULF2 co-expression with GPC3 is associated with cytoplasmic accumulation of β-catenin and promotes its nuclear localisation **(Figures 4.22 – 4.23).** GPC3 expression was absent in non-tumour tissues **(Figure 4.22)** and 16/60 tumours, but present in tumour cells in 44/60 (73%) cases, graded as 1 (cytoplasmic dot like or focal positivity, n=17), 2 (diffuse weak positivity in cytoplasm or membrane, n=9) or 3 (intensely positive membranous or cytoplasmic staining, n=18). Strong membranous or cytoplasmic GPC3 expression (Grade 3) was more common in cases with SULF2 expression in either tumour or stromal tissues (14/35 SULF2 present versus 4/25 SULF2 absent, p=0.046, Pearson Chi-Square).

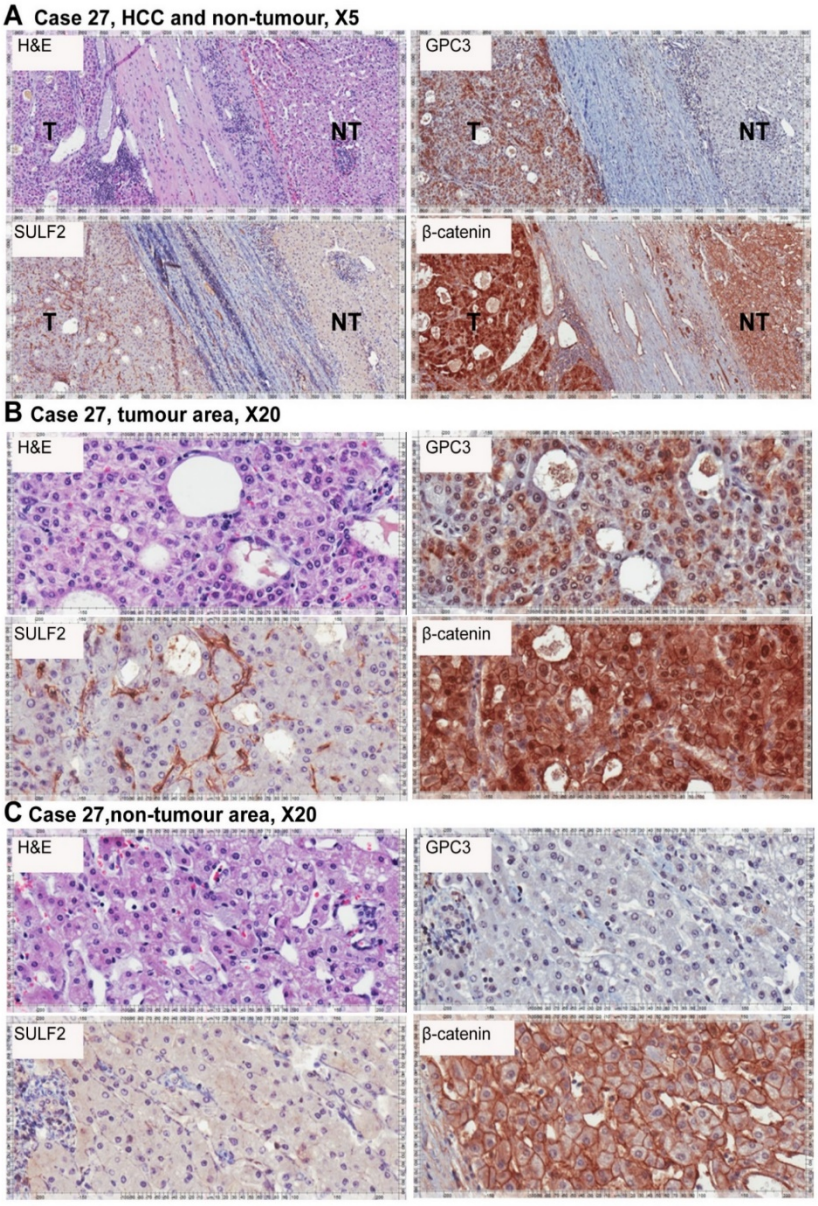

Figure 4.22 Tumour GPC3 and CAF SULF2, in association with nuclear β-catenin in HCC Representative images show H&E staining, GPC3, SULF2 and β- catenin IHC in both HCC (T) and adjacent non-tumour liver (NT). **(A)** GPC3, SULF2 and β- catenin was upregulated in T compared to NT. Nuclear β- catenin was evident in the T cells compared to NT, where its localisation was mainly membranous. **(B)** GPC3+ cells were present in T, with SULF2+ CAFs and nuclear β-catenin. **(C)** Shows NT, with no GPC3or SULF2 and membranous β-catenin. Images were captured using Aperio Imagescope software at x5 and x20 magnification.

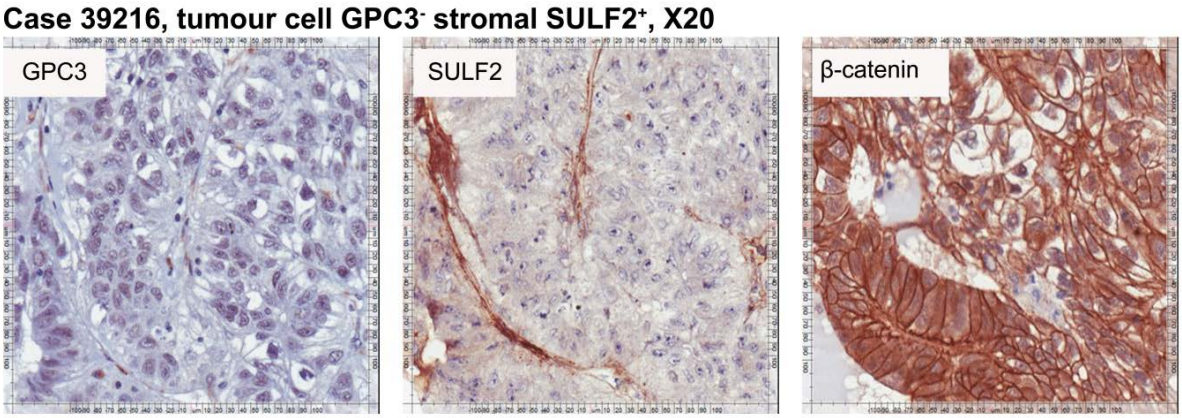

Figure 4.23 tumour cell β-catenin localisation is membranous in the absence of tumour GPC3 even in the presence of tumour stromal cells expressing SULF2. Representative images show a grade 2 HCC stained with GPC3 (left), SULF2 (middle), and β-catenin (right). SULF2 positive CAFs, GPC3 negative tumour cells and membranous β-catenin are shown. Images were captured using Aperio Imagescope software at x20 magnifications.

In our non-surgically treated patients (n=50), GPC3 expression (absent n=13 or present n=37) was not significantly associated with survival, although Grade 3 GPC3 identified a small group with a particularly poor prognosis (n=14, median survival 6.7 months). In contrast, stratification of all GPC3 positive cases based on SULF2 co-expression discriminated significantly between those with a good or poor prognosis. GPC3 and SULF2 co-expression remained significantly associated with poorer survival in a multivariate Cox Regression analysis (HR 3.63 (1.4-9.2), p=0.007) **(Figure 4.24)**.

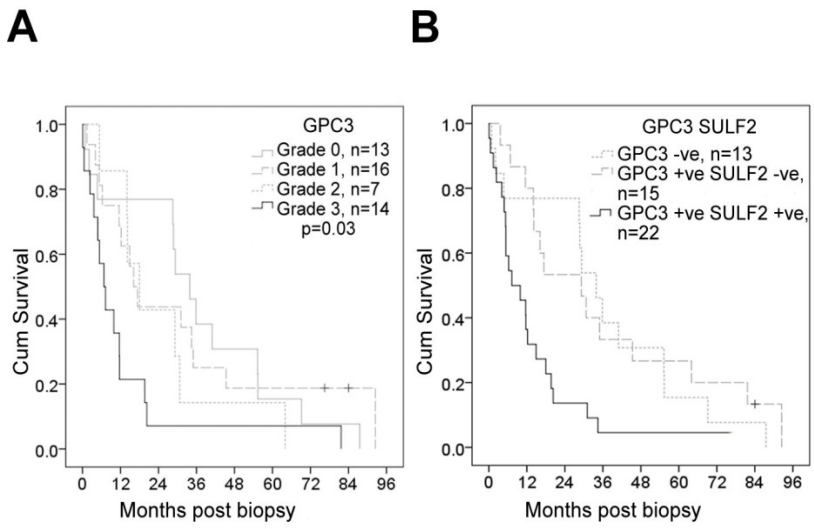

Figure 4.24 SULF2 co-expression discriminates prognosis in the presence of Glypican-3 Kaplan Meier curves show GPC3 only **(A)** or GPC3 and SULF2 co-expression **(B)** correlating with patient survival.

The relationship between SULF2, GPC3 and β-catenin was explored *in-vitro* in Huh7 cells, which express SULF2 in the presence of wild type (WT) Wnt/β-catenin signalling[60]. In WT Huh7 cells, stromal SULF2 induced GPC3 expression **(Figure 4.25A)** as well as membranous and cytoplasmic accumulation of β-catenin **(Figure 4.25B)**. Addition of Wnt3a promoted further cytoplasmic accumulation of β-catenin, with evidence of nuclear localisation **(Figure 4.25C)**. Taken together our in vitro data support the upregulation and activation of the GPC3 Wnt/β-catenin pathway as one mechanism by which stromal SULF2 induces HCC growth.

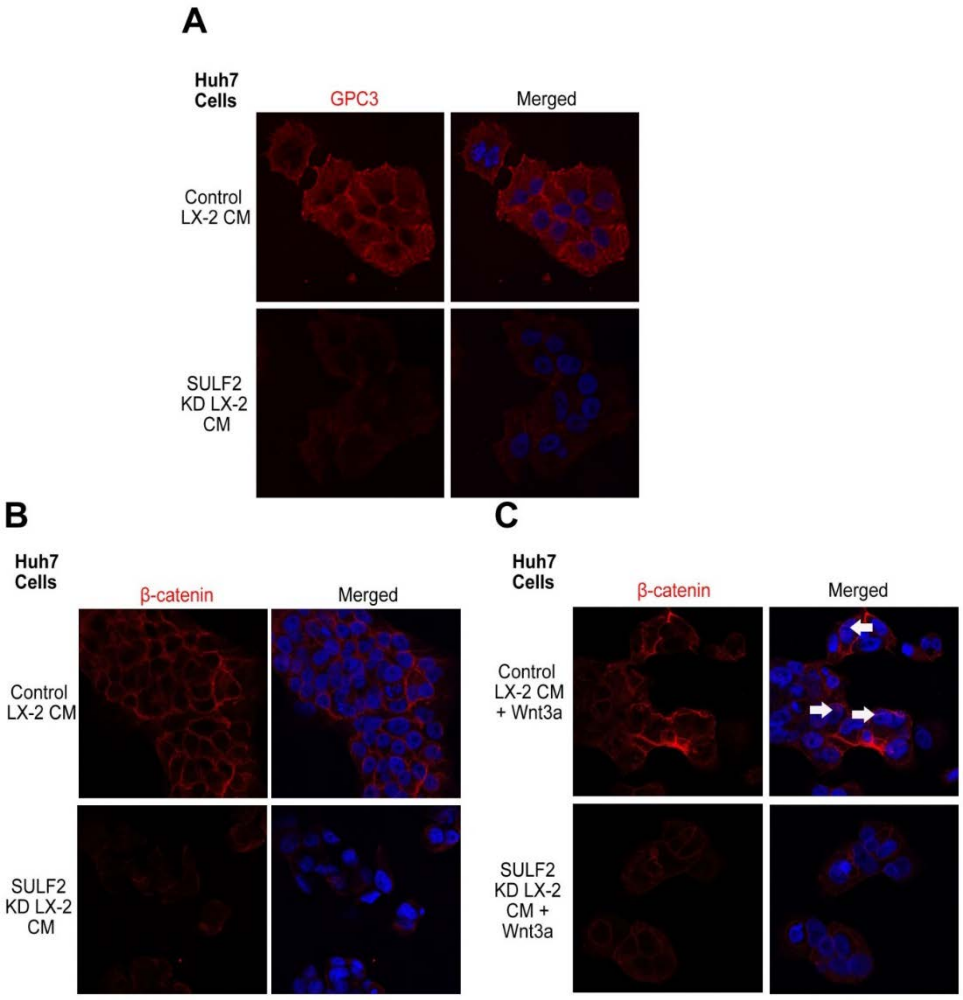

Figure 4.25 Stromal SULF2 upregulated membranous GPC3 and β-catenin in Huh7 cells Confocal images from the immuno-fluorescence staining of Glypican-3 expression in Huh7 cells treated with control LX-2 (SULF2 producing) or SULF2 KD LX-2 (no SULF2) cell CM **(A).** Confocal imaging from the immuno-fluorescence staining shows β-catenin expression and localisation in Huh7 cells treated with control LX-2 or SULF2 KD LX-2 cell CM ± frizzled receptor ligand Wnt-3a (100ng/ml), white arrows denote β-catenin nuclear positivity **(B&C)**, n=3 repeats.

Activation of Wnt signalling is one of the main regulators CSC phenotype in different cancers[366, 371], and given the fact that SULF2 activated Wnt signalling in our patient series, the association between Wnt signalling and NF-κB signalling was investigated. Notably, there was no correlation between nuclear β-catenin and RelA-P-ser536 (Pearson Chi-squared test p=0.331) or between β-catenin and CD44 (Pearson Chi-squared test p=0.336) in our cases, consistent with a SULF2 dependent phenotype.

4.9 Discussion

CAFs affect both the composition of the TME and the behaviour of the other cells in this niche. CAFs regulate many growth factors that bind different receptors, including integrins and laminins[372], as well as secreting ECM factors such as collagens, fibronectin and glycoseaminoglycans[335, 373, 374]. Deposition of these factors in the TME renders the tissue more rigid, a mechanical property that influences the phenotype of CAFs and tumour cells[335, 375, 376]. CAFs can also inhibit the infiltration of the lymphocytes to the tumours, decrease the survival of the mononuclear cells and increase the number of Treg cells that favour a more immuno-suppressive TME[377, 378]. Many angiogenic factors like VEGF[353, 379] or angiopoietins[380] are produced and secreted by the CAFs, initiating neo-angiogenesis by activating the relevant receptors in the endothelial cells. Finally, CAFs also regulate a plethora of cytokines and growth factors that can either directly or indirectly impact on the malignant cells, for example PDGF, IL-6, HGF and TGF-β [350, 381, 382].

Our mechanistic work aimed to characterise the role of stromal-SULF2 on the behaviour of the fibroblasts, but also to investigate the paracrine role of this novel SULF2 positive CAF phenotype, on activation of signalling pathways in the tumour cells. We used *in vitro, in silico* and human tissues to test and validate our hypotheses. Our results showed distinct SULF2-dependent pathways in both the fibroblasts and tumour cells. Some of these observations confirmed previously reported SULF2 dependant activities. The identification of SULF2 as a mediator of fibroblast cytokine production associated with a *CD44* stemness phenotype in tumour cells was particularly novel.

In an autocrine fashion, SULF2 induced PDGFRβ expression, leading to activation of the JNK pathway in fibroblasts. This SULF2-mediated activation of PDGFRβ/JNK pathway increased the production of the inflammatory cytokines IL-6 and IL-8 by fibroblasts, compatible with their known tumour-promoting role. The JNK pathway in fibroblasts has a key pro-tumorigenic role in HCC, with a previous study having shown that global KO of JNK1/2 in mice was protective

against HCC development[137]. Notably, the conditional KO of JNK1/2 from mice fibroblasts, but not from hepatocytes, rendered the mice protected against carcinogenic induction of HCC[137]. This cell-type dependent role of JNK pathway was attributed to an increase in IL-6 cytokine expression and production. Activation of the JNK pathway also has clinical relevance as the deregulation of JNK-associated genes in human HCC is reportedly associated with upregulation of CSC markers, early disease recurrence and a poorer prognosis[383]. Although not previously shown in HCC, the link between tumour SULF2 and IL-6 was previously reported in lung cancers[384]. Ionizing radiation induced IL-6 expression in lung cancer cell lines in a SULF-2 dependent manner leading to induction of metastasis and poorer outcome [384]. CAFs[385-387] and tumour associated macrophages[186] are major sources of IL-6 in the TME, with a paracrine impact on proliferation of adjacent tumour cells previously reported[186].

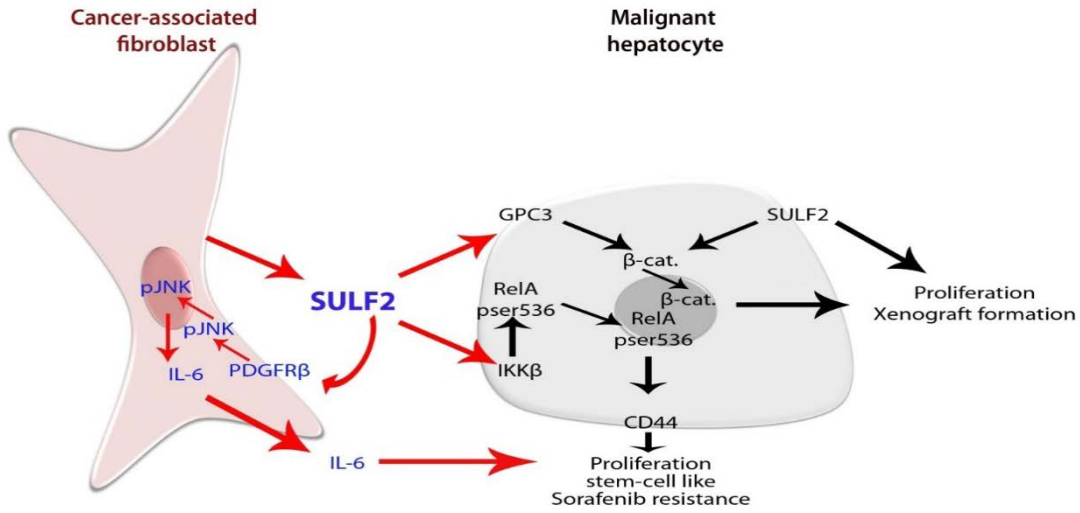

Figure 4.26 Schematic of a model depicting the key mechanistic findings from this study: SULF2-dependent pathways activated in the CAFs (with red arrows) and in the adjacent tumour cells (black arrows).

The cross-talk between tumour cells and CAFs within the TME is believed to be essential in maintaining tumour cell proliferation and give them resistance against environmental challenges. Here we have further characterised a novel paracrine pathway through which CAFs promote a more aggressive tumour phenotype. CAF-SULF2 and its regulated secretome activated IKKβ/NF-κB pathway in the tumour cells and was associated with a proliferative, invasive, CD44 expressing sorafenib resistant phenotype. These finding supported and bring together a previous *in silico* study linking *SULF2* with the progenitor cell, hepatoblast subclass in human HCC patients[388], and a study describing CAFs as regulators of stemness[352]. While the role of IKKβ cascade in the expansion of stem cell features in lung, breast[389] and intestinal cancer[390] was described, similar data in HCC was previously lacking. The role of RelA in the

development of inflammation-associated liver cancer has been previously reported[120], with the paracrine release of TNFα from the adjacent portal and inflammatory cells established. The Human biopsies data presented further validated a proposed paracrine role for SULF2, showing a strong association between CAF-SULF2 and the nuclear translocation of the RelA NF-κB subunit and CD44 membranous expression in neighbouring tumour cells. IL-6 production and therapy resistance associated with CSC features has been previously documented[186, 391], with IL-6 regulating both the transcription and the alternative splicing of *CD44* in multiple myeloma cell lines[392].

SULF2 has been previously implicated in the regulation of a number of signalling pathways in HCC, including activation of the Wnt pathway and upregulation of the well-known oncogene, GPC3[273, 304,393]. GPC3 is frequently expressed in HCC and often used as a diagnostic tissue biomarker. However, the pattern of GPC3 expression varies in HCC and prognostic associations with grade or outcome are not consistent as reviewed previously[270, 369]. Our data suggests that GPC3 co-expression with SULF2 offers a novel stratification for GPC3 positive cases, identifying those in whom GPC3 had poor prognostic relevance. *In vitro*, we also showed that stromal SULF2 upregulated GPC3 expression in the tumour cells. The role of SULF2 in the upregulation of GPC3 was previously reported[273], although our data cast a novel focus on the role of stromal SULF2 on upregulating GPC3 in the tumour cells. Targeting the component proteins or regulators of Wnt pathway has the potential to benefit many HCC patients[394]. Our clinical data suggests that the cross-talk between GPC3 in the tumour cells and SULF2 in the CAFs is important for the upregulation and nuclear translocation of β-catenin, thereby activating the Wnt/β-catenin signalling. *In vitro*, we showed that stromal SULF2 upregulated β-catenin, in the membrane of the tumour cells which was translocated to the cytoplasm and nucleus by adding Wnt3a to the SULF2 positive CM. Although the upregulation of membranous β-catenin in the SULF2 positive CM-treated Huh7 cells was evident, the nuclear translocation of β-catenin was not very convincing. Therefore, investigating the nuclear translocation of β-catenin using TopFlash/FopFlash reporter assay was used to confirm a potential role for stromal SULF2 in Wnt/β-catenin pathway activation.

Both Wnt/β-catenin and NF-κB signalling pathways are implicated in the regulation of liver cancer stemness[395-397]. CSCs are plastic cells and are able to self-renew, proliferate, migrate and resist chemotherapy[367, 398, 399]. Although a direct RelA-P-ser536/β-catenin/CD44 pathway

driving the expansion of CSCs in intestinal tumorigenesis[366] has recently been described, with RelA-P-ser536 promoting β-catenin translocation, we did not demonstrate a direct relationship between RelA-P-ser536 and nuclear β-catenin in our HCC cases. We do, however, highlight a novel mechanism whereby CAFs releasing SULF2 activates both NF-κB and β-catenin in association with the upregulation of CD44.

Our data derived from a combination of *in vitro* and *in vivo* studies are compelling and may have clinical relevance in a number of contexts. We corroborate that CAF-driven SULF2 expression has prognostic relevance in HCC. As an active protein released into the TME and associated with tumour progression, targeting SULF2 represents a novel therapeutic candidate. While there are currently no therapies directly targeting SULF2, its role potentially regulating stemness and therapy resistance make it noteworthy, as does the potential to use SULF2 expression in a predictive fashion. HCC SULF2 has been implicated in the regulation of the established morphogen, GPC3[273, 304]. Stromal SULF2 in part exerts its pro-tumorigenic actions through up-regulation and activation of the GPC3, Wnt/β-catenin signalling pathway in tumour cells and may similarly have biomarker potential in this context. Stratification of patients according to SULF2 and GPC3 tissue positivity provided a better prognostic tool, identifying those with poorest outcomes. These candidate biomarkers might also be useful for identifying patients less likely to respond to sorafenib, or perhaps more likely to respond to an inhibitor of GPC3 or SULF2 activity. In conclusion, SULF2 in the TME, derived from either tumour or stromal cells, has exciting therapeutic potential and is a candidate worthy of further study.

Chapter 5: Characterisation of SULF2 in Non-alcoholic fatty liver disease (NAFLD) and non-alcoholic steatohepatitis (NASH) *in vivo.*

5.1 Background.

NAFLD, or fat deposition in the liver in the absence of excessive alcohol consumption, describes a wide spectrum that ranges from mild simple steatosis to higher levels of fat with necro-inflammatory changes known as NASH[400]. The prevalence of NAFLD exceeds 25% of the population globally[39] and is typically associated with obesity, insulin resistance as well as other features of the metabolic syndrome like hypertension and hyperlipidaemia[401]. As a consequence of the breakthrough of direct acting antiviral agents (DAAs) in the treatment of HCV, in combination with the dramatically rising prevalence of global obesity, NAFLD is becoming one of the commonest causes of advanced liver diseases and HCC[41]. NAFLD-HCC arises in patients who are typically older, of male gender, with features of metabolic diseases[402, 403]. Approximately one third of NAFLD-HCC develops in the absence of cirrhosis, with NAFLD-HCC patients more likely to be non-cirrhotic compared to those with HCV-HCC[42]. Why people with non-cirrhotic NAFLD develop HCC is not well understood, but it is increasingly appreciated that people with the metabolic syndrome have a higher risk of developing cancers, with both obesity and T2DM independently associated with HCC risk, even in the absence of NAFLD[26]. Understanding the mechanisms involved will be key to the development of preventive strategies.

Previous studies have reported a link between SULF2 and obesity, with SULF2 having a role clearing remnant triglycerides and influencing blood triglyceride levels[404-406]. Glycomic focused microarray analyses in livers from obese mice, exploring various HSPG assembly-related genes, T2DM-related HSPG genes and genes involved in the posttranslational modification of HSPG structures, revealed a dramatic upregulation of *Sulf2*[404]. Mechanistic studies suggested that Sulf2 mediated the degradation of syndican-1 - a HSPG receptor on the surface of responsible for the uptake of apo-lipoprotein B (apoB) remnants. The upregulation of hepatic *Sulf2* was associated with decreased clearance of these atherogenic lipoproteins, which, in theory, could contribute an increased risk of developing atherosclerosis as a part of the metabolic syndrome in mice[404]. Notably, a single nucleotide polymorphism (SNP) rs2281279 in *SULF2* has been previously reported to be associated with lower *SULF2* levels and also with removal of postprandial triglyceride rich remnants in healthy donors[405].

Hepatic SULF2 expression in patients with NAFLD

In Prof Reeves lab, as part of an FP7 European Commission funded award entitled Fatty Liver Inhibition of Progression (FLIP), a role for SULF2 in NAFLD was explored in human tissues. SULF2 IHC was performed in 36 diagnostic biopsies from patients with NAFLD (by MRes student, Rebecca Harrison). Details of the pilot cohort are shown in **Table 5.1**. The histological severity of NAFLD was scored by liver pathology staff at the Newcastle upon Tyne Hospitals NHS Foundation Trust. SULF2 immunostained slides were assessed by two observers (Prof Reeves and liver pathologist, Dr Dina Tiniakos), blinded to clinical details at 100x magnification, as detailed in **Table 5.1**.

Table 5.1	**patients (36)**		**Patients (36)**
Age (median)	55	**Sex** (male/female)	26/13
BMI (median)	35.8		
T2DM no/yes	17/19		
Steatosis (0/1/2/3)	0/12/20/4	**ALT**	69.3 ± 5.8
Ballooning (0/1/2)	8/22/6	**AST**	47.2 ± 2.8
Lobular inflammation (0/1/2)	9/17/9	**ALP**	95.5 ± 6.7
Portal inflammation (0/1/2)	17/14/4	**Bilirubin**	9.5 ± 0.8
Mallory-Denk bodies (0/1/2)	14/18/2	**Albumin**	46.1 ± 0.5
Acid bodies (0/1/2)	21/5/1	**Prothrombin time (PT)**	10.6 ± 0.13
Megamitochondria (0/1)	28/2	**HBA1c**	8.2 ± 1.2
Lipogranuloma (0/1)	15/21	**Triglycerides**	2.1 ± 0.18
Fibrosis (0/1/2/3/4)	6/12/5/10/3	**LDL**	3.2 ± 0.22
NAS score* (1/2/3/4/5/6)	2/7/6/10/7/4	**HDL**	1.1 ± 0.04
SULF2 Immunohistochemistry - The percentage of SULF2-positive hepatocytes (cytoplasm, cell membrane, canalicular) was semi-quantitatively assessed with a score from 0-4 (0 = no hepatocytes positive, 1 = 1-25% positive, 2 = 26-50% positive, 3 = 51-75% positive, 4 = 76-100% positive). The SULF2-specific staining intensity (SI) was assessed with a score from 0-3 (0 = no staining, 1 = weak, 2 = moderate, 3 = strong). If a range of staining intensity was noted the predominant score was used. Presence and intensity of endothelial staining was recorded on all cases as an internal positive control.			
% Hepatocyte cytoplasmic score (0/1/2/3)	0/12/14/10		
Hepatocyte cytoplasm intensity score (0/1/2/3)	12/22/2/0		
Hepatocyte canalicular surface score (0/1/2/3)	1/28/3/4		
Hepatocyte cell membrane score (0/1/2/3/)	4/16/12/5		

Table 5.1: Demographic and clinico-pathological features of NAFLD/NASH patients Abbreviations: T2DM; Type-2 Diabetes mellitus, BMI; body-mass index, NAS score; NAFLD activity score, ALT; Alanine aminotransferase, AST; Aspartate aminotransferase, ALP; Alkaline phosphatase, LDL; Low density lipoprotein and HDL; High density lipoprotein. *NAS – NAFLD activity score derived from adding scores for steatosis, ballooning and lobular inflammation.

The median age of patients was 55 years, with a median BMI of 35.8. 26 were male (66%) and 19 patients (55.9%) had type 2 Diabetes mellitus (T2DM). Only 3 of 36 (8%) were graded histologically as having cirrhosis, but 10 had grade 3 fibrosis and 21 patients had a NAS score greater than 3 – indicating at least an element of NASH being present in over half of the cases.

SULF2 expression was elevated in patients with NAFLD

As previously described in Chapter 3, SULF2 was detected by IHC in bile ducts and in endothelial cells, serving as an internal positive control. In patients with simple steatosis, SULF2 expression was scant and detected on the canalicular surface of the hepatocytes, also as previously described in normal liver. In general, however, it was noted that while cytoplasmic hepatocyte expression of SULF2 is uncommon in normal liver, SULF2 was present at some level in the cytoplasm of every case with NAFLD. In 24/36, it was present in over 25% of hepatocytes. In fact, the % of hepatocytes with SULF2 cytoplasmic expression did not correlate with any markers of histological severity, and in a number of cases the intensity score overall was regarded as zero, as the majority of hepatocytes had no cytoplasmic SULF2. On the other hand, the intensity of SULF2 expression did have some notable associations, correlating with the steatosis score and the severity of portal inflammation (Spearman Correlation steatosis 0.357, p=0.033; portal inflammation 0.392, p=0.020).

Membranous SULF2 expression was increased in more advanced NAFLD

Prominent in some cases with NAFLD, was an increase in the % of hepatocytes with membranous expression of SULF2. Rather than expression on the canalicular surface, as is frequently observed at low levels in normal liver, this increase was most evident on the hepatocyte surface membrane. The data are summarised in **Table 5.1**, with examples shown in **Figure 5.1**. Notably, membranous expression of SULF2 was significantly associated with more severe NAFLD. It correlated weakly with the presence of ballooning (Spearman Rho 0.344, p=0.04), more so with portal inflammation (Spearman Rho 0.434, p=0.009), the presence of acidophil bodies (Spearman Rho 0.519, p=0.006) and megamitochondria (Spearman Rho 0.434, p=0.016), as well as with the severity of fibrosis (Spearman Rho 0.466, p=0.004).

SULF2 expression in non-parenchymal cells

In addition to expression of SULF2 in healthy bile ducts, positive cytoplasmic immunostaining of variable intensity was often noted in areas of ductular reaction, or proliferating immature bile ducts. Cytoplasmic expression was also noted in some portal lymphocytes and

macrophages, although not in every case. Similarly, positive Kupffer cells and lymphocytes were noted within sinusoids, but not in all cases.

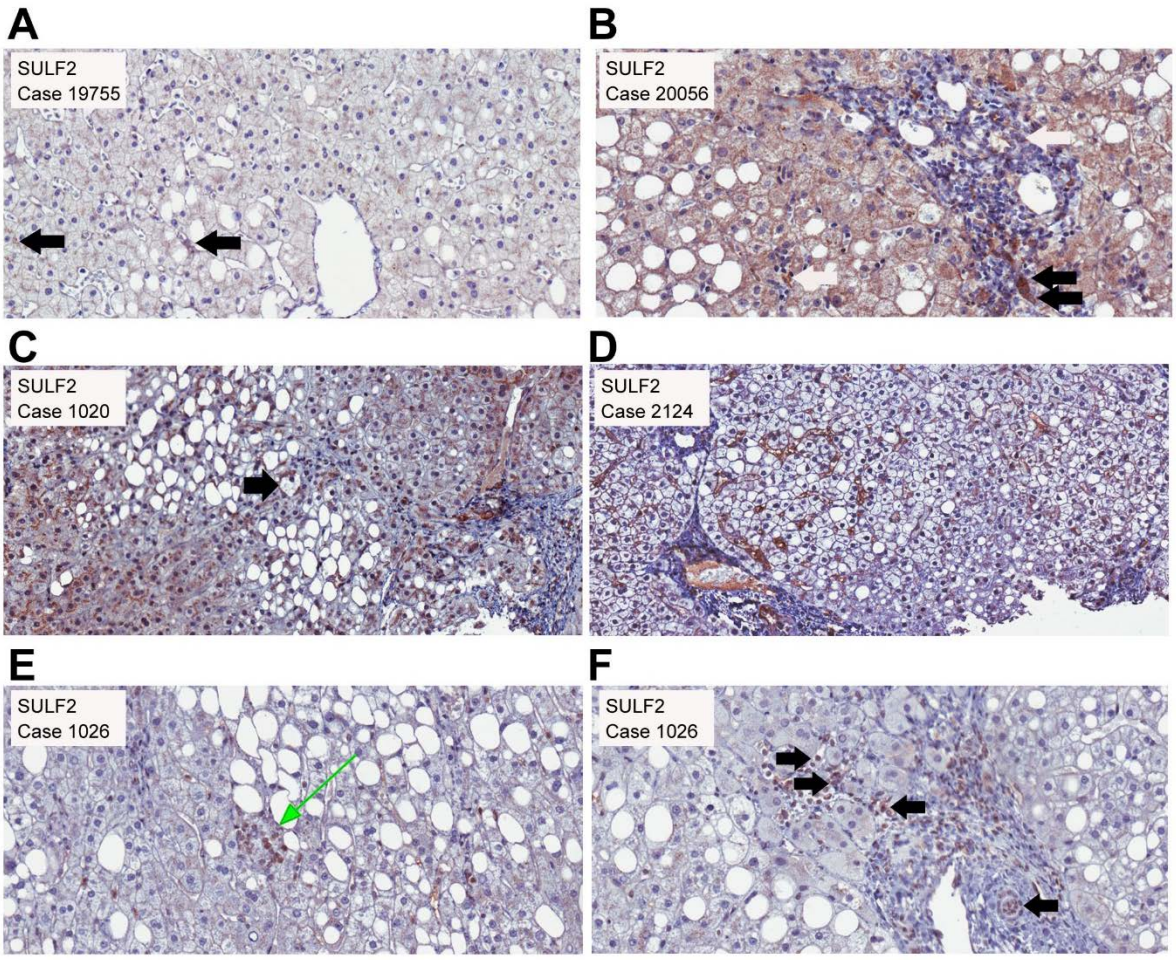

Figure 5.1 SULF2 expression patterns in NAFLD. Representative images show IHC staining of SULF2 in human biopsies from five patients with graded NAFLD **(A-F).** In **(A)**, with steatosis grade 1, no fibrosis and a NAS score of 1, SULF2 was scant, detected in the canalicular and sinusoidal areas (black arrows). In **(B)**, with grade 2 steatosis, stage 2 fibrosis and a NAS score of 5, SULF2 was present in the hepatocytes, inflammatory cells in the sinusoids, portal areas (white arrows) and immature bile ducts (black arrows). In **(C)**, with grade 1 steatosis, stage 2 fibrosis and a NAS score of 3, SULF2 was expressed in the membrane of ballooned hepatocytes (black arrow) and hepatocytes. In **(D)**, with grade 2 steatosis, stage 2 fibrosis and a NAS score of 4, membranous hepatocyte SULF2 was notable. In **(E and F)**, with grade 2 steatosis, stage 3 fibrosis and a NAS score of 6, SULF2 was present in inflammatory cells in areas of lobular inflammation (green arrow), in some sinusoidal cells **(E)**, and in inflammatory cells adjacent to portal tracts, (black arrows) **(F)**. Images were captured using Aperio Imagescope software at x20 magnification.

In summary, SULF2 was upregulated in liver biopsies from patients with NAFLD, with a distinct membranous pattern in those with more advanced disease. Expression in immunoregulatory cells was also noted. To explore further the expression of SULF2, in a longitudinal fashion in the development and progression of NAFLD, with an opportunity to characterise the

expression further in inflammatory cells as well as hepatocytes, we planned to characterise expression in a relevant in an animal model of disease.

5.2 Chapter 5 aims

5.2.1 To define the histological changes accompanying disease development in a diet-induced murine model of NAFLD-HCC.

5.2.2 To perform *SULF2* focused pathway analyses of RNA-sequencing data from the murine NAFLD-HCC model.

5.3 A relevant murine model for NAFLD/NASH and NASH/HCC

As part of the FP7 funded FLIP study referred to above, the Reeves/Oakley lab explored a number of different experimental mouse models, aiming to identify one that recapitulated the features of human NAFLD and NAFLD-HCC. Research Associate Dr Gillian Patman and research technician Anna Whitehead were responsible for delivering the model, including the handling of the blood and liver tissues. As it is aged patients with the metabolic syndrome and NAFLD that are more susceptible to developing HCC[402], the selected model centred on studying the impact of a fat-rich diet on ageing mice. For the purpose of studying the impact of the metabolic syndrome and HCC, C3H/He mice were chosen as they are known to develop impaired glucose tolerance and spontaneous HCC with age. C3H/He mice are less susceptible to HCC than B6C3F1 (a hybrid of C57BL/6 ♀ and C3H/He ♂) mice, but more susceptible to HCC than the relatively resistant strain C57BL/6. The mice were fed an American life style diet (ALIOS), with high fat and sugar water[330]. A pilot study in 2012 confirmed the development of steatosis and HCC at 1 year of age. *Sulf2* expression was assessed in mRNA extracted from whole liver by real time PCR. In the livers of mice fed the ALIOS diet, *Sulf2* was significantly elevated ($p=0.003$) and correlated with body weight (Spearman Rho 0.542, $p=0.011$), liver weight (Spearman Rho 0.599, $p=0.004$) as well as tumour number (Spearman Rho 0.752, $p<0.0001$) and size (Spearman Rho 0.447, $p=0.042$).

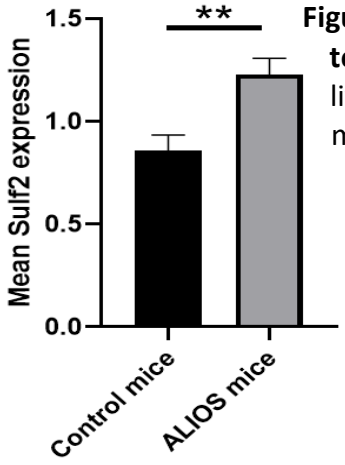

Figure 5.2 Hepatic Sulf2 is upregulated in ALIOS-fed mice compared to matched controls. Graph shows the expression of *Sulf2* in the liver of 10 control and 11 ALIOS-fed mice**.** Data are presented as mean± S.E.M, ** p<0.01**.**

Encouraged by these findings, a larger study including animals culled at different time points, with formal histopathology grading of NAFLD, was performed thereafter, as summarised below and described in more detail in Methods Chapter 2.

5.3.1 Gross features and Histological characterisation of the ALIOS-fed C3H/He model

Two groups of C3H/He mice were on control or ALIOS diet for 12, 24, 36 and 48 weeks, and two more groups were introduced where the Dietary intervention was co-administered with the carcinogen DEN **(Figure 5.3)**.

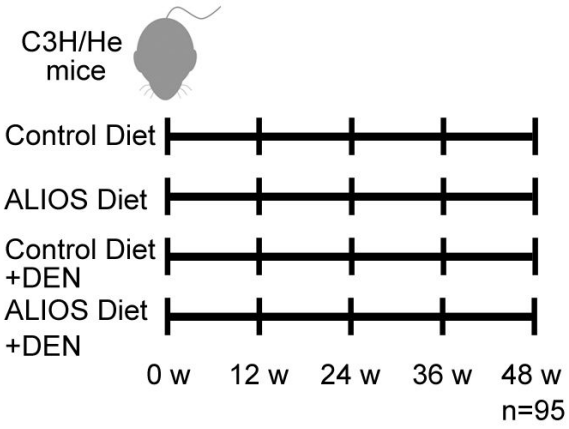

Figure 5.3: Work flow of the murine mouse model of diet-induced NASH/HCC. Mice on dietary intervention alone or with DEN liver carcinogen were culled 12, 24, 36 and 48 weeks after the intervention. Abbreviation: w; week, DEN; Diethyl nitrosamine, n; number of mice.

ALIOS-fed C3H/He mice exhibited obesity, represented by the increase in their body weight compared to the control group. This increase in body weight was significant throughout the whole study except for the 12 week time point **(Figure 5.4A)**. Similarly, the livers of ALIOS mice were bigger compared to the control group in all study time points **(Figure 5.4B)**.

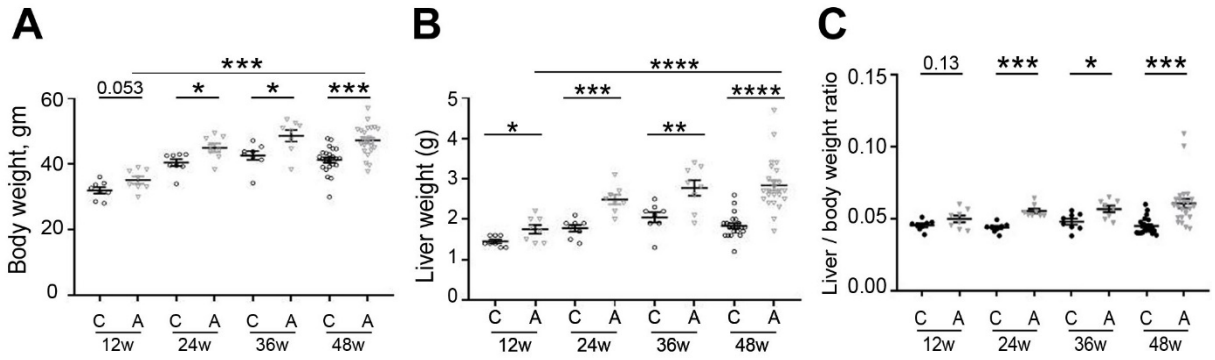

Figure 5.4: ALIOS diet induced obesity and higher liver weight in C3H/He mice. Graphs show the change of both body weight **(A)**, liver weight **(B)** and liver/body weight ratio **(C)** between control (C) and ALIOS (A) fed mice at 12 (n=8 per group), 24 (n=8 per group), 36 (n=8 per group) and 48 weeks (n=24 per group). Data are presented as mean ± S.E.M, * p<0.05; ** p<0.01, *** p=0.001, **** p<0.001.

The strongest Histological criteria associated the development of human NAFLD and NASH includes the grade of steatosis (scored 0-3), the severity of fibrosis (scored as 0-4 stages), the presence of lobular inflammation, the presence of hepatocyte ballooning and lipogranuloma[341]. Ancillary diagnostic features include microvesicular steatosis, pigmented kupffer cells, the presence of Mallory denk bodies and presence of megamitochodria. These histological features were comprehensively assessed in the livers of both the control- and ALIOS-fed mice and scores are listed in **(Table 5.2A and 5.2B)**.

At the 12 week time point, all ALIOS-fed mice developed steatosis scored as grade of 1 or 2 **(Figure 5.5A)**, while the control-fed mice were graded as 0 and 1 steatosis **(Figure 5.5C)**. Inflammatory changes, represented by portal inflammation and lobular inflammation, and architectural change (hepatocyte ballooning) were comparable between control and ALIOS fed mice at this time point, as was the NAS score **(Table 5.2A).** No fibrotic changes were observed **(Figure 5.5B&D)**. The ancillary features commonly seen in patients with NASH were not observed. These features are summarised in **Table 5.2B**

Table 5.2 Histological characterisation of the C3H/He mice fed with control or ALIOS diet

5.2A Classical features for diagnosis and severity assessment in NAFLD and NASH			
	Control Diet	**ALIOS diet**	**p value**
Steatosis grade (0/1/2/3)			
12 weeks	4/4/0/0	0/5/3/0	0.0196
24 weeks	0/1/7/0	0/2/5/1	>0.9999
36 weeks	2/2/4/0	0/0/6/2	0.0326
48 weeks	4/10/9/0	0/1/19/4	<0.0001
Hepatocellular ballooning (0/1/2)			
12 weeks	6/2/0	6/2/0	>0.9999
24 weeks	2/6/0	2/3/3	0.4671
36 weeks	3/4/1	5/3/0	0.4365
48 weeks	8/11/4	1/21/2	0.1213
Lobular Inflammation score (0/1/2)			
12 weeks	4/3/1	5/3/0	0.7063
24 weeks	7/1/0	5/3/0	0.5692
36 weeks	6/1/1	2/3/3	0.1058
48 weeks	12/11/0	1/17/6	<0.0001
NAFLD activity (NAS) score			
12 weeks	1.375 ± 0.3750	2.125 ± 0.3981	0.2752
24 weeks	2.750 ± 0.2500	3.500 ± 0.4226	0.2340
36 weeks	2.375 ± 0.3750	3.625 ± 0.4199	0.0665
48 weeks	2.522 ± 0.2802	4.417 ± 0.1989	<0.0001
Portal Inflammation score (0/1/2)			
12 weeks	1/6/1	2/2/4	0.3629
24 weeks	3/5/0	2/4/2	0.4499
36 weeks	0/6/2	0/1/7	0.0406
48 weeks	21/2/0	18/4/2	0.1914
Peri-sinusoidal fibrosis score (0/1)			
24 weeks	0/8	0/8	>0.9999
48 weeks	7/16	0/24	0.0039
Peri-portal fibrosis score (0/1/2)			
24 weeks	3/5	0/8	0.2000
48 weeks	17/6/0	12/11/1	0.1152
Fibrosis stage (0/1/2/3)			
24 weeks	0/6/2/0	0/1/7/0	0.0406
48 weeks	7/10/6/0	0/12/11/1	0.0097

At 24 weeks of age, steatosis in the livers of both ALIOS- and control-fed mice was scored as grade 1 and 2 with no statistical difference between the two groups **(Figure 5.6)**. Most of the ALIOS fed mice had a score 2 fibrosis, however, 75% of the aged matched mice had a fibrosis score of 1, and this higher fibrosis stage in the ALIOS group was statistically significant (p=0.0406) from that in the control diet **(Table 5.2A)**. Importantly, hepatocyte ballooning **(Figure 5.6A&C)** was similarly present in both groups. Portal and lobular inflammation appeared more common in the ALIOS mice compared to the matched control, but without statistical significance **(Figure 5.6C)**. Ancillary features of NASH features were absent in both groups at this time point **(Table 5.2B)**.

Table 5.2B	Ancillary Features of NASH		
	Control Diet	ALIOS diet	p.value
Lipogranuloma (0/1)			
12 weeks	8/0	8/0	>0.9999
24 weeks	8/0	8/0	>0.9999
36 weeks	8/0	8/0	>0.9999
48 weeks	22/1	3/21	<0.0001
Microvesicular steatosis (0/1)			
12 weeks	8/0	8/0	>0.9999
24 weeks	8/0	7/1	>0.9999
36 weeks	8/0	8/0	>0.9999
48 weeks	23/0	16/8	0.0039
Pigmented Kupffer cells (0/present)			
12 weeks	8/0	8/0	>0.9999
24 weeks	8/0	8/0	>0.9999
36 weeks	8/0	7/1	>0.9999
48 weeks	16/7	9/15	0.0454
Mallory Denk bodies (0/present)			
12 weeks	8/0	8/0	>0.9999
24 weeks	8/0	8/0	>0.9999
36 weeks	8/0	7/1	0.4286
48 weeks	18/5	10/14	0.0188
Megamitochondria (0/present)			
12 weeks	8/0	8/0	>0.9999
24 weeks	8/0	8/0	>0.9999
36 weeks	8/0	8/0	>0.9999
48 weeks	20/3	14/10	0.0509

Control mice had grades 0, 1 and 2 steatosis **(Figure 5.7A)** at the 36-week time point, whereas the ALIOS diet increased the steatosis grade in C3H/He mice towards grades 2 and 3 (p=0.03) **(Figure 5.7B)**. Consistent with the previous time point hepatocyte ballooning was evident in both groups **(Figure 5.7A&C)**, but the development of portal inflammation was statistically significant in the ALIOS-fed mice compared to the control group (P=0.04) **(Figure 5.7D)**. Other features of NAFLD/NASH remained unchanged **(Table 5.2B)**.

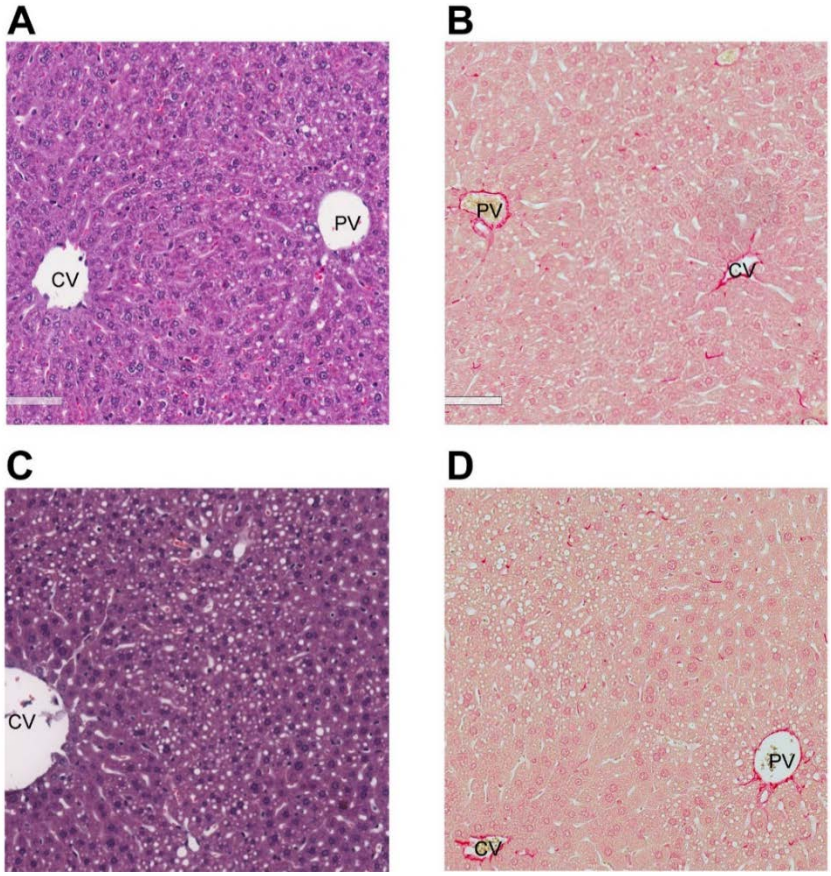

Figure 5.5 No major steatotic or fibrotic changes were observed in liver tissue from C3H/He mice fed on control or ALIOS diet at the 12-week time point. Representative images show H&E and Sirius red stained liver tissue from C3H/He mice fed with control **(A,B)** and ALIOS **(C,D)** diet. **(A)** Liver tissue from control-fed mouse, scored as 0 grade steatosis and 0 fibrosis **(B). (C)** Liver tissue from ALIOS-fed mouse, scored as 1 grade steatosis and stage 0 fibrosis **(D).** CV; central vein, PV; portal vein.

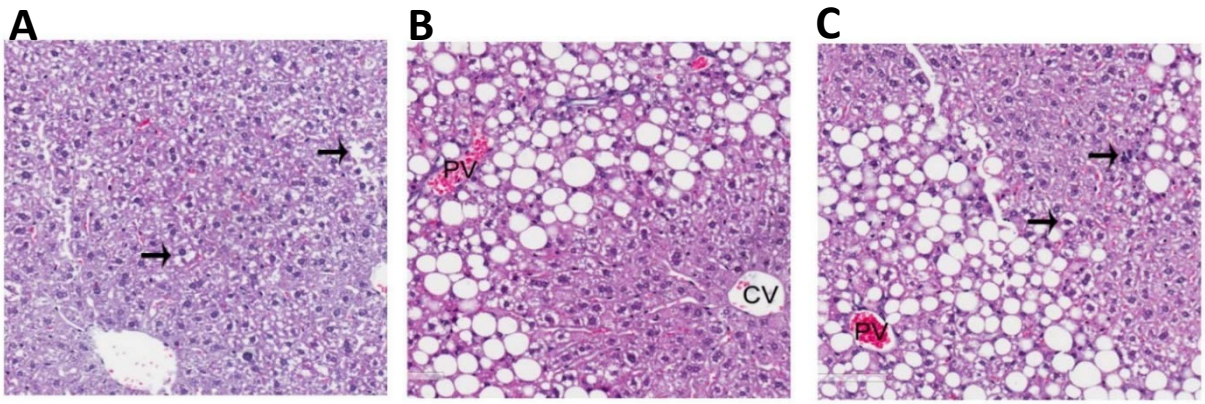

Figure 5.6 Both ALIOS and control-fed mice developed ballooning at 24 week time point. Representative images show H&E stained liver tissues from C3H/He mice fed with control **(A)** and ALIOS **(B&C)** diets. **(A)** Liver tissue from control-fed; this tissue showed few ballooned hepatocytes (grade1) (black arrows). **(B)** Liver tissue from ALIOS-fed mouse, scored as 2 grade steatosis, stage 2 fibrosis, hepatocellular ballooning (grade 2) (black arrow) and lobular inflammation (black arrow) **(C)**. CV; central vein, PV; portal vein.

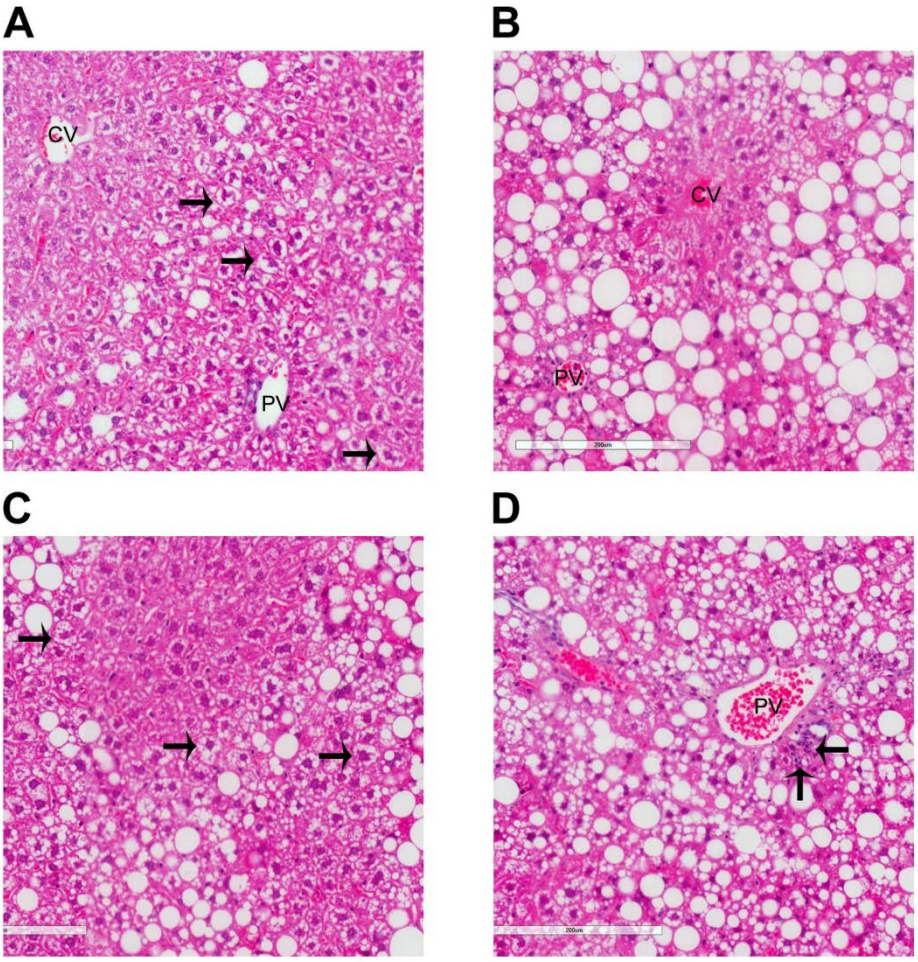

Figure 5.7 Increased steatosis with features of NASH in ALIOS-fed mice, but not the matched controls, at 36 weeks Representative images show H&E stain of liver tissues from C3H/He mice fed with control **(A)** and ALIOS **(B-D)** diet. **(A)** Liver tissue from control-fed mouse, scored as 1 grade steatosis with few ballooned hepatocytes (grade1) (black arrows)**. (B)** Liver tissue from ALIOS-fed mouse, scored as 3 grade steatosis and stage 2 fibrosis. **(C)** Hepatocellular ballooning was present (black arrow). **(D)** Portal inflammation was also evident in this ALIOS-fed mouse. CV; central vein, PV; portal vein.

At the 48-week time point, all ALIOS-fed mice developed (S2-S3) grade compared to age matched chow fed mice ($p<0.0001$) **(Figure 5.8A&B)**. The presence of lipogranuloma was also evident in the ALIOS fed mice but not the control mice ($p<0.0001$) **(Figure 5.8B)**. In addition, livers of the ALIOS-fed mice, but not control mice livers, showed strong fibrotic changes ($p=0.0097$) **(Figure 5.8C&D).** All of the ALIOS-fed mice (100%, 24/24) developed peri-sinusoidal fibrosis at compared to 69.5% (16/23) from the controls. Similarly, 74% (17/23) of the control mice did not develop peri-portal fibrosis and this percentage decreased to 50% when mice were fed on the ALIOS diet **(Table 5.2A)**. Only one mouse in the ALIOS-fed group didn't develop hepatocyte ballooning compared to 12 mice that lacked this feature in the

control group **(Figure 5.8E)**. Considering ballooning scored as (0/1/2), no significant differences were observed at any time point between the two groups.

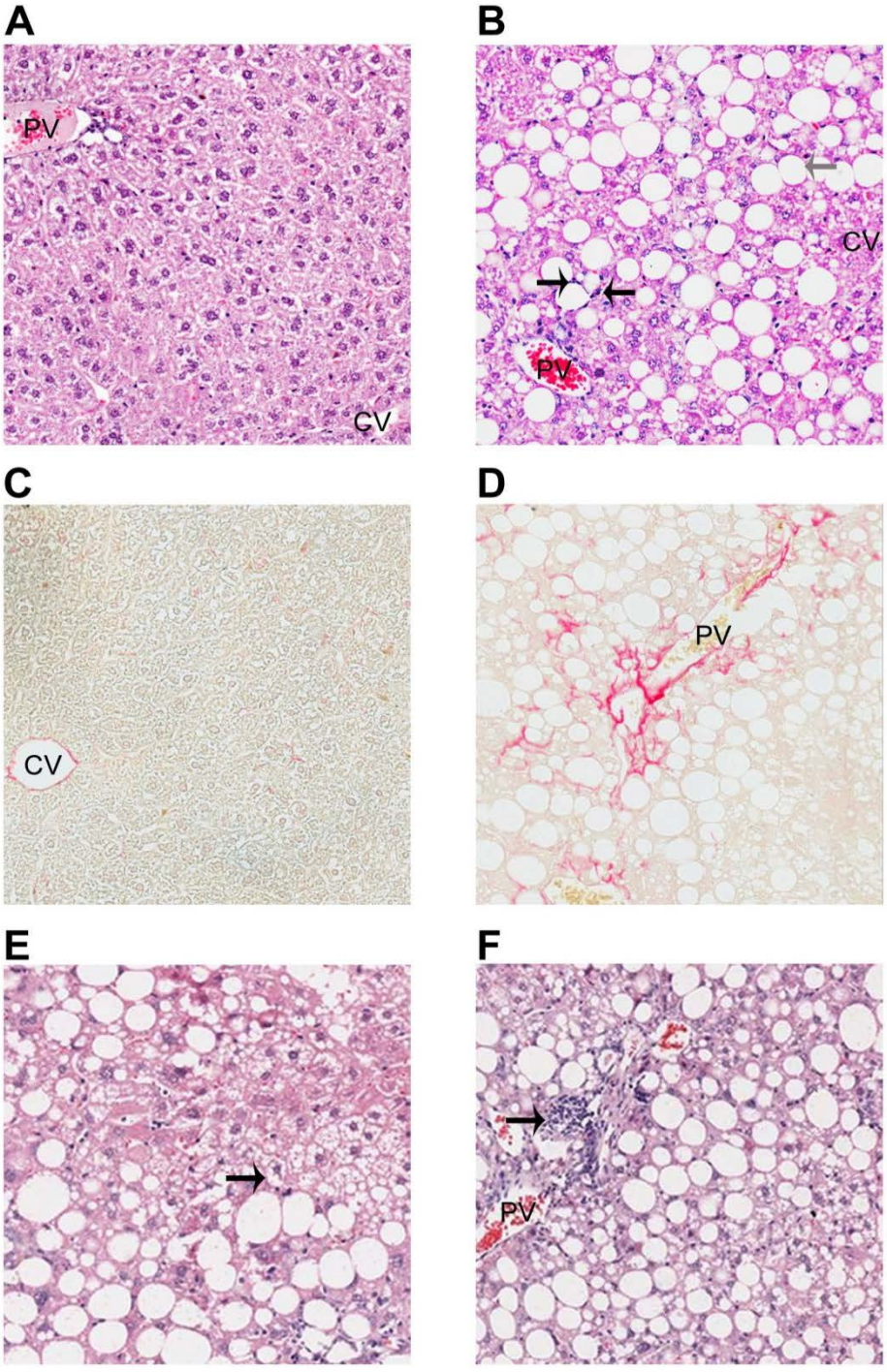

Figure 5.8 C3H/He mice fed the ALIOS diet developed characteristic features of human NAFLD/NASH at 48 weeks of age. Representative images show H&E and Sirius red staining of liver tissues from control **(A,C)** or ALIOS-fed mice **(B,D-F).** ALIOS diet induced more steatosis (grey arrow), lipogranulomas (black arrows) **(B)** and fibrosis **(D). (E)** Hepatocellular ballooning (black arrow) was evident in both groups, but this phenotype was more pronounced in ALIOS fed mice. **(F)** Portal inflammation was present in the ALIOS fed mice**.**

Although some control mice did develop quite marked ballooning, overall the presence of ballooning was more common in ALIOS fed mice. When ballooning was scored as present or absent, this was significantly different (95% of ALIOS diet fed mice versus 65% of control diet developed ballooning; p=0.0102). Lobular inflammation was also evident at 48 weeks in ALIOS mice, and as a consequence of these mentioned histological changes, the NAS score was higher in the ALIOS fed mice compared to the age matched control diet fed mice (p<0.0001) **(Figure 5.9**).

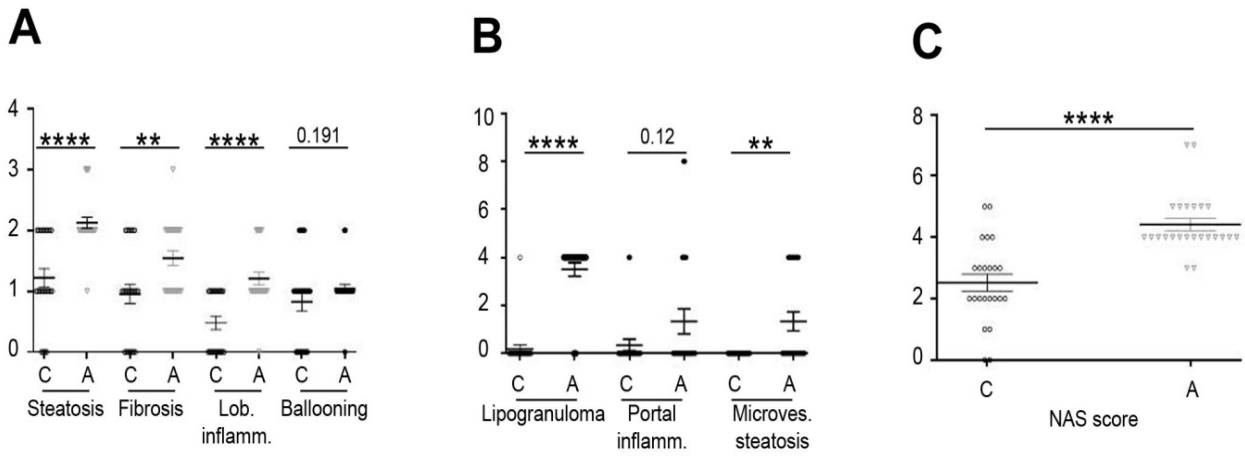

Figure 5.9 Histopathological differences in the livers of C3H/He mice at 48 weeks, fed either control or ALIOS diets. Graphs summarise the changes in steatosis, fibrosis, lobular inflammation (Lob. Inflamm) and hepatocyte ballooning **(A)**, lipogranuloma, portal inflammation (portal inflamm) and microvesicular steatosis (Microves. steatosis) **(B)**, or the NAS score **(C)** in mice fed with control (C) (n=23) or ALIOS (A) (n=24) diets. Data are presented as mean ± S.E.M, ** p<0.01, **** p<0.001.

Other features of NASH including microvesicular steatosis (p=0.0039), pigmented kupffer cells (p=0.045) and presence of Mallory denk bodies (p=0.018) were also evident in the ALIOS-fed mice rather than in the control group at the 48 week time point **(Table 5.2B)**. A trend towards increased in portal inflammation **(Figure 5.8F)** in ALIOS fed mice was not significantly different to control and neither was the presence of megamitochodria. It is important to note that none of the mice in either group or any of the study time points was scored as having stage 4 fibrosis, or cirrhosis **(Table 5.2A).**

Taken together, ALIOS feeding of C3H/He mice exacerbated the severity of fatty liver disease, more so as the mice aged. The phenotypic changes observed in the livers of the mice were similar to those observed in human NAFLD and NASH. A summary of all histological changes at the 48 week time point between the study groups is shown in **Figure 5.9.**

5.3.2 Development of HCC in ALIOS-fed C3H/He mice

As expected in this mouse strain, 5/23 of the control C3H/He mice developed small tumours at 48 weeks (21.7%). However, 23/24 (96%) of ALIOS-fed mice developed HCC in the same time frame **(Figure 5.10)**. Furthermore, the number of tumours developed in the ALIOS fed mice was significantly higher than in control diet mice (2.04±0.4 versus 0.3±0.1, p<0.0001), and were typically larger in size in ALIOS fed mice compared to the control group (7.6±1.1 versus 0.9±0.4, p=0.0003). Concurrent administration of the carcinogen DEN with the diet exacerbated the tumour development phenotype, with tumour number (7.9±2.1 versus 0.7±0.2, p=0.0025) and tumour size (6.3±1.7 versus 2.6±1.1, p=0.08) compared to mice that administered DEN and fed a control diet.

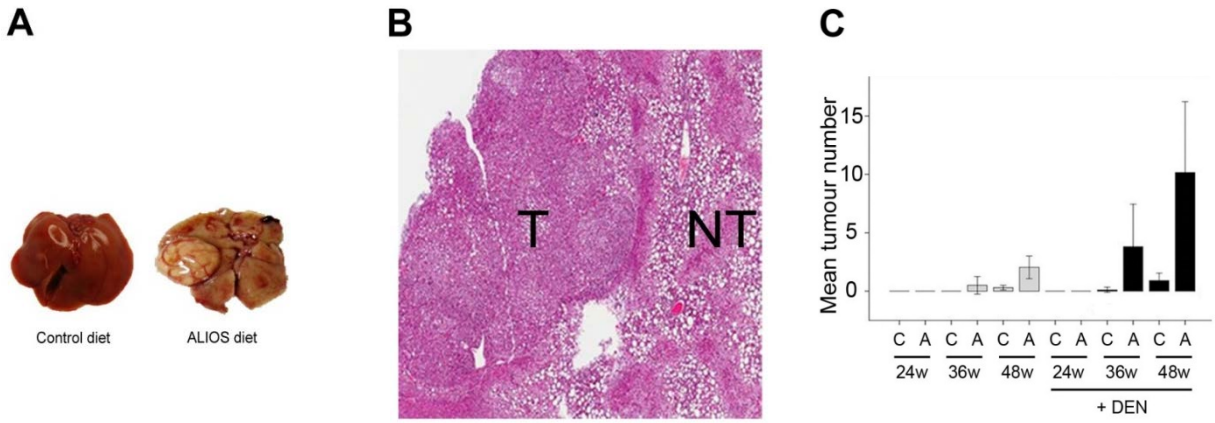

Figure 5.10 Aged C3H/He mice developed more HCC when challenged with ALIOS diet Representative images show a macroscopic tumour in a fatty liver from ALIOS-fed mice compared to a control liver **(A)**, and an H&E stained section of non-tumour (NT) fatty liver tissue from ALIOS-fed mouse with a tumour (T) **(B).** The graph **(C)** shows the number of tumours in livers of C3H/He mice fed with control (C) and ALIOS (A) alone (grey columns) or in combination with DEN (black columns) after 24, 36 and 48 weeks.

5.3.3 The gene expression profile in C3H/He mice

We wanted to explore changes in *Sulf2* in association with histopathological features of NAFLD and NASH in a temporal fashion. Also, with greater numbers, we hoped to establish if associations with HCC were independent of other contributory factors, such as diet, liver weight and histopathological features. Disappointingly, an exhaustive exploration failed to identify a sensitive and specific anti-mouse *Sulf2* antibody for the immunohistochemical characterisation of Sulf2 expression and cellular localisation in the mouse tissues. Consequently our assessments were limited to whole tissue studies at the RNA level. In the hope of characterising these in a more comprehensive fashion, RNA sequencing (RNAseq) was performed in tissues from 48 weeks old mice, including 23 non-tumour and 27 tumour liver

tissues from the control and ALIOS-fed C3H/He mice. The heat map in **Figure 5.11** was generated using R package software. The non-tumour and tumour transcriptomic data clustered into two distinct groups. A list of the top 100 differentially expressed genes based on the adjusted *p* value is included in the **Appendix 1**.

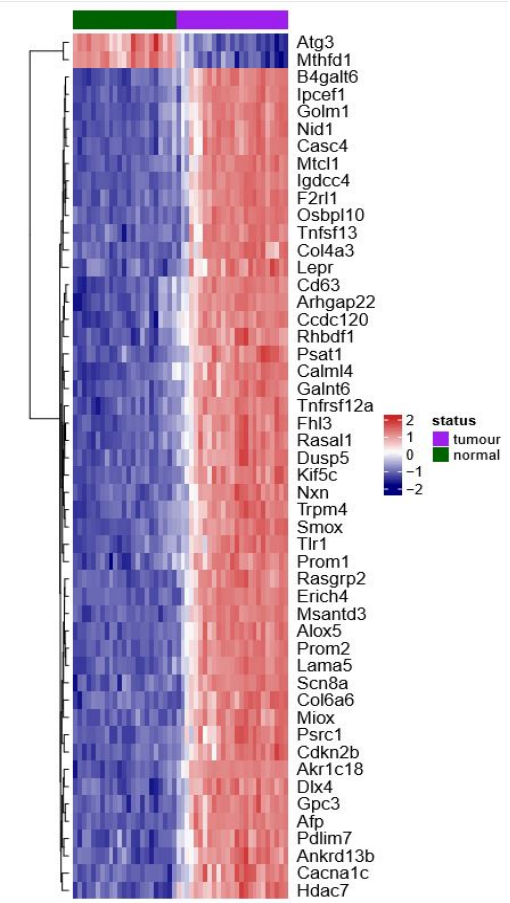

Figure 5.11 The landscape of C3H/He mice tumour and non-tumour transcriptomic data. The heat map shows the top 50 differentially expressed genes between the non-tumour tissue (green) and the tumour tissue (purple) transcriptomic data. Red colour indicates gene upregulation, while blue colour indicates gene downregulation.

Sulf2 was not markedly changed, but – as expected from the pilot study - it was upregulated in the ALIOS group compared to diet matched controls (p=0.0005), albeit with a small fold difference **(Figure 5.12A)**. The *Sulf2* level was comparable between the tumour and the non-tumour groups **(Figure 5.12B)**.

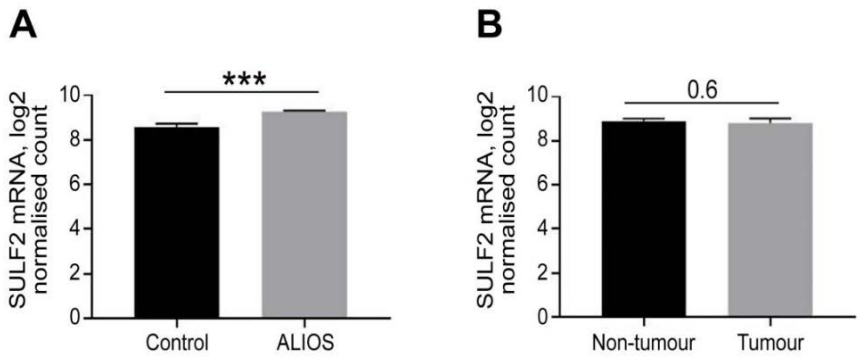

Figure 5.12 The mRNA expression levels of Sulf2 in non-tumour and tumour tissues Graphs show the difference in *sulf2* mRNA expression in the non-tumour liver tissue from control diet and ALIOS-fed mice (n=11 per group) is shown in **(A).** *Sulf2* expression in the non-tumour versus tumour liver tissues of the C3H/He mice (n=23 and 27 respectively) is shown in **(B)**. Data are presented as mean± S.E.M, *** p<0.001.

5.4 *Sulf2* associations with HCC in C3H/He mice

In keeping with the pilot study, *Sulf2* in the whole liver tissues – this time quantified by RNAseq – correlated significantly with the development of tumours (Spearman Rho 0.476, p=0.022), but more so with the number of tumours (Spearman Rho 0.551, p=0.006) and size of tumours (Spearman Rho 0.509, p=0.013) as well as with the tumour burden (Spearman Rho 0.576, p=0.004) as estimated using the sum of the diameter of all tumours in an individual mouse. The numbers studied were still relatively small and while interesting, by binary logistic regression of categorical variables (presence or absence of a tumour; tumours less than or greater than 5mm), the associations were not independent of other factors associated with tumour development, namely the diet, body weight and liver weight.

5.5 *Sulf2* and histological features of NAFLD in the livers of C3H/He mice

Bivariate associations between *Sulf2* and the graded histological features of NAFLD are summarised in **Table 5.3**, with notable highly significant associations with steatosis, inflammation and fibrosis, as well as with some of the other ancillary features of NASH.

	Sulf2 (continuous variable)	
	Spearman's Rho	*p* value
Diet (control vs ALIOS)	0.827	<0.0001
Body weight	0.582	0.004
Liver Weight	0.717	<0.0001
Steatosis (0/1/2/3)	**0.772**	**<0.0001**
Microvesicular steatosis (0/1)	**0.582**	**0.004**
Ballooning (0/1/2)	0.465	0.026
Lobular inflammation (0/1/2)	**0.639**	**0.001**
Portal inflammation (0/1/2)	**0.599**	**0.002**
Mallory-Denk bodies (0/1/2)	0.669	<0.0001
Megamitochondria	0.253	0.244
Apoptotic cells	0.373	0.079
Lipogranuloma (0/1)	**0.840**	**<0.0001**
Fibrosis (0/1/2/3/4)	**0.827**	**<0.0001**
NAS score (1/2/3/4/5/6)	**0.639**	**0.001**

Table 5.3 Association between *sulf2* and the histopathological features of the C3H/He mice

5.6 *Sulf2* pathways analysis in NAFLD development and progression in the C3H/He mice

The complete list of differentially expressed genes created by comparing transcriptomic data of the ALIOS fed mice versus control-fed mice is in **Appendix 2**. In this list, *Sulf2* was elevated in the ALIOS fed mice, although in a non-significant fashion after correction for multiple testing (adjusted p.value=0.06). Hampered by the lack of a suitable antibody to define more subtle changes in cellular source and location, but hypothesising an important biological role in NAFLD progression, this trend to *Sulf2* elevation was explored using a bioinformatics approach in groupings of mice based on grading of steatosis and fibrosis, as hallmarks of disease severity and progression. The first focus presented here was on fibrosis.

5.,6.1 Fibrosis directed bioinformatics analyses with a focus on Sulf2

Accordingly, mice were grouped into two groups; the first group included mice scored with high fibrotic changes (F(2-3); N3, N13, N14, N15, N16, N17, N18, N19, N20, N22, N23), while the second group involved mice with no or few fibrotic changes (F(0-1); N1, N2, N4, N5, N6, N7, N8, N9, N10, N11, N12, N21) **(Appendix3)**.

Running DE gene analysis between the above groups identified 2746 genes differentially expressed, with *Sulf2* upregulated (as expected) in the more advanced fibrosis group (Log2FC 0.56, q.value=0.002). Subsequent pathway analysis was performed using Ingenuity pathway analysis (IPA) software, after applying a cut off value of absolute Log2FC of 0.5 and an adjusted p value of 0.05. Activation of different inflammation-related canonical pathways, including activation of T-cell, natural killer T cells and phagosomes is shown in **(Figure 5.13)**.

A

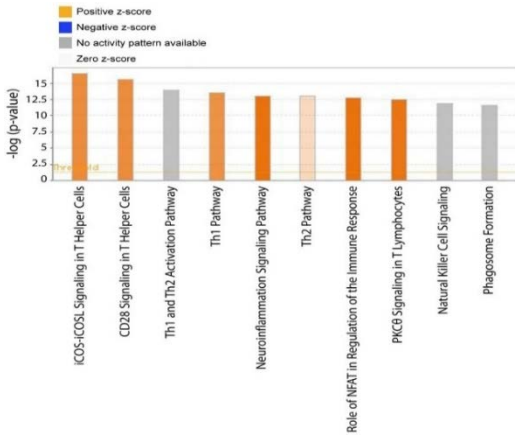

B

IPA canonical pathways	-log (p-value)	z-Score
iCOS-iCOSL Signaling in T Helper Cells	16.6	3.4
CD28 Signaling in T Helper Cells	15.5	3.411
Th1 and Th2 Activation Pathway	13.9	
Th1 Pathway	13.6	3.266
Neuroinflammation Signaling Pathway	13	4.23
Th2 Pathway	13	1.091
Role of NFAT in Regulation of the Immune Response	12.7	4.226
PKCθ Signaling in T Lymphocytes	12.5	4.131
Natural Killer Cell Signaling	11.8	
Phagosome Formation	11.6	

Figure 5.13 Activation of inflammatory pathways in association with more advanced fibrotic stages in C3H/He transcriptomic datasets. The bar chart **(A)** shows canonical pathways identified by IPA, ranked according to –log (q.value) of overlap. Orange represents activation, blue inhibition, and grey a z-score not calculated in the dataset. The intensity of colour is proportional to the increase in absolute activity z-score. The table **(B)** shows the –log (q.value) and z.score of the top 10 activated (orange) canonical pathways from the bar chart.

Notably, cell survival and cell viability were the top activated diseases and bio-functions in this high fibrosis associated list, together with activation of different inflammatory responses. Signalling pathways associated with different types of neoplasms were among the top inhibited diseases and functions **(Figure 5.14)**.

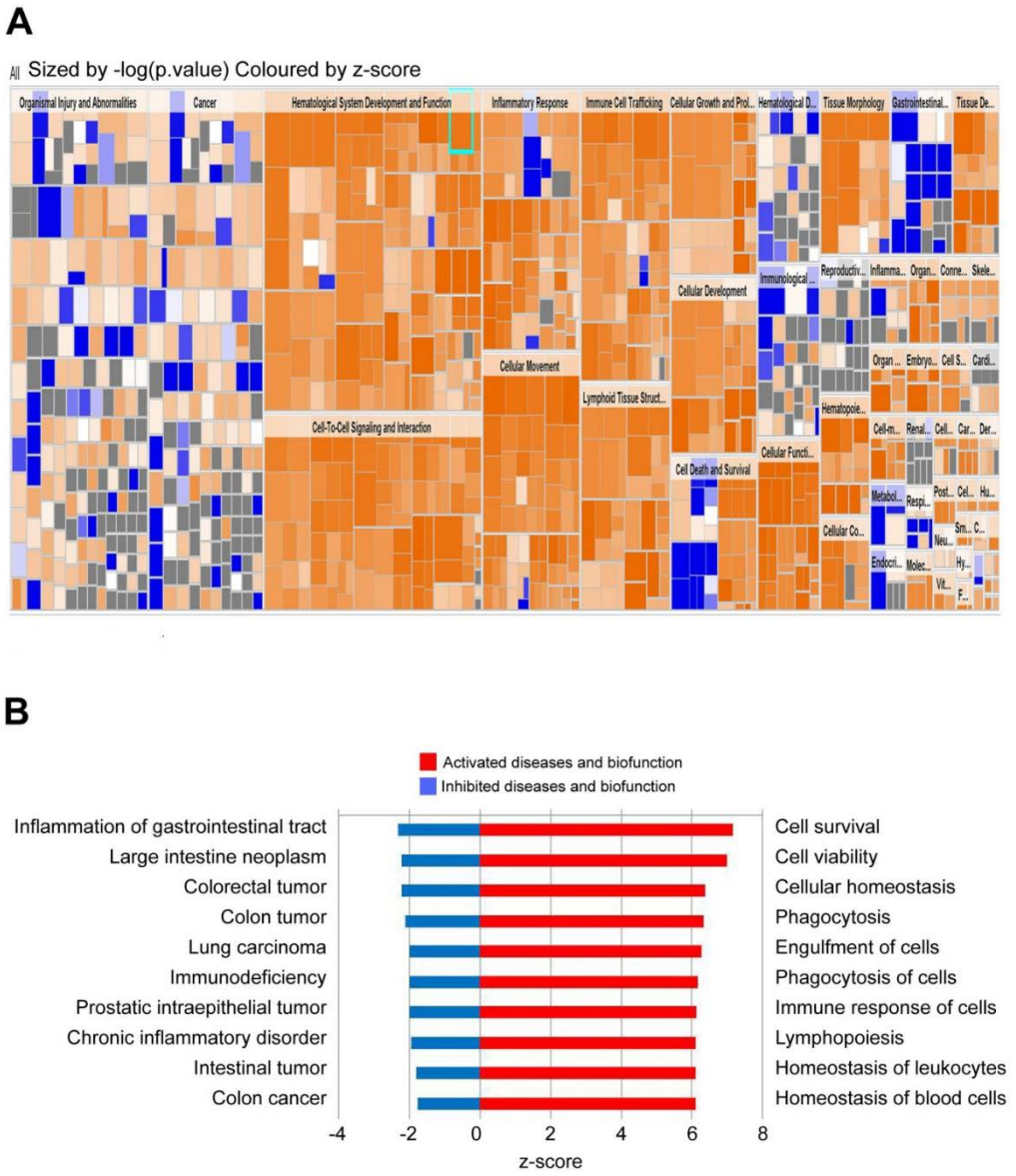

Figure 5.14 Viability, homeostasis and inflammation pathways were activated in the C3H/He mice liver transcriptome in association with fibrotic stages The Heat map **(A)** shows the IPA defined deregulation of different diseases and bio-functions, ranked according to –log (q.value) of overlap. Orange represents activation, blue inhibition, grey an uncalculated z-score and white an activity score of zero. The intensity of colour is proportional to the increase in absolute activity z-score. The bidirectional bar chart **(B)** shows the top 10 activated (red bars) and inhibited (blue bars) diseases and bio-functions defined, ranked according to the activation z.score.

As expected in this fibrotic directed list, IPA network analysis also identified pathways activated in connective tissue disorders, tissue development and cell-to-cell communications **(Figure 5.15A)**. Of note, fibrosis and activation hepatic stellate cells pathways were not among the top enriched ones in the dataset.

Sulf2 didn't appear in any of the top deregulated canonical pathways in this dataset, although diseases and bio-function analysis suggests the involvement of *Sulf2* in cytoskeleton organisation. This was supported by network analysis **(Figure 5.15B)** reporting *Sulf2* in "network 2". These were genes reportedly involved in directing cell morphology, but also associated with a cell-mediated immune response – introducing a previously unsuspected candidate role for *Sulf2*. Also interestingly, upstream analysis identified two novel candidates as potential regulators of *Sulf2* expression in liver, namely IL2 Inducible T Cell Kinase (Itk) and the Transferrin Receptor (Tfrc) **(Figure 5.16).**

A

	Molecules	Networks
1	34	Cell Cycle, Cellular Assembly and Organization, DNA Replication, Recombination, and Repair
2	30	Cell Morphology, Cell-mediated Immune Response, Cellular Movement
3	30	Antimicrobial Response, Inflammatory Response, Developmental Disorder
4	30	Connective Tissue Disorders, Hematological Disease, Organismal Injury and Abnormalities
5	29	Cell-To-Cell Signaling and Interaction, Molecular Transport, Small Molecule Biochemistry
6	29	DNA Replication, Recombination, and Repair, Connective Tissue Disorders, Developmental Disorder
7	29	Tissue Development, Cancer, Organismal Injury and Abnormalities
8	28	Cell-To-Cell Signaling and Interaction, Hematological System Development and Function, Immune Cell Trafficking
9	28	Immunological Disease, Endocrine System Disorders, Gastrointestinal Disease
10	28	Cellular Movement, Cell Cycle, Cell-To-Cell Signaling and Interaction

B

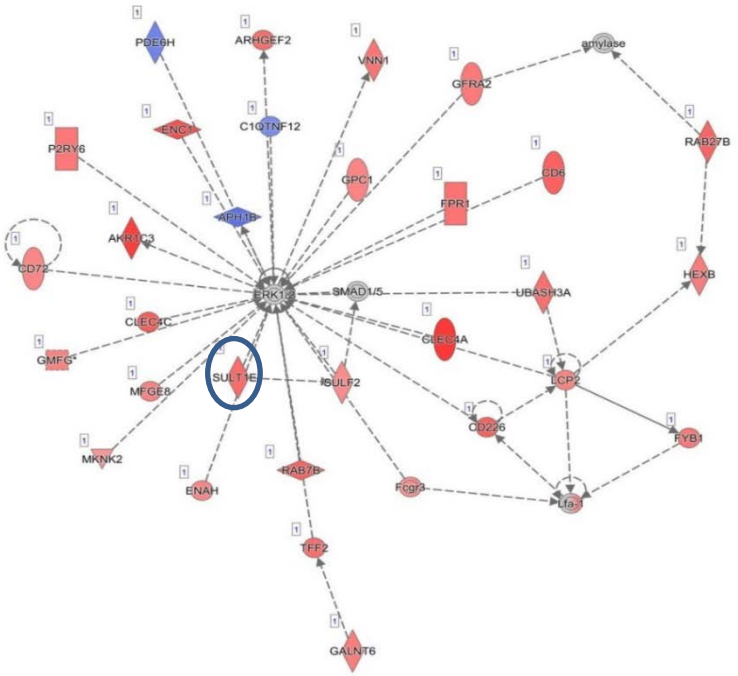

Figure 5.15 A sulf2-related network identified in association with advanced fibrosis in C3H/He liver tissues The Table **(A)** shows the top 10 IPA enriched networks, scored according to the number of genes in the mouse DE gene list overlapping the network. The image **(B)** shows the 2nd activated network in Table A, "cell morphology, cell-mediated immune response and cellular movement", in which *Sulf2* (circle) is involved. Red indicates gene upregulation, blue downregulation.

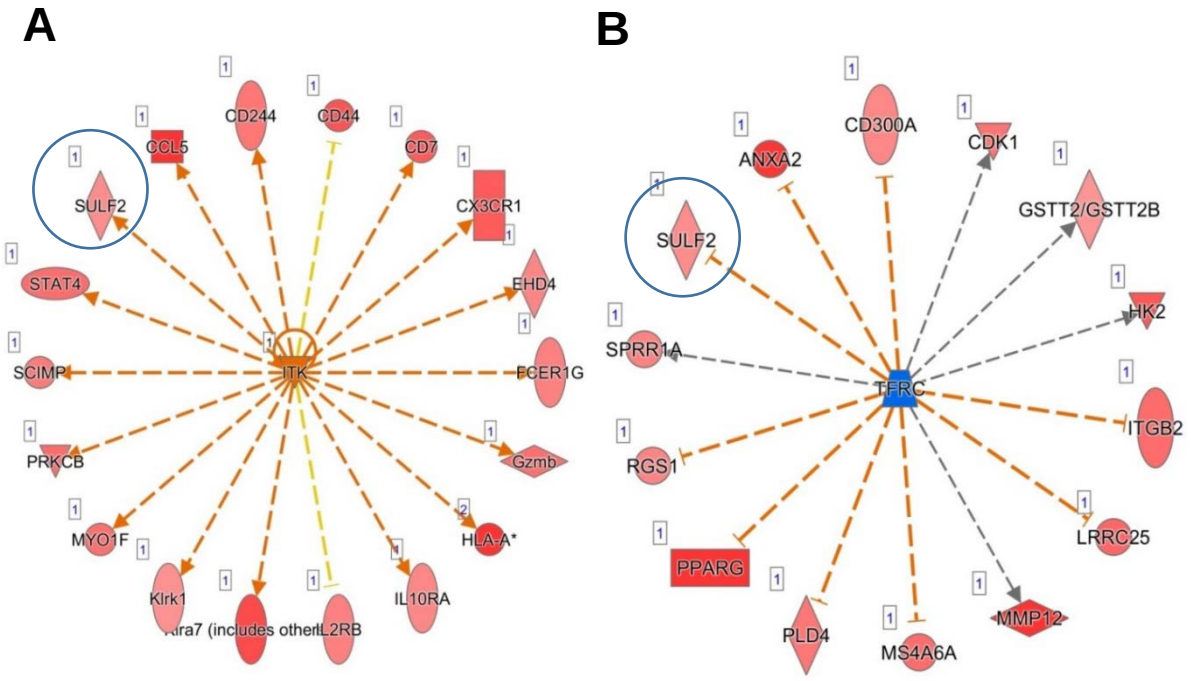

Figure 5.16 itk and tfrc identified as candidate regulators of liver fibrosis related Sulf2 expression The IPA generated Wheel charts suggest upstream regulators and their candidate downstream targets, based on relationships between gene expression in the tissues. *Sulf2* was identified in both Inducible T cell Kinase (*itk*) **(A)** and transferrin receptor (*tfrc*) **(B)** wheel charts, suggesting their involvement in the upstream regulation of *Sulf2* expression in association with more advanced fibrosis. Red indicates upregulation of the gene in the fibrotic tissues, orange indicates activation of the regulator, while blue indicates inhibition of the regulator. An orange line represents upregulation of the downstream gene consequent to activation **(A)** or inhibition **(B)** of the regulator. A yellow line indicates an inconsistent direction of change between downstream gene and the corresponding regulator.

5.6.2 The role of sulf2 in steatosis related pathways in the C3H/He mice

The second DE gene list created (using R package software) by grouping mice into two groups based on the histological scoring of fat deposition in liver tissue. The first group included mice with severe steatosis graded as 2-3 (N1, N2, N4, N11, N13, N14, N15, N16, N17, N18, N19, N20, N21, N22, N23), while the second group comprised mice that didn't develop steatosis or mice that had steatosis graded as 1 (N3, N5, N6, N7, N8, N9, N10, N12). In this DE gene list, *Sulf2* was among 1253 DE genes that were significantly upregulated (Log2FC 0.68, q.value=4.6 $x10^{-5}$) in the high steatosis group **(Appendix 4)**.

The subsequent IPA canonical pathway analysis of this DE gene list is summarised in **(Figure 5.17).** Inhibition of the LXR/RXR pathway and an increase in the degradation of Melatonin, Nicotine and Bupropion pathways were the most striking steatosis reported changes. *Sulf2* was not identified as a component gene in any of the IPA defined top canonical pathways.

A

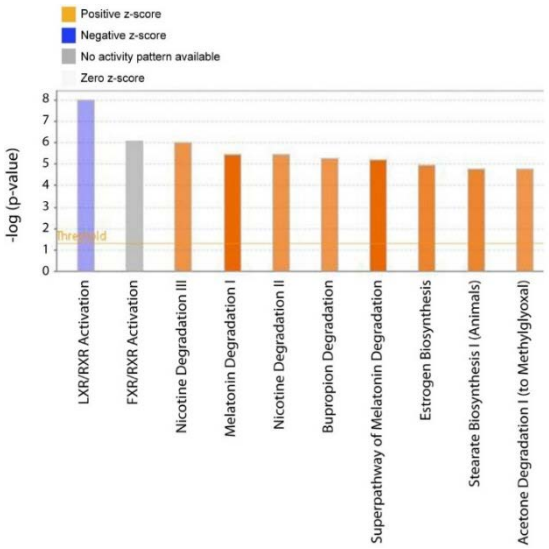

B

IPA canonical pathways	-log (p-value)	z-Score
LXR/RXR Activation	8.03	-0.905
FXR/RXR Activation	6.1	
Nicotine Degradation III	6.01	1.667
Melatonin Degradation I	5.45	2.333
Nicotine Degradation II	5.45	1.667
Bupropion Degradation	5.24	1.633
Superpathway of Melatonin Degradation	5.18	2.333
Estrogen Biosynthesis	4.98	1.89
Stearate Biosynthesis I (Animals)	4.77	1.89
Acetone Degradation I (to Methylglyoxal)	4.75	1.633

Figure 5.17 Changes in metabolic pathways in association with advanced steatosis The bar chart **(A)** shows the IPA top 10 changed canonical pathways, ranked according to the –log (q.value) of overlap. Orange represents activation, blue inhibition, and grey an uncalculated z-score, with intensity proportional to the increase in absolute activity. The table **(B)** shows the –log (q.value) and z.score of top 10 changed canonical pathways.

Pathways activated in diseases and associated with biofunctions were explored next and it wasn't surprising – given the DE gene list was created based of the degree of steatosis - to see "fatty acid metabolism" in the top ten list **(Figure 5.18)**, alongside two related to gluconeogenesis (synthesis of monosaccarhide and synthesis of D-glucose). Of note, a number of pathways related to immune cell infiltration and movement were inhibited in the presence of more advanced steatosis. Again, *Sulf2* was not involved in any of the aforementioned bio-functions.

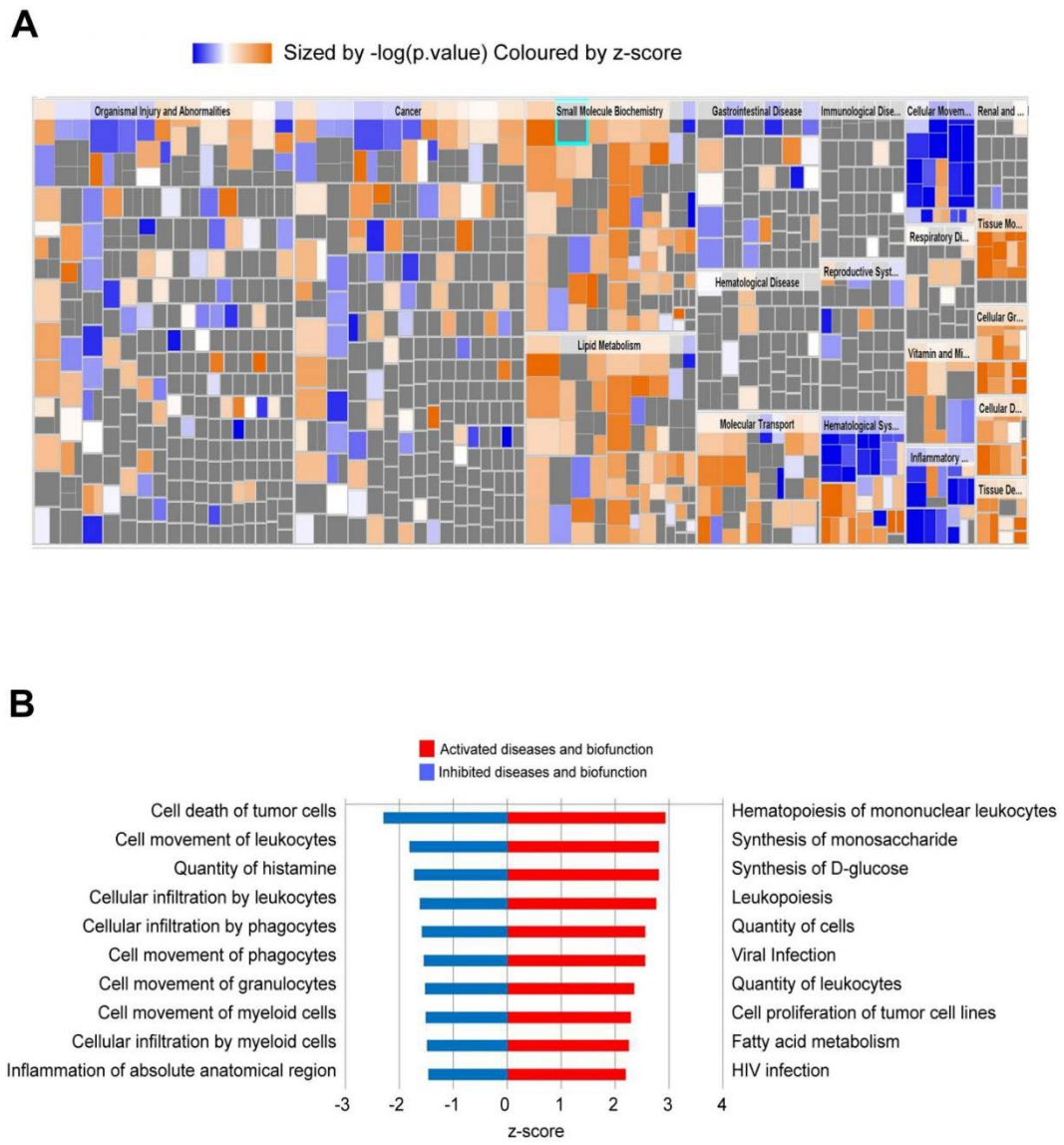

Figure 5.18 Diseases and bio-functions analysis of steatosis related hepatic gene expression in C3H/He liver tissues. The IPA heat map **(A)** shows the deregulation of different diseases and bio-functions in the mouse liver tissues, ranked according to –log (q.value) of overlap. Orange represents activation, blue inhibition, grey an uncalculated z-score and white represents a zero activity score. The intensity of colour is proportional to the increase in absolute activity z-score. The bidirectional bar chart **(B)** shows the top 10 activated (red) and inhibited (blue) pathways in steatotic livers, ranked according to the activation z.score.

A

	Molecules	Networks
1	30	Lipid Metabolism, Molecular Transport, Small Molecule Biochemistry
2	29	Cell Cycle, DNA Replication, Recombination, and Repair, Connective Tissue Disorders
3	25	Cancer, Endocrine System Disorders, Organismal Injury and Abnormalities
4	24	Carbohydrate Metabolism, Lipid Metabolism, Small Molecule Biochemistry
5	23	Cellular Movement, Cellular Growth and Proliferation, Tissue Development
6	22	Lipid Metabolism, Molecular Transport, Small Molecule Biochemistry
7	22	Lipid Metabolism, Small Molecule Biochemistry, Drug Metabolism
8	20	Connective Tissue Development and Function, Tissue Morphology, Cellular Movement
9	20	Drug Metabolism, Amino Acid Metabolism, Endocrine System Development and Function
10	19	Energy Production, Lipid Metabolism, Small Molecule Biochemistry

B

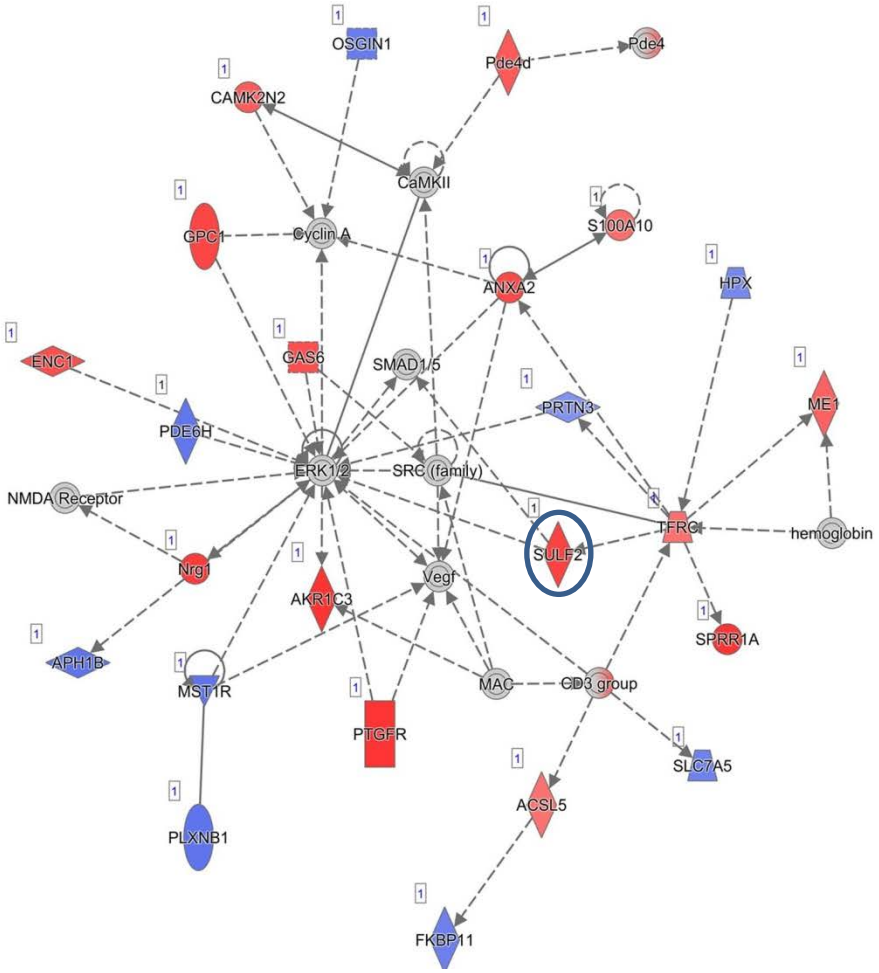

Figure 5.19 A metabolic role for Sulf2 in suggested by Ingenuity Pathway Analysis (IPA) The table **(A)** shows the steatosis associated top 10 enriched networks in the mouse fatty liver, scored according to the number of steatosis DE gene overlapping the network. The image **(B)** shows the network '4', entitled "Carbohydrate metabolism, lipid metabolism, small molecule biochemistry", in which upregulated *Sulf2* (circle) may play a part. Red indicates gene upregulation, blue indicates gene downregulation, while grey indicates non DE genes.

IPA was also used to explore lipid metabolism, molecular transport and small molecule biochemistry-related networks **(Figure 5.19)**. *Sulf2* was identified as controlling carbohydrate metabolism, lipid metabolism and small molecule biochemistry, shown as network 4 in the table in **Figure 5.19A** and graphically in **Figure 5.19B**.

In summary, *Sulf2* was upregulated in the whole liver tissues of 48 week C3H/He mice with dietary induced fatty liver, by *Sulf2* real time PCR in a pilot study of 21 mice and by exploration of its transcript in RNAseq analyses in an independent experiment including 23 mice. However, *Sulf2* was not identified as a significant dietary intervention induced DE genes by bioinformatics analyses of the RNAseq cohort. When the mice were grouped according to the histological scoring, *Sulf2* was differentially expressed in some of the lists created, but was not one of the top changing genes. Fold differences in Sulf2 were not as striking as other genes, perhaps because changes were present in a minority of cells or a particular cellular compartment not so well captured in 'whole tissues analyses'. Despite this limitation, the bioinformatics analyses have raised some interesting associations.

5.8 Discussion

Over the last decade a number of approaches have been adopted to find clinically relevant biomarkers and novel therapeutic targets for NAFLD/NASH. The wide spectrum of the disease and the lack of experimental models that accurately reflect the whole range of the human disease have proved challenging. The increasing burden of NAFLD-HCC, even in the absence of cirrhosis, further emphasizes the need for research in this area, including the development of experimental models that recapitulate the features of human disease[407].

In the introduction to this chapter, I have put together and presented IHC data generated previously by our group, exploring SULF2 expression in biopsies from human NAFLD/NASH patients. SULF2 was expressed in a number of different cell types in normal liver, including in endothelial cells and bile ducts, as well as at low levels on the canalicular surface of hepatocytes, in keeping with essential roles in the liver microenvironment. Notably, cytoplasmic expression of SULF2 was present to come degree in every patient with NAFLD. Within patients with NAFLD, the more pathological association was with an increase in surface membrane expression of SULF2, often associated with a reduction of expression at the canalicular surface. This increase was significant associated with both the presence of ballooning and portal inflammation, but most notably with the presence of fibrosis. Also observed was SULF2 expression in immune cells such as lymphocytes and macrophages, more

noticeable in those cases with histologically more advanced disease. These data complement the pivotal role we believe stromal SULF2 plays in the progression of HCC and the aim of our group was to develop an animal model which would enable the further exploration of *Sulf2*.

Moving forward, I have described here the tissue characterisation of *Sulf2* in a pilot study of dietary induced fatty liver disease and HCC, confirming it to be increased and associated with tumour stage.

Subsequently I have analysed phenotypic data in a larger follow up study in C3H/He mice, fed with control or ALIOS diet, in which the histopathology of NAFLD and the cancers was comprehensively scored by liver pathologist, Dr Dina Tiniakos. While the ALIOS diet in murine models of NAFLD was reported previously[330, 331], the use of the C3H/He adipogenic mouse strain in the diet-induced NASH was a novel aspect. In similar studies focused on C57BL/6 mice challenged with ALIOS diet, ballooned hepatocytes, Mallory-Denk bodies and liver fibrosis have not been reported[330]. Although C57BL/6 mice develop liver tumours, these are just a few mm in diameter and too small to characterise[330]. In our C3H/He mice, in addition to the obesity, hyperlipidaemia and impaired glucose tolerance (data not shown), mice also developed steatosis, fibrosis, lobular inflammation, Mallory-denk bodies and lipogranuloma – regarded as key features of human NASH. In addition, the presence of ballooned hepatocytes – an essential diagnostic feature of human NASH - was a common feature in control diet aged (48 weeks) C3H/He mice liver (12/23, 52%), exacerbated by ALIOS feeding (23/24, 96%).

We had aimed to characterise Sulf2 by IHC, exploring temporal relationships in different cellular compartments as NAFLD develops and progresses to fibrosis and/or HCC. However, the lack of a suitable sensitive and specific antibody has been a major limitation. The only useful human antibody is a mouse monoclonal and despite significant investment – both in technician time and alternative antibody generation – it has not yet been possible to characterise murine Sulf2 in the way we had hoped.

My subsequent focus in this chapter, was on whole liver RNA-seq data from the C3H/He mice. Cluster analysis defined two groups which reassuringly reproduced the non-tumour and the tumour tissues. As described previously, the *Sulf2* increase in liver tissue of ALIOS-fed mice compared to control mice was modest and did not reach statistical significance after adjusting for multiple comparisons in the whole RNAseq dataset. We have proposed that this reflects the use of whole tissues, lacking the sensitivity to capture increases in a small subset of cells.

Regarding the parenchymal cells or hepatocytes, which make up 90% of all liver cells, our human data suggest that modest heterogeneous increases in the cytoplasm in the presence of even minor degrees of NAFLD – present actually in the majority of our mice. In Human disease, even striking membranous increases were heterogeneous in character, localised in steatotic regions. Furthermore, the human data suggested expression in non-parenchymal cells, most consistently bile ducts and endothelial cells present in all tissues regardless of NAFLD stage (hence contributing to background), but also present in a variable fashion in inflammatory cells which contribute a relatively small proportion of whole liver RNA. These patterns of expression may be biologically important, but challenging to capture by whole liver transcriptomic analysis. The generation suitable tool antibodies to characterise mouse sulf2 will be important for future work and their generation is being pursued with collaborators. In the absence of an antibody, an alternative may be to use another techniques like RNA-scope, for detecting *sulf2* in the mouse tissue.

Despite the limitations of whole tissues analysis, *Sulf2* was differentially regulated in the presence of steatosis or fibrosis, corroborating the Human IHC data showing its cytoplasmic and membranous elevation in the presence of steatosis, correlating with fibrosis. Furthermore, IPA analysis of disease stage specific gene lists has suggested *Sulf2* involvement in cytoskeleton organisation- and small molecule biochemistry-related networks. Of particular note was the suggested relationship between *Sulf2* and *Itk* in the liver tissue. ITK is a non-tyrosine receptor kinase present in the plasma membrane of T cells, NKT cells and mast cells, and it is involved in T cell activation[408-410]. ITK regulates the Th2 response in different organs and initiates the production of different cytokines and growth factors[411-413]. Further exploration of the interaction between *Sulf2* and *Itk* would be worth pursuing in the future, potentially identifying a novel role for Sulf2 in T cell function.

In conclusion, SULF2 is an exciting candidate contributing to the pathogenesis of NAFLD/NASH. For future work, Golbal sulf2 $^{-/-}$ knock-out (KO) mice are available and challenging these mice with different diets may be worthwhile, to explore if they are protected from NAFLD or its progression to fibrosis and/or HCC. Studies of this nature, in combination with antibody generation or tools such as RNAscope, may help to define the roles on mechanisms of this extracellular sulfatase in fatty liver disease. If confirmed as a key driver or master regulator of progression, the development of inhibitory molecules or antibodies would be worthy of pursuit.

Chapter 6: Non hypothesis-driven investigation of regulators of NAFLD progression to NASH and HCC

6.1 Background

Tumourigenesis is a complicated and multistep process involving tumour initiation, development and progression[414]. Tumours usually arise on a background of inherited or acquired genetic alterations that divert the affected cells from regulatory mechanisms and encourage clonal expansion and invasion[415, 416]. Genetic alterations can destabilise an organs gene expression leading to phenotypic changes that promote cancer- liver tumours arising in diseased liver being the focus here. Characterising the transcriptomic changes and genetic aberrations associated with premalignant disease and analysing network deregulation involved in the development and progression of HCC may identify pathways worthy of pursuit as predictive biomarkers or therapeutic targets. Highly heterogeneous in nature, the common changes in HCC gene expression have been extensively studied in the hope of understanding the tumours biology and generating tumour subclasses useful for guiding therapy[57-59, 87, 229, 417]. As yet these efforts have not impacted clinical practice, but transcriptomic analyses combined with 'immunophenotyping' of the tumour and its microenvironment may change that. The *Llovet* group[229] has recently used this kind of approach to show that HCC can be categorized into an "immune active" and "immune inactive" subclasses, with the 'immune active class' potentially including the patients most likely to benefit from treatment with checkpoint inhibitors. Thus, these types of study may have particular importance for the translation of immunotherapies, helping to identify the patients most likely to benefit, as well as those best treated with combination approaches or entry into ongoing clinical trials.

In the previous chapters, we demonstrated that the presence of SULF2 in the TME was a poor prognostic marker in HCC patients. Moreover, SULF2 had a unique expression pattern in human NAFLD, associated with the presence of NASH and fibrosis. We then explored of *Sulf2* in the livers of C3H/He mice, demonstrating its upregulation in association with steatosis and fibrosis in a targeted or 'hypothesis' driven fashion, while identifying some interesting candidate upstream regulators and mechanisms that may be relevant to NAFLD progression. Although this directional-driven transcriptomic analysis was biologically relevant and underpinned by a human NAFLD scoring system[341] adapted for ALIOS mice, recent studies suggest that this supervised grouping approach has limited value as it does not necessarily reflect 'real changes' in the tissues and changes in mice often poorly mirror the most

important changes in the human context[418]. Notably, there were DE genes identified in both supervised and unsupervised clustering that had far greater magnitude change and significance than *Sulf2*. Thus, non-directional analysis of the transcriptomic data may, in theory, help to identify novel pathways and candidate therapeutic targets involved in disease progression[418].

6.2 Chapter 6 aims

6.2.1 To perform an un-supervised clustering of the transcriptomic landscape of the non-tumour liver tissues of the C3H/He mice to identify candidate drivers of tumour development.

6.2.2 To explore identified candidates in biopsies from patients with NAFLD.

6.2.3 To assess the overlap between the human HCC transcriptome and C3H/He tumour transcriptome.

6.3 Non-hypothesis driven exploration of the C3H/He NAFLD transcriptome

6.3.1 Unsupervised clustering of the transcriptomic data of C3H/He mice non-tumour liver tissue

Unsupervised clustering of the mouse non-tumour transcriptomic data identified two sub-clusters **(Figure 6.1)**. The first group was defined as group 1 (G1) and included all the control-fed mice plus two ALIOS-fed mice. The second group was defined as group 2 (G2) and included all the ALIOS-fed mice plus one control-fed mice **(Figure 6.2A)**.

Assessment of the correlation between the transcriptomic clustering and different gross and histopathological criteria of the C3H/He mice revealed that mice in G2 cluster were obese with bigger livers and higher VAT weight than G1 mice **(Figure 6.2)**. Non-tumour liver tissue of the G2 mice had higher steatosis grade, more fibrotic changes, a higher NAS score and more lipogranulomas compared to tissues of G1 mice **(Figure 6.2)**. Notably, tumours in G2 mice were larger than tumours in G1 mice **(Figure 6.2)**. Professor *Reeves* previously analysed the predictors of tumour development in the C3H/He mice **(Appendix-5)** showing that the liver weight, body weight, presence of lipogranuloma and steatosis grade were strongly associated with HCC development. This implies that unsupervised clustering of the C3H/He mice transcriptome was associated with the key predictors of the tumour development. Of note,

most of the mice in G2 cluster developed tumours compared to mice in G1; however, with no statistical significance **(Figure 6.2P)**.

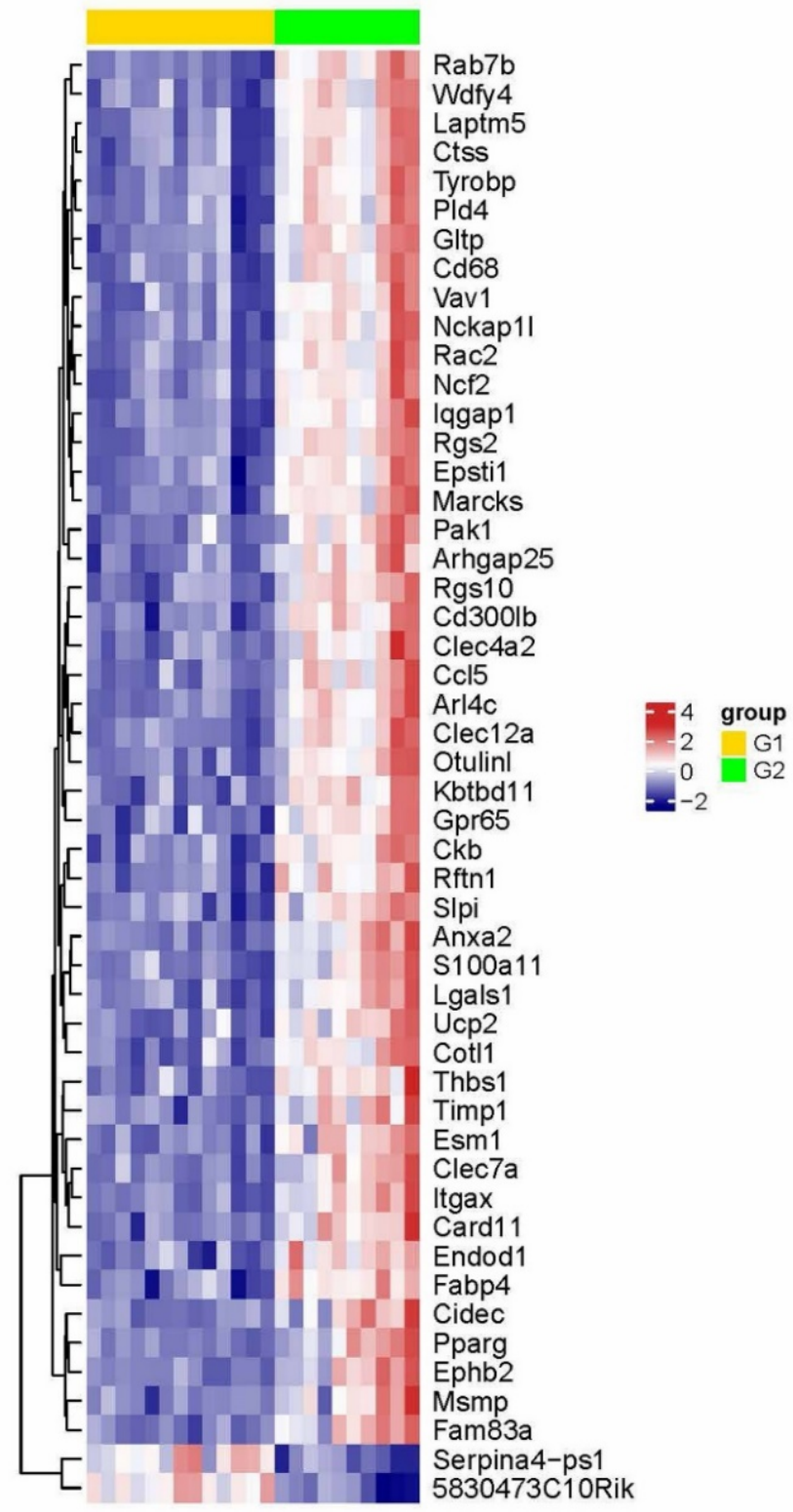

Figure 6.1 Identification of two distinct hepatic non-tumour sub-clusters in the C3H/He mouse transcriptomic data The heat map shows the top 50 DE genes in the G1 and G2 mice. G1 group is colour coded yellow, while G2 group is colour-coded green. Upregulated genes are denoted in red and downregulated genes are denoted in blue.

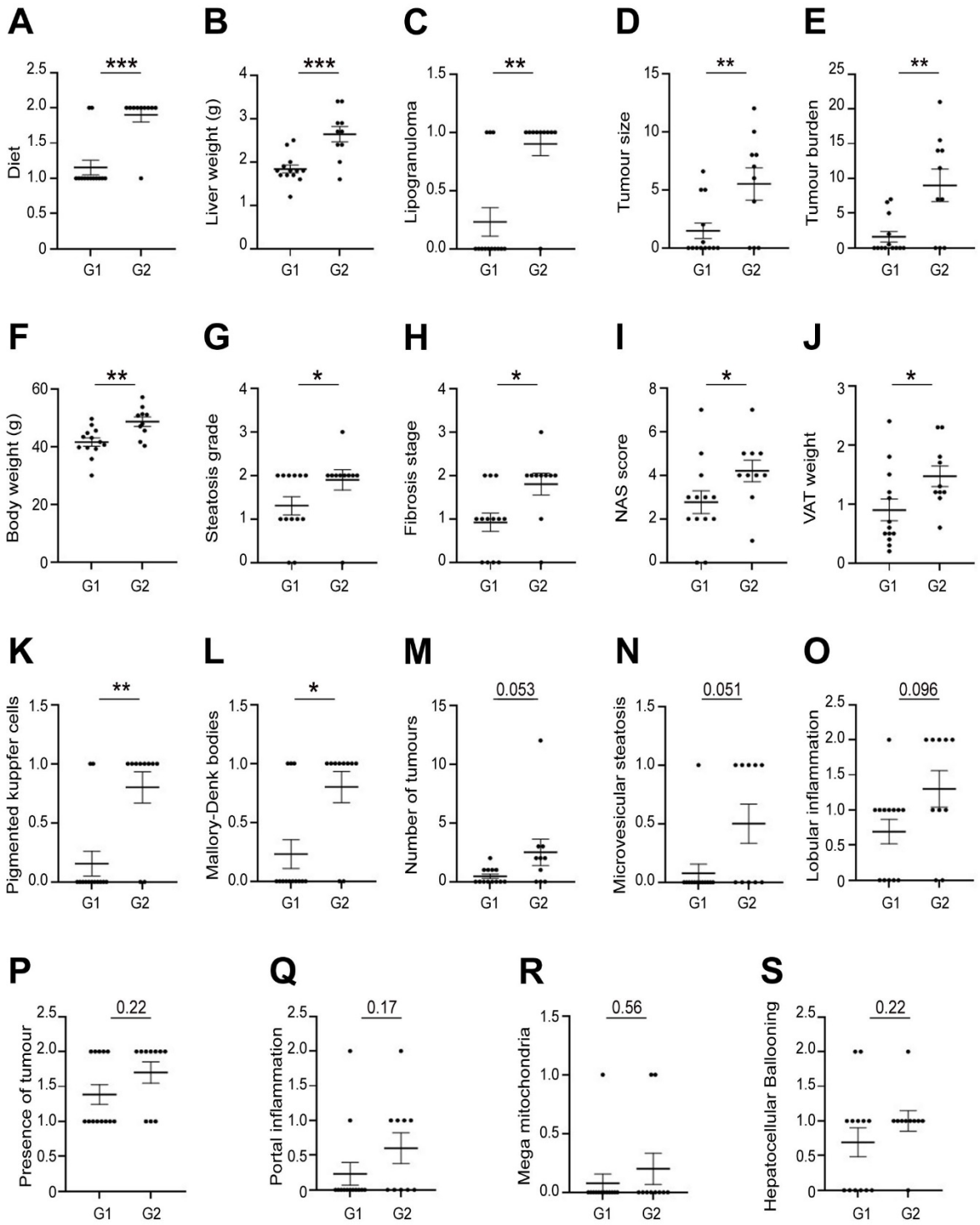

Figure 6.2 Unsupervised hepatic clustering of C3H/He mice transcriptome was associated with features of the metabolic syndrome, more advanced NAFLD and HCC. Graphs show the grouping of mice in G1 and G2 clusters based on diet **(A),** liver weight **(B)**, Lipogranuloma **(C)**, Tumour size **(D)**, tumour burden **(E)**, Body weight **(F)**, steatosis **(G)**, fibrosis **(H)**, NAS score **(I)**, VAT weight **(J)**, pigmented Kuppfer cells **(K)**, Mallory-Denk body **(L)**, tumour number **(M)**, microvesicular steatosis **(N)**, lobular inflammation **(O)**, presence of tumour **(P)**, portal inflammation **(Q),** megamitochondria **(R)** and hepatocellular ballooning **(S)**. Data is presented as mean±s.e.m, *p<0.05, **p<0.01 and ***p<0.001.

6.3.2 Pathway analysis of the G2 versus G1 DE gene list using IPA

A list of DE gene between G2 group (more diseased) and G1 group (less diseased) was created and included 3900 DE genes between the two groups **(Appendix-6)**, exceeding the number identified in supervised clustering studies based on histological characterisations of mice liver tissue in **(chapter 5)** – supporting a role for un-supervised analysis when looking at gene expression data. The Top 10 enriched canonical pathways in the IPA analysis were exclusively T cell-related **(Figure 6.3)**, strongly supporting the association between lobular inflammation and tumour development in the C3H/He mice **(Appendix-5)**.

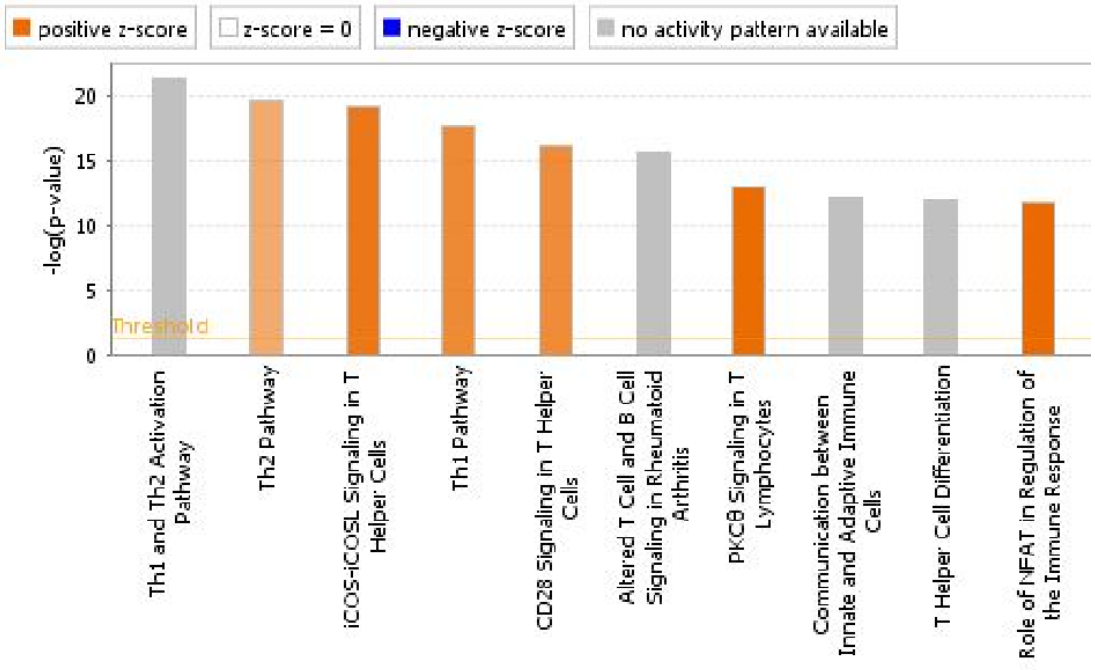

Figure 6.3 Activation of T cell canonical pathways was evident in the C3H/He non-tumour subclass G2 versus G1 comparison The IPA bar chart shows the top 10 activated canonical pathways in the mouse non-tumour tissue, ranked according to –log (q.value) of overlap. Orange represents pathway activation, blue represents pathway inhibition, grey represents an uncalculated z-score and white represents zero activity score. The intensity of colour is proportional to the increase in absolute activity z-score.

Cell survival and cell viability were the top 'disease and bio-function pathways' activated in the G2 group transcriptomic data compared to G1, while 'organismal death and apoptosis bio-function' pathways were inhibited **(Figure 6.4)**. This supported data previously generated by PhD student, Ahmed Mahdi. He showed that the number of Ki67 positive hepatocyte nuclei, where Ki67 is a marker of cell proliferation, was elevated in the non-tumour tissue of the

C3H/He mice fed the ALIOS diet and correlated with the development of HCC in our murine model (Data not shown).

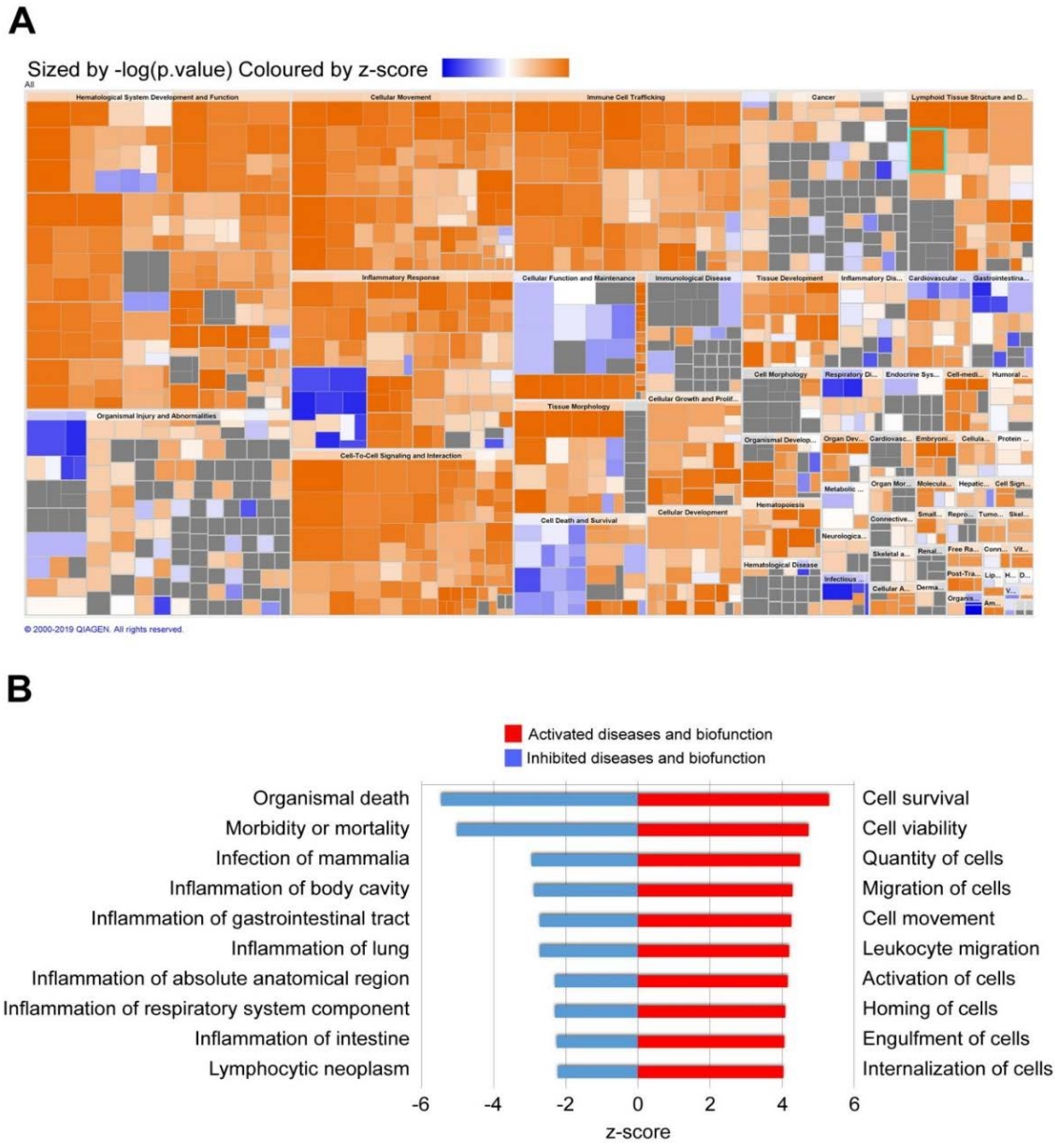

Figure 6.4 Cell survival was the top IPA identified bio-function activated in C3H/He non-tumour tissue subclass G2 versus G1 The heat map **(A)** shows the deregulation of different diseases and bio-function pathways in the mouse non-tumour tissues, ranked according to –log (q.value) of overlap. Colour orange represents bio-function activation, blue represents bio-function inhibition, grey represents an uncalculated z-score and white represents an activity score of zero. The intensity of colour is proportional to the increase in absolute activity z-score. The bidirectional bar chart **(B)** shows the top 10 activated (red bars) and inhibited (blue bars) diseases and bio-functions in the mouse non-tumour tissue, ranked according to the activation z.score.

The IPA upstream analysis tool was used to identify candidate regulatory molecules that potentially control the transcription of genes in the analysed list. *Csf2*, *Ifnγ*, *Cd44*, *Mitf* and

Ptger2 were the top regulators identified in the non-tumour gene list. *Cd44* was the regulator with the greatest level of expression in G2 versus G1 **(Figure 6.5)**.

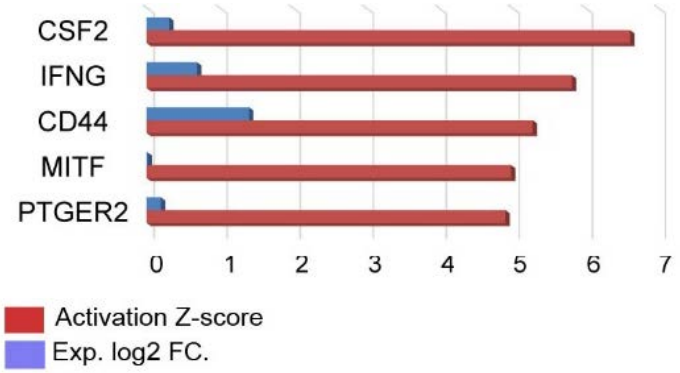

Figure 6.5 IPA upstream analysis identifies the top upstream regulators in the hepatic non-tumour G2-G1 comparison in C3H/He mice. The bar graph shows the top 5 regulators of the expression of DE genes in the G2-G1 list. Red bars represent the activation z-score of the upstream regulators, and the blue bars represent the log2FC of their expression.

Regulator-effect analysis, using an IPA tool that links the top upstream regulators with top changing diseases and bio-function, ranked *Cd44* first amid other regulators (**Table 6.1)**, followed by *Il27*. Bioinformatics suggested a role for *Cd44* in the recruitment of T lymphocytes to the diseased liver via regulating the expression of key chemokines and T cell attractors **(Figure 6.6)**.

Rank	Symbol	Disease and functions	Consistency score
1	Cd44	Homing of T lymphocytes	3.479
2	Il27	Differentiation of mononuclear leukocytes	3.357
3	Il27	Hematopoiesis of mononuclear leukocytes	3.357
4	Il17	Lymphopoiesis	3.357
5	Tcr	Cytotoxicity	3.207

Table 6.1 The top 5 molecules in the IPA regulator-effect analysis of G2-G1 DE gene list. *Cd44* was ranked first molecule regulating T cell recruitment in diseased mice liver

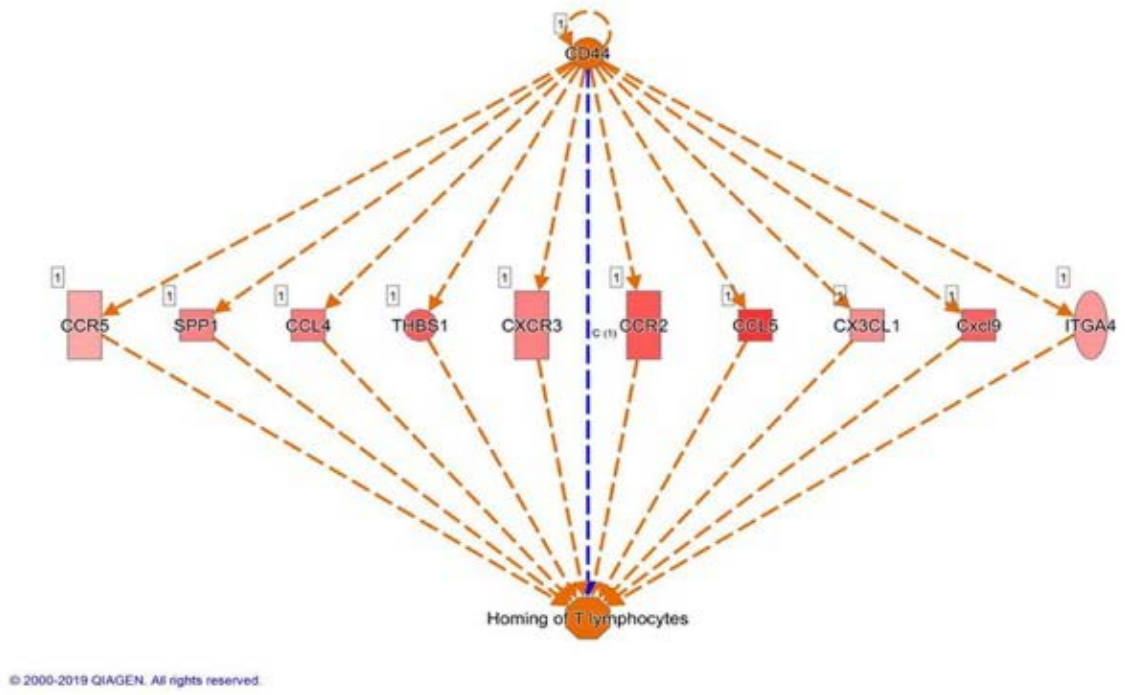

Figure 6.6 Cd44 regulates the expression of key chemokines responsible for T cell recruitment Network analysis identified the elevated expression of genes regulated by *Cd44*, including those involved in recruitment of T cells to the site of injury in diseased non-tumour liver tissues of C3H/He mice. The colour orange of *Cd44* indicates positive regulation of the process. Red colour indicates upregulation of genes downstream to *Cd44*. The orange colour of the "homing of T lymphocytes" function indicates activation of the process as a results of upregulation of upstream genes.

In conclusion, IPA suggested an important role for T cells in the pathogenesis of NAFLD and NAFLD-HCC in the C3H/He mice. Upregulation of T cells chemokines, influenced by *Cd44*, potentially drives the infiltration of T cells to the liver in response to fat associated damage.

6.3.3 Pathway analysis of the G2 versus G1 DE gene list using GSEA

Gene set enrichment analysis (GSEA) is another powerful platform for analysing gene lists and is commonly cited in peer reviewed publications. The G2-G1 gene list was analysed against the GSEA molecular signatures database (MSigDB) that is composed of hallmark, positional, curated, motif, computational, gene ontology (GO), oncogenic and immunological gene lists. GSEA identified Macrophage-Enriched Metabolic Network (MEMN) as the top enriched network amongst all pathways in the MSigDB **(Figure 6.7A)** suggesting a role for macrophages in disease progression. Complementing the IPA analysis, the top 10 GSEA immune panel-enriched pathways showed activation of CD4 and Treg cells, together with activation of other immune cell-related pathways like B cells and myeloid cells **(Figure 6.7B)**.

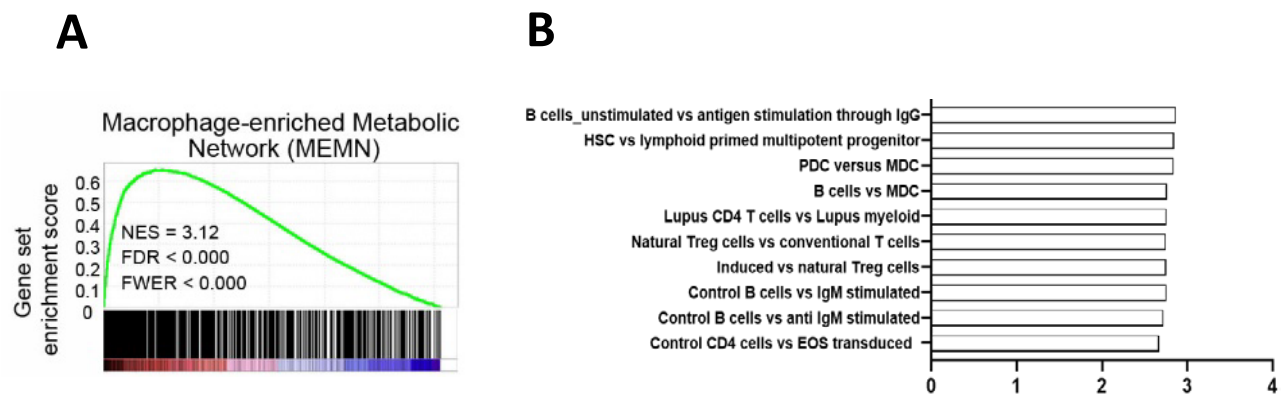

Figure 6.7 GSEA analysis confirms the activation of immune cell-related pathways in the G2-G1 comparison Panel **(A)** shows the gene set enrichment of the 'macrophage enriched metabolic network'. Key: NES; normalised enrichment score, FDR; false discover rate, FWER; family wise error rate. The graph in **(B)** shows the top 10 enriched pathways in GSEA immune signatures. Data are ranked according to the normalised enrichment score (NES).

The GSEA Hallmark signature analysis revealed activation of a number of different mechanistic pathways, including activation of NF-kB and IL6/STAT3 pathways **(Figure 6.8)**. This finding was of particular note due to the reported link between their activation in the non-tumour tissue of patients and the recurrence of HCC[57]. In other words, activation of these pathways in the C3H/He non-tumour mouse liver tissues supports the validity of the preclinical model as one relevant to the study of the development of HCC in human disease.

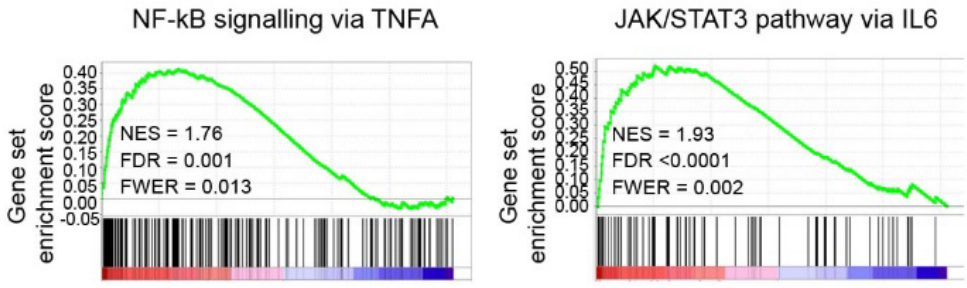

Figure 6.8 GSEA hallmark analysis showed activation of NF-kB and STAT3 pathways in livers of G2 versus G1 mice Gene set enrichment of NF-kB and STAT3 pathways G2-G1 comparison. Key: NES; normalised enrichment score, FDR; false discover rate, FWER; family wise error rate.

In summary, GSEA analysis supported IPA findings, highlighting the importance of T cell pathways in the disease progression in C3H/He mice. In addition, GSEA identified macrophages as potential contributors to this tumour-favouring environment. Activation of

key inflammatory molecular pathways might explain the progression of simple steatosis to advanced stages including HCC.

6.4 Investigating the role of macrophages and T cells in livers of C3H/He mice

6.4.1 Expression of Cd44 in mouse liver tissue

Pathway analysis of the non-tumour tissue proposed a role of macrophages and T cells in liver disease progression in C3H/He mice, with a suggested link between *Cd44* and the process of T cell infiltration. Cd44 IHC was performed to explore the protein levels and cellular source of Cd44 in liver tissue of C3H/He mice, together with IHC staining for Cd68 and F4/80 macrophage markers. Notably, Cd44 was expressed exclusively in macrophages in both control and ALIOS groups **(Figure 6.9)**. The number of Cd44 positive macrophages in control-fed mice was 5 fold less than Cd44 positive macrophages in ALIOS fed mice (14.32±2.39 in control mice versus 88.79±9.099 in ALIOS-fed mice). There was a modest increase in Cd68 (66.67±4.066 versus 93.46±4.4 positive cells/HPF) and F4/80 (49.91±6.44 versus 118±22.34 positive cells/HPF) **(Figure 6.9)** positive macrophages. In combination, given the higher fold diet induced change in Cd44 macrophage count relative to total macrophage count, the data support increased infiltration but also the acquisition of Cd44 positive macrophage phenotype.

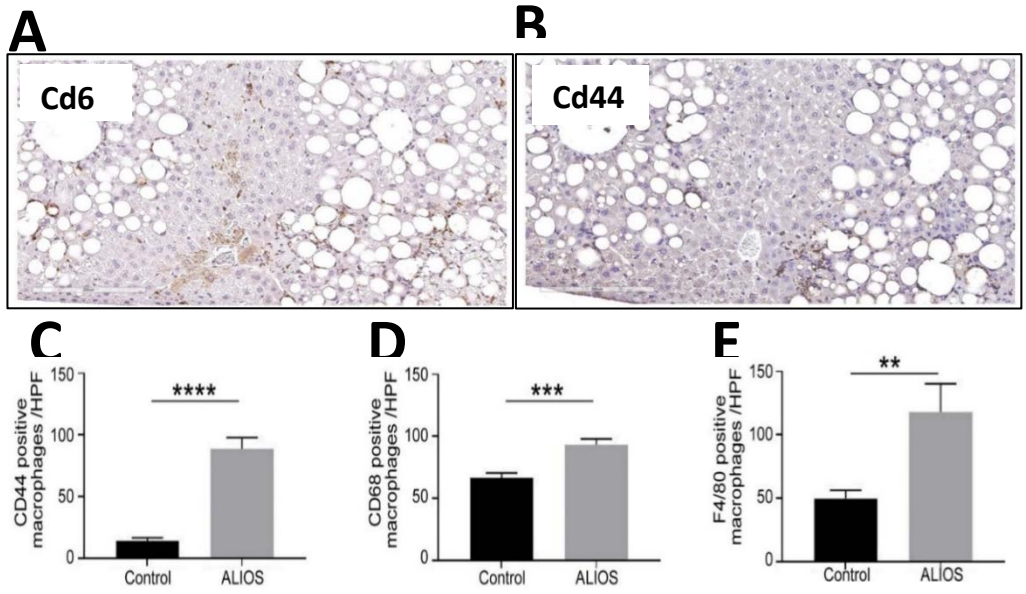

Figure 6.9 A preferential increase in Cd44 positive macrophages in lipogranuloma rich areas of steatosis in ALIOS-fed C3H/He mice Representative images show IHC stain for Cd68 **(A)** and Cd44 **(B)** in liver tissues of ALIOS-fed mouse. Lipogranulomas were Cd68 and Cd44 positive. Images were captured using Aperio Imagescope software at x20 magnification. Graphs show the number of Cd44 **(C)**, Cd68 **(D)** and F4/80 **(E)** positive macrophages in control and ALIOS-fed mice (n=12 per group). Data are presented as mean ± s.e.m; ** p<0.01, *** p=0.001, **** p<0.001.

Histological assessment also revealed that lipogranulomas, congregations of macrophages around cell-free lipid droplets, were the strongest predictor of HCC development in the C3H/He mice, and were rich in Cd44 and Cd68 positive cells. When mice were grouped into Cd44 high (above median number of Cd44 positive macrophages) and Cd44 low (below median), a significant association between Cd44 and the presence of lipogranuloma was confirmed (lipogranuloma was absent in 10/11 of Cd44 low mice, while all Cd44 high mice had lipogranuloma, chi square $p<0.0001$). On applying similar groupings to Cd68 and f4/80 macrophages, there were no significant associations with the presence of lipogranulomas (Cd68 p=0.084; f4/80 p=0.198). The development of tumours in C3H/He mice correlated with the number of Cd44 (Spearman rho 0.561, p=0.007) and Cd68 (Spearman rho 0.509, p=0.019), but not f4/80 (Spearman rho 0.401, p=0.065) positive macrophages.

In summary, macrophages surrounding the lipogranulomas in the C3H/He mice acquired a Cd44 positive macrophage phenotype that was associated with the development of HCC.

6.4.2 CD44 positive macrophages and HCC development in patients with NAFLD

The translational impact of the association between Cd44 and the development of HCC in the C3H/He mice was assessed in human disease by counting the number of CD44 and CD68 positive macrophages in non-tumour liver biopsies from patients with NAFLD, with and without HCC. This cohort included 42 patients with a median age of 67 years, 64.3% of whom (27/42) had developed HCC. In keeping with the animal model (NAFLD-HCC in the absence of cirrhosis), cirrhosis was absent in 31/42 (75.6%) of patients. The median BMI of the patients was 31.35 and 23/42 (57.5%) had T2DM.

The number of CD44 and CD68 positive macrophages in livers of patients with NAFLD-HCC was significantly higher than that in NAFLD patients who didn't have HCC **(Figure 6.10)**.

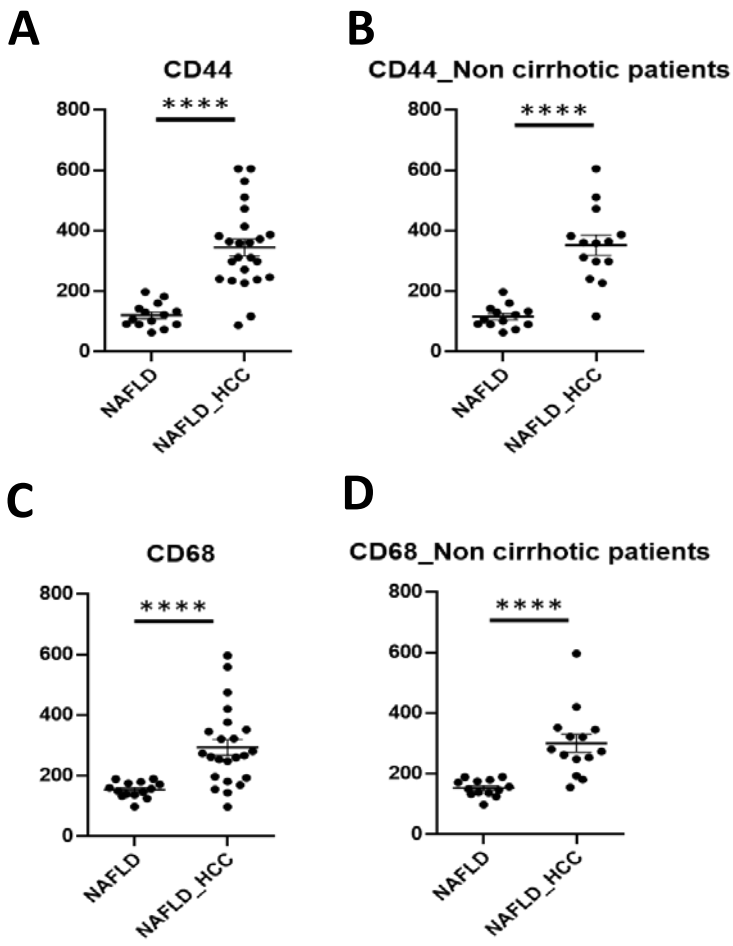

Figure 6.10 CD44 and CD68 positive macrophages were elevated in non-tumour tissues of NAFLD-HCC Graphs show numbers of CD44 positive **(A &B)** and CD68 positive **(C & D)** macrophages per at least 5 HPF, in the non-tumour liver biopsies from NAFLD patients with and without HCC, in all cases (n=42) (**A,C**) or excluding cirrhotic cases (n=31) (**B,D)** excluded the cirrhotic cases. Data are presented in mean±s.e.m, ****p<0.0001.

The number of CD44 positive macrophages was also strongly associated with age (Spearman rho 0.660, p<0.0001), and tumour number (Spearman rho 0.758, p<0.0001) with a weaker association with T2DM (Spearman rho 0.344, p=0.04). When considering only the macrophage counts in the non-cirrhotic cases, the number of CD44 positive macrophages remained significantly higher in patients who developed HCC **(Figure 6.10)**. The association between the number of CD44 and CD68 positive macrophages was very strong regardless of presence or absence of cirrhosis (Spearman rho 0.736, p<0.0001 for all patients and Spearman rho 0.744, p<0.0001 for the non-cirrhotic cases) **(Figure 6.11)**.

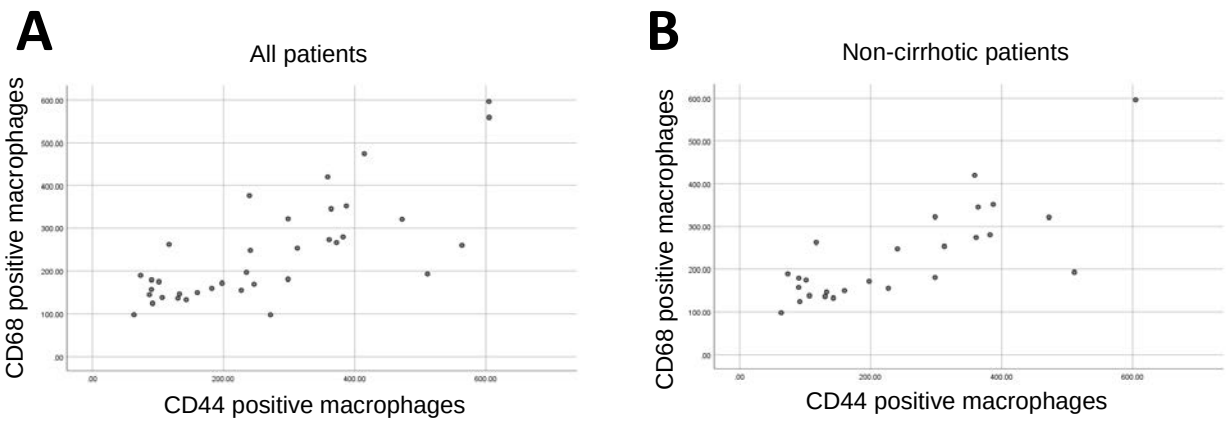

Figure 6.11 The number of CD44 positive macrophages in NAFLD correlated with the number of CD68 positive macrophages. Graphs show the association between the number of CD44 and CD68 positive macrophages in all patients **(A)** and in non-cirrhotic cases **(B)**.

In conclusion, macrophage counts in the non-tumour tissues of patients with NAFLD was higher in those with HCC compared to those without, supporting a role for CD44 in tumour development. The association between CD44 and CD68 cell counts supports the observation that macrophages were the primary cell source of CD44 in diseased human liver. The number of CD44 positive macrophages remained higher in liver biopsies of NAFLD patients who developed HCC independently of the presence of cirrhosis.

6.4.3 Exploring the role of different chemokines in macrophage recruitment in mice

Increased infiltration of steatotic livers with macrophages raised questions about the processes underlying their accumulation, with suspected roles for increased expression and production of certain monocyte/macrophage chemokines. These include CCL5, CCL4 and SPP1, released in response to damage, that attract macrophages to sites of injury[419, 420]. Investigation of the expression level of these macrophage-attracting chemokines in the non-tumour DE gene list confirmed upregulation of *Ccl5* ($p<0.0001$), but not *Ccl2* ($p=0.25$) in the liver of ALIOS mice compared to the control mice. *Spp1* or osteopontin, a known ligand of CD44[421], was also upregulated in ALIOS mice ($p=0.001$). mRNA validation of this by RT-PCR confirmed the upregulation of *Ccl5* and *Spp1* in ALIOS versus control mice, but the upregulation of *Spp1* didn't reach the statistical significance **(Figure 6.12)**. Looking for the cellular source of chemokines, recent reports suggested hepatocytes as one possible source of the expression of Ccl5[422] and Spp1[423], so the expression of both genes was investigated *in vitro* in lipid loaded mouse hepatocytes.

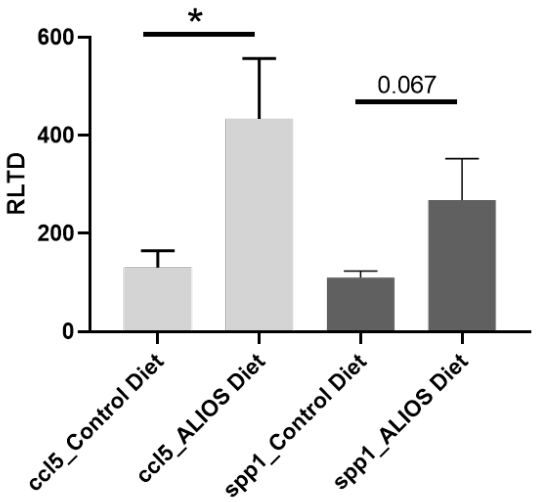

Figure 6.12 Hepatic expressions of Ccl5 and Spp1 were upregulated in ALIOS versus control C3H/He mice. Graph shows the upregulation of *Ccl5* (light grey) and *Spp1* (dark grey) in ALIOS versus control-fed mice (n=12 per group). Expression is shown as the relative level of transcriptional difference (RLTD) using *gapdh* as a control. Data are expressed as mean ± s.e.m; *P<0.05.

Hepatocytes isolated from C57BL/6 mice were treated with either bovine serum albumin (BSA) or Oleate/palmitate for 24 hours to see the effect of lipid on the expression profile of *Ccl5* and *Spp1*. The levels of *Ccl5* and *Spp1* in lipid loaded hepatocytes; however, didn't change **(Figure 6.13)** compared to their level in hepatocytes treated with BSA control.

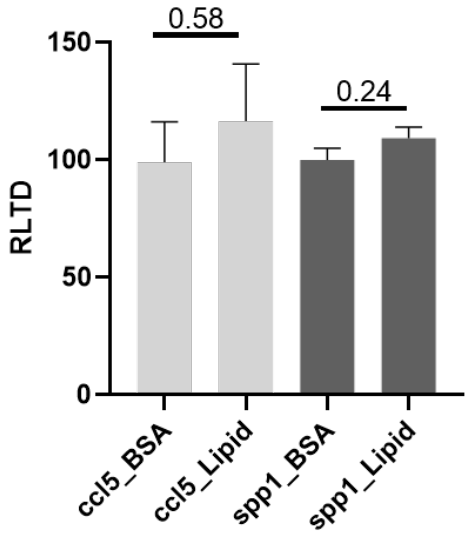

Figure 6.13 ccl5 and spp1 levels were comparable between control and lipid loaded mouse hepatocytes in vitro. Graph shows non-significant upregulation of *Ccl5* (light grey) and *Spp1* (dark grey) in hepatocytes treated with control or with oleate/palmitate for 24 hours. Expression is shown as the relative level of transcriptional difference (RLTD) using *gapdh* as a control. Data are presented as mean±s.e.m of 3 biological replicates (n=3).

In summary, liver expression of *Ccl5* and *Spp1* was upregulated in response to the ALIOS diet *in vivo,* and this might contribute to higher macrophage counts in the ALIOS mouse tissue. Lipid loading of hepatocytes *in vitro* was not associated with increases in these chemokines. If damaged hepatocytes are the source, this might be in association with other DAMPs and/or TGFβ with lipids, rather than lipid loading alone. Alternatively, these chemokines may be secreted from other cell types in response to injury.

6.4.4 Investigating the link between macrophages and T cells recruitment

6.4.4.1 The association between the macrophages and T cell counts in C3H/He mice

The link between the macrophages and HCC was supported by the bioinformatics analyses and IHC studies in murine and human tissues. IPA and GSEA analyses also implicated another type of immune filtrate, suggesting a role for T cells in disease pathogenesis. Given that monocytes and macrophages may favour T cell tolerance within the diseased liver environment[424], we next investigated the interplay between T cells and macrophages. Joao Mauricio, a PhD student in our group, did IHC staining and scoring for Cd4, Cd8 and Foxp3 T cell subtypes **(Appendix-7)**. Although the counts of the three T cell types were significantly higher in the ALIOS mice compared to control mice, the number of Cd4 T cells (Spearman Rho 0.701, p<0.0001) rather than Cd8 T cell counts (Spearman Rho 0.410, P=0.058) was associated with tumour development. In addition, the number of Foxp3 positive Cd4 T cells was higher in mice who developed HCC compared to those who didn't (16.33±3.20 versus 8.35±2.68; p=0.041). This supported the GSEA immune-signature analysis **(Figure 6.7)** that revealed an enrichment of Cd4 and Foxp3-related pathways. We created categorical datasets by dividing C3H/He mice into two groups, based on the median number of counts, for each immune cell subtype in order to study associations between different macrophage phenotypes and the T cell subsets. **Table 6.2** shows a strong association between macrophages of Cd44 phenotype and the infiltration of different T cell subtypes into the liver of C3H/he mice. There was no association between Cd68 or F4/80 with T cell counts.

	Cd4			**Foxp3**			**Cd8**		
	Fisher t.test	**Spearman Rho**	**Spearman p.value**	**Fisher t.test**	**Spearman Rho**	**Spearman p.value**	**Fisher t.test**	**Spearman Rho**	**Spearman p.value**
cd44	**0.009**	**0.636**	**0.001**	**0.03**	**0.548**	**0.008**	**0.009**	**0.636**	**0.001**
cd68	0.198	0.365	0.095	1	0.083	0.712	0.67	0.183	0.416
f4/80	0.086	**0.455**	**0.035**	0.198	0.365	0.095	0.395	0.273	0.219

Table 6.2 Hepatic Cd44 positive macrophages were positively associated with different T cell subsets. Fisher exact t.test and Spearman correlation were used to explore associations between categorical data. Significant associations are shown in bold.

The strong association between Cd44 counts and Foxp3 and Cd4 positive cells was notable given that the three cell counts were also associated with the development of HCC in C3H/He mice **(Figure 6.14)**. Interestingly, Foxp3 positive T cells were detected in the periportal steatotic areas in mice liver tissues where lipogranuloma were common **(Figure 6.15)** and the number of Foxp3 positive T cells was significantly associated with the presence of lipogranuloma (Spearman Rho 0.533, p=0.009). The presence of lipogranulomas was also associated with Cd4 and Cd8 T cell count (Cd4 Spearman Rho 0.525, p=0.01; Cd8 Spearman Rho 0.502, p=0.019).

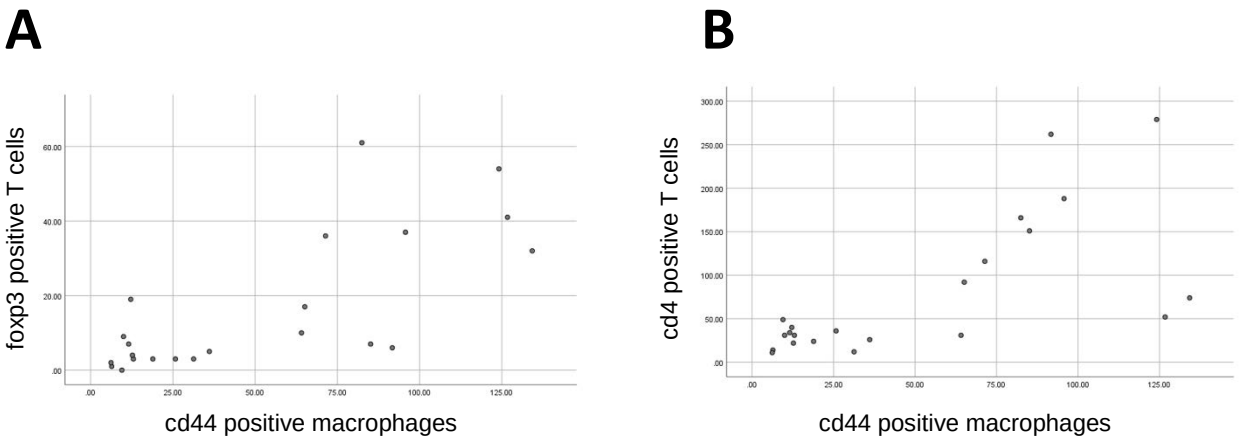

Figure 6.14 Cd44 macrophages correlated with Foxp3 and Cd4 T cell counts. Graphs show the associations between the numbers of Cd44 positive macrophages and the number of Foxp3 **(A)** and Cd4 **(B)** positive T cells in C3H/He mice (n=12 per group).

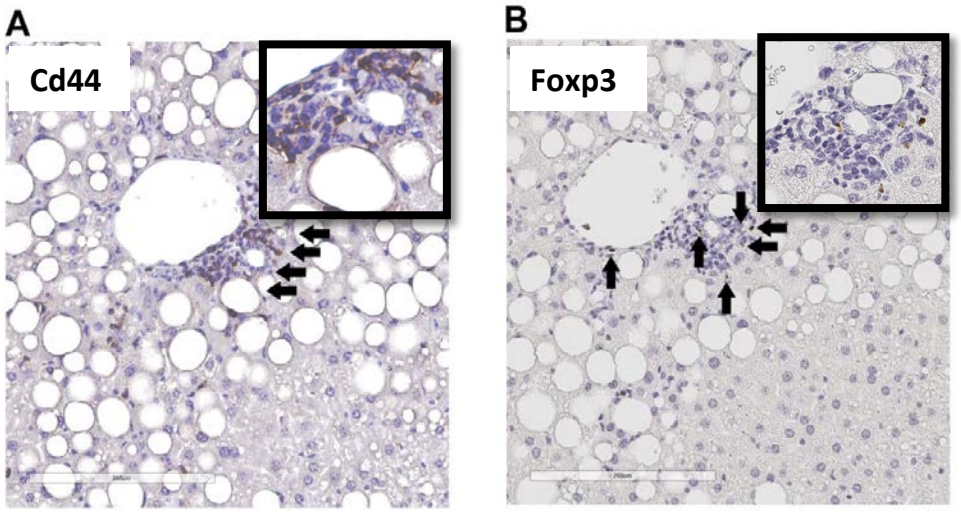

Figure 6.15 Accumulation of T-reg cells in areas rich with Cd44 positive macrophages. Representative images show IHC stain for Cd44 **(A)** and Foxp3 **(B)** in liver of ALIOS-fed mouse. Cd44 positive macrophages accumulated in the portal areas around lipogranuloma (**A**; black

arrows); an area enriched with Foxp3 positive Cd4 T-reg cells (**B**; black arrows). Images were captured using Aperio Imagescope software at x20 magnification.

6.4.4.2 Exploring the T cell chemokines responsible for T cell recruitment in C3H/He mice

Mining the list of DE genes to identify candidate T cell chemokines revealed an elevated expression of classical T cell attractants *Cxcl9* (p=7.85E-08) and *Cxcl10* (p=2.53E-07) in livers of ALIOS-fed mice compared to age matched controls. In addition, the level of the specific Treg attractant *Ccl22* (p=0.013), but not *Ccl17*, was also upregulated in the steatotic livers. This was confirmed at the mRNA level **(Figure 6.16)** in both control and ALIOS-fed mice and the results were reproducible.

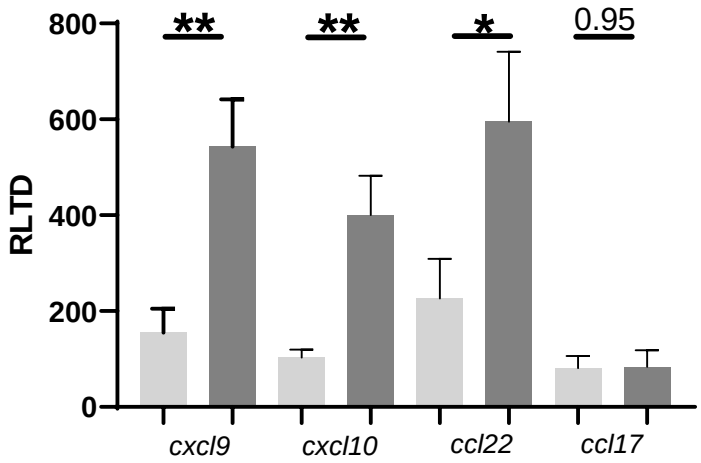

Figure 6.16 Upregulation of different T cell chemoattractants in vivo in livers of ALIOS fed C3H/He mice. Graph shows the increased expression of *Cxcl9, Cxcl10* and *Ccl22*, but not *Ccl17* in control- (light grey) and ALIOS- (dark grey) fed mice. Expression is shown as the relative level of transcriptional difference (RLTD) using *Gapdh* as a control. Data are expressed as mean ± s.e.m; *P<0.05; ** p<0.01, n=12 mice per group.

The association between hepatic *Cxcl9*, *Cxcl10* and *Ccl22* and the count of different T cell subsets is listed in **table 6.3.** In summary, *Cxcl9* was the only chemokine that was associated with the T cell counts in the C3H/He mice, while *Cxcl10* showed no significant associations with different T cell infiltrates. Interestingly, *Ccl22* was strongly associated with the infiltration of foxp3 T cells and cd4 cells, but not the Cd8 T cells, confirming the specificity of this chemokine in attracting T cells of Foxp3 regulatory phenotype.

	Cd4		Foxp3		Cd8	
	Spearman Rho	Spearman p.value	Spearman Rho	Spearman p.value	Spearman Rho	Spearman p.value
Cxcl9	**0.609**	**0.003**	**0.647**	**0.001**	**0.517**	**0.016**
Cxcl10	0.409	0.052	0.410	0.053	0.119	0.599
Ccl22	**0.466**	**0.025**	**0.671**	**<0.0001**	0.371	0.089

Table 6.3 Cxcl9 and Ccl22 levels were associated with Cd4 and Foxp3 T cell counts. Spearman correlations between categorical datasets are shown. Significant associations are in bold.

6.4.4.3 Investigation of the link between macrophages and T cell chemokines

We have shown the Cd44 macrophage count to be associated with the infiltration of different T cell subsets, and we have also suggested an association between Cd44 positive macrophages, Cd4 and Foxp3 positive T cells and the development of HCC. This association between macrophages and T cells might be a result of macrophage-induced expression of T cell chemoattractants, as suggested from the IPA regulator analysis **(Figure 6.6).** In fact, the number of Cd44 positive macrophages was strongly associated with *Cxcl9* (Spearman Rho 0.603, p=0.004) and *Ccl22* (Spearman Rho 0.597, p=0.003) **(Figure 6.17)**; both of which were strongly associated with recruitment of Cd4 and Foxp3 positive T cells to the injured liver.

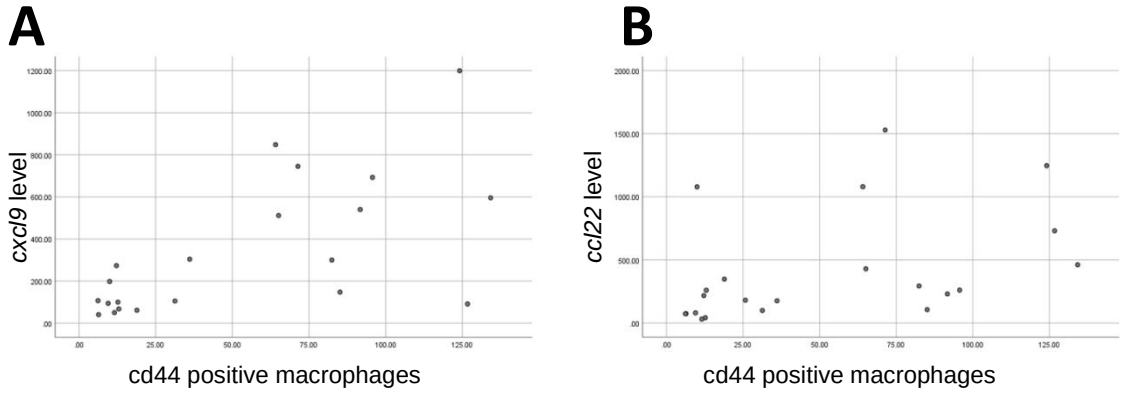

Figure 6.17 Cd44 positive macrophages correlated with key T cell recruiting chemokines in C3H/He mice Graphs show the association between the numbers of Cd44 positive macrophages and *Cxcl9* **(A)** and *Ccl22* **(B)** levels in the non-tumour livers of C3H/He mice, n=21.

Notably, none of the other macrophage phenotypes (Cd68 or F4/80 positive macrophages) were associated with the expression of the above cytokines, adding another tier of support a role for Cd44 in recruitment of T cells to the fat-loaded livers of C3H/He mice **(Table 6.4)**.

	Cxcl9		*Ccl22*	
	Spearman Rho	**Spearman p.value**	**Spearman Rho**	**Spearman p.value**
Cd44	**0.603**	**0.004**	**0.597**	**0.003**
Cd68	0.362	0.116	0.343	0.128
F4/80	0.399	0.073	0.075	0.740

Table 6.4 cd44 positive macrophages were associated with T cell chemokine expression in C3H/He mice. Spearman correlation was used. Significant associations are in bold.

The above association might imply that macrophages (of Cd44 phenotype) can modify the liver microenvironment, increasing the recruitment of T cells and consequently the development of HCC in C3H/He mice. Depending on the cellular source of each T cell chemokine, this macrophage-regulated cross-talk could be directly via macrophage-secreted chemotactic factors or indirectly via interaction with other cell types within the diseased liver niche.

6.4.4.4 Investigation of the effect of macrophage polarisation on the autocrine secretion of T cell chemokines

Bone marrow-derived monocytes (BMDMs) were isolated from C57BL/6 mice as described in the materials and methods. Polarisation of BMDMs from M0 (unpolarised macrophages) into M1 classical inflammatory macrophage phenotype or M2 restorative macrophage phenotype was confirmed morphologically **(Figure 6.18)** and at the mRNA levels **(Figure 6.19).**

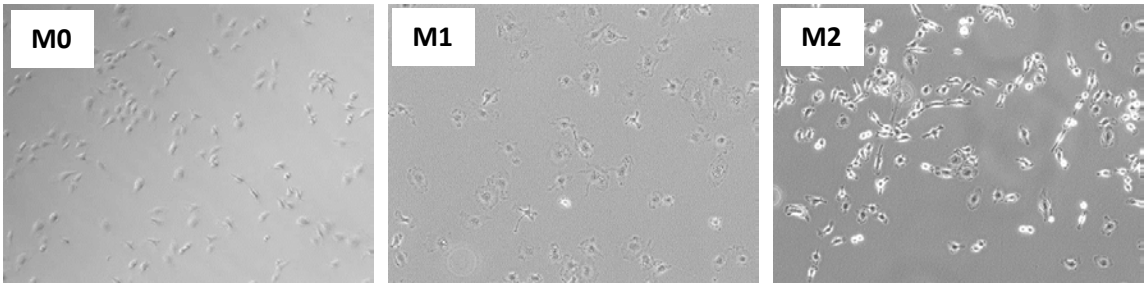

Figure 6.18 Treatment of mouse BMDMs with LPS/Ifny or Il4/Il13 changed their polarisation into M1 and M2 macrophages respectively. Images show the morphological changes accompanying the change from (M0) into the inflammatory macrophage (M1) or restorative macrophages (M2) phenotypes. M1 macrophages acquired a rounded, fried-egg like morphology, while M2 macrophages were more elongated and spindle in shaped. Images were taken at 50x magnification using Zeiss software, n=3 biological replicates.

Upon stimulation with lipopolysaccharides (LPS) and interferon-γ (Ifny), the unpolarised M0 macrophages acquired an M1 fried-egg like shape, while M0 macrophages treated with both Il4 and Il13 adopted a spindle like shape typical of the M2 phenotype **(Figure 6.18)**. Gene expression profiles for markers of different macrophage phenotypes was explored**,** and M1 macrophages showed upregulation of *Il6, Tnfα* and *Nos2* markers compared to M0 and M2 macrophages **(Figure 6.19A).** On the other hand, M2 macrophages showed the upregulation of the M2 classical markers *Arg1* and *Ch3i3,* compared to M1 and M0 macrophages **(Figure 6.19B)** further supporting the success in the induction of macrophage polarisation. Other markers of M2 macrophages were, on the other hand, comparable between the three phenotypes **(Figure 6.19B).**

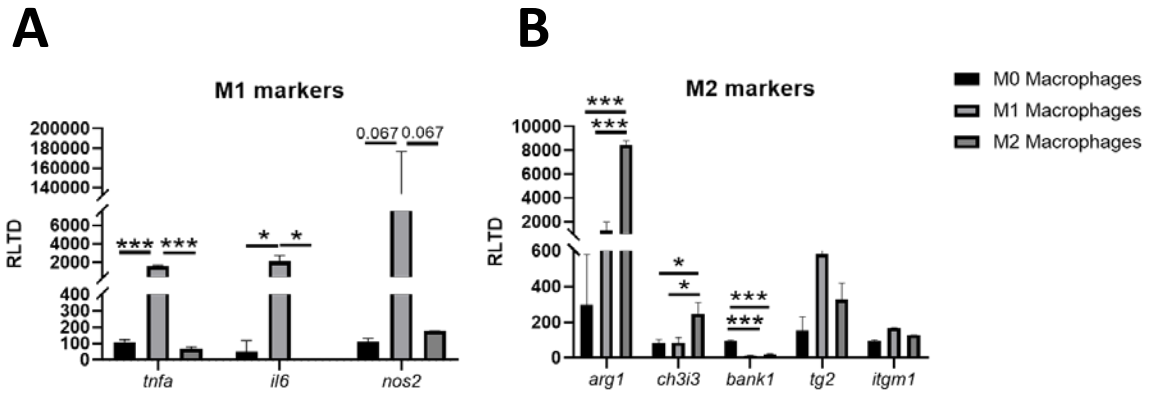

Figure 6.19 Upregulation of classical M1 and M2 markers in BMDMs polarised with either LPS/Ifny or Il4/Il13. Graphs show the gene expression of the classical M1 markers *tnfa, Il6* and *Nos2* **(A)** and M2 markers *Arg1, Ch3i3, Bank1, Tg2* and *Itgm1* **(B)** in M0 (black bars), M1 (light grey) and M2 (dark grey) macrophages. Expression is shown as the relative level of transcriptional difference (RLTD) using *Gapdh* as a control. Data are presented as mean ± s.e.m of 2 biological replicates (n=2), * p<0.05, ***p<0.001.

The *Cd44* level was comparable between M0 and M1, while slightly decreased in M2 macrophages, albeit with no statistical significance **(Figure 6.20A)**. Notably, *Cd44* was highly expressed in all the three macrophage phenotypes (average cycle number of 22), suggesting a poor correlation with hepatic macrophages (low in resident macrophages by IHC) and those derived from Bone Marrow, with limited relevance for further parallels in the Cd44 context. On the other hand, M1 polarised macrophages showed strong upregulation of *Ccl22* and *Ccl17* compared to M0 and M2 macrophages **(Figure 6.20B).** This upregulation was significant in *Ccl22* rather than *Ccl17*.

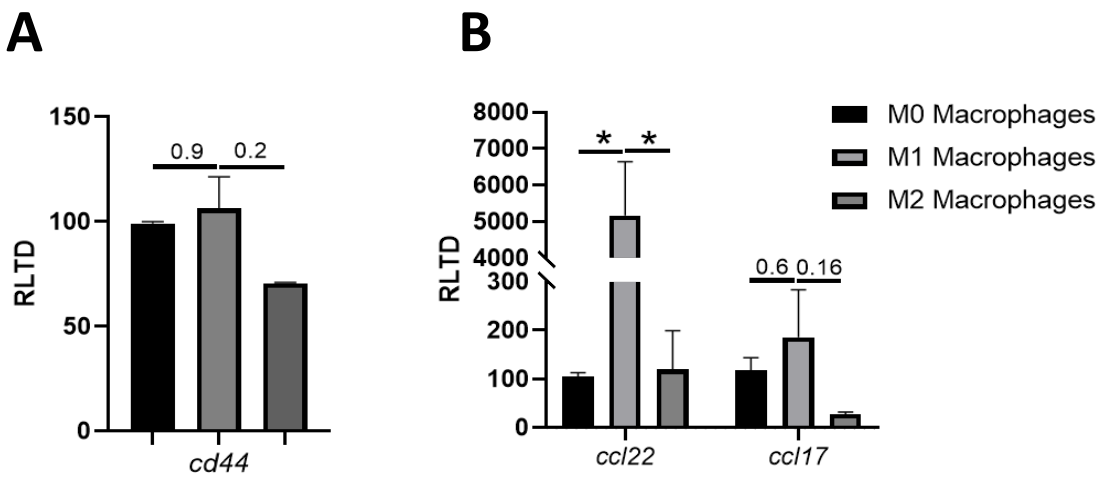

Figure 6.20 Polarisation of mouse BMDMs show difference in the level of ccl22, but not cd44 and ccl17. Graphs show the levels of *Cd44* **(A),** *Ccl22* and *Ccl17* **(B)** in M0 (black bars), M1 (light grey) and M2 (dark grey) macrophages. Expression is shown as the relative level of transcriptional difference (RLTD) using *Gapdh* as a control. Data are presented as mean ± s.e.m of 2 biological replicates (n=2), * $p<0.05$.

In summary, polarisation of DMDMs into M1 and M2 macrophage phenotypes was successfully achieved. M1 macrophages showed higher levels of the Treg chemokine *Ccl22* (formerly called macrophage derived chemokines (MDC)) compared to other macrophage phenotypes, while *Ccl17* and *Cd44* levels were comparable among different phenotypes. A better way to study the phenotype of the Cd44 positive macrophage would ideally be comparing the polarisation status of macrophages isolated from diet- challenged C3H/He mice based on their cd44 expression pattern ($Cd44^{high}$ versus $Cd44^{low}$).

6.4.4.5 Investigation of the effect of macrophage polarisation on the paracrine secretion of T cell chemokines from hepatocytes

CXCL9 and CXCL10 were reported to be expressed by diseased hepatocytes in patients with chronic HCV infection[425], so we hypothesised that macrophages might stimulate hepatocytes to produce chemokines that, in turn, induce the recruitment of T cells. Isolated mouse hepatocytes were treated *in vitro* with CM from M0, M1 and M2 macrophages for 24 hours, and the expression of *Cxcl9* and *Cxcl10* was measured. Hepatocytes treated with M1 macrophages showed dramatic upregulation of *cxcl9* and *cxl10* compared to hepatocytes treated with M0 and M2 CM **(Figure 6.21)**.

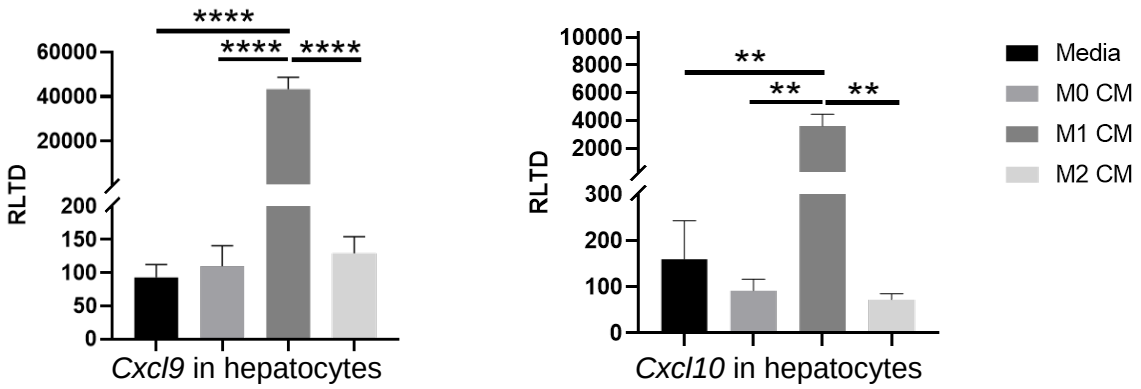

Figure 6.21 The upregulation of Cxcl9 and Cxcl10 in mouse hepatocytes is induced by M1 macrophage secretome. Graphs show the levels of *Cxcl9* and *Cxcl10* in mouse primary hepatocytes treated with complete media or CM from in M0, M1 and M2 macrophages. Expression is shown as the relative level of transcriptional difference (RLTD) using *Gapdh* as a control. Data are presented as mean ± s.e.m of 3 biological replicates (n=3), ** p<0.001, ****P<0.0001.

In summary, *in vitro* studies showed that M1 macrophages contributed to the recruitment of T cells in an autocrine fashion (production of Ccl22 from macrophages) or in a paracrine fashion via cross-talk with parenchymal cells to produce *Cxcl9* and *Cxcl10*. Further validation for the role of Cd44 in the production of T cell chemokines is still outstanding.

6.5 The association between human and mouse tumour transcriptomic data

6.5.1 Exploring the overlap between the mouse tumour RNA-seq data and the human TCGA gene expression profile

The reason for analysing the C3H/He mice non-tumour transcriptomic data was to detect factors which might contribute to the development of NAFLD-HCC in the absence of cirrhosis. In order to investigate whether the HCC developed in the C3H/He mice would mirror human HCC, we compared C3H/He tumour RNA-seq data with publically available Tumour Cancer Genome Atlas (TCGA) transcriptomic database. Sirintra Nakjang from the Newcastle bioinformatics unit has analysed the human TCGA of 374 patients and 50 normal tissue samples. Unsupervised class discovery of the human data identified 6 robust HCC metagene signatures (defined as V1-V6, blue colour) and one non-tumour tissue signature (defined as V7, light green colour) shown in the heat map **(Figure 6.22).**

NAFLD-HCC transcriptome data (denoted in dark blue) in this cohort distributed between different metagenes and failed to form coherent signature, implying that the presence of other stronger factors driving this metagene signature.

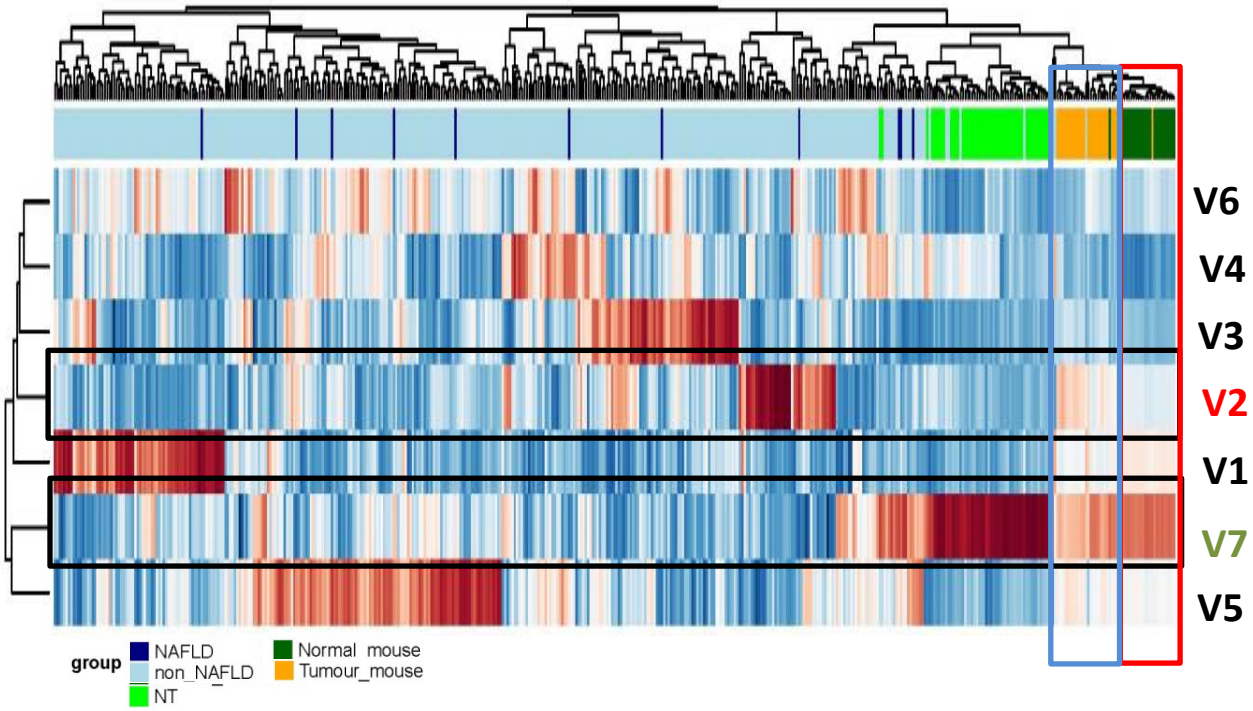

Figure 6.22 Overlapping signatures between Human TCGA and C3H/He mice transcriptome. The heat map shows the TGCA gene expression derived metgene level (V1-V7), which defined subgroup membership (red indicates high metagene levels, blue indicates low levels). Each row represents a metagene and columns are different samples. These 7 metagenes split normal tissue (NT) from tumour tissues (NAFLD and non-NAFLD) as well as splitting tumours samples into several subgroups. Overlapped metagenes are defined by black boxes, mouse non-tumour and tumour transcriptome are highlighted by green box and orange boxes.

The mouse non-tumour transcriptome overlapped with the human non-tumour tissue metagene (V7 signature; denoted in green **Figure 6.22**). Of note, mouse tumour transcriptome also overlapped with the human non-tumour signature, but to lesser extent compared to the non-tumour tissue. The reason for this might be due to the contamination of the sequenced mice tumours from the adjacent non-tumour liver tissue. In contrast, the mouse tumour transcriptome profile, but not the non-tumour profile, showed a signature in the human HCC V2 metagene (denoted in red; **Figure 6.22)** reflecting a resemblance between C3H/He mice tumour transcriptome and a certain subclass of human HCC.

6.5.2 Investigating the gene signature shared between C3H/He and human TCGA tumour data

The DE gene list was created comparing gene transcription profile of V2 human metagene with other human metagenes **(Appendix-8)**. GSEA analysis of this list showed strong enrichment of a particular human HCC subclass with DE genes in this metagene **(Figure 6.23)**.

A

Enriched gene signatures	Genes (overlap genes)	-log (FDR q.value)
Human liver cancer proliferation subclass characterized by high levels of serum AFP, and chromosomal instability.	179 (113)	149.9
Liver selected genes	244 (122)	144.8
Genes highly expressed in human hepatocellular carcinoma with good survival.	185 (87)	98.8
Genes from 'subtype S3' signature of hepatocellular carcinoma (HCC): hepatocyte differentiation.	266 (80)	71.8
Genes down-regulated in liver samples of liver-specific knockout of HNF4A	149 (60)	62.1

B

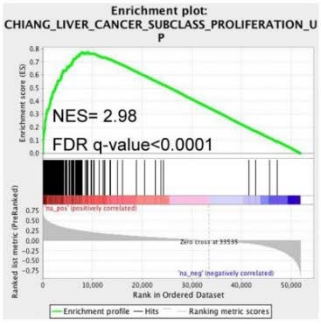

C

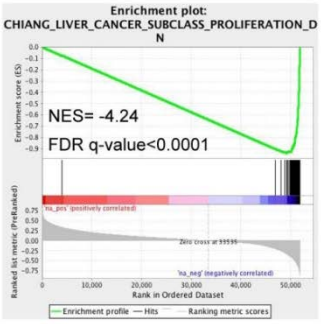

Figure 6.23 Mouse tumour gene expression profile represents a specific subclass of HCC patients. The table **(A)** shows the top 5 overlapping human HCC subgroups with the human V2 metagene signature using GSEA. Gene set enrichment scores of the top enriched human HCC subclass that is characterised by high proliferation and high AFP levels **(B-C)**.

This human HCC subclass was characterised by high proliferation, chromosomal aberration and high AFP levels. The above data was complimented from the fact that *afp* was the top DE gene when comparing mouse tumour versus mouse non-tumour expression profile **(Appendix-1)**. Thus, tumours in C3H/He mice might provide a good preclinical model, relevant particularly to the human HCC subclass characterised by high proliferation index.

6.5.3 Exploring common causative oncogenic pathways in C3H/He tumours and V2 human metagene

Analysing the DE lists of the human V2 metagene and the mouse tumour versus non-tumour against the GSEA oncogenic signatures revealed common pathways responsible for tumour progression, as shown in **Figure 6.24**

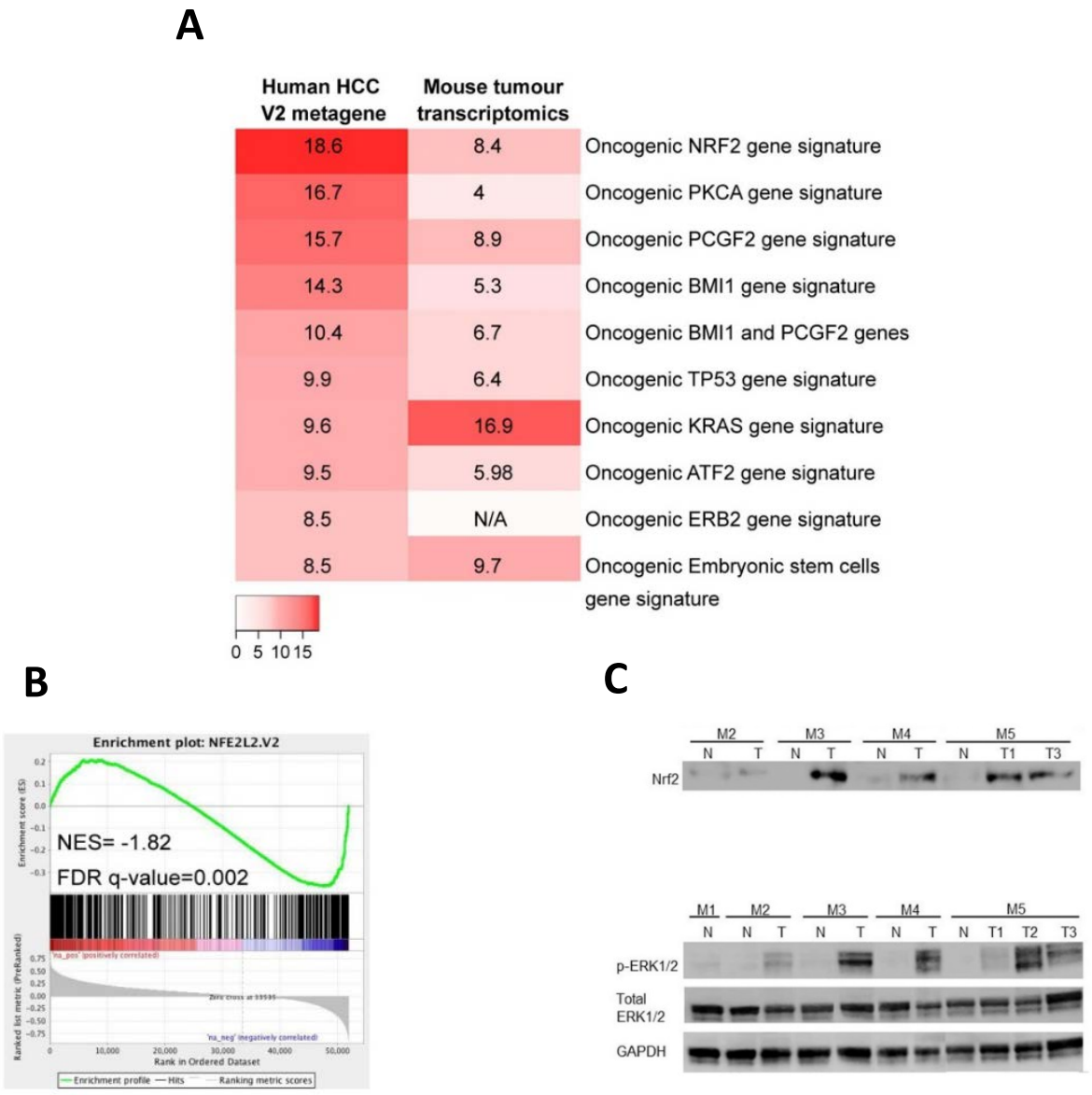

Figure 6.24 Top oncogenic pathways shared between the human V2 signature and mouse tumour transcriptomics The heat map **(A)** shows the top 10 activated oncogenic pathways in the human metagene V2 and mouse tumour transcriptomics using GSEA software, represented by –log (qvalue of overlap)**.** Gene set enrichment score of the NRF2 pathway in the human V2 signature is shown in **(B)** . Western blotting of NRF2, pERK1/2, total ERK1/2 and GAPDH house keeping gene in tissue lysates from tumour and matched non-tumour of 4 different ALIOS-fed mice **(C)**.

The NRF2 oncogenic pathway was the top activated pathway in the human V2 metagene and was also activated in the mouse tumour tissue **(Figure 6.24)**. On the other hand, activation of KRAS pathway was the top enriched pathway in the mouse tumour versus normal data with similar activation in the human signature. In fact, this data confirmed what Gillian Patman, from our group, showed by WB years ago. She noticed an upregulation of both NRF2 and

pERK1/2 proteins in mouse tumour tissue compared to matched non-tumour controls **(Figure 6.24)**. In conclusion, the tumour developed on the background of ALIOS diet resembled a group of HCC patients with unique phenotypic features. This subclass was characterised by the activation of NRF2 and ERK oncogenic pathways.

6.7 Discussion

Early molecular programming studies used microarray analysis to link the change in organism's gene expression profile with different physiological and pathological features[426, 427]. This research area was significantly improved after the introduction of the whole genome high throughput next generation sequencing (NGS) that provided a faster and more cost-effective way to study molecular datasets[428, 429]. The combination of RNAseq, with advanced data analysis pipelines has aided comprehensive characterisation of the molecular landscape and gene expression of different pathological conditions, especially in the cancer field[430]. Early microarray studies in paraffin embedded formalin fixed resections from HCC in patients undergoing resection failed to characterise a tumour gene signature predicting patients' prognosis[57]. Instead, this study identified a liver non-tumour gene signature that predicted HCC patients' outcome. Authors also found an enrichment of different inflammatory pathways in the non-tumour tissue of patients, like IL6/STAT3 and NF-kB pathways[57]. Other studies centred on HCC molecular classifications were discussed in the introduction chapter.

In this chapter, unsupervised clustering of the non-tumour C3H/He mice transcriptomic data identified an important role of inflammation in HCC development. Interrogation of IPA and GSEA analyses of this DE list revealed an enrichment of macrophages, CD4 and FOXP3-related pathways. Analysis also showed an enrichment of cell proliferation and survival pathway in line with activation of STAT3 and NF-kB pathways in the diseased non-tumour tissue. The RNAseq pathway analysis corroborated the previous histopathology characterisation showing that during accumulation of lipids in ALIOS-mice tissue, Lipogranulomas - cell free fat droplets surrounded by macrophages - were the strongest predictor of HCC development in the mice. This macrophage phenotype was particularly characterised by Cd44 and Cd68, rather than F4/80 positive. A previous study has suggested a cancer associated role for CD44, showing CD44 expression in the non-tumour liver tissue to predict poorer HCC patients' outcome[431]. Another study showed that the presence of CD68 positive monocytes in the peri-tumoral regions was also associated with poorer outcome in HCC patients[432].

As shown by the bioinformatic analysis, the number of different T cell subsets was higher in livers of ALIOS fed mice. The number of Cd4 positive and Foxp3 positive, rather than Cd8 positive, T cells were associated with the tumour development. Cd44 positive macrophages were the only macrophage phenotype associated with the number of infiltrating T cell subsets. Histological assessment of ALIOS-liver tissue showed an enrichment of Treg cells in the areas with Cd44 positive lipogranuloma. Moreover, Cd44 positive macrophages were associated with chemokines responsible for the recruitment of Treg cells. In combination, these data support a key role for Cd44 in the induction of immune suppressive premalignant microenvironment characterised by increase the infiltration of Treg cells[424].

Rather than analysing the DE gene list produced by comparing the ALIOS tumour and the non-tumour transcriptomic data, we projected these data against the tumour and non-tumour metagene signatures provided by our non-hypothesis clustering of the human TCGA data. This human HCC 6 signature classification was previously created by another group[433]. The normal human liver metagene was enriched from the mouse non-tumour transcriptomic data, while a certain human tumour metagene was exclusively enriched from our mouse tumour data. Further analysis of the human subclass represented by this metagene identified a unique group of patients with high proliferation and activation of ERK/NRF2 pathways. This patient subclass was originally described by Chiang[58] among 5 different HCC subclasses and it was characterised also by higher frequencies of 4q loss and 13q loss and lower frequencies of 6q loss.

In conclusion, the ALIOS fed C3H/He mice recapitulated the features of human NASH and NASH/HCC. This model represents a valuable tool to study the mechanisms related to the development of and progression of HCC in the patients with the metabolic syndrome, particularly in the absence of cirrhosis.

Chapter 7: Discussion, conclusion and future directions

The current staging systems and treatment options of human HCC

The global incidence of HCC is 1/10000 person per year ranking the sixth most common cancer and the third cause of cancer related mortality[5]. HCC is the predominant form of primary liver cancer and is mostly preceded by chronic liver diseases[434]. The development of HCC in Asia and sub-Saharan Africa is attributed to the prevalence of HBV infection and ingestion of Aflatoxin-B[435], while HCV, alcohol consumption, and metabolic syndrome are among the common causes of HCC in USA and Europe[41, 436]. Prevalence of HCC reached a plateau in certain areas in Europe and Japan; however, HCC is on the rise in the USA and developing countries[437]. The advant of DAAs in the eradication of viral hepatitis reduced the number of chronically-infected patients who are more likely to develop HCC with age[24, 438]. Safety profile and the non-inferior risk for HCC development once the cirrhosis is established are the major limitations of treatment with the DDAs[25]. A large body of evidence supports the increased risk of HCC development on the background of metabolic syndrome and its other co-morbidities. In NAFLD patients, retrospective studies made an association between obesity, T2DM and metabolic syndrome with the development of HCC[439]. Male, aged NAFLD patients with high BMI are more likely to develop HCC compared to non-obese controls[440], and T2DM is reported to be an independent risk factor for the development of HCC[441]. To this end, the active role of NAFLD and metabolic syndrome in setting the stage for the development of HCC primes the need for more in depth studies to characterise and validate novel therapeutic targets to HCC. Median life expectancy of HCC patients is stage-dependent, but at best, it doesn't exceed 2 years in the advanced stage HCC[349, 442], so novel therapeutic targets might be efficient alone or in concert with the existing treatment protocols to improve the outcome of HCC patients.

The Barcelona Clinic Liver Cancer (BCLC) prognostic assessment system is paired with treatment protocols to manage patients with HCC taking into account the stage of the tumour, other related symptoms and the degree of liver function preservation[443]. Patients who had solitary tumour of less than 5cm, or up to three nodules of less than 3 cm with preserved liver functions and no extrahepatic diseases are staged as BCLC-0 and BCLC-A, and they benefit from tumour resection, ablation or transplantation[444]. Absence of cirrhosis is the benchmark for tumour resection in early stage patients with HCC. Tumour recurrence and absence of approved adjuvant or neo-adjuvant therapies for patients undergoing resection are the main limitation of the procedure[444]. Despite the high survival rate in patients undergoing liver

transplantation as a better alternative to resection in early stage HCC, the availability of donor remains the main obstacle[445]. No adjuvant therapy is given to those who are in the waiting list for liver transplantation, thereby increasing the risk of disease progression[446]. Necrosis-inducing ablation is the third option for early stage HCC patients, and is highly recommended for patients with single malignant focus[447]. Ablation is considered curative in single nodules less than 2cm in size, and the survival of Child-pugh stage-A patients undergoing ablation is similar to those having resection[448]. If histological examination is not necessary for the treatment strategy and the liver transplantation is not possible, resection should be a second line therapy after ablation in very early stage HCC patients[444]. Patients with larger multifocal tumours, preserved liver functions and no distant metastasis are staged as BCLC stage-B and would benefit from transarterial chemoembolization[449]. Repeating the chemoembolization should be considered if the necrosis is established after two rounds, or if the second chemoembolization induces substantial necrosis after initial progression following the first treatment[444]. If tumour progresses upon transarterial chemoembolization, treatment with sorafenib should be considered. The only available treatment for patients with advanced HCC (BCLC-C stage) is the tyrosine kinase inhibitors sorafenib[349] as a first line therapy, and regorafenib[442] and cabozantinib[450] as second line treatment. Patients with end-stage HCC (BCLC-D) are not amenable for transplantation as they have the poorest survival and the best supportive care seems to be the only treatment for this category[444]. Despite the efforts exerted in the management of HCC, the 5-year survival of patients with HCC doesn't exceed at best 12%[434] priming the need for more effective therapy.

The role of immune editing in the development of HCC

The development of HCC is mostly preceded by chronic liver diseases, and the inflammatory response is an integral part of the liver damaged state. The activation of the non-parenchymal cells within liver microarchitecture and the infiltration of inflammatory cells help the resolution of acute liver damage caused by drugs, viral infection or fat deposition. However, repeated cycles of damage, hepatocyte regeneration, release of reactive oxygen species (ROS) and DNA damage together with the presence of different immune cell subtypes provide a fertile environment for the development of HCC[216, 451]. An elegant study by *Llovet et al*, published in Gastroenterology in July 2019[452], supports the substantial role of the immune infiltrate in the non-tumour chronically-diseased livers in patient progression into HCC in cirrhotic patients. Authors of this study identified an immune cancer field (ICF) in the

surrounding non-tumour liver tissue in more than half of patients who developed early stage HCC. Activation of classical inflammatory pathways (NF-kB, IL6/STAT3 and IL2/STAT5) as well as different T cells and macrophage pathways was the hallmark in the analysed non-neoplastic tissues. Interestingly, this non-tumour ICF signature was associated with poor prognosis in the analysed cohort, in line with other studies about the role of the non-tumour signatures in predicting the prognosis of HCC patients[57]. Three distinct molecular subtypes were further identified within the ICF group, and were defined as high infiltrate ICF (characterised by more T, B cell and macrophage infiltration pathways), immunosuppressive ICF (characterised by T cell exhaustion and M2 macrophages pathways) and pro-inflammatory ICF (IFNɣ activation and M1 macrophage pathways). Validation of the ICF signature in another cohort of cirrhotic patients within the HCC surveillance programs confirmed its existence in nearly 51% of patients. Among the three ICF subgroups, the presence of the immunosuppressive ICF was the strongest predictor for the development of HCC. Finally, there was no correlation with this ICF signature and the peri- or intra-tumoral immune infiltration reflecting that once the tumour is established, the stromal infiltration is regulated by the tumour cells themselves rather than by the surrounding tissue[452].

We focused on combining the RNA-sequencing, unsupervised clustering, and pathway analysis to leverage the impact of the murine model of NAFLD-HCC established in our group. In particular, we aimed for unleashing the contributing factors and the features responsible for the development of dietary induced-HCC in C3H/He mice in the absence of established cirrhosis. C3H/He mice challenged with the ALIOS diet faithfully recapitulated the histological features of the human NAFLD and NASH. In addition, C3H/He mice developed HCC with age, and this phenotype was exacerbated in mice on the ALIOS diet. The liver weight, the presence of lipogranuloma, steatosis grade, lobular inflammation and stage of fibrosis strongly predicted the development of HCC regardless to the diet.

The gene expression data of the C3H/He non-tumour liver tissue split into two groups, and most of the ALIOS-fed mice were clustered in the G2 group that represented more chronically injured liver. Mice in G2 group showed all features associated with the development of HCC; namely, larger liver weight, lipogranuloma and higher tumour burden and tumour size compared to mice in G1 cluster. Analysing the DE gene list resulting from comparing the above non-tumour clusters showed the activation of macrophage and T cell pathways consistent with what was shown in Llovet's study in human non-tumour liver tissues[452]. Histological

characterisation to the different immune infiltrates in the non-tumour tissue revealed a significant increase in the number of macrophages and the T cell infiltrates in the diseased livers. Of these, the number of cd4 positive T cells and foxp3 positive cells and the number of cd68 positive macrophages were associated with tumour development. Bioinformatics suggested cd44 as one of the main drivers in the G2 *vs* G1 comparison, and IHC stain for cd44 in mice showed a predominant expression in the macrophages. The number of cd44 positive macrophages was strongly associated with the presence of lipogranuloma; the strongest predictor of HCC. The cd44 macrophage count was also strongly associated with the development of HCC in C3H/He; a finding that was validated in human NAFLD/NASH non-tumour tissues. The number of CD44 positive macrophages was higher in the non-tumour tissue of NAFLD/NASH patients who developed HCC compared to those who didn't develop HCC regardless to the presence of cirrhosis. This is clinically relevant in many aspects; first, CD44 macrophage count can be considered as predictive marker for tumour development in non-cirrhotic NAFLD patients by setting up a certain threshold for CD44 positive macrophage above which NAFLD patient could develop HCC. This subclass of patients is not subjected to the surveillance programs[453], and lack of predictive markers increases patients' risk of developing HCC with age. Preventive strategies against HCC development could also consider targeting CD44 in macrophage as a prophylactic therapy against HCC in the high risk patients.

Virtually all reports about CD44 in non-malignant conditions link its expression with different immune cell activation, trafficking and homing processes[454-458]. *Wang J* and *Kubes P*[458] showed that sterile liver injury stimulates the infiltration of peritoneal cavity macrophages in a cd44 dependent manner. Once recruited to the liver, these macrophages acquire the restorative M2 macrophage phenotype contributing to the process of injury repair and healing[458]. It is noteworthy saying that authors didn't measure cd44 level in the liver-recruited macrophages once acquired the M2 phenotype to see whether or not this phenotype switch changes cd44 expression. $cd44^{-/-}$ KO mice challenged with Methionine-choline deficient (MCDD) diet showed macrophages skewed to M2 polarisation compared to control mice. In the same context, macrophages isolated from $cd44^{-/-}$ KO mice were less responsive to LPS activation[456]. Expression of cd44 in different macrophage phenotypes showed counterintuitive results. Stimulation of human THP1 monocyte cell line with M1 and M2 stimuli showed increased CD44 expression in M1 macrophage phenotype compared to M0 and M2 macrophages. M2-polarised THP1 cells; however, expressed CD44 isoform v6 that was associated with better

uptake of hyaluronic acid-based material compared to M1-polarised macrophages that had the strongest CD44 expression[459]. Another study by a different group showed upregulation of cd44 in bone marrow-derived monocytes stimulated with either LPS/IFNɣ (M1 stimuli) or with IL4 (M2 stimuli) adding more complexity to identify the association between cd44 expression and different macrophage polarisation[460]. Further studies are needed to confirm the phenotype associated with CD44 expression.

Regardless to the phenotype of the cd44 positive macrophages, IPA analysis and the association between cd44 macrophage counts with cell count of T cell subsets suggested a role of cd44 in regulating the homing of different T cell subsets in the lipid-loaded livers. The infiltration of T cells to the injured livers was influenced by the upregulation of *cxcl9* in mice tissue, and *cxcl9* expression in the C3H/He mice was strongly associated with the number of cd44 positive macrophages. *In vitro*, *cxcl9* level was strongly upregulated in isolated mouse hepatocytes incubated with CM from M1 classical macrophages compared to hepatocytes stimulated with CM from other macrophage polarization. In line with this, the level of *ccl22*, another T cell chemoattractant whose mRNA levels were associated with cd44 positive macrophages, was upregulated in the *in vitro* experiments in M1 macrophages compared to other macrophage phenotypes. Of note, CCL22 was reported to be associated with the TAM phenotype[461, 462]. This might be explained by the difference between the tumour infiltrating macrophages and macrophages that exist in the precancerous-lesion. The paradigm of M1-M2-TAM is grossly challenged with recent findings of macrophages that carry shared M1/M2 features[463-465]. Further work is needed to characterise the macrophage phenotype in the C3H/He mice that is linked with infiltration of immune suppressive T cells and with the development of HCC.

CAFs are important modulators of human HCC progression

The HCC milieu includes the transformed hepatocytes as well as other non-parenchymal cells including CAFs, TMAs, infiltrating T cells and angiogenic factors[466]. The role of the stromal components within the tumour microenvironment is to induce the proliferation and metastasis of the tumour cells, to favour immunosuppressive environment and to increase the tumour vasculature[466]. In line with this, the infiltration of αSMA-positive CAFs is associated with tumour recurrence after resection in HCC patients[351]. The accumulation of TAMs in HCC is also associated with the larger tumour size and poor patients' outcome[225]. Elevation of

serum VEGF is associated with tumour stage and size and worse prognosis[467]. Hence, tumour stroma is rewarding target to downstage tumour and improve patient outcome.

The elevation of *SULF2* in HCC resections was associated with post-resection tumour recurrence[304]; however, the cellular source of SULF2 and its prognostic role in diagnostic HCC biopsies was yet to be determined. Our studies showed that CAFs were the predominant source of SULF2 in the HCC biopsies, and patients whose HCC biopsies were CAF-SULF2 positive showed the poorest survival. *In vitro* studies using fibroblast cell line with manipulated SULF2 level supported the profound role of stromal SULF2 in inducing aggressive tumour microenvironment. HCC cells cultured in SULF2-rich CM or co-cultured with SULF2 expressing fibroblasts were more proliferative, migratory and invasive compared with cells grown in the absence of SULF2. Moreover, tumour spheroids grown in stromal SULF2 positive media were less amenable to the cytostatic effect exerted by sorafenib in comparison with spheroids grown in SULF2 deficient conditions. This finding was further supported by IHC stain for SULF2 in biopsies from sorafenib-treated HCC patients where the CAF-SULF2 positivity was associated with sorafenib tolerability and poor survival. SULF2 works in different, but yet complimentary, mechanisms depending on its cellular source. SULF2 KD from the fibroblasts reduced the activation of PDGFRβ/JNK/STAT3 pathway leading to deficient secretion of the pro-tumourigenic cytokines IL6 and IL8. Previous studies showed that *in vivo* activation of JNK pathway in mice liver stromal cells was responsible for regulating the fibroblast secretome preceding the development of experimental HCC[137]. Consistently, the role of SULF2 in the expression and production of IL6 in lung cancer cell lines was previously proved[384]. Yet, this is the first study to link SULF2 with the production of IL6 and IL8 cytokines in the context of HCC. SULF2 and SULF2-regulated secretome activated NF-kB pathway in the tumour cells in a paracrine fashion. This SULF2-dependent activation of NF-kB pathway upregulated the stemness marker *CD44* in the tumour cells and this was associated with the proliferation and invasion seen in the HCC cell lines. Activation of NF-kB pathway and upregulation of *CD44* was evident even if the cells were treated with sorafenib, thereby suggesting this pathway as the driver of sorafeib resistance being a feature of CAF-SULF2. This finding was further supported from HCC biopsies where SULF2 positive CAFS existed in the vicinity of tumour cells with positive membranous CD44 and nuclear Pp65 (RelA) positivity. Recently, *Michael Karin's* group has published an elegant study that support the role of CD44 in the process of HCC development and progression[186]. In this study, IL6 secreted from activated macrophages was

associated with CD44 expression in hepatocytes and progenitor cells, treatment of primary hepatocytes with recombinant IL6 induced CD44 expression. CD44 was then responsible for switching of P53 surveillance program leading to the development and progression of HCC[186]. As a regulator of IL6 production and secretion, we provide a novel evidence about the role of SULF2/IL6/CD44 axis in the transformed/malignant hepatocytes.

In 2017, *Llovet* and his group identified a novel immune profile of HCC[229] by integration of transcriptome analysis, IHC stain and patients data. HCCs in this immune class showed more T cell infiltration and more PD1 and PDL1 positivity compared to the immune-null group. Further dissection of the immune profile within the immune class showed two distinct groups; namely referred as "immune active" and "immune exhausted" groups. The immune active class was characterised by less active stroma, better patient outcomes and activation of different effector cell pathways like IFNɣ reflecting the activation of the anti-tumour immunity. In clear contrast to the immune active class, the immune exhausted class was characterised by the enrichment of T cell exhaustion, M2 macrophages and worse patient prognosis. Notably, this class was associated with active stroma and activation of TGFβ as a driver pathway to this immune class[229]. Accumulating data from our group has suggested a role of SULF2 to this immune exhausted class. We show that *SULF2* level was significantly higher in the "immune exhausted" subclass compared to the "immune active2 and "immune-null" classes. IHC stain to CD45, CD4, CD8, CD68 and CD66b in HCC biopsies previously stained with SULF2 showed an association between CAF-SULF2 and the CD45 and CD68 positive counts (data not shown). Given the strong upregulation of SULF2 in the LX2 cells upon treatment with rhTGFβ, we propose another inevitable role of SULF2, as an integral part of the active tumour stroma, in the infiltration of macrophages and leukocytes to the tumour; and this role is mediated by TGFβ. These data were collected in the time course after completion of this thesis and are considered as supporting material for the CAF-SULF2 manuscript.

Conclusion

In summary, the focus of the current study was to explore the active role of different non-parenchymal cells present in the proximity of the tumour niche on the development and progression of HCC. This study used both hypothesis driven and non-hypothesis driven approach to reveal the irrefutable role of SULF2 within the tumour microenvironment side by

side with characterization of cd44, cxcl9 and ccl22 as possible novel therapeutic targets that predispose malignancy in the chronically injured livers.

Future directions

- As a part of the Epos grant, RNAseq was performed on NAFLD/NASH patients with different disease stage in a multi-centre study in Europe. Among different DE genes, *SULF2* was upregulated in the advanced disease stage compared to simple steatosis. In addition, SULF2 was differentially hypo-methylated in patients with more advanced disease explaining the *SULF2* upregulation in the RNAseq. These data corroborated our preliminary SULF2 IHC in NAFLD/NASH patients, thereby encouraging further characterisation of SULF2 as a rewarding therapeutic target in NAFLD/NASH.
- *Sulf2* expression in the murine mouse model of NAFLD-HCC was associated with certain histopathological criteria of mice, most importantly with the development and the size of the developed tumours. $Sulf2^{-/-}$ mice are available, and challenging $Sulf2^{-/-}$ mice with ALIOS diet might give an insight about the role of Sulf2 in tumour development and progression.
- Bioinformatics suggested a novel association between *Sulf2* and *Itk* in the fibrosis-related DE gene list linking Sulf2 with inflammatory changes accompanying fibrosis. Exploring this association between SULF2 and inflammation could provide a novel therapeutic angle in fibrotic patients, but could also indirectly reduce the number of patients developing HCC after deposition of the fibrotic scars. Isolation and FACS sorting of peripheral and liver resident T cells can identify the SULF2-specific T cell subtype and its clinical and translational relevance.
- Unsupervised clustering of the non-tumour tissue provided a significant role of the inflammatory changes in setting the scene for the development of HCC reassuringly reproducing what was very recently published. CD44 positive macrophages orchestrate the microenvironment favouring an immune suppressive and anti-tumour evasion mechanisms. The phenotype of CD44 positive macrophages should be carefully characterised with the hope to produce tool therapy that could, in theory, reduce CD44 levels and confer the reduction of the tumour development of the preclinical NAFLD-HCC models before testing in diseased NAFLD/NASH patients. Rerunning the ALIOS model with isolation and characterisation of the CD44 positive macrophages is one of the important future directions for our group.

- The interplay between different cell compartments in the liver microarchitecture could influence the infiltration of immune subsets preceding the development of malignancy. On the other hand, certain immune cells are responsible for the anti-tumour activity and removal of senescent liver parenchymal cells. Careful investigation should dissect the pathways responsible for the tumour development from these responsible for tumour eradication before adopting immune-related therapeutic strategies in the diseased patients.

Erratum

Myofibroblast cells used in these studies were subsequently confirmed to be of primate COS cell origin, rather than being human hepatic stellate 'LX-2' cells.

After submission of this thesis to the post graduate office for examination, Professor Oakley was informed by a collaborator performing routine checks on shared 'LX-2 cells', that they were likely of primate rather than human origin. Our group have subsequently confirmed that the cells called 'LX-2' cells used in this thesis are in fact derived from COS monkey embryonic fibroblasts. While the SULF2 mechanistic *in-vitro* experiments presented remain valid, as COS cells are frequently used as a tool cell line producing SULF2, submission of my first author SULF2 manuscript for publication has been delayed pending confirmatory mechanistic studies in additional validated human cells. The thesis examiners were subsequently informed and it was agreed that an addendum be added, to highlight this issue, in the final copy of the thesis, post examiners corrections, submitted to Newcastle University.

References

1. Global Burden of Disease Cancer C, Fitzmaurice C, Akinyemiju TF, et al. Global, Regional, and National Cancer Incidence, Mortality, Years of Life Lost, Years Lived With Disability, and Disability-Adjusted Life-Years for 29 Cancer Groups, 1990 to 2016: A Systematic Analysis for the Global Burden of Disease Study. JAMA Oncol 2018;4:1553-1568.
2. El-Serag HB. Hepatocellular carcinoma: an epidemiologic view. J Clin Gastroenterol 2002;35:S72-8.
3. Parkin DM, Bray F, Ferlay J, et al. Global cancer statistics, 2002. CA Cancer J Clin 2005;55:74-108.
4. McGlynn KA, Tsao L, Hsing AW, et al. International trends and patterns of primary liver cancer. Int J Cancer 2001;94:290-6.
5. IARC. Fact sheets by Population-Globocan-IARC. 2016.
6. Lozano R, Naghavi M, Foreman K, et al. Global and regional mortality from 235 causes of death for 20 age groups in 1990 and 2010: a systematic analysis for the Global Burden of Disease Study 2010. Lancet 2012;380:2095-128.
7. Ciernik IF. Risk factors for hepatocellular carcinoma in patients with chronic liver diseases. N Engl J Med 1993;329:1897; author reply 1897-8.
8. Mair RD, Valenzuela A, Ha NB, et al. Incidence of hepatocellular carcinoma among US patients with cirrhosis of viral or nonviral etiologies. Clin Gastroenterol Hepatol 2012;10:1412-7.
9. Mancebo A, Gonzalez-Dieguez ML, Cadahia V, et al. Annual incidence of hepatocellular carcinoma among patients with alcoholic cirrhosis and identification of risk groups. Clin Gastroenterol Hepatol 2013;11:95-101.
10. Sangiovanni A, Prati GM, Fasani P, et al. The natural history of compensated cirrhosis due to hepatitis C virus: A 17-year cohort study of 214 patients. Hepatology 2006;43:1303-10.
11. Parkin DM. The global health burden of infection-associated cancers in the year 2002. Int J Cancer 2006;118:3030-44.
12. Yang JD, Kim WR, Coelho R, et al. Cirrhosis is present in most patients with hepatitis B and hepatocellular carcinoma. Clin Gastroenterol Hepatol 2011;9:64-70.
13. Mittal S, El-Serag HB. Epidemiology of hepatocellular carcinoma: consider the population. J Clin Gastroenterol 2013;47 Suppl:S2-6.
14. Fattovich G, Bortolotti F, Donato F. Natural history of chronic hepatitis B: special emphasis on disease progression and prognostic factors. J Hepatol 2008;48:335-52.
15. Chen CJ, Yang HI, Su J, et al. Risk of hepatocellular carcinoma across a biological gradient of serum hepatitis B virus DNA level. JAMA 2006;295:65-73.
16. Fasani P, Sangiovanni A, De Fazio C, et al. High prevalence of multinodular hepatocellular carcinoma in patients with cirrhosis attributable to multiple risk factors. Hepatology 1999;29:1704-7.
17. Yoshizawa H. Hepatocellular carcinoma associated with hepatitis C virus infection in Japan: projection to other countries in the foreseeable future. Oncology 2002;62 Suppl 1:8-17.
18. Stroffolini T, Andreone P, Andriulli A, et al. Gross pathologic types of hepatocellular carcinoma in Italy. Oncology 1999;56:189-92.
19. Armstrong GL, Alter MJ, McQuillan GM, et al. The past incidence of hepatitis C virus infection: implications for the future burden of chronic liver disease in the United States. Hepatology 2000;31:777-82.
20. Donato F, Tagger A, Gelatti U, et al. Alcohol and hepatocellular carcinoma: the effect of lifetime intake and hepatitis virus infections in men and women. Am J Epidemiol 2002;155:323-31.
21. Lemon SM, McGivern DR. Is hepatitis C virus carcinogenic? Gastroenterology 2012;142:1274-8.
22. Bralet MP, Regimbeau JM, Pineau P, et al. Hepatocellular carcinoma occurring in nonfibrotic liver: epidemiologic and histopathologic analysis of 80 French cases. Hepatology 2000;32:200-4.

23. Morgan RL, Baack B, Smith BD, et al. Eradication of hepatitis C virus infection and the development of hepatocellular carcinoma: a meta-analysis of observational studies. Ann Intern Med 2013;158:329-37.
24. Singal AK, Singh A, Jaganmohan S, et al. Antiviral therapy reduces risk of hepatocellular carcinoma in patients with hepatitis C virus-related cirrhosis. Clin Gastroenterol Hepatol 2010;8:192-9.
25. Reig M, Boix L, Marino Z, et al. Liver Cancer Emergence Associated with Antiviral Treatment: An Immune Surveillance Failure? Semin Liver Dis 2017;37:109-118.
26. Reeves HL, Zaki MY, Day CP. Hepatocellular Carcinoma in Obesity, Type 2 Diabetes, and NAFLD. Dig Dis Sci 2016;61:1234-45.
27. Simon TG, Bonilla H, Yan P, et al. Atorvastatin and fluvastatin are associated with dose-dependent reductions in cirrhosis and hepatocellular carcinoma, among patients with hepatitis C virus: Results from ERCHIVES. Hepatology 2016;64:47-57.
28. Chen HP, Shieh JJ, Chang CC, et al. Metformin decreases hepatocellular carcinoma risk in a dose-dependent manner: population-based and in vitro studies. Gut 2013;62:606-15.
29. Yuan JM, Govindarajan S, Arakawa K, et al. Synergism of alcohol, diabetes, and viral hepatitis on the risk of hepatocellular carcinoma in blacks and whites in the U.S. Cancer 2004;101:1009-17.
30. Marrero JA, Fontana RJ, Fu S, et al. Alcohol, tobacco and obesity are synergistic risk factors for hepatocellular carcinoma. J Hepatol 2005;42:218-24.
31. Hassan MM, Hwang LY, Hatten CJ, et al. Risk factors for hepatocellular carcinoma: synergism of alcohol with viral hepatitis and diabetes mellitus. Hepatology 2002;36:1206-13.
32. Naccarato R, Farinati F. Hepatocellular carcinoma, alcohol, and cirrhosis: facts and hypotheses. Dig Dis Sci 1991;36:1137-42.
33. Bressac B, Kew M, Wands J, et al. Selective G to T mutations of p53 gene in hepatocellular carcinoma from southern Africa. Nature 1991;350:429-31.
34. Kubicka S, Trautwein C, Niehof M, et al. Target gene modulation in hepatocellular carcinomas by decreased DNA-binding of p53 mutations. Hepatology 1997;25:867-73.
35. Omer RE, Kuijsten A, Kadaru AM, et al. Population-attributable risk of dietary aflatoxins and hepatitis B virus infection with respect to hepatocellular carcinoma. Nutr Cancer 2004;48:15-21.
36. Chen CJ, Wang LY, Lu SN, et al. Elevated aflatoxin exposure and increased risk of hepatocellular carcinoma. Hepatology 1996;24:38-42.
37. Wang JS, Qian GS, Zarba A, et al. Temporal patterns of aflatoxin-albumin adducts in hepatitis B surface antigen-positive and antigen-negative residents of Daxin, Qidong County, People's Republic of China. Cancer Epidemiol Biomarkers Prev 1996;5:253-61.
38. Sun Z, Lu P, Gail MH, et al. Increased risk of hepatocellular carcinoma in male hepatitis B surface antigen carriers with chronic hepatitis who have detectable urinary aflatoxin metabolite M1. Hepatology 1999;30:379-83.
39. Younossi ZM, Koenig AB, Abdelatif D, et al. Global epidemiology of nonalcoholic fatty liver disease-Meta-analytic assessment of prevalence, incidence, and outcomes. Hepatology 2016;64:73-84.
40. Chalasani N, Younossi Z, Lavine JE, et al. The diagnosis and management of non-alcoholic fatty liver disease: Practice guideline by the American Association for the Study of Liver Diseases, American College of Gastroenterology, and the American Gastroenterological Association. Am J Gastroenterol 2012;107:811-26.
41. Dyson J, Jaques B, Chattopadyhay D, et al. Hepatocellular cancer: the impact of obesity, type 2 diabetes and a multidisciplinary team. J Hepatol 2014;60:110-7.
42. Mittal S, Sada YH, El-Serag HB, et al. Temporal trends of nonalcoholic fatty liver disease-related hepatocellular carcinoma in the veteran affairs population. Clin Gastroenterol Hepatol 2015;13:594-601 e1.
43. Michelotti GA, Machado MV, Diehl AM. NAFLD, NASH and liver cancer. Nat Rev Gastroenterol Hepatol 2013;10:656-65.

44. Sanyal A, Poklepovic A, Moyneur E, et al. Population-based risk factors and resource utilization for HCC: US perspective. Curr Med Res Opin 2010;26:2183-91.
45. Davila JA, Morgan RO, Shaib Y, et al. Diabetes increases the risk of hepatocellular carcinoma in the United States: a population based case control study. Gut 2005;54:533-9.
46. La Vecchia C, Negri E, Decarli A, et al. Risk factors for hepatocellular carcinoma in northern Italy. Int J Cancer 1988;42:872-6.
47. Lawson DH, Gray JM, McKillop C, et al. Diabetes mellitus and primary hepatocellular carcinoma. Q J Med 1986;61:945-55.
48. Lagiou P, Kuper H, Stuver SO, et al. Role of diabetes mellitus in the etiology of hepatocellular carcinoma. J Natl Cancer Inst 2000;92:1096-9.
49. Huo TI, Wu JC, Lee SD. Are alcohol, tobacco and obesity genuine risk factors for hepatocellular carcinoma? J Hepatol 2005;42:941; author reply 941-2.
50. Nair S, Mason A, Eason J, et al. Is obesity an independent risk factor for hepatocellular carcinoma in cirrhosis? Hepatology 2002;36:150-5.
51. Regimbeau JM, Colombat M, Mognol P, et al. Obesity and diabetes as a risk factor for hepatocellular carcinoma. Liver Transpl 2004;10:S69-73.
52. Bosman FT, Carneiro, F., Hruban, R.H., Theise, N.D. WHO Classification of Tumours of the Digestive System, Fourth Edition

WHO Classification of Tumours,

IARC WHO Classification of Tumours. 2010;Volume 3.
53. Nagtegaal ID, Odze RD, Klimstra D, et al. The 2019 WHO classification of tumours of the digestive system. Histopathology 2019.
54. Pittman ME, Brunt EM. Anatomic pathology of hepatocellular carcinoma: histopathology using classic and new diagnostic tools. Clin Liver Dis 2015;19:239-59.
55. Edmondson HA, Steiner PE. Primary carcinoma of the liver: a study of 100 cases among 48,900 necropsies. Cancer 1954;7:462-503.
56. Boyault S, Rickman DS, de Reynies A, et al. Transcriptome classification of HCC is related to gene alterations and to new therapeutic targets. Hepatology 2007;45:42-52.
57. Hoshida Y, Villanueva A, Kobayashi M, et al. Gene expression in fixed tissues and outcome in hepatocellular carcinoma. N Engl J Med 2008;359:1995-2004.
58. Chiang DY, Villanueva A, Hoshida Y, et al. Focal gains of VEGFA and molecular classification of hepatocellular carcinoma. Cancer Res 2008;68:6779-88.
59. Hoshida Y, Nijman SM, Kobayashi M, et al. Integrative transcriptome analysis reveals common molecular subclasses of human hepatocellular carcinoma. Cancer Res 2009;69:7385-92.
60. Lachenmayer A, Alsinet C, Savic R, et al. Wnt-pathway activation in two molecular classes of hepatocellular carcinoma and experimental modulation by sorafenib. Clin Cancer Res 2012;18:4997-5007.
61. Mao TL, Chu JS, Jeng YM, et al. Expression of mutant nuclear beta-catenin correlates with non-invasive hepatocellular carcinoma, absence of portal vein spread, and good prognosis. J Pathol 2001;193:95-101.
62. Villanueva A, Hoshida Y, Battiston C, et al. Combining clinical, pathology, and gene expression data to predict recurrence of hepatocellular carcinoma. Gastroenterology 2011;140:1501-12 e2.
63. Lee JS, Chu IS, Heo J, et al. Classification and prediction of survival in hepatocellular carcinoma by gene expression profiling. Hepatology 2004;40:667-76.
64. Coulouarn C, Factor VM, Thorgeirsson SS. Transforming growth factor-beta gene expression signature in mouse hepatocytes predicts clinical outcome in human cancer. Hepatology 2008;47:2059-67.
65. Kaposi-Novak P, Lee JS, Gomez-Quiroz L, et al. Met-regulated expression signature defines a subset of human hepatocellular carcinomas with poor prognosis and aggressive phenotype. J Clin Invest 2006;116:1582-95.

66. Cairo S, Armengol C, De Reynies A, et al. Hepatic stem-like phenotype and interplay of Wnt/beta-catenin and Myc signaling in aggressive childhood liver cancer. Cancer Cell 2008;14:471-84.
67. Yamashita T, Forgues M, Wang W, et al. EpCAM and alpha-fetoprotein expression defines novel prognostic subtypes of hepatocellular carcinoma. Cancer Res 2008;68:1451-61.
68. International Consensus Group for Hepatocellular NeoplasiaThe International Consensus Group for Hepatocellular N. Pathologic diagnosis of early hepatocellular carcinoma: a report of the international consensus group for hepatocellular neoplasia. Hepatology 2009;49:658-64.
69. Nahon P, Zucman-Rossi J. Single nucleotide polymorphisms and risk of hepatocellular carcinoma in cirrhosis. J Hepatol 2012;57:663-74.
70. Yoon YJ, Chang HY, Ahn SH, et al. MDM2 and p53 polymorphisms are associated with the development of hepatocellular carcinoma in patients with chronic hepatitis B virus infection. Carcinogenesis 2008;29:1192-6.
71. Migita K, Miyazoe S, Maeda Y, et al. Cytokine gene polymorphisms in Japanese patients with hepatitis B virus infection--association between TGF-beta1 polymorphisms and hepatocellular carcinoma. J Hepatol 2005;42:505-10.
72. Tarhuni A, Guyot E, Rufat P, et al. Impact of cytokine gene variants on the prediction and prognosis of hepatocellular carcinoma in patients with cirrhosis. J Hepatol 2014;61:342-50.
73. Wang Y, Kato N, Hoshida Y, et al. Interleukin-1beta gene polymorphisms associated with hepatocellular carcinoma in hepatitis C virus infection. Hepatology 2003;37:65-71.
74. Nahon P, Sutton A, Rufat P, et al. Myeloperoxidase and superoxide dismutase 2 polymorphisms comodulate the risk of hepatocellular carcinoma and death in alcoholic cirrhosis. Hepatology 2009;50:1484-93.
75. Suenaga M, Yamada S, Fujii T, et al. A functional polymorphism in the epidermal growth factor gene predicts hepatocellular carcinoma risk in Japanese hepatitis C patients. Onco Targets Ther 2013;6:1805-12.
76. Kumar V, Kato N, Urabe Y, et al. Genome-wide association study identifies a susceptibility locus for HCV-induced hepatocellular carcinoma. Nat Genet 2011;43:455-8.
77. Liu YL, Patman GL, Leathart JB, et al. Carriage of the PNPLA3 rs738409 C >G polymorphism confers an increased risk of non-alcoholic fatty liver disease associated hepatocellular carcinoma. J Hepatol 2014;61:75-81.
78. Wang B, Huang G, Wang D, et al. Null genotypes of GSTM1 and GSTT1 contribute to hepatocellular carcinoma risk: evidence from an updated meta-analysis. J Hepatol 2010;53:508-18.
79. Hartmann D, Srivastava U, Thaler M, et al. Telomerase gene mutations are associated with cirrhosis formation. Hepatology 2011;53:1608-17.
80. Calado RT, Young NS. Telomere diseases. N Engl J Med 2009;361:2353-65.
81. Nault JC, Calderaro J, Di Tommaso L, et al. Telomerase reverse transcriptase promoter mutation is an early somatic genetic alteration in the transformation of premalignant nodules in hepatocellular carcinoma on cirrhosis. Hepatology 2014;60:1983-92.
82. Pilati C, Letouze E, Nault JC, et al. Genomic profiling of hepatocellular adenomas reveals recurrent FRK-activating mutations and the mechanisms of malignant transformation. Cancer Cell 2014;25:428-41.
83. Sung WK, Zheng H, Li S, et al. Genome-wide survey of recurrent HBV integration in hepatocellular carcinoma. Nat Genet 2012;44:765-9.
84. Nault JC, Datta S, Imbeaud S, et al. Recurrent AAV2-related insertional mutagenesis in human hepatocellular carcinomas. Nat Genet 2015;47:1187-93.
85. Poon SL, Pang ST, McPherson JR, et al. Genome-wide mutational signatures of aristolochic acid and its application as a screening tool. Sci Transl Med 2013;5:197ra101.
86. Tolba R, Kraus T, Liedtke C, et al. Diethylnitrosamine (DEN)-induced carcinogenic liver injury in mice. Lab Anim 2015;49:59-69.

87. Llovet JM, Villanueva A, Lachenmayer A, et al. Advances in targeted therapies for hepatocellular carcinoma in the genomic era. Nat Rev Clin Oncol 2015;12:436.
88. Schulze K, Imbeaud S, Letouze E, et al. Exome sequencing of hepatocellular carcinomas identifies new mutational signatures and potential therapeutic targets. Nat Genet 2015;47:505-511.
89. Harris CC. p53 tumor suppressor gene: from the basic research laboratory to the clinic--an abridged historical perspective. Carcinogenesis 1996;17:1187-98.
90. Hofseth LJ, Hussain SP, Harris CC. p53: 25 years after its discovery. Trends Pharmacol Sci 2004;25:177-81.
91. Moinzadeh P, Breuhahn K, Stutzer H, et al. Chromosome alterations in human hepatocellular carcinomas correlate with aetiology and histological grade--results of an explorative CGH meta-analysis. Br J Cancer 2005;92:935-41.
92. Oren M, Rotter V. Introduction: p53--the first twenty years. Cell Mol Life Sci 1999;55:9-11.
93. Ratovitski EA, Patturajan M, Hibi K, et al. p53 associates with and targets Delta Np63 into a protein degradation pathway. Proc Natl Acad Sci U S A 2001;98:1817-22.
94. Srivatanakul P, Sriplung H, Deerasamee S. Epidemiology of liver cancer: an overview. Asian Pac J Cancer Prev 2004;5:118-25.
95. Haber DA, Housman DE. Rate-limiting steps: the genetics of pediatric cancers. Cell 1991;64:5-8.
96. Scorsone KA, Zhou YZ, Butel JS, et al. p53 mutations cluster at codon 249 in hepatitis B virus-positive hepatocellular carcinomas from China. Cancer Res 1992;52:1635-8.
97. Aguilar F, Hussain SP, Cerutti P. Aflatoxin B1 induces the transversion of G-->T in codon 249 of the p53 tumor suppressor gene in human hepatocytes. Proc Natl Acad Sci U S A 1993;90:8586-90.
98. Kress S, Jahn UR, Buchmann A, et al. p53 Mutations in human hepatocellular carcinomas from Germany. Cancer Res 1992;52:3220-3.
99. Oda T, Tsuda H, Scarpa A, et al. p53 gene mutation spectrum in hepatocellular carcinoma. Cancer Res 1992;52:6358-64.
100. Ozturk M. p53 mutation in hepatocellular carcinoma after aflatoxin exposure. Lancet 1991;338:1356-9.
101. Arbuthnot P, Capovilla A, Kew M. Putative role of hepatitis B virus X protein in hepatocarcinogenesis: effects on apoptosis, DNA repair, mitogen-activated protein kinase and JAK/STAT pathways. J Gastroenterol Hepatol 2000;15:357-68.
102. Bergsland EK. Molecular mechanisms underlying the development of hepatocellular carcinoma. Semin Oncol 2001;28:521-31.
103. Jia L, Wang XW, Harris CC. Hepatitis B virus X protein inhibits nucleotide excision repair. Int J Cancer 1999;80:875-9.
104. Guichard C, Amaddeo G, Imbeaud S, et al. Integrated analysis of somatic mutations and focal copy-number changes identifies key genes and pathways in hepatocellular carcinoma. Nat Genet 2012;44:694-8.
105. Ahn SM, Jang SJ, Shim JH, et al. Genomic portrait of resectable hepatocellular carcinomas: implications of RB1 and FGF19 aberrations for patient stratification. Hepatology 2014;60:1972-82.
106. Sawey ET, Chanrion M, Cai C, et al. Identification of a therapeutic strategy targeting amplified FGF19 in liver cancer by Oncogenomic screening. Cancer Cell 2011;19:347-58.
107. Di Tommaso L, Sangiovanni A, Borzio M, et al. Advanced precancerous lesions in the liver. Best Pract Res Clin Gastroenterol 2013;27:269-84.
108. Totoki Y, Tatsuno K, Covington KR, et al. Trans-ancestry mutational landscape of hepatocellular carcinoma genomes. Nat Genet 2014;46:1267-73.
109. Zucman-Rossi J, Villanueva A, Nault JC, et al. Genetic Landscape and Biomarkers of Hepatocellular Carcinoma. Gastroenterology 2015;149:1226-1239 e4.

110. de La Coste A, Romagnolo B, Billuart P, et al. Somatic mutations of the beta-catenin gene are frequent in mouse and human hepatocellular carcinomas. Proc Natl Acad Sci U S A 1998;95:8847-51.
111. Satoh S, Daigo Y, Furukawa Y, et al. AXIN1 mutations in hepatocellular carcinomas, and growth suppression in cancer cells by virus-mediated transfer of AXIN1. Nat Genet 2000;24:245-50.
112. Bai F, Nakanishi Y, Takayama K, et al. Codon 64 of K-ras gene mutation pattern in hepatocellular carcinomas induced by bleomycin and 1-nitropyrene in A/J mice. Teratog Carcinog Mutagen 2003;Suppl 1:161-70.
113. Boix-Ferrero J, Pellin A, Blesa JR, et al. K-ras Gene Mutations in Liver Carcinomas from a Mediterranean Area of Spain. Int J Surg Pathol 2000;8:267-270.
114. Cerutti P, Hussain P, Pourzand C, et al. Mutagenesis of the H-ras protooncogene and the p53 tumor suppressor gene. Cancer Res 1994;54:1934s-1938s.
115. Challen C, Guo K, Collier JD, et al. Infrequent point mutations in codons 12 and 61 of ras oncogenes in human hepatocellular carcinomas. J Hepatol 1992;14:342-6.
116. Soman NR, Wogan GN. Activation of the c-Ki-ras oncogene in aflatoxin B1-induced hepatocellular carcinoma and adenoma in the rat: detection by denaturing gradient gel electrophoresis. Proc Natl Acad Sci U S A 1993;90:2045-9.
117. Takada S, Koike K. Activated N-ras gene was found in human hepatoma tissue but only in a small fraction of the tumor cells. Oncogene 1989;4:189-93.
118. Tsuda H, Hirohashi S, Shimosato Y, et al. Low incidence of point mutation of c-Ki-ras and N-ras oncogenes in human hepatocellular carcinoma. Jpn J Cancer Res 1989;80:196-9.
119. Karin M, Greten FR. NF-kappaB: linking inflammation and immunity to cancer development and progression. Nat Rev Immunol 2005;5:749-59.
120. Pikarsky E, Porat RM, Stein I, et al. NF-kappaB functions as a tumour promoter in inflammation-associated cancer. Nature 2004;431:461-6.
121. Barnes PJ, Karin M. Nuclear factor-kappaB: a pivotal transcription factor in chronic inflammatory diseases. N Engl J Med 1997;336:1066-71.
122. Hudson JD, Shoaibi MA, Maestro R, et al. A proinflammatory cytokine inhibits p53 tumor suppressor activity. J Exp Med 1999;190:1375-82.
123. Fausto N. Liver regeneration. J Hepatol 2000;32:19-31.
124. Maeda S, Kamata H, Luo JL, et al. IKKbeta couples hepatocyte death to cytokine-driven compensatory proliferation that promotes chemical hepatocarcinogenesis. Cell 2005;121:977-90.
125. Vakkila J, Lotze MT. Inflammation and necrosis promote tumour growth. Nat Rev Immunol 2004;4:641-8.
126. Zeh HJ, 3rd, Lotze MT. Addicted to death: invasive cancer and the immune response to unscheduled cell death. J Immunother 2005;28:1-9.
127. Curiel TJ, Coukos G, Zou L, et al. Specific recruitment of regulatory T cells in ovarian carcinoma fosters immune privilege and predicts reduced survival. Nat Med 2004;10:942-9.
128. Coussens LM, Werb Z. Inflammation and cancer. Nature 2002;420:860-7.
129. Karin M, Cao Y, Greten FR, et al. NF-kappaB in cancer: from innocent bystander to major culprit. Nat Rev Cancer 2002;2:301-10.
130. Pollard JW. Tumour-educated macrophages promote tumour progression and metastasis. Nat Rev Cancer 2004;4:71-8.
131. Weinreich DM, Elaraj DM, Puhlmann M, et al. Effect of interleukin 1 receptor antagonist gene transduction on human melanoma xenografts in nude mice. Cancer Res 2003;63:5957-61.
132. Eferl R, Wagner EF. AP-1: a double-edged sword in tumorigenesis. Nat Rev Cancer 2003;3:859-68.
133. Hui L, Zatloukal K, Scheuch H, et al. Proliferation of human HCC cells and chemically induced mouse liver cancers requires JNK1-dependent p21 downregulation. J Clin Invest 2008;118:3943-53.

134. Schwabe RF, Bradham CA, Uehara T, et al. c-Jun-N-terminal kinase drives cyclin D1 expression and proliferation during liver regeneration. Hepatology 2003;37:824-32.
135. Behrens A, Sibilia M, David JP, et al. Impaired postnatal hepatocyte proliferation and liver regeneration in mice lacking c-jun in the liver. EMBO J 2002;21:1782-90.
136. Tournier C, Hess P, Yang DD, et al. Requirement of JNK for stress-induced activation of the cytochrome c-mediated death pathway. Science 2000;288:870-4.
137. Das M, Garlick DS, Greiner DL, et al. The role of JNK in the development of hepatocellular carcinoma. Genes Dev 2011;25:634-45.
138. Takeda H, Lyle S, Lazar AJ, et al. Human sebaceous tumors harbor inactivating mutations in LEF1. Nat Med 2006;12:395-7.
139. Tanaka K, Kitagawa Y, Kadowaki T. Drosophila segment polarity gene product porcupine stimulates the posttranslational N-glycosylation of wingless in the endoplasmic reticulum. J Biol Chem 2002;277:12816-23.
140. Willert K, Brown JD, Danenberg E, et al. Wnt proteins are lipid-modified and can act as stem cell growth factors. Nature 2003;423:448-52.
141. Goodman RM, Thombre S, Firtina Z, et al. Sprinter: a novel transmembrane protein required for Wg secretion and signaling. Development 2006;133:4901-11.
142. Korkut C, Ataman B, Ramachandran P, et al. Trans-synaptic transmission of vesicular Wnt signals through Evi/Wntless. Cell 2009;139:393-404.
143. Bhanot P, Brink M, Samos CH, et al. A new member of the frizzled family from Drosophila functions as a Wingless receptor. Nature 1996;382:225-30.
144. Dann CE, Hsieh JC, Rattner A, et al. Insights into Wnt binding and signalling from the structures of two Frizzled cysteine-rich domains. Nature 2001;412:86-90.
145. Janda CY, Waghray D, Levin AM, et al. Structural basis of Wnt recognition by Frizzled. Science 2012;337:59-64.
146. Li VS, Ng SS, Boersema PJ, et al. Wnt signaling through inhibition of beta-catenin degradation in an intact Axin1 complex. Cell 2012;149:1245-56.
147. Boon EM, van der Neut R, van de Wetering M, et al. Wnt signaling regulates expression of the receptor tyrosine kinase met in colorectal cancer. Cancer Res 2002;62:5126-8.
148. Brabletz T, Jung A, Dag S, et al. beta-catenin regulates the expression of the matrix metalloproteinase-7 in human colorectal cancer. Am J Pathol 1999;155:1033-8.
149. Chamorro MN, Schwartz DR, Vonica A, et al. FGF-20 and DKK1 are transcriptional targets of beta-catenin and FGF-20 is implicated in cancer and development. EMBO J 2005;24:73-84.
150. He TC, Sparks AB, Rago C, et al. Identification of c-MYC as a target of the APC pathway. Science 1998;281:1509-12.
151. Hendrix ND, Wu R, Kuick R, et al. Fibroblast growth factor 9 has oncogenic activity and is a downstream target of Wnt signaling in ovarian endometrioid adenocarcinomas. Cancer Res 2006;66:1354-62.
152. Koh TJ, Bulitta CJ, Fleming JV, et al. Gastrin is a target of the beta-catenin/TCF-4 growth-signaling pathway in a model of intestinal polyposis. J Clin Invest 2000;106:533-9.
153. Rodilla V, Villanueva A, Obrador-Hevia A, et al. Jagged1 is the pathological link between Wnt and Notch pathways in colorectal cancer. Proc Natl Acad Sci U S A 2009;106:6315-20.
154. Shimokawa T, Furukawa Y, Sakai M, et al. Involvement of the FGF18 gene in colorectal carcinogenesis, as a novel downstream target of the beta-catenin/T-cell factor complex. Cancer Res 2003;63:6116-20.
155. Shtutman M, Zhurinsky J, Simcha I, et al. The cyclin D1 gene is a target of the beta-catenin/LEF-1 pathway. Proc Natl Acad Sci U S A 1999;96:5522-7.
156. Tetsu O, McCormick F. Beta-catenin regulates expression of cyclin D1 in colon carcinoma cells. Nature 1999;398:422-6.
157. Zhang T, Otevrel T, Gao Z, et al. Evidence that APC regulates survivin expression: a possible mechanism contributing to the stem cell origin of colon cancer. Cancer Res 2001;61:8664-7.
158. Cadoret A, Ovejero C, Terris B, et al. New targets of beta-catenin signaling in the liver are involved in the glutamine metabolism. Oncogene 2002;21:8293-301.

159. Giera S, Braeuning A, Kohle C, et al. Wnt/beta-catenin signaling activates and determines hepatic zonal expression of glutathione S-transferases in mouse liver. Toxicol Sci 2010;115:22-33.
160. Loeppen S, Koehle C, Buchmann A, et al. A beta-catenin-dependent pathway regulates expression of cytochrome P450 isoforms in mouse liver tumors. Carcinogenesis 2005;26:239-48.
161. Nejak-Bowen K, Monga SP. Wnt/beta-catenin signaling in hepatic organogenesis. Organogenesis 2008;4:92-9.
162. Ovejero C, Cavard C, Perianin A, et al. Identification of the leukocyte cell-derived chemotaxin 2 as a direct target gene of beta-catenin in the liver. Hepatology 2004;40:167-76.
163. Sekine S, Lan BY, Bedolli M, et al. Liver-specific loss of beta-catenin blocks glutamine synthesis pathway activity and cytochrome p450 expression in mice. Hepatology 2006;43:817-25.
164. Tan X, Behari J, Cieply B, et al. Conditional deletion of beta-catenin reveals its role in liver growth and regeneration. Gastroenterology 2006;131:1561-72.
165. Peifer M, McCrea PD, Green KJ, et al. The vertebrate adhesive junction proteins beta-catenin and plakoglobin and the Drosophila segment polarity gene armadillo form a multigene family with similar properties. J Cell Biol 1992;118:681-91.
166. Nejak-Bowen KN, Monga SP. Beta-catenin signaling, liver regeneration and hepatocellular cancer: sorting the good from the bad. Semin Cancer Biol 2011;21:44-58.
167. Cadoret A, Ovejero C, Saadi-Kheddouci S, et al. Hepatomegaly in transgenic mice expressing an oncogenic form of beta-catenin. Cancer Res 2001;61:3245-9.
168. Harada N, Miyoshi H, Murai N, et al. Lack of tumorigenesis in the mouse liver after adenovirus-mediated expression of a dominant stable mutant of beta-catenin. Cancer Res 2002;62:1971-7.
169. Harada N, Oshima H, Katoh M, et al. Hepatocarcinogenesis in mice with beta-catenin and Ha-ras gene mutations. Cancer Res 2004;64:48-54.
170. Nejak-Bowen KN, Thompson MD, Singh S, et al. Accelerated liver regeneration and hepatocarcinogenesis in mice overexpressing serine-45 mutant beta-catenin. Hepatology 2010;51:1603-13.
171. Tan X, Apte U, Micsenyi A, et al. Epidermal growth factor receptor: a novel target of the Wnt/beta-catenin pathway in liver. Gastroenterology 2005;129:285-302.
172. Ban KC, Singh H, Krishnan R, et al. GSK-3beta phosphorylation and alteration of beta-catenin in hepatocellular carcinoma. Cancer Lett 2003;199:201-8.
173. Merle P, de la Monte S, Kim M, et al. Functional consequences of frizzled-7 receptor overexpression in human hepatocellular carcinoma. Gastroenterology 2004;127:1110-22.
174. Nambotin SB, Lefrancois L, Sainsily X, et al. Pharmacological inhibition of Frizzled-7 displays anti-tumor properties in hepatocellular carcinoma. J Hepatol 2011;54:288-99.
175. Tong Y, Lin Y, Zhang Y, et al. Association between TCF7L2 gene polymorphisms and susceptibility to type 2 diabetes mellitus: a large Human Genome Epidemiology (HuGE) review and meta-analysis. BMC Med Genet 2009;10:15.
176. Abou-Shady M, Baer HU, Friess H, et al. Transforming growth factor betas and their signaling receptors in human hepatocellular carcinoma. Am J Surg 1999;177:209-15.
177. Idobe Y, Murawaki Y, Kitamura Y, et al. Expression of transforming growth factor-beta 1 in hepatocellular carcinoma in comparison with the non-tumor tissue. Hepatogastroenterology 2003;50:54-9.
178. Ito N, Kawata S, Tamura S, et al. Positive correlation of plasma transforming growth factor-beta 1 levels with tumor vascularity in hepatocellular carcinoma. Cancer Lett 1995;89:45-8.
179. Matsuzaki K, Date M, Furukawa F, et al. Autocrine stimulatory mechanism by transforming growth factor beta in human hepatocellular carcinoma. Cancer Res 2000;60:1394-402.
180. Song BC, Chung YH, Kim JA, et al. Transforming growth factor-beta1 as a useful serologic marker of small hepatocellular carcinoma. Cancer 2002;94:175-80.

181. Tsai JF, Chuang LY, Jeng JE, et al. Clinical relevance of transforming growth factor-beta 1 in the urine of patients with hepatocellular carcinoma. Medicine (Baltimore) 1997;76:213-26.
182. Tsai JF, Jeng JE, Chuang LY, et al. Clinical evaluation of urinary transforming growth factor-beta1 and serum alpha-fetoprotein as tumour markers of hepatocellular carcinoma. Br J Cancer 1997;75:1460-6.
183. Seoane J, Gomis RR. TGF-beta Family Signaling in Tumor Suppression and Cancer Progression. Cold Spring Harb Perspect Biol 2017;9.
184. Chen J, Zaidi S, Rao S, et al. Analysis of Genomes and Transcriptomes of Hepatocellular Carcinomas Identifies Mutations and Gene Expression Changes in the Transforming Growth Factor-beta Pathway. Gastroenterology 2018;154:195-210.
185. Buchert M, Burns CJ, Ernst M. Targeting JAK kinase in solid tumors: emerging opportunities and challenges. Oncogene 2016;35:939-51.
186. Dhar D, Antonucci L, Nakagawa H, et al. Liver Cancer Initiation Requires p53 Inhibition by CD44-Enhanced Growth Factor Signaling. Cancer Cell 2018;33:1061-1077 e6.
187. Chang Q, Daly L, Bromberg J. The IL-6 feed-forward loop: a driver of tumorigenesis. Semin Immunol 2014;26:48-53.
188. Langowski JL, Zhang X, Wu L, et al. IL-23 promotes tumour incidence and growth. Nature 2006;442:461-5.
189. Niu G, Briggs J, Deng J, et al. Signal transducer and activator of transcription 3 is required for hypoxia-inducible factor-1alpha RNA expression in both tumor cells and tumor-associated myeloid cells. Mol Cancer Res 2008;6:1099-105.
190. Niu G, Wright KL, Huang M, et al. Constitutive Stat3 activity up-regulates VEGF expression and tumor angiogenesis. Oncogene 2002;21:2000-8.
191. Xu Q, Briggs J, Park S, et al. Targeting Stat3 blocks both HIF-1 and VEGF expression induced by multiple oncogenic growth signaling pathways. Oncogene 2005;24:5552-60.
192. Bowman T, Broome MA, Sinibaldi D, et al. Stat3-mediated Myc expression is required for Src transformation and PDGF-induced mitogenesis. Proc Natl Acad Sci U S A 2001;98:7319-24.
193. Jarnicki A, Putoczki T, Ernst M. Stat3: linking inflammation to epithelial cancer - more than a "gut" feeling? Cell Div 2010;5:14.
194. Masuda M, Suzui M, Yasumatu R, et al. Constitutive activation of signal transducers and activators of transcription 3 correlates with cyclin D1 overexpression and may provide a novel prognostic marker in head and neck squamous cell carcinoma. Cancer Res 2002;62:3351-5.
195. Rahaman SO, Harbor PC, Chernova O, et al. Inhibition of constitutively active Stat3 suppresses proliferation and induces apoptosis in glioblastoma multiforme cells. Oncogene 2002;21:8404-13.
196. Stephanou A, Brar BK, Knight RA, et al. Opposing actions of STAT-1 and STAT-3 on the Bcl-2 and Bcl-x promoters. Cell Death Differ 2000;7:329-30.
197. Grivennikov SI, Wang K, Mucida D, et al. Adenoma-linked barrier defects and microbial products drive IL-23/IL-17-mediated tumour growth. Nature 2012;491:254-8.
198. Huang M, Wang J, Lee P, et al. Human non-small cell lung cancer cells express a type 2 cytokine pattern. Cancer Res 1995;55:3847-53.
199. Miteva LD, Stanilov NS, Deliysky TS, et al. Significance of -1082A/G polymorphism of IL10 gene for progression of colorectal cancer and IL-10 expression. Tumour Biol 2014;35:12655-64.
200. Sellon RK, Tonkonogy S, Schultz M, et al. Resident enteric bacteria are necessary for development of spontaneous colitis and immune system activation in interleukin-10-deficient mice. Infect Immun 1998;66:5224-31.
201. Kaplan DH, Shankaran V, Dighe AS, et al. Demonstration of an interferon gamma-dependent tumor surveillance system in immunocompetent mice. Proc Natl Acad Sci U S A 1998;95:7556-61.
202. Shankaran V, Ikeda H, Bruce AT, et al. IFNgamma and lymphocytes prevent primary tumour development and shape tumour immunogenicity. Nature 2001;410:1107-11.

203. Street SE, Trapani JA, MacGregor D, et al. Suppression of lymphoma and epithelial malignancies effected by interferon gamma. J Exp Med 2002;196:129-34.
204. Zhou L, Huang Y, Li J, et al. The mTOR pathway is associated with the poor prognosis of human hepatocellular carcinoma. Med Oncol 2010;27:255-61.
205. Liu D, Wong CC, Fu L, et al. Squalene epoxidase drives NAFLD-induced hepatocellular carcinoma and is a pharmaceutical target. Sci Transl Med 2018;10.
206. Matter MS, Decaens T, Andersen JB, et al. Targeting the mTOR pathway in hepatocellular carcinoma: current state and future trends. J Hepatol 2014;60:855-65.
207. Inoki K, Li Y, Xu T, et al. Rheb GTPase is a direct target of TSC2 GAP activity and regulates mTOR signaling. Genes Dev 2003;17:1829-34.
208. Tee AR, Fingar DC, Manning BD, et al. Tuberous sclerosis complex-1 and -2 gene products function together to inhibit mammalian target of rapamycin (mTOR)-mediated downstream signaling. Proc Natl Acad Sci U S A 2002;99:13571-6.
209. Calvisi DF, Wang C, Ho C, et al. Increased lipogenesis, induced by AKT-mTORC1-RPS6 signaling, promotes development of human hepatocellular carcinoma. Gastroenterology 2011;140:1071-83.
210. Cui J, Gong Z, Shen HM. The role of autophagy in liver cancer: molecular mechanisms and potential therapeutic targets. Biochim Biophys Acta 2013;1836:15-26.
211. Janku F, McConkey DJ, Hong DS, et al. Autophagy as a target for anticancer therapy. Nat Rev Clin Oncol 2011;8:528-39.
212. Andersen JB, Spee B, Blechacz BR, et al. Genomic and genetic characterization of cholangiocarcinoma identifies therapeutic targets for tyrosine kinase inhibitors. Gastroenterology 2012;142:1021-1031 e15.
213. Menon S, Manning BD. Common corruption of the mTOR signaling network in human tumors. Oncogene 2008;27 Suppl 2:S43-51.
214. Zhang ZJ, Zheng ZJ, Shi R, et al. Metformin for liver cancer prevention in patients with type 2 diabetes: a systematic review and meta-analysis. J Clin Endocrinol Metab 2012;97:2347-53.
215. Singh S, Singh PP, Singh AG, et al. Anti-diabetic medications and the risk of hepatocellular cancer: a systematic review and meta-analysis. Am J Gastroenterol 2013;108:881-91; quiz 892.
216. Hernandez-Gea V, Toffanin S, Friedman SL, et al. Role of the microenvironment in the pathogenesis and treatment of hepatocellular carcinoma. Gastroenterology 2013;144:512-27.
217. Lok AS, Seeff LB, Morgan TR, et al. Incidence of hepatocellular carcinoma and associated risk factors in hepatitis C-related advanced liver disease. Gastroenterology 2009;136:138-48.
218. Wong CM, Ng IO. Molecular pathogenesis of hepatocellular carcinoma. Liver Int 2008;28:160-74.
219. Darvin P, Toor SM, Sasidharan Nair V, et al. Immune checkpoint inhibitors: recent progress and potential biomarkers. Exp Mol Med 2018;50:165.
220. Zamarron BF, Chen W. Dual roles of immune cells and their factors in cancer development and progression. Int J Biol Sci 2011;7:651-8.
221. Fu J, Xu D, Liu Z, et al. Increased regulatory T cells correlate with CD8 T-cell impairment and poor survival in hepatocellular carcinoma patients. Gastroenterology 2007;132:2328-39.
222. Wynn TA, Vannella KM. Macrophages in Tissue Repair, Regeneration, and Fibrosis. Immunity 2016;44:450-462.
223. Lucas T, Abraham D, Aharinejad S. Modulation of tumor associated macrophages in solid tumors. Front Biosci 2008;13:5580-8.
224. Wu SD, Ma YS, Fang Y, et al. Role of the microenvironment in hepatocellular carcinoma development and progression. Cancer Treat Rev 2012;38:218-25.
225. Ding T, Xu J, Wang F, et al. High tumor-infiltrating macrophage density predicts poor prognosis in patients with primary hepatocellular carcinoma after resection. Hum Pathol 2009;40:381-9.

226. Affo S, Yu LX, Schwabe RF. The Role of Cancer-Associated Fibroblasts and Fibrosis in Liver Cancer. Annu Rev Pathol 2017;12:153-186.
227. Kalluri R, Zeisberg M. Fibroblasts in cancer. Nat Rev Cancer 2006;6:392-401.
228. Bhowmick NA, Neilson EG, Moses HL. Stromal fibroblasts in cancer initiation and progression. Nature 2004;432:332-7.
229. Sia D, Jiao Y, Martinez-Quetglas I, et al. Identification of an Immune-specific Class of Hepatocellular Carcinoma, Based on Molecular Features. Gastroenterology 2017;153:812-826.
230. Esko JD, Zhang L. Influence of core protein sequence on glycosaminoglycan assembly. Curr Opin Struct Biol 1996;6:663-70.
231. Stanford KI, Bishop JR, Foley EM, et al. Syndecan-1 is the primary heparan sulfate proteoglycan mediating hepatic clearance of triglyceride-rich lipoproteins in mice. J Clin Invest 2009;119:3236-45.
232. Ori A, Wilkinson MC, Fernig DG. A systems biology approach for the investigation of the heparin/heparan sulfate interactome. J Biol Chem 2011;286:19892-904.
233. Baeg GH, Lin X, Khare N, et al. Heparan sulfate proteoglycans are critical for the organization of the extracellular distribution of Wingless. Development 2001;128:87-94.
234. Bellaiche Y, The I, Perrimon N. Tout-velu is a Drosophila homologue of the putative tumour suppressor EXT-1 and is needed for Hh diffusion. Nature 1998;394:85-8.
235. Han C, Yan D, Belenkaya TY, et al. Drosophila glypicans Dally and Dally-like shape the extracellular Wingless morphogen gradient in the wing disc. Development 2005;132:667-79.
236. Takei Y, Ozawa Y, Sato M, et al. Three Drosophila EXT genes shape morphogen gradients through synthesis of heparan sulfate proteoglycans. Development 2004;131:73-82.
237. Belov AA, Mohammadi M. Molecular mechanisms of fibroblast growth factor signaling in physiology and pathology. Cold Spring Harb Perspect Biol 2013;5.
238. Brown A, Robinson CJ, Gallagher JT, et al. Cooperative heparin-mediated oligomerization of fibroblast growth factor-1 (FGF1) precedes recruitment of FGFR2 to ternary complexes. Biophys J 2013;104:1720-30.
239. DiGabriele AD, Lax I, Chen DI, et al. Structure of a heparin-linked biologically active dimer of fibroblast growth factor. Nature 1998;393:812-7.
240. Mohammadi M, Olsen SK, Ibrahimi OA. Structural basis for fibroblast growth factor receptor activation. Cytokine Growth Factor Rev 2005;16:107-37.
241. Xu D, Young JH, Krahn JM, et al. Stable RAGE-heparan sulfate complexes are essential for signal transduction. ACS Chem Biol 2013;8:1611-20.
242. Gralle M, Botelho MG, Wouters FS. Neuroprotective secreted amyloid precursor protein acts by disrupting amyloid precursor protein dimers. J Biol Chem 2009;284:15016-25.
243. Xue Y, Lee S, Wang Y, et al. Crystal structure of the E2 domain of amyloid precursor protein-like protein 1 in complex with sucrose octasulfate. J Biol Chem 2011;286:29748-57.
244. Lietha D, Chirgadze DY, Mulloy B, et al. Crystal structures of NK1-heparin complexes reveal the basis for NK1 activity and enable engineering of potent agonists of the MET receptor. EMBO J 2001;20:5543-55.
245. Goodsell DS, Olson AJ. Structural symmetry and protein function. Annu Rev Biophys Biomol Struct 2000;29:105-53.
246. Shaw AS, Filbert EL. Scaffold proteins and immune-cell signalling. Nat Rev Immunol 2009;9:47-56.
247. Iozzo RV. Basement membrane proteoglycans: from cellar to ceiling. Nat Rev Mol Cell Biol 2005;6:646-56.
248. Fransson LA, Belting M, Cheng F, et al. Novel aspects of glypican glycobiology. Cell Mol Life Sci 2004;61:1016-24.
249. Filmus J, Selleck SB. Glypicans: proteoglycans with a surprise. J Clin Invest 2001;108:497-501.
250. Bezakova G, Ruegg MA. New insights into the roles of agrin. Nat Rev Mol Cell Biol 2003;4:295-308.

251. Bernfield M, Gotte M, Park PW, et al. Functions of cell surface heparan sulfate proteoglycans. Annu Rev Biochem 1999;68:729-77.
252. Alexopoulou AN, Multhaupt HA, Couchman JR. Syndecans in wound healing, inflammation and vascular biology. Int J Biochem Cell Biol 2007;39:505-28.
253. Turnbull J, Powell A, Guimond S. Heparan sulfate: decoding a dynamic multifunctional cell regulator. Trends Cell Biol 2001;11:75-82.
254. Jorpes JE, Gardell S. On heparin monosulfuric acid. J Biol Chem 1948;176:267-76.
255. Ori A, Wilkinson MC, Fernig DG. The heparanome and regulation of cell function: structures, functions and challenges. Front Biosci 2008;13:4309-38.
256. Esko JD, Selleck SB. Order out of chaos: assembly of ligand binding sites in heparan sulfate. Annu Rev Biochem 2002;71:435-71.
257. Maccarana M, Sakura Y, Tawada A, et al. Domain structure of heparan sulfates from bovine organs. J Biol Chem 1996;271:17804-10.
258. Murphy KJ, Merry CL, Lyon M, et al. A new model for the domain structure of heparan sulfate based on the novel specificity of K5 lyase. J Biol Chem 2004;279:27239-45.
259. Kato M, Wang H, Bernfield M, et al. Cell surface syndecan-1 on distinct cell types differs in fine structure and ligand binding of its heparan sulfate chains. J Biol Chem 1994;269:18881-90.
260. Orellana A, Hirschberg CB, Wei Z, et al. Molecular cloning and expression of a glycosaminoglycan N-acetylglucosaminyl N-deacetylase/N-sulfotransferase from a heparin-producing cell line. J Biol Chem 1994;269:2270-6.
261. Aikawa J, Grobe K, Tsujimoto M, et al. Multiple isozymes of heparan sulfate/heparin GlcNAc N-deacetylase/GlcN N-sulfotransferase. Structure and activity of the fourth member, NDST4. J Biol Chem 2001;276:5876-82.
262. Mulloy B, Forster MJ. Conformation and dynamics of heparin and heparan sulfate. Glycobiology 2000;10:1147-56.
263. Safaiyan F, Lindahl U, Salmivirta M. Structural diversity of N-sulfated heparan sulfate domains: distinct modes of glucuronyl C5 epimerization, iduronic acid 2-O-sulfation, and glucosamine 6-O-sulfation. Biochemistry 2000;39:10823-30.
264. Rong J, Habuchi H, Kimata K, et al. Substrate specificity of the heparan sulfate hexuronic acid 2-O-sulfotransferase. Biochemistry 2001;40:5548-55.
265. Rong J, Habuchi H, Kimata K, et al. Expression of heparan sulphate L-iduronyl 2-O-sulphotransferase in human kidney 293 cells results in increased D-glucuronyl 2-O-sulphation. Biochem J 2000;346 Pt 2:463-8.
266. Habuchi H, Tanaka M, Habuchi O, et al. The occurrence of three isoforms of heparan sulfate 6-O-sulfotransferase having different specificities for hexuronic acid adjacent to the targeted N-sulfoglucosamine. J Biol Chem 2000;275:2859-68.
267. Tatrai P, Egedi K, Somoracz A, et al. Quantitative and qualitative alterations of heparan sulfate in fibrogenic liver diseases and hepatocellular cancer. J Histochem Cytochem 2010;58:429-41.
268. Barth H, Schafer C, Adah MI, et al. Cellular binding of hepatitis C virus envelope glycoprotein E2 requires cell surface heparan sulfate. J Biol Chem 2003;278:41003-12.
269. Schulze A, Gripon P, Urban S. Hepatitis B virus infection initiates with a large surface protein-dependent binding to heparan sulfate proteoglycans. Hepatology 2007;46:1759-68.
270. Filmus J, Capurro M. Glypican-3: a marker and a therapeutic target in hepatocellular carcinoma. FEBS J 2013;280:2471-6.
271. Zhou F, Shang W, Yu X, et al. Glypican-3: A promising biomarker for hepatocellular carcinoma diagnosis and treatment. Med Res Rev 2018;38:741-767.
272. Di Tommaso L, Franchi G, Park YN, et al. Diagnostic value of HSP70, glypican 3, and glutamine synthetase in hepatocellular nodules in cirrhosis. Hepatology 2007;45:725-34.
273. Lai JP, Oseini AM, Moser CD, et al. The oncogenic effect of sulfatase 2 in human hepatocellular carcinoma is mediated in part by glypican 3-dependent Wnt activation. Hepatology 2010;52:1680-9.

274. Diez-Roux G, Ballabio A. Sulfatases and human disease. Annu Rev Genomics Hum Genet 2005;6:355-79.
275. Sardiello M, Annunziata I, Roma G, et al. Sulfatases and sulfatase modifying factors: an exclusive and promiscuous relationship. Hum Mol Genet 2005;14:3203-17.
276. Dhoot GK, Gustafsson MK, Ai X, et al. Regulation of Wnt signaling and embryo patterning by an extracellular sulfatase. Science 2001;293:1663-6.
277. Morimoto-Tomita M, Uchimura K, Bistrup A, et al. Sulf-2, a proangiogenic heparan sulfate endosulfatase, is upregulated in breast cancer. Neoplasia 2005;7:1001-10.
278. Izvolsky KI, Shoykhet D, Yang Y, et al. Heparan sulfate-FGF10 interactions during lung morphogenesis. Dev Biol 2003;258:185-200.
279. Kreuger J, Jemth P, Sanders-Lindberg E, et al. Fibroblast growth factors share binding sites in heparan sulphate. Biochem J 2005;389:145-50.
280. Kreuger J, Salmivirta M, Sturiale L, et al. Sequence analysis of heparan sulfate epitopes with graded affinities for fibroblast growth factors 1 and 2. J Biol Chem 2001;276:30744-52.
281. Pye DA, Vives RR, Hyde P, et al. Regulation of FGF-1 mitogenic activity by heparan sulfate oligosaccharides is dependent on specific structural features: differential requirements for the modulation of FGF-1 and FGF-2. Glycobiology 2000;10:1183-92.
282. Lyon M, Deakin JA, Mizuno K, et al. Interaction of hepatocyte growth factor with heparan sulfate. Elucidation of the major heparan sulfate structural determinants. J Biol Chem 1994;269:11216-23.
283. Mahalingam Y, Gallagher JT, Couchman JR. Cellular adhesion responses to the heparin-binding (HepII) domain of fibronectin require heparan sulfate with specific properties. J Biol Chem 2007;282:3221-30.
284. Feyzi E, Lustig F, Fager G, et al. Characterization of heparin and heparan sulfate domains binding to the long splice variant of platelet-derived growth factor A chain. J Biol Chem 1997;272:5518-24.
285. Ono K, Hattori H, Takeshita S, et al. Structural features in heparin that interact with VEGF165 and modulate its biological activity. Glycobiology 1999;9:705-11.
286. Morimoto-Tomita M, Uchimura K, Werb Z, et al. Cloning and characterization of two extracellular heparin-degrading endosulfatases in mice and humans. J Biol Chem 2002;277:49175-85.
287. Hanson SR, Best MD, Wong CH. Sulfatases: structure, mechanism, biological activity, inhibition, and synthetic utility. Angew Chem Int Ed Engl 2004;43:5736-63.
288. Tang R, Rosen SD. Functional consequences of the subdomain organization of the sulfs. J Biol Chem 2009;284:21505-14.
289. Rosen SD, Lemjabbar-Alaoui H. Sulf-2: an extracellular modulator of cell signaling and a cancer target candidate. Expert Opin Ther Targets 2010;14:935-49.
290. Ai X, Do AT, Kusche-Gullberg M, et al. Substrate specificity and domain functions of extracellular heparan sulfate 6-O-endosulfatases, QSulf1 and QSulf2. J Biol Chem 2006;281:4969-76.
291. Lamanna WC, Frese MA, Balleininger M, et al. Sulf loss influences N-, 2-O-, and 6-O-sulfation of multiple heparan sulfate proteoglycans and modulates fibroblast growth factor signaling. J Biol Chem 2008;283:27724-35.
292. Nagamine S, Keino-Masu K, Shiomi K, et al. Proteolytic cleavage of the rat heparan sulfate 6-O-endosulfatase SulfFP2 by furin-type proprotein convertases. Biochem Biophys Res Commun 2010;391:107-12.
293. Ambasta RK, Ai X, Emerson CP, Jr. Quail Sulf1 function requires asparagine-linked glycosylation. J Biol Chem 2007;282:34492-9.
294. Kalus I, Salmen B, Viebahn C, et al. Differential involvement of the extracellular 6-O-endosulfatases Sulf1 and Sulf2 in brain development and neuronal and behavioural plasticity. J Cell Mol Med 2009;13:4505-21.
295. Holst CR, Bou-Reslan H, Gore BB, et al. Secreted sulfatases Sulf1 and Sulf2 have overlapping yet essential roles in mouse neonatal survival. PLoS One 2007;2:e575.

296. Ai X, Kitazawa T, Do AT, et al. SULF1 and SULF2 regulate heparan sulfate-mediated GDNF signaling for esophageal innervation. Development 2007;134:3327-38.
297. Seffouh A, Milz F, Przybylski C, et al. HSulf sulfatases catalyze processive and oriented 6-O-desulfation of heparan sulfate that differentially regulates fibroblast growth factor activity. FASEB J 2013;27:2431-9.
298. Uchimura K, Morimoto-Tomita M, Bistrup A, et al. HSulf-2, an extracellular endoglucosamine-6-sulfatase, selectively mobilizes heparin-bound growth factors and chemokines: effects on VEGF, FGF-1, and SDF-1. BMC Biochem 2006;7:2.
299. Uchimura K, Morimoto-Tomita M, Rosen SD. Measuring the activities of the Sulfs: two novel heparin/heparan sulfate endosulfatases. Methods Enzymol 2006;416:243-53.
300. Viviano BL, Paine-Saunders S, Gasiunas N, et al. Domain-specific modification of heparan sulfate by Qsulf1 modulates the binding of the bone morphogenetic protein antagonist Noggin. J Biol Chem 2004;279:5604-11.
301. Chen G, Nakamura I, Dhanasekaran R, et al. Transcriptional Induction of Periostin by a Sulfatase 2-TGFbeta1-SMAD Signaling Axis Mediates Tumor Angiogenesis in Hepatocellular Carcinoma. Cancer Res 2017;77:632-645.
302. He X, Brenchley PE, Jayson GC, et al. Hypoxia increases heparanase-dependent tumor cell invasion, which can be inhibited by antiheparanase antibodies. Cancer Res 2004;64:3928-33.
303. Vreys V, David G. Mammalian heparanase: what is the message? J Cell Mol Med 2007;11:427-52.
304. Lai JP, Sandhu DS, Yu C, et al. Sulfatase 2 up-regulates glypican 3, promotes fibroblast growth factor signaling, and decreases survival in hepatocellular carcinoma. Hepatology 2008;47:1211-22.
305. Lai JP, Sandhu DS, Yu C, et al. Sulfatase 2 protects hepatocellular carcinoma cells against apoptosis induced by the PI3K inhibitor LY294002 and ERK and JNK kinase inhibitors. Liver Int 2010;30:1522-8.
306. Adamsen BL, Kravik KL, Clausen OP, et al. Apoptosis, cell cycle progression and gene expression in TP53-depleted HCT116 colon cancer cells in response to short-term 5-fluorouracil treatment. Int J Oncol 2007;31:1491-500.
307. Chau BN, Diaz RL, Saunders MA, et al. Identification of SULF2 as a novel transcriptional target of p53 by use of integrated genomic analyses. Cancer Res 2009;69:1368-74.
308. Shachaf CM, Kopelman AM, Arvanitis C, et al. MYC inactivation uncovers pluripotent differentiation and tumour dormancy in hepatocellular cancer. Nature 2004;431:1112-7.
309. Calvisi DF, Conner EA, Ladu S, et al. Activation of the canonical Wnt/beta-catenin pathway confers growth advantages in c-Myc/E2F1 transgenic mouse model of liver cancer. J Hepatol 2005;42:842-9.
310. Conner EA, Lemmer ER, Sanchez A, et al. E2F1 blocks and c-Myc accelerates hepatic ploidy in transgenic mouse models. Biochem Biophys Res Commun 2003;302:114-20.
311. Ju HL, Han KH, Lee JD, et al. Transgenic mouse models generated by hydrodynamic transfection for genetic studies of liver cancer and preclinical testing of anti-cancer therapy. Int J Cancer 2016;138:1601-8.
312. Katz SF, Lechel A, Obenauf AC, et al. Disruption of Trp53 in livers of mice induces formation of carcinomas with bilineal differentiation. Gastroenterology 2012;142:1229-1239 e3.
313. Liu Y, Qi X, Zeng Z, et al. CRISPR/Cas9-mediated p53 and Pten dual mutation accelerates hepatocarcinogenesis in adult hepatitis B virus transgenic mice. Sci Rep 2017;7:2796.
314. Orban PC, Chui D, Marth JD. Tissue- and site-specific DNA recombination in transgenic mice. Proc Natl Acad Sci U S A 1992;89:6861-5.
315. Li Y, Erzurumlu RS, Chen C, et al. Whisker-related neuronal patterns fail to develop in the trigeminal brainstem nuclei of NMDAR1 knockout mice. Cell 1994;76:427-37.
316. Hastie AR, Pruitt SC. Yeast two-hybrid interaction partner screening through in vivo Cre-mediated Binary Interaction Tag generation. Nucleic Acids Res 2007;35:e141.
317. Pitot HC, Dragan YP. Facts and theories concerning the mechanisms of carcinogenesis. FASEB J 1991;5:2280-6.

318. Rao KV, Vesselinovitch SD. Age- and sex-associated diethylnitrosamine dealkylation activity of the mouse liver and hepatocarcinogenesis. Cancer Res 1973;33:1625-7.
319. Bakiri L, Wagner EF. Mouse models for liver cancer. Mol Oncol 2013;7:206-23.
320. Yoshimoto S, Loo TM, Atarashi K, et al. Obesity-induced gut microbial metabolite promotes liver cancer through senescence secretome. Nature 2013;499:97-101.
321. He L, Tian DA, Li PY, et al. Mouse models of liver cancer: Progress and recommendations. Oncotarget 2015;6:23306-22.
322. Morton JJ, Bird G, Refaeli Y, et al. Humanized Mouse Xenograft Models: Narrowing the Tumor-Microenvironment Gap. Cancer Res 2016;76:6153-6158.
323. Zhou Q, Facciponte J, Jin M, et al. Humanized NOD-SCID IL2rg-/- mice as a preclinical model for cancer research and its potential use for individualized cancer therapies. Cancer Lett 2014;344:13-19.
324. Nakagawa H, Umemura A, Taniguchi K, et al. ER stress cooperates with hypernutrition to trigger TNF-dependent spontaneous HCC development. Cancer Cell 2014;26:331-343.
325. Mauad TH, van Nieuwkerk CM, Dingemans KP, et al. Mice with homozygous disruption of the mdr2 P-glycoprotein gene. A novel animal model for studies of nonsuppurative inflammatory cholangitis and hepatocarcinogenesis. Am J Pathol 1994;145:1237-45.
326. Rinella ME, Green RM. The methionine-choline deficient dietary model of steatohepatitis does not exhibit insulin resistance. J Hepatol 2004;40:47-51.
327. Ibrahim SH, Hirsova P, Malhi H, et al. Animal Models of Nonalcoholic Steatohepatitis: Eat, Delete, and Inflame. Dig Dis Sci 2016;61:1325-36.
328. Hebbard L, George J. Animal models of nonalcoholic fatty liver disease. Nat Rev Gastroenterol Hepatol 2011;8:35-44.
329. Asgharpour A, Cazanave SC, Pacana T, et al. A diet-induced animal model of non-alcoholic fatty liver disease and hepatocellular cancer. J Hepatol 2016;65:579-88.
330. Tetri LH, Basaranoglu M, Brunt EM, et al. Severe NAFLD with hepatic necroinflammatory changes in mice fed trans fats and a high-fructose corn syrup equivalent. Am J Physiol Gastrointest Liver Physiol 2008;295:G987-95.
331. Dowman JK, Hopkins LJ, Reynolds GM, et al. Development of hepatocellular carcinoma in a murine model of nonalcoholic steatohepatitis induced by use of a high-fat/fructose diet and sedentary lifestyle. Am J Pathol 2014;184:1550-61.
332. EASL-EORTC. European Association for the Study of the Liver, European Organisation for Research and Treatment of Cancer: EASL-EORTC clinical practice guidelines: management of hepatocellular carcinoma. J Hepatol 2012;56:43.
333. Xu L, Hui AY, Albanis E, et al. Human hepatic stellate cell lines, LX-1 and LX-2: new tools for analysis of hepatic fibrosis. Gut 2005;54:142-51.
334. Coulouarn C, Corlu A, Glaise D, et al. Hepatocyte-stellate cell cross-talk in the liver engenders a permissive inflammatory microenvironment that drives progression in hepatocellular carcinoma. Cancer Res 2012;72:2533-42.
335. Carloni V, Luong TV, Rombouts K. Hepatic stellate cells and extracellular matrix in hepatocellular carcinoma: more complicated than ever. Liver Int 2014;34:834-43.
336. Uyama N, Shimahara Y, Kawada N, et al. Regulation of cultured rat hepatocyte proliferation by stellate cells. J Hepatol 2002;36:590-9.
337. Lehner B, Sandner B, Marschallinger J, et al. The dark side of BrdU in neural stem cell biology: detrimental effects on cell cycle, differentiation and survival. Cell Tissue Res 2011;345:313-28.
338. Terranova VP, Hujanen ES, Loeb DM, et al. Use of a reconstituted basement membrane to measure cell invasiveness and select for highly invasive tumor cells. Proc Natl Acad Sci U S A 1986;83:465-9.
339. Wartenberg M, Ling FC, Muschen M, et al. Regulation of the multidrug resistance transporter P-glycoprotein in multicellular tumor spheroids by hypoxia-inducible factor (HIF-1) and reactive oxygen species. FASEB J 2003;17:503-5.

340. Chen R, Dong Y, Xie X, et al. Screening candidate metastasis-associated genes in three-dimensional HCC spheroids with different metastasis potential. Int J Clin Exp Pathol 2014;7:2527-35.
341. Kleiner DE, Brunt EM, Van Natta M, et al. Design and validation of a histological scoring system for nonalcoholic fatty liver disease. Hepatology 2005;41:1313-21.
342. Gordon H. SHH. A simple method for the silver impregnation of reticulin. American Journal of Pathology 1936;12:545.
343. Babicki S, Arndt D, Marcu A, et al. Heatmapper: web-enabled heat mapping for all. Nucleic Acids Res 2016;44:W147-53.
344. Murtagh F, Legendre P. Ward's Hierarchical Agglomerative Clustering Method: Which Algorithms Implement Ward's Criterion? Journal of Classification 2014;31:274-295.
345. Mootha VK, Lindgren CM, Eriksson KF, et al. PGC-1alpha-responsive genes involved in oxidative phosphorylation are coordinately downregulated in human diabetes. Nat Genet 2003;34:267-73.
346. Subramanian A, Tamayo P, Mootha VK, et al. Gene set enrichment analysis: a knowledge-based approach for interpreting genome-wide expression profiles. Proc Natl Acad Sci U S A 2005;102:15545-50.
347. Llovet JM, Hernandez-Gea V. Hepatocellular carcinoma: reasons for phase III failure and novel perspectives on trial design. Clin Cancer Res 2014;20:2072-9.
348. El-Khoueiry AB, Sangro B, Yau T, et al. Nivolumab in patients with advanced hepatocellular carcinoma (CheckMate 040): an open-label, non-comparative, phase 1/2 dose escalation and expansion trial. Lancet 2017;389:2492-2502.
349. Llovet JM, Ricci S, Mazzaferro V, et al. Sorafenib in advanced hepatocellular carcinoma. N Engl J Med 2008;359:378-90.
350. Amann T, Bataille F, Spruss T, et al. Activated hepatic stellate cells promote tumorigenicity of hepatocellular carcinoma. Cancer Sci 2009;100:646-53.
351. Ju MJ, Qiu SJ, Fan J, et al. Peritumoral activated hepatic stellate cells predict poor clinical outcome in hepatocellular carcinoma after curative resection. Am J Clin Pathol 2009;131:498-510.
352. Lau EY, Lo J, Cheng BY, et al. Cancer-Associated Fibroblasts Regulate Tumor-Initiating Cell Plasticity in Hepatocellular Carcinoma through c-Met/FRA1/HEY1 Signaling. Cell Rep 2016;15:1175-89.
353. Ankoma-Sey V, Wang Y, Dai Z. Hypoxic stimulation of vascular endothelial growth factor expression in activated rat hepatic stellate cells. Hepatology 2000;31:141-8.
354. Drost J, Clevers H. Organoids in cancer research. Nat Rev Cancer 2018;18:407-418.
355. Radisky DC, Bissell MJ. Cancer. Respect thy neighbor! Science 2004;303:775-7.
356. Lai KK, Shang S, Lohia N, et al. Extracellular matrix dynamics in hepatocarcinogenesis: a comparative proteomics study of PDGFC transgenic and Pten null mouse models. PLoS Genet 2011;7:e1002147.
357. Ji J, Eggert T, Budhu A, et al. Hepatic stellate cell and monocyte interaction contributes to poor prognosis in hepatocellular carcinoma. Hepatology 2015;62:481-95.
358. Zhang DY, Goossens N, Guo J, et al. A hepatic stellate cell gene expression signature associated with outcomes in hepatitis C cirrhosis and hepatocellular carcinoma after curative resection. Gut 2016;65:1754-64.
359. Breslin S, O'Driscoll L. Three-dimensional cell culture: the missing link in drug discovery. Drug Discov Today 2013;18:240-9.
360. Gill BJ, West JL. Modeling the tumor extracellular matrix: Tissue engineering tools repurposed towards new frontiers in cancer biology. J Biomech 2014;47:1969-78.
361. Terris B, Pineau P, Bregeaud L, et al. Close correlation between beta-catenin gene alterations and nuclear accumulation of the protein in human hepatocellular carcinomas. Oncogene 1999;18:6583-8.
362. Clevers H, Nusse R. Wnt/beta-catenin signaling and disease. Cell 2012;149:1192-205.

363. Mukozu T, Nagai H, Matsui D, et al. Serum VEGF as a tumor marker in patients with HCV-related liver cirrhosis and hepatocellular carcinoma. Anticancer Res 2013;33:1013-21.
364. Sneddon JB, Werb Z. Location, location, location: the cancer stem cell niche. Cell Stem Cell 2007;1:607-11.
365. Morrison SJ, Spradling AC. Stem cells and niches: mechanisms that promote stem cell maintenance throughout life. Cell 2008;132:598-611.
366. Schwitalla S, Fingerle AA, Cammareri P, et al. Intestinal tumorigenesis initiated by dedifferentiation and acquisition of stem-cell-like properties. Cell 2013;152:25-38.
367. Ma S, Chan KW, Hu L, et al. Identification and characterization of tumorigenic liver cancer stem/progenitor cells. Gastroenterology 2007;132:2542-56.
368. Jia D, Yang W, Li L, et al. beta-Catenin and NF-kappaB co-activation triggered by TLR3 stimulation facilitates stem cell-like phenotypes in breast cancer. Cell Death Differ 2015;22:298-310.
369. Capurro M, Wanless IR, Sherman M, et al. Glypican-3: a novel serum and histochemical marker for hepatocellular carcinoma. Gastroenterology 2003;125:89-97.
370. Capurro MI, Xiang YY, Lobe C, et al. Glypican-3 promotes the growth of hepatocellular carcinoma by stimulating canonical Wnt signaling. Cancer Res 2005;65:6245-54.
371. Zhan T, Rindtorff N, Boutros M. Wnt signaling in cancer. Oncogene 2017;36:1461-1473.
372. Hynes RO. The extracellular matrix: not just pretty fibrils. Science 2009;326:1216-9.
373. Santamato A, Fransvea E, Dituri F, et al. Hepatic stellate cells stimulate HCC cell migration via laminin-5 production. Clin Sci (Lond) 2011;121:159-68.
374. Rombouts K, Carloni V. The fibrotic microenvironment as a heterogeneity facet of hepatocellular carcinoma. Fibrogenesis Tissue Repair 2013;6:17.
375. Lu P, Weaver VM, Werb Z. The extracellular matrix: a dynamic niche in cancer progression. J Cell Biol 2012;196:395-406.
376. Levental KR, Yu H, Kass L, et al. Matrix crosslinking forces tumor progression by enhancing integrin signaling. Cell 2009;139:891-906.
377. Zhao W, Su W, Kuang P, et al. The role of hepatic stellate cells in the regulation of T-cell function and the promotion of hepatocellular carcinoma. Int J Oncol 2012;41:457-64.
378. Zhao W, Zhang L, Yin Z, et al. Activated hepatic stellate cells promote hepatocellular carcinoma development in immunocompetent mice. Int J Cancer 2011;129:2651-61.
379. Lin N, Chen Z, Lu Y, et al. Role of activated hepatic stellate cells in proliferation and metastasis of hepatocellular carcinoma. Hepatol Res 2015;45:326-36.
380. Torimura T, Ueno T, Kin M, et al. Overexpression of angiopoietin-1 and angiopoietin-2 in hepatocellular carcinoma. J Hepatol 2004;40:799-807.
381. Song J, Ge Z, Yang X, et al. Hepatic stellate cells activated by acidic tumor microenvironment promote the metastasis of hepatocellular carcinoma via osteopontin. Cancer Lett 2015;356:713-20.
382. Mikula M, Proell V, Fischer AN, et al. Activated hepatic stellate cells induce tumor progression of neoplastic hepatocytes in a TGF-beta dependent fashion. J Cell Physiol 2006;209:560-7.
383. Chang Q, Chen J, Beezhold KJ, et al. JNK1 activation predicts the prognostic outcome of the human hepatocellular carcinoma. Mol Cancer 2009;8:64.
384. Jung CH, Ho JN, Park JK, et al. Involvement of SULF2 in γ-irradiation-induced invasion and resistance of cancer cells by inducing IL-6 expression. Oncotarget 2016;7:16090-103.
385. Osuala KO, Sameni M, Shah S, et al. Il-6 signaling between ductal carcinoma in situ cells and carcinoma-associated fibroblasts mediates tumor cell growth and migration. BMC Cancer 2015;15:584.
386. Qiao Y, Zhang C, Li A, et al. IL6 derived from cancer-associated fibroblasts promotes chemoresistance via CXCR7 in esophageal squamous cell carcinoma. Oncogene 2018;37:873-883.
387. Nagasaki T, Hara M, Nakanishi H, et al. Interleukin-6 released by colon cancer-associated fibroblasts is critical for tumour angiogenesis: anti-interleukin-6 receptor antibody

suppressed angiogenesis and inhibited tumour-stroma interaction. Br J Cancer 2014;110:469-78.
388. Yang JD, Sun Z, Hu C, et al. Sulfatase 1 and sulfatase 2 in hepatocellular carcinoma: associated signaling pathways, tumor phenotypes, and survival. Genes Chromosomes Cancer 2011;50:122-35.
389. Chen C, Cao F, Bai L, et al. IKKbeta Enforces a LIN28B/TCF7L2 Positive Feedback Loop That Promotes Cancer Cell Stemness and Metastasis. Cancer Res 2015;75:1725-35.
390. Greten FR, Eckmann L, Greten TF, et al. IKKbeta links inflammation and tumorigenesis in a mouse model of colitis-associated cancer. Cell 2004;118:285-96.
391. Korkaya H, Kim GI, Davis A, et al. Activation of an IL6 inflammatory loop mediates trastuzumab resistance in HER2+ breast cancer by expanding the cancer stem cell population. Mol Cell 2012;47:570-84.
392. Vincent T, Mechti N. IL-6 regulates CD44 cell surface expression on human myeloma cells. Leukemia 2004;18:967-75.
393. Nakamura I, Fernandez-Barrena MG, Ortiz-Ruiz MC, et al. Activation of the transcription factor GLI1 by WNT signaling underlies the role of SULFATASE 2 as a regulator of tissue regeneration. J Biol Chem 2013;288:21389-98.
394. Pez F, Lopez A, Kim M, et al. Wnt signaling and hepatocarcinogenesis: molecular targets for the development of innovative anticancer drugs. J Hepatol 2013;59:1107-17.
395. Marquardt JU, Factor VM, Thorgeirsson SS. Epigenetic regulation of cancer stem cells in liver cancer: current concepts and clinical implications. J Hepatol 2010;53:568-77.
396. Vlantis K, Wullaert A, Sasaki Y, et al. Constitutive IKK2 activation in intestinal epithelial cells induces intestinal tumors in mice. J Clin Invest 2011;121:2781-93.
397. Marquardt JU, Gomez-Quiroz L, Arreguin Camacho LO, et al. Curcumin effectively inhibits oncogenic NF-kappaB signaling and restrains stemness features in liver cancer. J Hepatol 2015;63:661-9.
398. Yamashita T, Ji J, Budhu A, et al. EpCAM-positive hepatocellular carcinoma cells are tumor-initiating cells with stem/progenitor cell features. Gastroenterology 2009;136:1012-24.
399. Yang ZF, Ho DW, Ng MN, et al. Significance of CD90+ cancer stem cells in human liver cancer. Cancer Cell 2008;13:153-66.
400. Anstee QM, Targher G, Day CP. Progression of NAFLD to diabetes mellitus, cardiovascular disease or cirrhosis. Nat Rev Gastroenterol Hepatol 2013;10:330-44.
401. Wong VW, Wong GL, Choi PC, et al. Disease progression of non-alcoholic fatty liver disease: a prospective study with paired liver biopsies at 3 years. Gut 2010;59:969-74.
402. Mittal S, El-Serag HB, Sada YH, et al. Hepatocellular Carcinoma in the Absence of Cirrhosis in United States Veterans is Associated With Nonalcoholic Fatty Liver Disease. Clin Gastroenterol Hepatol 2016;14:124-31 e1.
403. Yasui K, Hashimoto E, Komorizono Y, et al. Characteristics of patients with nonalcoholic steatohepatitis who develop hepatocellular carcinoma. Clin Gastroenterol Hepatol 2011;9:428-33; quiz e50.
404. Chen K, Liu ML, Schaffer L, et al. Type 2 diabetes in mice induces hepatic overexpression of sulfatase 2, a novel factor that suppresses uptake of remnant lipoproteins. Hepatology 2010;52:1957-67.
405. Matikainen N, Burza MA, Romeo S, et al. Genetic variation in SULF2 is associated with postprandial clearance of triglyceride-rich remnant particles and triglyceride levels in healthy subjects. PLoS One 2013;8:e79473.
406. Wu X, Williams KJ. NOX4 pathway as a source of selective insulin resistance and responsiveness. Arterioscler Thromb Vasc Biol 2012;32:1236-45.
407. Brown ZJ, Heinrich B, Greten TF. Mouse models of hepatocellular carcinoma: an overview and highlights for immunotherapy research. Nat Rev Gastroenterol Hepatol 2018;15:536-554.
408. Schmidt U, Boucheron N, Unger B, et al. The role of Tec family kinases in myeloid cells. Int Arch Allergy Immunol 2004;134:65-78.

409. Tomlinson MG, Kane LP, Su J, et al. Expression and function of Tec, Itk, and Btk in lymphocytes: evidence for a unique role for Tec. Mol Cell Biol 2004;24:2455-66.
410. Smith CI, Islam TC, Mattsson PT, et al. The Tec family of cytoplasmic tyrosine kinases: mammalian Btk, Bmx, Itk, Tec, Txk and homologs in other species. Bioessays 2001;23:436-46.
411. Takesono A, Horai R, Mandai M, et al. Requirement for Tec kinases in chemokine-induced migration and activation of Cdc42 and Rac. Curr Biol 2004;14:917-22.
412. Sahu N, Mueller C, Fischer A, et al. Differential sensitivity to Itk kinase signals for T helper 2 cytokine production and chemokine-mediated migration. J Immunol 2008;180:3833-8.
413. Fischer AM, Mercer JC, Iyer A, et al. Regulation of CXC chemokine receptor 4-mediated migration by the Tec family tyrosine kinase ITK. J Biol Chem 2004;279:29816-20.
414. Feitelson MA, Sun B, Satiroglu Tufan NL, et al. Genetic mechanisms of hepatocarcinogenesis. Oncogene 2002;21:2593-604.
415. Cahill DP, Kinzler KW, Vogelstein B, et al. Genetic instability and darwinian selection in tumours. Trends Cell Biol 1999;9:M57-60.
416. Wong KM, Hudson TJ, McPherson JD. Unraveling the genetics of cancer: genome sequencing and beyond. Annu Rev Genomics Hum Genet 2011;12:407-30.
417. Nault JC, De Reynies A, Villanueva A, et al. A hepatocellular carcinoma 5-gene score associated with survival of patients after liver resection. Gastroenterology 2013;145:176-87.
418. Teufel A, Itzel T, Erhart W, et al. Comparison of Gene Expression Patterns Between Mouse Models of Nonalcoholic Fatty Liver Disease and Liver Tissues From Patients. Gastroenterology 2016;151:513-525 e0.
419. Westerbacka J, Kolak M, Kiviluoto T, et al. Genes involved in fatty acid partitioning and binding, lipolysis, monocyte/macrophage recruitment, and inflammation are overexpressed in the human fatty liver of insulin-resistant subjects. Diabetes 2007;56:2759-65.
420. Many GM, Yokosaki Y, Uaesoontrachoon K, et al. OPN-a induces muscle inflammation by increasing recruitment and activation of pro-inflammatory macrophages. Exp Physiol 2016;101:1285-1300.
421. Senbanjo LT, Chellaiah MA. CD44: A Multifunctional Cell Surface Adhesion Receptor Is a Regulator of Progression and Metastasis of Cancer Cells. Front Cell Dev Biol 2017;5:18.
422. Li BH, He FP, Yang X, et al. Steatosis induced CCL5 contributes to early-stage liver fibrosis in nonalcoholic fatty liver disease progress. Transl Res 2017;180:103-117 e4.
423. Zhu C, Kim K, Wang X, et al. Hepatocyte Notch activation induces liver fibrosis in nonalcoholic steatohepatitis. Sci Transl Med 2018;10.
424. Breous E, Somanathan S, Vandenberghe LH, et al. Hepatic regulatory T cells and Kupffer cells are crucial mediators of systemic T cell tolerance to antigens targeting murine liver. Hepatology 2009;50:612-21.
425. Zeremski M, Petrovic LM, Chiriboga L, et al. Intrahepatic levels of CXCR3-associated chemokines correlate with liver inflammation and fibrosis in chronic hepatitis C. Hepatology 2008;48:1440-50.
426. Kononen J, Bubendorf L, Kallioniemi A, et al. Tissue microarrays for high-throughput molecular profiling of tumor specimens. Nat Med 1998;4:844-7.
427. Shalon D, Smith SJ, Brown PO. A DNA microarray system for analyzing complex DNA samples using two-color fluorescent probe hybridization. Genome Res 1996;6:639-45.
428. Wang Z, Gerstein M, Snyder M. RNA-Seq: a revolutionary tool for transcriptomics. Nat Rev Genet 2009;10:57-63.
429. Nagalakshmi U, Waern K, Snyder M. RNA-Seq: a method for comprehensive transcriptome analysis. Curr Protoc Mol Biol 2010;Chapter 4:Unit 4 11 1-13.
430. Shyr D, Liu Q. Next generation sequencing in cancer research and clinical application. Biol Proced Online 2013;15:4.
431. Tovuu LO, Imura S, Utsunomiya T, et al. Role of CD44 expression in non-tumor tissue on intrahepatic recurrence of hepatocellular carcinoma. Int J Clin Oncol 2013;18:651-6.

432. Kuang DM, Zhao Q, Peng C, et al. Activated monocytes in peritumoral stroma of hepatocellular carcinoma foster immune privilege and disease progression through PD-L1. J Exp Med 2009;206:1327-37.
433. Calderaro J, Couchy G, Imbeaud S, et al. Histological subtypes of hepatocellular carcinoma are related to gene mutations and molecular tumour classification. J Hepatol 2017;67:727-738.
434. El-Serag HB. Hepatocellular carcinoma. N Engl J Med 2011;365:1118-27.
435. El-Serag HB. Epidemiology of viral hepatitis and hepatocellular carcinoma. Gastroenterology 2012;142:1264-1273 e1.
436. Morgan TR, Mandayam S, Jamal MM. Alcohol and hepatocellular carcinoma. Gastroenterology 2004;127:S87-96.
437. Bertuccio P, Turati F, Carioli G, et al. Global trends and predictions in hepatocellular carcinoma mortality. J Hepatol 2017;67:302-309.
438. Papatheodoridis GV, Chan HL, Hansen BE, et al. Risk of hepatocellular carcinoma in chronic hepatitis B: assessment and modification with current antiviral therapy. J Hepatol 2015;62:956-67.
439. Degasperi E, Colombo M. Distinctive features of hepatocellular carcinoma in non-alcoholic fatty liver disease. Lancet Gastroenterol Hepatol 2016;1:156-164.
440. Calle EE, Rodriguez C, Walker-Thurmond K, et al. Overweight, obesity, and mortality from cancer in a prospectively studied cohort of U.S. adults. N Engl J Med 2003;348:1625-38.
441. Schlesinger S, Aleksandrova K, Pischon T, et al. Diabetes mellitus, insulin treatment, diabetes duration, and risk of biliary tract cancer and hepatocellular carcinoma in a European cohort. Ann Oncol 2013;24:2449-55.
442. Bruix J, Qin S, Merle P, et al. Regorafenib for patients with hepatocellular carcinoma who progressed on sorafenib treatment (RESORCE): a randomised, double-blind, placebo-controlled, phase 3 trial. Lancet 2017;389:56-66.
443. Bruix J, Reig M, Sherman M. Evidence-Based Diagnosis, Staging, and Treatment of Patients With Hepatocellular Carcinoma. Gastroenterology 2016;150:835-53.
444. Forner A, Reig M, Bruix J. Hepatocellular carcinoma. Lancet 2018;391:1301-1314.
445. Mazzaferro V, Regalia E, Doci R, et al. Liver transplantation for the treatment of small hepatocellular carcinomas in patients with cirrhosis. N Engl J Med 1996;334:693-9.
446. Sapisochin G, Bruix J. Liver transplantation for hepatocellular carcinoma: outcomes and novel surgical approaches. Nat Rev Gastroenterol Hepatol 2017;14:203-217.
447. Hasegawa K, Kokudo N, Makuuchi M, et al. Comparison of resection and ablation for hepatocellular carcinoma: a cohort study based on a Japanese nationwide survey. J Hepatol 2013;58:724-9.
448. Cucchetti A, Piscaglia F, Cescon M, et al. Cost-effectiveness of hepatic resection versus percutaneous radiofrequency ablation for early hepatocellular carcinoma. J Hepatol 2013;59:300-7.
449. Llovet JM, Real MI, Montana X, et al. Arterial embolisation or chemoembolisation versus symptomatic treatment in patients with unresectable hepatocellular carcinoma: a randomised controlled trial. Lancet 2002;359:1734-9.
450. Abou-Alfa GK, Borgman-Hagey AE, Kelley RK. Cabozantinib in Hepatocellular Carcinoma. N Engl J Med 2018;379:1384-1385.
451. Llovet JM, Zucman-Rossi J, Pikarsky E, et al. Hepatocellular carcinoma. Nat Rev Dis Primers 2016;2:16018.
452. Moeini A, Torrecilla S, Tovar V, et al. An Immune Gene Expression Signature Associated With Development of Human Hepatocellular Carcinoma Identifies Mice That Respond to Chemopreventive Agents. Gastroenterology 2019.
453. Fingas CD, Best J, Sowa JP, et al. Epidemiology of nonalcoholic steatohepatitis and hepatocellular carcinoma. Clin Liver Dis (Hoboken) 2016;8:119-122.

454. Bollyky PL, Falk BA, Long SA, et al. CD44 costimulation promotes FoxP3+ regulatory T cell persistence and function via production of IL-2, IL-10, and TGF-beta. J Immunol 2009;183:2232-41.
455. Liu T, Soong L, Liu G, et al. CD44 expression positively correlates with Foxp3 expression and suppressive function of CD4+ Treg cells. Biol Direct 2009;4:40.
456. Patouraux S, Rousseau D, Bonnafous S, et al. CD44 is a key player in non-alcoholic steatohepatitis. J Hepatol 2017;67:328-338.
457. Kang HS, Liao G, DeGraff LM, et al. CD44 plays a critical role in regulating diet-induced adipose inflammation, hepatic steatosis, and insulin resistance. PLoS One 2013;8:e58417.
458. Wang J, Kubes P. A Reservoir of Mature Cavity Macrophages that Can Rapidly Invade Visceral Organs to Affect Tissue Repair. Cell 2016;165:668-78.
459. Rios de la Rosa JM, Tirella A, Gennari A, et al. The CD44-Mediated Uptake of Hyaluronic Acid-Based Carriers in Macrophages. Adv Healthc Mater 2017;6.
460. Ruffell B, Poon GF, Lee SS, et al. Differential use of chondroitin sulfate to regulate hyaluronan binding by receptor CD44 in Inflammatory and Interleukin 4-activated Macrophages. J Biol Chem 2011;286:19179-90.
461. Yeung OW, Lo CM, Ling CC, et al. Alternatively activated (M2) macrophages promote tumour growth and invasiveness in hepatocellular carcinoma. J Hepatol 2015;62:607-16.
462. Yang P, Li QJ, Feng Y, et al. TGF-beta-miR-34a-CCL22 signaling-induced Treg cell recruitment promotes venous metastases of HBV-positive hepatocellular carcinoma. Cancer Cell 2012;22:291-303.
463. Chow A, Huggins M, Ahmed J, et al. CD169(+) macrophages provide a niche promoting erythropoiesis under homeostasis and stress. Nat Med 2013;19:429-36.
464. Chavez-Galan L, Olleros ML, Vesin D, et al. Much More than M1 and M2 Macrophages, There are also CD169(+) and TCR(+) Macrophages. Front Immunol 2015;6:263.
465. Georgoudaki AM, Prokopec KE, Boura VF, et al. Reprogramming Tumor-Associated Macrophages by Antibody Targeting Inhibits Cancer Progression and Metastasis. Cell Rep 2016;15:2000-11.
466. Hanahan D, Coussens LM. Accessories to the crime: functions of cells recruited to the tumor microenvironment. Cancer Cell 2012;21:309-22.
467. Zhu AX, Duda DG, Sahani DV, et al. HCC and angiogenesis: possible targets and future directions. Nat Rev Clin Oncol 2011;8:292-301.

Appendix

Appendix-1 List of top 100 DE genes in tumour versus non-tumour comparison

symbol	log2FoldChange	pvalue	padj
Afp	8.44263783	1.87E-179	4.14E-175
Akr1c18	8.840960881	1.97E-163	2.18E-159
Igdcc4	8.615427477	2.77E-125	2.05E-121
Gpc3	8.170529223	3.29E-119	1.83E-115
Alox5	8.730666917	8.86E-105	3.93E-101
Kif5c	8.030015624	4.74E-102	1.75E-98
Msantd3	5.605312611	3.11E-95	9.86E-92
Ipcef1	6.562819115	7.56E-93	2.10E-89
Galnt6	5.825448131	2.00E-92	4.94E-89
Prom2	10.04177835	4.95E-92	1.10E-88
Rasgrp2	3.57811106	1.49E-91	3.01E-88
Col4a3	6.950164867	1.68E-89	3.10E-86
Lama5	4.910575041	4.21E-87	7.18E-84
Dusp5	5.335998931	3.20E-86	5.07E-83
Tnfrsf12a	3.748370371	7.15E-86	1.06E-82
B4galt6	4.589440132	4.47E-83	6.20E-80
Cdkn2b	6.001067766	3.08E-82	4.02E-79
Erich4	9.386133729	1.32E-81	1.63E-78
Rhbdf1	2.643264609	9.39E-80	1.10E-76
Nid1	4.402575535	1.50E-79	1.66E-76
Psrc1	8.877126359	7.11E-79	7.51E-76
Fhl3	4.328825075	2.24E-78	2.26E-75
Scn8a	4.845982965	2.68E-78	2.59E-75
Smox	4.043392409	6.38E-78	5.90E-75
Mtcl1	6.387750686	2.97E-77	2.64E-74
Golm1	4.528479505	2.24E-76	1.92E-73
Rasal1	5.675415429	1.33E-75	1.10E-72
Cacna1c	6.309070622	2.36E-75	1.87E-72
Dlx4	4.517503056	1.95E-74	1.50E-71
Ccdc120	4.039612377	1.51E-73	1.11E-70
Casc4	4.651520753	1.61E-73	1.15E-70
Nxn	3.921810917	2.87E-73	1.99E-70
Psat1	5.071135972	1.59E-72	1.07E-69
Col6a6	4.914607104	3.84E-71	2.51E-68
Pdlim7	1.953325248	1.08E-70	6.84E-68
Miox	8.891304282	1.45E-70	8.95E-68
Hdac7	1.612690754	3.01E-69	1.76E-66
Calml4	4.400926207	3.01E-69	1.76E-66
Ankrd13b	2.63750931	6.24E-69	3.56E-66

Tlr1	6.141791134	1.42E-68	7.90E-66
Cd63	4.486462294	1.57E-68	8.48E-66
Trpm4	3.958149081	1.78E-67	9.42E-65
Prom1	5.290290336	3.39E-67	1.75E-64
Mthfd1	-0.951720594	7.48E-67	3.78E-64
F2rl1	7.800368191	1.02E-66	5.06E-64
Tnfsf13	4.224962755	1.10E-66	5.31E-64
Osbpl10	4.958871016	1.14E-66	5.37E-64
Arhgap22	6.206632025	1.85E-66	8.55E-64
Lepr	4.649332481	2.10E-66	9.53E-64
Atg3	-0.787483744	1.02E-65	4.52E-63
NA	3.890633773	2.29E-65	9.98E-63
Airn	3.383042887	4.53E-65	1.93E-62
Panx1	3.479654956	7.04E-65	2.95E-62
Glp2r	7.589349413	1.08E-64	4.45E-62
Fst	4.086710818	3.68E-64	1.48E-61
Gria3	3.472563135	3.86E-64	1.53E-61
Adamtsl5	4.802755354	1.38E-63	5.39E-61
Card10	1.961035451	2.53E-63	9.69E-61
Ajuba	3.278486537	2.79E-63	1.05E-60
Abcc5	2.815835715	2.87E-63	1.06E-60
Adamts14	3.90103299	3.25E-62	1.18E-59
Rhoc	2.792729513	9.60E-62	3.39E-59
Lysmd2	4.777428706	9.62E-62	3.39E-59
Nrg1	4.017130998	1.11E-61	3.86E-59
Fblim1	5.293882663	1.28E-61	4.37E-59
5330417C22Rik	4.873890377	2.63E-61	8.85E-59
Cd40	4.371609382	2.71E-61	8.97E-59
Hid1	3.845462044	3.73E-61	1.22E-58
Phgdh	6.774008614	4.06E-61	1.31E-58
Tspan8	7.1040849	4.21E-61	1.34E-58
Zfp57	3.709452738	7.17E-61	2.24E-58
Plxna3	3.411804361	8.38E-61	2.58E-58
Clip2	2.494554733	8.63E-60	2.63E-57
Ica1	3.047246986	1.02E-59	3.07E-57
NA	4.220050901	1.13E-59	3.35E-57
Dlx4os	7.997350123	1.44E-59	4.19E-57
Mtmr11	3.016697042	1.71E-59	4.92E-57
Clcf1	3.534213256	3.43E-59	9.75E-57
Kcp	3.879972734	1.02E-58	2.87E-56
Tnfrsf10b	4.348620754	1.18E-58	3.27E-56
Bmp8b	6.360670146	1.67E-58	4.59E-56
Fhdc1	4.855459185	2.06E-58	5.58E-56
Tmem54	7.453598065	2.59E-58	6.93E-56

Itih5	4.096294696	2.82E-58	7.45E-56
Ndfip1	-0.967808705	7.39E-58	1.93E-55
Pde6c	4.964818634	4.46E-57	1.15E-54
Zfp641	4.525732005	1.42E-56	3.61E-54
Hes1	1.971872516	4.28E-56	1.08E-53
Cth	-1.76997674	5.95E-56	1.48E-53
Gch1	-0.968384519	1.60E-55	3.95E-53
Ifnlr1	4.042596974	1.75E-55	4.26E-53
Scn1b	3.205679602	4.24E-55	1.02E-52
Ugt2a3	-1.601522954	5.36E-55	1.28E-52
Itpr3	2.758916634	8.99E-55	2.12E-52
Aldh7a1	-1.067539235	1.79E-54	4.18E-52
Myo7b	5.700391531	2.39E-54	5.54E-52
Pck2	3.128338573	4.53E-54	1.04E-51
Drc1	3.576981609	1.11E-53	2.52E-51
Scd2	4.736960337	1.43E-53	3.22E-51
Golga7b	8.768351906	1.86E-53	4.13E-51

Appendix-2 List of top 100 DE genes in the non-tumour tissue of ALIOS versus control-fed mice comparison

symbol	log2FoldChange	pvalue	padj
NA	1.203581	9.80E-12	4.49E-07
B430212C06Rik	2.174045	2.20E-09	5.05E-05
Spink1	2.206168	4.48E-09	6.84E-05
Tmem86a	1.241054	3.22E-08	0.00036848
Arhgap10	1.064582	6.38E-08	0.00058431
Limch1	1.351157	9.84E-08	0.00075132
Fam46a	-0.89141	1.26E-07	0.0008231
Apoa4	1.226494	2.09E-07	0.00106526
S100g	1.930044	1.96E-07	0.00106526
Syt14	1.380868	3.44E-07	0.00152379
Cyp2b10	2.280894	3.66E-07	0.00152379
Setbp1	1.030734	4.26E-07	0.0016275
NA	1.956681	5.27E-07	0.00185646
Rbm24	2.96117	8.40E-07	0.00256543
Fam83a	2.478311	8.16E-07	0.00256543
Nuggc	-1.99918	1.25E-06	0.00358803
Ucp2	1.30328	1.48E-06	0.00398737
Spink5	-1.14312	1.64E-06	0.00411803
Gstp1	-1.03052	1.71E-06	0.00411803
Slc22a26	3.098045	2.68E-06	0.00613869
Atp9a	0.323367	3.50E-06	0.00728592
Slc22a29	2.001839	3.47E-06	0.00728592
Tiam2	-2.18443	4.10E-06	0.00749819
Kdm2b	-0.272	3.89E-06	0.00749819
Obp2a	-2.50107	4.26E-06	0.00749819
Slc22a27	3.005928	4.13E-06	0.00749819
Smpd3	1.815372	4.43E-06	0.00751388
Tnfrsf22	0.764335	4.71E-06	0.00760088
Csf2rb	0.886089	4.81E-06	0.00760088
Bend7	-0.44156	5.25E-06	0.00800963
Slc35f2	2.010912	6.38E-06	0.0088517
Fez2	0.63717	6.32E-06	0.0088517
Slc47a2	0.616851	6.22E-06	0.0088517
Defb1	1.379134	6.89E-06	0.00928424
Stambpl1	0.898633	9.93E-06	0.0103455
Acot9	0.813928	9.55E-06	0.0103455
Man2b2	0.379897	7.97E-06	0.0103455
Cgref1	1.143292	9.82E-06	0.0103455
Cspg5	-1.79421	9.71E-06	0.0103455
Pygo1	1.378602	9.79E-06	0.0103455
Cyp2b13	3.503563	8.71E-06	0.0103455
Serpina1e	-4.11431	9.94E-06	0.0103455
Cyp2a4	4.698236	8.80E-06	0.0103455

Gcnt4	-1.65543	9.70E-06	0.0103455
Ly6d	2.794496	1.03E-05	0.01051052
Ctsb	0.380842	1.30E-05	0.0125216
Ctnna1	0.23484	1.27E-05	0.0125216
Tox	1.533001	1.31E-05	0.0125216
Stk10	0.74585	1.48E-05	0.0132576
Vldlr	1.71538	1.42E-05	0.0132576
Mlph	0.743616	1.45E-05	0.0132576
Dlgap1	-0.94123	1.52E-05	0.01338657
Plscr2	0.540279	1.58E-05	0.01361593
Folh1	1.242719	1.76E-05	0.01417218
Myl12b	0.453084	1.72E-05	0.01417218
Dcaf12l1	0.744704	1.76E-05	0.01417218
Sort1	-0.76496	1.69E-05	0.01417218
Adap1	1.044579	1.82E-05	0.01438838
Smarca4	0.296511	1.88E-05	0.0145966
Mogat1	2.747028	1.94E-05	0.01474762
Eps8	0.944197	1.96E-05	0.01474762
Cntnap1	1.554633	2.09E-05	0.01484594
Ptgfr	1.357083	2.05E-05	0.01484594
Sepw1	0.363593	2.06E-05	0.01484594
Sod3	0.663615	2.11E-05	0.01484594
Angpt1	1.14017	2.20E-05	0.01504337
Ttc39a	2.069874	2.19E-05	0.01504337
Gnai1	1.071366	2.33E-05	0.01544841
NA	1.242254	2.30E-05	0.01544841
Vav1	0.903681	2.65E-05	0.01660274
Olfr701	-1.35204	2.61E-05	0.01660274
NA	-0.56911	2.58E-05	0.01660274
NA	-0.79381	2.62E-05	0.01660274
Ranbp3l	-0.82942	2.69E-05	0.0166614
Hexb	0.811295	2.75E-05	0.0167877
Tinag	2.21548	2.88E-05	0.01726866
Tmem98	0.6856	2.90E-05	0.01726866
Klhl13	0.64054	3.07E-05	0.01803087
Paip1	0.279145	3.12E-05	0.01808459
Tnfrsf21	0.600979	3.49E-05	0.01965515
Chchd6	0.754959	3.51E-05	0.01965515
NA	0.92577	3.52E-05	0.01965515
Krt23	2.005001	3.90E-05	0.02008102
Crebbp	-0.25335	4.02E-05	0.02008102
Grm8	-1.6227	4.01E-05	0.02008102
Zfp639	-0.28836	4.12E-05	0.02008102
Cabp1	-0.70562	3.86E-05	0.02008102
Gdf3	0.992756	4.07E-05	0.02008102
Myh14	0.407161	3.73E-05	0.02008102

Car14	-0.93733	3.91E-05	0.02008102
Ccdc68	0.612122	3.77E-05	0.02008102
Mmd2	-1.30357	4.10E-05	0.02008102
Snord104	-0.5595	4.05E-05	0.02008102
NA	1.574364	3.74E-05	0.02008102
NA	0.539028	4.21E-05	0.02028305
Slc45a4	0.285824	4.25E-05	0.02028305
Isoc2b	0.477184	4.40E-05	0.02079475
Cd300lb	0.81459	4.52E-05	0.02110037
Rai2	0.467298	4.70E-05	0.02174073
Klc1	-0.41189	4.87E-05	0.02231879

Appendix-3 List of top 100 DE genes in the non-tumour tissue of high fibrosis versus low fibrosis comparison

symbol	log2FoldChange	pvalue	padj
Nuggc	-1.694798196	8.15E-19	1.45E-14
Ucp2	1.106164153	2.85E-15	2.54E-11
Sort1	-0.81540868	1.05E-14	5.10E-11
Slc22a29	1.673442977	1.15E-14	5.10E-11
Inpp4a	-0.510388481	1.88E-14	5.58E-11
NA	1.694951006	1.62E-14	5.58E-11
Pparg	1.777016638	3.93E-14	9.99E-11
Tox	1.530517023	8.77E-14	1.73E-10
Fam83a	1.660347528	8.15E-14	1.73E-10
Cgref1	1.128553642	2.58E-13	4.59E-10
Slc22a26	1.693763312	4.98E-13	8.06E-10
Vldlr	1.557519943	6.72E-13	9.96E-10
Sh3bgrl3	0.712243064	1.71E-12	2.33E-09
S100a11	1.244066063	1.96E-12	2.49E-09
Acot9	0.737037245	3.57E-12	4.23E-09
Spsb4	-0.672310537	3.87E-12	4.30E-09
Apoa4	0.999837597	4.97E-12	5.20E-09
Limch1	1.400578989	6.33E-12	6.26E-09
Ctsb	0.339310065	1.10E-11	1.03E-08
NA	1.036288427	1.24E-11	1.10E-08
Cidec	1.581462773	1.55E-11	1.31E-08
S100g	1.567274145	1.64E-11	1.32E-08
Tgfbr2	0.950053027	2.05E-11	1.59E-08
Ephb2	1.533610905	3.98E-11	2.95E-08
Cspg5	-1.512323669	5.63E-11	4.01E-08
Anxa2	0.992554304	6.79E-11	4.64E-08
Aqp7	1.498185994	7.05E-11	4.64E-08
Itgax	1.446424971	1.01E-10	6.44E-08
S100pbp	-0.355281846	1.36E-10	8.36E-08
Angpt1	1.250545996	1.95E-10	1.16E-07
Capns1	0.251083573	3.11E-10	1.79E-07
Fignl1	1.428863659	3.57E-10	1.98E-07
Obp2a	-1.464956678	4.50E-10	2.29E-07
Tmem86a	0.932759144	4.26E-10	2.29E-07
Lgals1	1.05237804	4.51E-10	2.29E-07
Mmp12	1.452292066	6.11E-10	3.02E-07
Clec7a	1.254561251	6.71E-10	3.22E-07
Cyp2u1	-0.78799999	8.93E-10	4.13E-07
Ccnd1	1.132089917	9.16E-10	4.13E-07
Setbp1	1.197797937	9.28E-10	4.13E-07
Ccbl1	-0.522586273	1.01E-09	4.38E-07

Eps8	0.962550481	1.12E-09	4.75E-07
Cntnap1	1.219619995	1.41E-09	5.77E-07
Rcan2	1.371658326	1.43E-09	5.77E-07
Psmd8	0.223676429	1.48E-09	5.86E-07
Cars	-0.413808172	1.69E-09	6.52E-07
NA	-1.380935393	1.92E-09	7.25E-07
Kcp	-0.895890518	2.14E-09	7.95E-07
Myl12b	0.365309009	2.46E-09	8.79E-07
H2-M2	1.401146428	2.47E-09	8.79E-07
Ehbp1	-0.43784295	2.58E-09	9.00E-07
Pea15a	0.353897514	2.94E-09	1.00E-06
Zmym5	-0.249198041	3.22E-09	1.07E-06
Fez2	0.537128198	3.25E-09	1.07E-06
Znf512b	-0.467199981	3.34E-09	1.08E-06
Fras1	-0.855714398	3.41E-09	1.08E-06
NA	-0.707802036	3.48E-09	1.09E-06
Plekha2	0.561161188	3.70E-09	1.13E-06
Dcbld1	0.674542949	4.17E-09	1.26E-06
B4galt6	0.825236448	4.74E-09	1.40E-06
Mmp13	1.361988	5.42E-09	1.58E-06
Fam46a	-0.749469887	6.00E-09	1.72E-06
Rims4	1.280515152	6.09E-09	1.72E-06
Tm4sf4	0.337542188	6.39E-09	1.78E-06
Arhgap10	0.944014344	7.12E-09	1.95E-06
Msmp	1.355861973	7.58E-09	2.04E-06
Krt23	1.343020312	8.14E-09	2.16E-06
NA	-0.69478318	8.89E-09	2.32E-06
NA	-0.447989931	8.98E-09	2.32E-06
Anxa5	0.426144753	9.41E-09	2.39E-06
Bend7	-0.440216791	1.09E-08	2.74E-06
Defb1	1.244117371	1.18E-08	2.91E-06
Stambpl1	0.989316789	1.21E-08	2.95E-06
Gstp1	-0.860320047	1.23E-08	2.96E-06
Simc1	-0.420084415	1.32E-08	3.13E-06
Ccdc80	0.73684706	1.57E-08	3.66E-06
Capg	0.857028219	1.74E-08	3.98E-06
Hao2	1.321117656	1.72E-08	3.98E-06
Ly6d	1.321679487	1.80E-08	4.06E-06
Mcm5	1.145466109	1.84E-08	4.09E-06
Cotl1	0.534441909	2.00E-08	4.34E-06
Tnfsf15	1.279424754	2.00E-08	4.34E-06
Mbp	1.116772136	2.17E-08	4.64E-06
Fbxo22	-0.286223861	2.23E-08	4.67E-06
Ywhah	0.359249748	2.21E-08	4.67E-06
Stk10	0.653813006	2.36E-08	4.89E-06
Ptgfr	1.26782392	2.55E-08	5.21E-06

Iqgap1	0.616734606	2.64E-08	5.30E-06
Snhg18	0.860271327	2.65E-08	5.30E-06
Slc16a5	1.073261323	2.69E-08	5.32E-06
Gal3st1	1.162094172	2.93E-08	5.72E-06
Mogat1	1.280469532	3.35E-08	6.47E-06
Marcks	0.502725439	3.43E-08	6.56E-06
Slc22a27	1.289934666	3.50E-08	6.63E-06
Scai	-0.784151879	4.00E-08	7.50E-06
NA	-0.798988768	4.14E-08	7.68E-06
Myof	0.819387187	4.49E-08	8.24E-06
Wisp3	-1.246717446	4.59E-08	8.33E-06
Fgd3	0.858406947	4.66E-08	8.37E-06
Hexb	0.643159219	5.50E-08	9.78E-06

Appendix-4 List of top 100 DE genes in the non-tumour tissue of high fibrosis versus low steatosis comparison

symbol	log2FoldChange	pvalue	padj
Fam83a	1.464684233	5.02E-14	8.69E-10
Csf2rb	0.841191668	7.73E-13	6.68E-09
Tff3	-1.325676425	7.98E-12	4.60E-08
Dnaic1	-1.270247442	2.77E-11	1.20E-07
Itpr2	-0.462814735	1.01E-10	3.51E-07
Dntt	1.036542481	2.10E-10	5.40E-07
Tusc3	0.552252214	2.19E-10	5.40E-07
Atp9a	0.274288437	2.62E-10	5.67E-07
Slc22a29	1.25819665	5.53E-10	1.06E-06
Aph1b	-0.914399935	6.49E-10	1.12E-06
Myl12b	0.310224903	1.06E-09	1.68E-06
Apoa4	0.886582781	1.29E-09	1.72E-06
Saa3	-1.087077598	1.22E-09	1.72E-06
Serpina9	-1.238211362	1.76E-09	2.18E-06
Def8	0.32456576	1.89E-09	2.18E-06
NA	-1.208283027	2.04E-09	2.20E-06
Inpp4a	-0.366722298	3.09E-09	3.14E-06
H2-Q1	1.064788455	3.26E-09	3.14E-06
Ucp2	0.806640382	6.60E-09	6.01E-06
Msmp	1.177557703	1.22E-08	1.05E-05
Fitm1	1.042384176	1.35E-08	1.12E-05
Ly6d	1.167650391	1.52E-08	1.20E-05
NA	-1.104865173	1.68E-08	1.26E-05
Enho	-1.160114012	1.99E-08	1.44E-05
Isoc2b	0.464017062	2.32E-08	1.58E-05
Gm19619	0.876048553	2.38E-08	1.58E-05
Fads1	0.712966091	2.64E-08	1.69E-05
Ccbl1	-0.433225214	3.27E-08	2.02E-05
Capns1	0.195122229	4.38E-08	2.61E-05
Gcnt4	-1.054276755	4.62E-08	2.66E-05
Cntnap1	1.033838061	6.01E-08	3.25E-05
Ccnd1	0.907973169	5.84E-08	3.25E-05
Lpar6	-0.270146494	6.74E-08	3.54E-05
Sulf2	**0.684330083**	**9.16E-08**	**4.66E-05**
Vat1	0.381589361	1.18E-07	5.75E-05
Spink5	-1.033271422	1.20E-07	5.75E-05
NA	-1.015343286	1.77E-07	8.26E-05
Tead3	-0.366988793	2.17E-07	9.38E-05
Gngt1	0.784452313	2.16E-07	9.38E-05
Dcaf12l1	0.666412274	2.17E-07	9.38E-05
Cdkl2	0.41264676	2.28E-07	9.51E-05

Slc35f2	1.069397697	2.31E-07	9.51E-05
S100g	1.059979629	2.47E-07	9.95E-05
Znrf1	-0.404760579	2.64E-07	0.000104
Acmsd	-0.754450922	2.76E-07	0.000106
Apoc2	0.577477286	3.23E-07	0.000122
Ip6k1	-0.209673909	3.31E-07	0.000122
Tpst1	-0.552946968	3.81E-07	0.000137
NA	-0.976173487	4.03E-07	0.000142
Mcm4	0.75597425	4.54E-07	0.000156
Cotl1	0.421261455	4.60E-07	0.000156
Tmem86a	0.757317985	4.92E-07	0.000162
Ern1	-0.441395258	4.96E-07	0.000162
B430212C06Rik	0.98045074	5.27E-07	0.000169
Sall4	1.022186981	5.94E-07	0.000187
M6pr	0.176396552	6.35E-07	0.000193
Mogat1	0.999937948	6.29E-07	0.000193
NA	1.008817016	6.90E-07	0.000206
Cops7b	-0.341836561	7.09E-07	0.000206
Rarres1	0.670831504	7.14E-07	0.000206
Scd2	1.010883222	7.78E-07	0.000221
Tbc1d31	0.709228526	8.19E-07	0.000228
Acot9	0.524055917	9.44E-07	0.000259
Fads2	0.750787347	1.08E-06	0.000292
Anxa5	0.329673711	1.10E-06	0.000292
Tspan33	-0.722069367	1.14E-06	0.000298
Dynll1	-0.7392959	1.24E-06	0.000305
Abcd1	0.553755222	1.22E-06	0.000305
Pnpla3	1.002720547	1.21E-06	0.000305
5830473C10Rik	-0.428465402	1.25E-06	0.000305
Klhl33	-0.840886577	1.25E-06	0.000305
Adgrf1	-0.991756836	1.30E-06	0.000313
Mllt10	-0.252573512	1.43E-06	0.000339
Gpc1	0.667060399	1.47E-06	0.000343
NA	-0.389839517	1.49E-06	0.000345
Acad9	0.294541598	1.55E-06	0.000353
Srxn1	0.373457503	1.63E-06	0.000362
Bmp6	-0.446832862	1.63E-06	0.000362
BC026585	0.407562337	1.65E-06	0.000362
Dlgap1	-0.953628566	1.77E-06	0.00037
Sh3bgrl3	0.4661017	1.73E-06	0.00037
Arhgap10	0.790588897	1.73E-06	0.00037
Maml3	-0.528651182	1.77E-06	0.00037
Taok2	-0.369297046	1.81E-06	0.000373
Gm17296	-0.495441871	1.83E-06	0.000373
NA	-0.411192336	1.91E-06	0.000385
Ctsb	0.246168451	2.03E-06	0.000403

Lama3	-0.926681279	2.10E-06	0.000414
Cyp2c39	0.831997064	2.16E-06	0.000415
Polr2c	-0.245169655	2.15E-06	0.000415
NA	-0.848701492	2.18E-06	0.000415
C1ql4	-0.958805894	2.27E-06	0.000422
Ctnna1	0.171837308	2.25E-06	0.000422
Cidec	0.964732798	2.34E-06	0.000426
NA	-0.793084899	2.33E-06	0.000426
Nqo1	0.653664599	2.80E-06	0.000484
Brd4	-0.171298807	2.72E-06	0.000484
Smpd3	0.914781269	2.83E-06	0.000484
Smarca4	0.262645781	2.81E-06	0.000484
Fam46a	-0.620283507	2.72E-06	0.000484

Appendix-5 the histological predictors of HCC development in the C3H/He mice

Chi^2 test was performed between categorical variables, while Spearman correlation was performed between different variables.

	Tumour development				
	Chi^2			**Spearman correlation**	
	NO	**Yes**	**p value**	**Correlation**	**p value**
Gross phenotype features					
Liver weight	**1.93 ± 0.11**	**2.67 ± 0.13**		**0.686**	**<0.001**
Liver/body weight ratio	**0.05 ± 0.002**	**0.058 ± 0.002**		**0.66**	**<0.001**
Body weight	**42.18 ± 1.12**	**45.95 ± 0.92**		**0.381**	**0.008**
Histological parameters					
Steatosis grade (0/1/2/3)	**4/7/8/1**	**0/4/20/3**	**0.01**	**0.429**	**0.003**
Microvesicular steatosis	19/1	20/7	0.059	**0.382**	**0.008**
Hepatocellular ballooning (0/1/2)	5/12/3	4/20/3	0.579	0.058	0.699
Mallory Denk bodies (0/present)	14/6	13/13	0.172	0.305	0.1039
Lipogranuloma (0/present)	15/5	9/17	**0.007**	**0.481**	**0.001**
Lobular Inflammation score (0/1/2)	9/10/1	4/18/5	0.06	**0.421**	**0.003**
Portal Inflammation score (0/1/2)	18/1/1	21/5/1	0.507	0.276	0.060
Megamitochondria (0/present)	16/4	17/9	0.275	0.031	0.839
Apoptotic cells (0/present)	15/5	22/4	0.145	-0.114	0.452
Pigmented Kupffer cells (0/present)	13/7	11/15	0.127	0.280	0.060
Perisinusoidal fibrosis score(0/1)	6/14	1/26	0.012	0.361	0.013
Fibrosis stage (0/1/2/3)	6/8/6	1/14/11/1	0.064	**0.355**	**0.014**
NAS score (sum)				**0.465**	**0.001**

Appendix-6 List of top 100 DE genes in the non-tumour tissue G2-G1 comparison

symbol	log2FoldChange	pvalue	padj
Rab7b	1.359134316	8.56E-18	1.56E-13
Rgs2	1.326200401	1.17E-16	1.07E-12
Itgax	3.070569217	5.29E-16	3.22E-12
Ephb2	5.037418963	2.23E-15	1.02E-11
Fam83a	2.959473584	3.55E-15	1.30E-11
Ccl5	2.810290262	6.37E-15	1.94E-11
Rgs10	1.259532556	1.08E-14	2.46E-11
Esm1	2.871008568	1.04E-14	2.46E-11
Pparg	4.08289923	1.41E-14	2.86E-11
Arl4c	1.210437925	1.74E-14	3.18E-11
Clec12a	1.382969639	3.41E-14	5.37E-11
Marcks	0.808501292	3.53E-14	5.37E-11
Clec7a	2.06592789	7.76E-14	1.09E-10
Iqgap1	0.95801272	1.06E-13	1.25E-10
Rac2	1.456875313	1.09E-13	1.25E-10
Fabp4	1.014439538	1.03E-13	1.25E-10
Anxa2	1.50396261	1.35E-13	1.45E-10
Epsti1	1.247936037	1.77E-13	1.80E-10
Ncf2	1.091980182	2.08E-13	2.00E-10
Cd300lb	1.141537474	2.32E-13	2.12E-10
Tyrobp	1.152122859	3.40E-13	2.96E-10
Slpi	2.829778489	3.83E-13	3.18E-10
Laptm5	1.241558944	4.21E-13	3.25E-10
Ctss	1.313986275	4.28E-13	3.25E-10
Lgals1	1.750814714	4.44E-13	3.25E-10
S100a11	1.946599023	4.69E-13	3.30E-10
Card11	2.36672697	4.96E-13	3.35E-10
Gltp	0.928456203	9.90E-13	6.46E-10
Timp1	3.260114433	1.19E-12	7.45E-10
Wdfy4	1.155041207	1.22E-12	7.45E-10
Fam105a	1.435609461	1.43E-12	8.42E-10
Rftn1	0.988664999	1.87E-12	1.07E-09
Cd68	0.989247112	2.02E-12	1.09E-09
Vav1	1.133073448	2.03E-12	1.09E-09
Ckb	1.099940398	2.23E-12	1.17E-09
Endod1	0.969749043	2.68E-12	1.36E-09
Thbs1	1.940743741	2.76E-12	1.36E-09
Kbtbd11	1.635367339	3.11E-12	1.49E-09
Nckap1l	1.187748515	3.21E-12	1.51E-09
Arhgap25	1.304362396	4.79E-12	2.19E-09
Cidec	3.185851928	7.45E-12	3.32E-09

Ucp2	1.373021954	7.76E-12	3.36E-09
Msmp	3.396284509	7.90E-12	3.36E-09
Pld4	1.117857684	9.70E-12	4.03E-09
Cotl1	0.814243272	1.06E-11	4.29E-09
NA	-4.079536802	1.65E-11	6.54E-09
Clec4a2	1.672108973	1.72E-11	6.55E-09
5830473C10Rik	-0.688594907	1.72E-11	6.55E-09
Gpr65	1.390705015	1.80E-11	6.70E-09
Pak1	1.338584911	2.24E-11	8.20E-09
Trem2	2.447214461	3.58E-11	1.19E-08
Sash3	1.509624283	3.44E-11	1.19E-08
Rap2b	0.900109359	3.54E-11	1.19E-08
B4galt6	1.151351281	3.45E-11	1.19E-08
Ms4a4b	1.87320898	3.52E-11	1.19E-08
Uhrf1	2.780330841	3.68E-11	1.20E-08
Tnfrsf23	1.382085065	3.86E-11	1.24E-08
Capg	1.36288818	3.98E-11	1.25E-08
Ly6d	3.248552011	4.06E-11	1.26E-08
Gnai1	1.527483917	4.32E-11	1.32E-08
Hr	2.234750158	4.40E-11	1.32E-08
Myl12b	0.495840381	4.56E-11	1.34E-08
Lpxn	1.126618128	5.08E-11	1.47E-08
Dock2	1.317705168	6.39E-11	1.82E-08
Amz1	1.831023718	7.30E-11	2.05E-08
Ly86	1.140937813	9.25E-11	2.52E-08
Hip1	0.687771282	9.17E-11	2.52E-08
Mbp	1.894942589	1.04E-10	2.78E-08
Csf1r	0.974790629	1.18E-10	3.11E-08
Was	1.190245519	1.19E-10	3.11E-08
Cybb	1.316363724	1.36E-10	3.50E-08
Sh3pxd2b	1.216376464	1.43E-10	3.63E-08
Fcer1g	1.039992004	1.70E-10	4.25E-08
Ppm1h	0.98991467	1.81E-10	4.47E-08
Myo1f	1.313352426	2.38E-10	5.79E-08
Ms4a7	2.301540961	2.47E-10	5.85E-08
Acot9	0.928396503	2.46E-10	5.85E-08
Tnfaip8l2	1.176264257	2.67E-10	6.10E-08
Gpsm3	0.784568538	2.66E-10	6.10E-08
Dna2	-0.623830814	2.64E-10	6.10E-08
Cyba	1.06235638	3.02E-10	6.81E-08
H2-M2	3.752112724	3.10E-10	6.92E-08
Cd52	1.801688923	3.19E-10	7.02E-08
Cxcl9	1.874650962	3.61E-10	7.85E-08
Fam129a	1.035352159	3.74E-10	8.03E-08

NA	1.21220214	3.88E-10	8.23E-08
Wisp2	3.191471438	3.98E-10	8.35E-08
Arhgap22	2.827918458	4.11E-10	8.54E-08
Cyth4	1.108570951	4.43E-10	9.10E-08
Ppp4r3a	-0.432994015	4.80E-10	9.74E-08
Myof	1.198870527	4.98E-10	1.00E-07
Trim30d	0.999994332	5.16E-10	1.03E-07
Pdcd1	5.134805636	5.41E-10	1.06E-07
Ccnd1	1.695752427	5.47E-10	1.06E-07
Sh3bgrl3	0.952296721	5.55E-10	1.07E-07
Cd48	1.291535518	6.20E-10	1.18E-07
Slc7a8	0.86707134	6.39E-10	1.20E-07
Rinl	1.15276684	6.55E-10	1.22E-07
Scube1	2.236732896	6.70E-10	1.24E-07
Ifit3b	1.183226877	7.13E-10	1.30E-07

Appendix-7 Different subsets of T cells were increased in the non-tumour livers of ALIOS mice compared to control mice

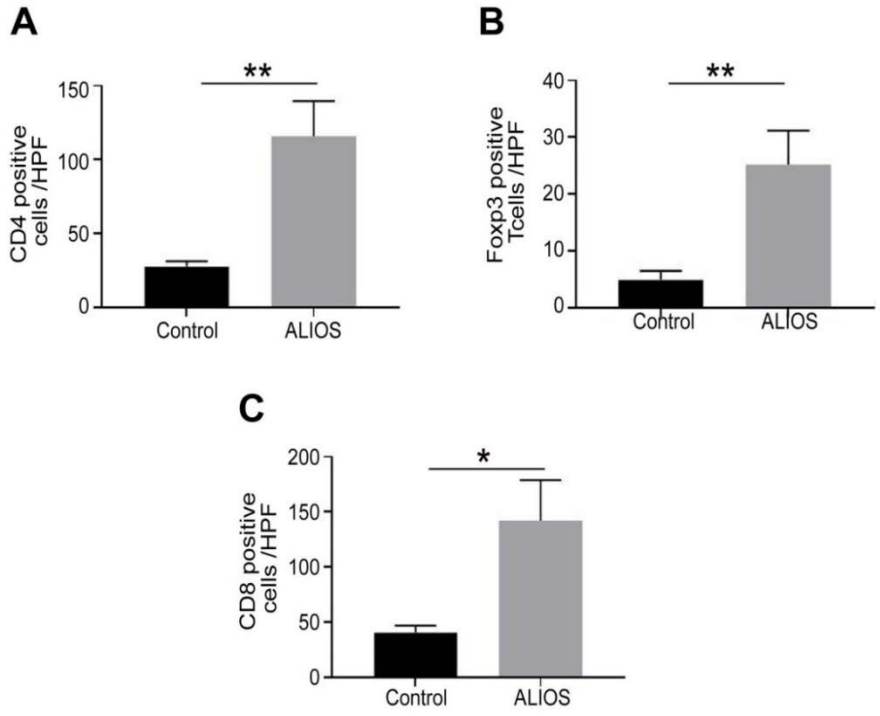

Graphs show the number of CD4 **(A)**, FOXP3 **(B)** and CD8 **(C)** positive T cells in control and ALIOS-fed mice. Data are presented as mean ± s.e.m of positive T cells in 10 high power fields (HPF); * $p<0.05$; ** $p<0.01$

Appendix-8 List of top 100 DE genes in the V2 human signature

symbol	log2FoldChange	pvalue	padj
AHSG	-6.058814897	2.18E-145	7.98E-141
SERPINC1	-5.864260687	1.22E-142	2.23E-138
SLC38A3	-4.32787323	3.41E-115	4.17E-111
NR1I3	-5.077516278	9.36E-114	8.59E-110
CYP27A1	-3.761003529	3.47E-111	2.55E-107
DAO	-5.30121174	2.27E-105	1.39E-101
AQP9	-5.827279902	1.52E-104	7.98E-101
ITGA3	4.093904398	2.37E-102	1.09E-98
PKLR	-5.024888729	3.07E-102	1.25E-98
ASPDH	-5.651603803	1.42E-101	5.22E-98
PLCD3	3.178424327	2.25E-100	7.50E-97
PCK2	-3.849325744	1.77E-97	5.41E-94
SPEG	5.026713439	1.71E-96	4.83E-93
XYLB	-2.787220725	8.60E-96	2.14E-92
UPB1	-4.895203928	8.76E-96	2.14E-92
CCL16	-5.622741858	2.29E-95	5.24E-92
PIPOX	-3.786150019	9.99E-92	2.16E-88
CYB5A	-2.833150413	2.04E-91	4.15E-88
PFKFB1	-4.750818837	7.94E-91	1.53E-87
ACOX2	-3.649710094	4.20E-90	7.69E-87
HNF4A-AS1	-5.163825422	2.20E-88	3.85E-85
APOH	-4.200464675	7.10E-88	1.18E-84
TTR	-5.406958674	3.29E-87	5.24E-84
APOM	-4.265832381	3.82E-85	5.83E-82
SARDH	-3.673712608	6.37E-85	9.34E-82
PROC	-3.273232451	7.37E-84	1.04E-80
ECI2	-2.150274885	3.33E-83	4.53E-80
KHK	-3.40762185	1.75E-82	2.29E-79
PEBP1	-2.25206221	1.77E-81	2.24E-78
SORD	-3.502276203	2.03E-81	2.49E-78
F7	-3.432238683	2.64E-81	3.13E-78
PKM	3.596431766	1.25E-80	1.43E-77
SPDYC	-4.28566513	1.19E-79	1.32E-76
EPHX1	-3.439875415	2.37E-79	2.56E-76
KNG1	-3.954819654	4.51E-79	4.73E-76
AC022816.1	-5.839594708	4.74E-79	4.83E-76
GLYCTK	-2.90651005	5.35E-79	5.30E-76
AQP11	-2.683675169	2.16E-78	2.09E-75
F12	-4.107137695	4.00E-78	3.76E-75
SLC27A5	-4.772009392	4.30E-78	3.95E-75

SERPIND1	-3.746392669	1.11E-77	9.94E-75
AC021074.3	-5.831658028	9.45E-77	8.25E-74
SULT2A1	-4.93932307	2.46E-76	2.10E-73
ADORA2A-AS1	-3.551117611	6.17E-75	5.14E-72
TWIST1	5.432555672	3.93E-74	3.20E-71
AC008549.1	-6.04860657	4.72E-74	3.76E-71
METTL7A	-2.473909794	5.38E-74	4.20E-71
APOA2	-4.46842969	9.28E-74	7.09E-71
SLC9A1	2.131903526	1.55E-73	1.16E-70
CYP2J2	-3.346562801	4.33E-73	3.18E-70
CDR2L	2.941236853	2.17E-72	1.55E-69
MMP14	2.904909685	2.20E-72	1.55E-69
A1BG	-4.397457218	4.17E-72	2.89E-69
CYP7A1	-6.926743868	7.67E-72	5.21E-69
KIF3C	3.124123625	2.21E-71	1.47E-68
ETNK2	-3.887780034	2.49E-70	1.63E-67
LRP8	3.465482861	2.59E-70	1.67E-67
TF	-3.853450718	4.18E-70	2.64E-67
ACSM2A	-4.532556786	5.26E-70	3.27E-67
PECR	-2.422936635	5.76E-70	3.52E-67
FUOM	-2.832956547	6.66E-70	4.00E-67
EHHADH	-3.489821075	7.18E-70	4.25E-67
HJV	-4.430666485	1.07E-69	6.24E-67
ALDH5A1	-2.532000497	1.51E-69	8.54E-67
ITGB4	3.432284927	1.76E-69	9.77E-67
GPX8	2.866805273	3.18E-69	1.74E-66
CRYL1	-2.550857174	8.95E-69	4.83E-66
BDH1	-3.211456961	9.33E-69	4.96E-66
DMGDH	-3.838883465	3.42E-68	1.79E-65
DCXR	-3.937391633	3.75E-67	1.94E-64
F2	-3.543676345	2.51E-66	1.28E-63
SLC10A1	-5.785933174	7.88E-66	3.96E-63
HCN3	-3.069305026	1.10E-65	5.40E-63
IL27	-3.935477941	1.10E-65	5.40E-63
ITPR2	-2.49202564	1.21E-65	5.85E-63
ITIH5	5.453709016	4.69E-65	2.23E-62
FETUB	-5.503162238	6.01E-65	2.83E-62
BHMT	-5.333131215	7.34E-65	3.41E-62
APOC3	-4.444012796	1.05E-64	4.80E-62
ATP8A2	5.293811671	1.69E-64	7.66E-62
MLXIPL	-2.717543987	3.92E-64	1.75E-61
ITIH1	-3.582177583	5.41E-64	2.39E-61
ACSM2B	-4.074571727	2.39E-63	1.02E-60

UGT2B10	-4.914562509	3.52E-63	1.49E-60
HSD17B4	-2.189682806	1.60E-62	6.68E-60
RGN	-3.167765448	1.76E-62	7.26E-60
AP003716.1	-5.300365241	1.93E-62	7.86E-60
NMNAT2	4.80080227	2.46E-62	9.93E-60
NADK2	-2.466323193	2.56E-62	1.02E-59
NUGGC	-4.365618537	1.22E-61	4.82E-59
ARID3C	-4.163819483	1.67E-61	6.51E-59
ADH6	-3.778221661	2.29E-61	8.85E-59
GIPR	4.380258306	2.56E-61	9.79E-59
CES2	-3.221900834	4.26E-61	1.61E-58
CAT	-2.615856239	1.84E-60	6.90E-58
DHTKD1	-2.45025276	1.91E-60	7.07E-58
AMT	-2.184604271	2.14E-60	7.83E-58
SCTR	5.415163599	4.22E-60	1.53E-57
MITF	2.755409371	6.89E-60	2.45E-57
RTP3	-4.903151221	9.49E-60	3.35E-57

Bibliography

Personal Data	
Name	Marco Youssef William Zaki
Gender	Male
Date of Birth	21.12.1987
Nationality	Egyptian
Marital Status	Married
Languages	Arabic
	English
Degree	BSc. pharmaceutical Sciences, MSc. Biochemistry.
Position	Assistant lecturer in the department of biochemistry, Faculty of Pharmacy, Minia university, Egypt.
	PhD student in the Northern institute for cancer research/ institute of cellular medicine, Newcastle university, UK.
Email	m.y.w.zaki2@newcastle.ac.uk
	Marcyoussef87@yahoo.com
Education	
2004-2009	Pharmaceutical sciences, faculty of pharmacy, Minia university, Egypt
2009	BSc in Pharmaceutical Sciences, Faculty of Pharmacy, Minia University, Egypt
2014	MSc in Biochemistry, "Investigation of possible changes of HDGF expression in hepato-carcinogenic mouse model", Minia University, Egypt
2015 to date	PhD student at the NICR/ICM, school of medical sciences, Newcastle University-Newcastle Upon Tyne, England.
Training	
2010	Effective presentation skills course, **Minia University, Egypt**
2010	Self-education training course, **Minia University, Egypt**
2010	Laboratory safety training course, **Minia University, Egypt**
2011	Information & communication Technology Project (ICTP) inclusive course, **Minia University, Egypt**
2012	Practical training in Institute of Biochemistry and molecular biology, Faculty of medicine, **Bonn University, Germany**
2013	Training course in Quality parameters in the educational process, **Minia University, Egypt**

	Training course in " Communication skills, **Minia University, Egypt**
2015	Biological safety, CHOSHH and GM training, **Newcastle university, UK**
2017	Animal handling course – Pil AB, **Newcastle University, UK**
2017	ePortfolio and Personal Development Planning course
2017	Molecular Pathology Node - Training Day, **Newcastle University, UK**
2017	SPSS Beginners course, **Newcastle University, UK**
2018	Training in Cancer Research UK MedImmune Alliance, Granta park, **Cambridge, UK** for the development of active SULFATASE-2 recombinant protein.
2018	Animal tissue processing in MRC Harwell, **Oxford, UK** as a part from current project for an important regulator of NAFLD/HCC.

Techniques and skills

2010-2014 *Characterisation of HDGF protein levels in different stages of HCC development in murine mouse models*

1- Synthesis of recombinant proteins.

2- Rabbit immunisation, Antibody production and purification.

3- Western blotting.

4- Immunohistochemistry.

2015 to Date *Project 1: Characterisation of SULF2 cellular source, function and mechanistic role in human HCC*

1- Molecular biology: Synthesis of recombinant protein, Western blotting, Quantitative Real time PCR (q-PCR)

2- Gene manipulation: CRISPR/CAS9 gene knock-out technique, shRNA gene silencing techniques.

3- Cell based techniques: Cell culture; cell lines and primary cells, Proliferation assays (MTT, BrdU assays), Cell migration assay, Cell invasion assay.

4- 2D and 3D in vitro models: Trans-well 2D cell co-culture techniques, 3D tumour spheroid techniques.

5- ELISA: In-house ELISA optimisation; antibody/protein coating, antibody labelling, target protein measurement.

6- Tissue and cell staining: Immunohistochemistry (IHC), Immunocytochemistry (ICC), Immunofluorescence (IF)

7- Tumour xenograft mouse model.

8- Statistics: Graph-pad prism, SPSS

Project 2: Investigating the role of different immune cells in the development of HCC in a dietary mouse model

1- Bioinformatics tools; Principles of bioinformatics analysis R package, Dealing with big transcriptomic data; Analysing differentially expressed gene lists using Ingenuity pathway analysis (IPA), Gene set enrichment analysis (GSEA) and panther software

2- Tissue and cell staining: Immunohistochemistry (IHC), Immunocytochemistry (ICC), Immunofluorescence (IF)

3- Molecular biology: Synthesis of recombinant protein, Western blotting, Quantitative Real time PCR (q-PCR).

4- Animal work; Animal blood and tissue sampling and manipulation and processing, GTT test for mice

5- Primary cell cultures: Isolation of primary hepatocytes and bone marrow derived monocytes for *in vitro* work

6- statistics

Project 3: The role of Obeticholic acid in restoring cognitive function declined in primary Biliary cholangitis

Bioinformatics tools; Analysing differentially expressed gene lists using Ingenuity pathway analysis (IPA), Gene set enrichment analysis (GSEA) and panther software.

Project 4: MeCP2 in organ fibrosis

1- Primary cell culture: Monitoring isolated mouse hepatic stellate cells with specific MeCP2 knock-out.

2- Immunohistochemistry staining.

Project 5: cRel in organ fibrosis and cancer

1- Bioinformatics tools; Analysing differentially expressed gene lists using Ingenuity pathway analysis (IPA).

2- Immunofluorescence staining

3- 3D tumour spheroid co-culture*Project 6: The development of a novel bioreactor technique for precision-cut liver slices*

Immunohistochemistry

Project 7: Vanin1 single nucleotide polymorphism (SNP) in the development and progression of non-alcoholic fatty liver diseases

Cell based assays; proliferation assays

Quantitative Real time PCR (q-PCR)

Project 8: Non-parenchymal TREM2 in HCC

3D tumour spheroid co-culture

Oral talks (As presenting author)

2019 **Marco Zaki**, Misti V Mccain, Ahmed K Mahdi, Joao Mauricio, Caroline Wilson, Gillian Patman, Anna Whitehead, John Lunec, Ruchi Shukla, Quentin M Anstee, Dina Tiniakos, Fiona Oakley, Helen Louise Reeves-*"Genome wide RNA expression analysis identifies CD44 positive macrophages as promoters of hepatocyte proliferation and the development of NAFLD-HCC"*, EASL HCC summit, Lisbon, Portugal.

Link to the talk: https://easl.meta-dcr.com/hcc2019/crs/abstract-presentation-genome-wide-rna-expression-analysis-identifies-cd44-positive-macrophages-as-promoters-of-hepatocyte-proliferation-and-the-development-of-nafld-hcc

2018	Ahmed Mahdi, **Marco Zaki**, Joao Muricio, Catherine Willoughby, Misti McCain, Olivier Govaere, Jill Patman, Quentin Anstee, John Lunec, Dina Tiniakos, Fiona Oakley and Helen Reeves- *" What drives development of HCC in non-cirrhotic NAFLD?"*, EASL international liver conference, Paris, France.
2018	**Marco Zaki**, Sari Alhasan, Lee Borthwick, Ruchi Shukla, Fiona Oakley and Helen Reeves*, "The role of Stromal SULFATASE-2 in the progression of Hepatocellular carcinoma",* British association for the study of the liver (BASL), Derbyshire, UK.
2017	**Marco Zaki** ,Sari Al-Hasan , Lee Borthwick, Ruchi Shukla, Fiona Oakley and Helen Reeves – *"Stromal SULFATASE-2 promotes Human hepatocellular carcinoma cell growth and is a potential novel therapeutic target",* Oral presentation in the EASL HCC summit in Geneva, Switzerland.

Oral talks (as co-author)

2019	Lucy Gee, Ben Millar, Jack Leslie, Claire Richardson, Diana Jurk, Saimir Luli, **Marco Youssef William Zaki**, Fiona LeBeau, Elizabeth Stoll, David Jones, Fiona Oakley- *"Obeticholic acid limits cholestasis induced cognitive decline by maintaining blood-brain barrier integrity and preserving neuronal health"*, accepted for oral presentation in the international liver congress, Vienna, Austria.

Poster presentations

2019	**Marco Zaki**, Misti Mccain, Ben Barksby, Lee Borthwick, Olivier Govaere, Dina Tiniakos, Ruchi Shukla, Helen Louise Reeves, Fiona Oakley -"*Sulfatase-2 (SULF2) in the hepatocellular carcinoma microenvironment orchestrates disease progression and therapy resistance"*, EASL HCC summit, Lisbon, Portugal.
2019	Aitor Esparza-Baquer, Ibone Labiano, Omar Sharif, Fiona Oakley, Pedro Miguel Rodrigues, Elizabeth Hijona, Raul Jimenez-Aguero, Adelaida La Casta, **Marco Youssef William Zaki**, Colm O Rourke, Patricia Munoz-Garrido, Jesper Andersen , Sylvia Knapp, Derek A Mann, Luis Bujanda, Jesús María Banales, María Jesús Perugorria -*" Non-parenchymal TREM2 halts hepatocarcinogenesis through the inhibition of liver inflammation and hepatocyte proliferation"*, EASL HCC summit, Lisbon, Portugal.
2019	Lucy Gee*, **Marco Zaki*,** Graham Smith, Dave Jones, Fiona Oakley- *"High throughput RNA Sequencing Unravels Pathways Associated with Cognitive Deficit in Primary Billiary Cholangitis"*, EASL international liver congress, Vienna, Austria.
2018	Olivier Govaere, Jeremy Palmer, Mingqiang Zhuang, **Marco Zaki**, Emma Scott, Simon Cockell, Ann K Daly, Quentin M. Anstee- *"The vanin 1-cysteamine pathway regulates immune tolerance upon lipidinduced oxidative stress in non-alcoholic fatty liver disease"*, accepted for poster presentation in the international liver congress in Paris, France.
2017	**Marco Y. Zaki**, Lee Borthwick, Sari Alhasan, Julie Worrell, Ruchi Shukla, Dina Tiniakos, Helen Reeves, Fiona Oakley, *" Stromal Sulfatase-2 – a critical regulator of hepatocellular carcinoma growth and migration"*, AASLD Liver meeting, Washington DC, USA.
2017	**Marco Zaki**, Sari Alhasan, Lee Borthwick, Ruchi Shukla, Julie C Worrell, Helen Reeves and Fiona Oakley – *"Stromal SULFATASE-2 promotes Human hepatocellular carcinoma cell growth",* the director's Day, ICM, school of medical sciences, Newcastle University, UK.
2017	**Marco Zaki**, Sari Alhasan, Lee Borthwick, Ruchi Shukla, Fiona Oakley and Helen Reeves – *"SULFATASE-2, secreted from Cancer-associated fibroblasts, promotes Human hepatocellular carcinoma cell growth"*, BACR tumour microenvironment conference, Nottingham, UK.

2017	Worrell JC, Leslie J, Smith G, O'Reilly S, **Zaki M**, van Laar JM, Mann DA and Oakley F – "*Regulation Of Fibroblast Phenotype, Functionality And Matrix Production By The Nf- Kb Subunit C-Rel In Fibrosis",* poster in 15th international workshop on scleroderma research, university of Pittsburgh, USA.
2014	**Marco Y. William Zaki**, Heba M. eltahir, Nabil M. Abdel-hamid and Mekky M M Abouzied - *"Production and Characterization of Rabbit Anti-mouse Hepatoma Derived Growth Factor (HDGF) IgG for Western Blotting and Immunohistochemistry"*, Poster presentation in Assiut University 9th international pharmaceutical sciences conference, Assiut, Egypt.

Publications

2019	**Marco Zaki**, Ahmed K Mahdi, Gillian L Patman, Joao Mauricio, Misti V McCain, Anna Whitehead, Despina Televantou, Robyn Watson, Jack Leslie, John Lunec, Derek Mann, Quentin M Anstee, Dina Tiniakos, Fiona Oakley, Sirintra Nakjang, Ruchi Shukla, Helen L Reeves, *" A macrophage response to free liver fat drives proliferation and hepatocellular carcinoma in non-alcoholic fatty liver disease". **Manuscript is under review in "Journal of Hepatology".***
2019	Eva Moran-Salvador*, Marina Garcia-Macia*, Ashwin Sivaharan*, Laura Sabater, **Marco Y.W. Zaki**, Fiona Oakley, Amber Knox, Agata Page, Saimir Luli, Mann J* and Mann DA*- *"MeCP2 regulates the myofibroblast RNA landscape and its fibrogenic activity is controlled by site-specific phosphorylation", **Gastroenterology.***
2019	Hannah Paish, Lee Reed, Helen Brown, Mark Bryan, Olivier Govaere, Jack Leslie, Ben Barksby, Marina Garcia Macia, Abigail Watson, Xin Xu, **Marco Y. W. Zaki**, Laura Greaves, Julia Whitehall, Jeremy French, Steven White, Derek Manas, Stuart Robinson, Gabriele Spoletini, Clive Griffiths, Derek Mann, Lee A Borthwick, Michael J Drinnan, Jelena Mann* and Fiona Oakley*- *"A novel bioreactor technology for modelling fibrosis in human and rodent precision-cut liver slices", **Hepatology***.
2019	Jack Leslie, Julie C. Worrell, Saimir Luli, William Reilly, Hannah L Paish, Marina García Macia, Amber Knox, Ben S Barksby, Lucy Gee, **Marco Y.W. Zaki**, Hannah Hepton, Charlotte Bragg, Xin Xu, Git W Chung, Colin DA Brown, Andrew D. Blanchard, Carmel B. Nanthakumar, Morten Karsdal, Jelena Mann, Stuart M Robinson, Derek M Manas, Gourab Senn, Jeremy French, Steven A White, Johannes L Zakrzewski, Ulf Klein, Andrew J Fisher, Neil S Sheerin, Lee A Borthwick, Derek A Mann and Fiona Oakley- *"c-Rel orchestrates energy-dependant epithelial and macrophage reprogramming in fibrosis",* **Revisions are performed for resubmission to *Nature metabolism*.**
2019	Aitor Esparza-Baquer, Ibone Labiano, Omar Sharif, Fiona Oakley, Pedro M. Rodrigues, Elizabeth Hijona, Raul Jimenez-Agüero, Adelaida La Casta, **Marco Y. W. Zaki**, Colm J. O'Rourke, Patricia Munoz-Garrido, Gernot Schabbauer, Jesper B. Andersen, Sylvia Knapp, Derek A Mann, Luis Bujanda, Jesus M. Banales, and Maria J. Perugorria- "TREM2 defends the liver against Hepatocellular Carcinoma through multifactorial protective mechanisms", **Revisions are performed for resubmission to *Gut*.**
2019	Ramy Younes, Olivier Govaere, Salvatore Petta, Luca Miele, Anna L. Fracanzani, Chiara Rosso, Maria J. Garcia Blanco, Angelo Armandi, Gian Paolo Caviglia, **Marco Y.W. Zaki**, Antonio Liguori, Paolo Francione, Grazia Pennisi, Luca Valenti, *Quentin M. Anstee & *Elisabetta Bugianesi, "Long-term clinical and prognostic significance of serum antinuclear autoantibodies in patients with non-alcoholic fatty liver diseases", Paper circulated to co-authors before submission to ***Hepatology***.
2018	**Marco Y. W. Zaki**, Helen L. Reeves – "Long intergenic non-coding RNAs in hepatocellular carcinoma – a focus on Linc00176", Editorial, ***Non-coding RNA Investigation journal.***

2016	Reeves HL, **Zaki MY,** Day CP – "Hepatocellular Carcinoma in Obesity, Type 2 Diabetes, and NAFLD", Review article, in ***Digestive Diseases and Sciences journal****.*
2016	**Marco Y. W. Zaki**, Helen L. Reeves – "*The genetic heterogeneity of hepatocellular carcinoma and the implications for personalised medicine"*, Editorial in ***Translational Cancer Research.***
2011	Nabil M Abdel-Hamid, Maiiada H Nazmy, Ahmed Wahid, Michael A Fawzy, and **Marco Youssof** - *"A Survey on herbal management of hepatocellular carcinoma".* Review article in ***world journal of gastroenterology.***

Peer reviewed manuscripts

2018	OncoTargets and Therapy
2019	Hepatology
2019	Liver international

Memberships

2017	Member of the European Association for the Study of liver Diseases "EASL".
2017-2018	Member of the British Association of cancer research.
2018	Member of the European Association for the Study of liver Diseases "EASL".
2019	Member of the European Association for the Study of liver Diseases "EASL".
2020	Member of the European Association for the Study of liver Diseases "EASL".

Awards and funding

2015	"Newton fund" to support PhD scholarship in Newcastle, United Kingdom.
2017	Best poster award in the ICM Directors day for the poster entitled: SULFATASE-2, secreted from Cancer-associated fibroblasts, promotes Human hepatocellular carcinoma cell growth.
2017	Young investigator full Bursary award to attend the EASL HCC Summit in Geneva, Switzerland.
2018	Young investigator full Bursary award to attend the EASL international liver conference, Paris, France.
2019	2 x Young investigator full Bursary awards to attend the EASL HCC summit, Lisbon, Portugal.
2019	Post submission scholarship-academic development scheme, Newcastle University.